



HAL
open science

Modeling and control of an urban wind turbine intended to be integrated into an electrical microgrid

Jamila Aourir Mazian

► **To cite this version:**

Jamila Aourir Mazian. Modeling and control of an urban wind turbine intended to be integrated into an electrical microgrid. Electric power. Université de Technologie de Compiègne, 2022. English. NNT : 2022COMP2669 . tel-04098235

HAL Id: tel-04098235

<https://theses.hal.science/tel-04098235>

Submitted on 15 May 2023

HAL is a multi-disciplinary open access archive for the deposit and dissemination of scientific research documents, whether they are published or not. The documents may come from teaching and research institutions in France or abroad, or from public or private research centers.

L'archive ouverte pluridisciplinaire **HAL**, est destinée au dépôt et à la diffusion de documents scientifiques de niveau recherche, publiés ou non, émanant des établissements d'enseignement et de recherche français ou étrangers, des laboratoires publics ou privés.

Par **Jamila AOURIR MAZIAN**

*Modeling and control of an urban wind turbine
intended to be integrated into an electrical microgrid*

Thèse présentée
pour l'obtention du grade
de Docteur de l'UTC



Soutenue le 30 mars 2022
Spécialité : Génie Électrique : Laboratoire Avenues - EA-7284

D2669

UNIVERSITÉ DE TECHNOLOGIE DE COMPIÈGNE

THESE

Pour obtenir le grade de

DOCTEUR

Spécialité : Génie Électrique

Jamila AOURIR MAZIAN

Modeling and control of an urban wind turbine intended to be integrated into an electrical microgrid

Laboratoire AVENUES, EA 7284

Soutenance le 30 mars 2022 devant le jury composé de :

Rapporteurs: Prof. Franck BETIN, LTI, Université de Picardie Jules Verne-Amiens

Prof. Raphaël ROMARY, LSEE, Université d'Artois-Béthune

Examineurs: Prof. Vincent LANFRANCHI, LEC, UTC-Compiègne

Prof. Delphine RIU, G2Elab, Grenoble INP UGA-Grenoble

Directeur de thèse: Prof Fabrice LOCMONT, AVENUES, UTC Compiègne

Université de Technologie de Compiègne – AVENUES

Rue Roger Couttolenc, 60203 Compiègne

Abstract

The high global consumption of fossil energy fuels is accelerating their depletion and threatening the Earth's environmental balance. For that, new categories of energy based on renewable sources are developed to build a new diversified and decarbonized energy mix. In order to allow a massive penetration of these renewable energy sources (RESs) into the conventional grid, the use of new electrical system structures seems to be a promising solution, taking into account several aspects such as the costs, the security of supply, and the ease of implementation. Thus, microgrids (MGs) constituted by decentralized energy sources and energy storage systems have been developed to replace or complement the main centralized grid. They can ensure some support functions, i.e., enhancement of the grid stability, black-start operation, replacement of diesel generators, etc. In addition, the consumers become producers and are able to inject a part of their surplus of energy into the public grid. In urban areas, the solar photovoltaic (PV) system has been extensively examined for decades and is widely used thanks to its many advantages such as low environmental impact, easy integration in buildings, reduction of transportation losses, etc. Recently, small-scale wind turbines (SSWTs) are also becoming more and more used, as a complementary source for PV systems, especially for applications near ground level and in urban areas where wind speed is a few meters per second. However, the use of wind power is still nowadays a challenge for the urban MG. In this present thesis, two different types of studies are conducted for a SSWT. i) the first one concerns new power control strategies for a SSWT. It deals with limited power point tracking (LPPT) as an emerging new technology for power management controllers for SSWTs. The LPPT operates in such a way that power requested by the user can be extracted from the wind turbine (WT) while respecting constraints and limitations. However, operating in LPPT mode still requires a deep understanding to obtain a compromise between minimizing power oscillations and transient response. For that, three LPPT power control strategies for a SSWT based on the perturb and observe (P&O) principle are investigated. The proposed algorithms are P&O with fixed step size, P&O based on Newton's method, and P&O based on the fuzzy logic (FL) technique. The experimental results highlight that all methods function correctly and reach the limited power point (LPP). The FL method shows good dynamic performances with more steady oscillations around LPP compared to other methods. ii) in the second study in this thesis, the integration of a SSWT into a direct current (DC) MG was investigated. The RESs (PV sources and WT), storage, and public grid are included and a supervisory system is suggested to manage the power. The power balance is ensured thanks to the real-time power management in the operational layer of the supervisory system. The power is managed based on the rules made according to several aspects, such as every component's energy cost or tariff and its physical limitations. Excess of power produced by PV sources and WT is one of the problems that face the reliability of the MG and should be resolved. Thus, a strategy to limit power from each source is suggested. It is based on two coefficients, α and γ , called "shedding coefficients" that have the role of calculating the quantity of power that should be limited from each source. Simulation tests are carried out

using two power management strategies: optimization and without optimization (storage priority). The results reveal that the coefficient γ reduces the overall cost and whatever the coefficient that is applied, optimization still provides good performances and significantly reduces the global cost.

Keywords: DC microgrid; small-scale wind turbine; limited power point tracking; energy management; power management; supervisory system; optimization; shedding constraints.

Acknowledgements

First and foremost I am extremely grateful to my supervisor, Professor Fabrice LOCMET for his invaluable advice, continuous support, and patience during my Ph.D. study. His immense knowledge and plentiful experience have encouraged me all the time in my academic research and daily life. I would also like to thank Professor Manuela SECHILARIU for accepting me in AVENUES laboratory and revising one of my publications.

I also express my very gratitude to Professor Raphaël ROMARY and Professor Franck BETIN, who have made detailed reports and remarks on my thesis, which help a lot in improving the quality of my thesis for both research content and presentation. Thanks also to Professor Delphine RIU, chairman of the thesis committee, and Professor Vincent LANFRANCHI for their interest in my work. I would also like to thank Professor Arnaud HUBERT and Professor Alain RASSINEUX for their technical support of my study during the individual monitoring committee

I would like to thank my colleagues and research team in AVENUES laboratory and the department of Génie Urbain (GU): Josiane GILLES, Nassima MOUHOUS-VOYNEAU, Nathalie MOLINES, Nancy DOBAIRE, Jean-louis BATOZ, Fabien LAMARQUE, Eduard ANTALUCA, Gilles MOREL, Hipolito MARTELL-FLORES, Justin EMERY, Berk CELIK, and Carine HENRIOT for a cherished time spent together in the lab, and in social settings.

I also thank my colleagues (Ph.D. students) and friends: Soundouss MESSOUDI, Sana BENHAMAI, Saray CHAVEZ, Dian WANG, Wenshuai BAI, Saleh CHEIKH-MOHAMAD, Soelarsou SOELARSO, Amine BEN DAOUED, Fadi AGHA KASSAB and Ghada TAY for the good ambiance, for sharing the Ph.D. and life experience, for discussions on culture and customs, as well as on the study.

My appreciation also goes out to my parents, my sister, my brother, my husband, and all my family members. Without their tremendous understanding and encouragement in the past few years, it would be impossible for me to achieve my goals. Thank you for your encouragement and support all through my studies.

Finally, I would like to present my sincere thankfulness to Lydie DELETTRE who passed away before seeing me complete my thesis successfully. I am grateful for your friendship and your support at a very difficult time in this adventure.

Table of content

Acknowledgements	4
List of figures	9
List of tables	13
Abbreviations	14
Nomenclature	17
Publications associated with this PhD thesis	21
General introduction	22
Chapitre I. Connection and integration of renewable energies in utility grid.....	27
I.1. Towards the next generation of electricity grid: the emergence of smart grids concept	27
I.1.1. Smart grid characteristics and literature survey.....	28
I.1.1.1. Smart grid definition.....	28
I.1.1.2. Smart grid characteristics	29
I.1.1.3. Smart grid advantages.....	29
I.2. Microgrid: the backbone of smart grid	30
I.2.1. Definition.....	30
I.2.2. MG Architecture: AC, DC, and Hybrid.....	31
I.3. DC MG	34
I.3.1. Introduction.....	34
I.3.2. Motivations behind rethinking of DC deployment.....	34
I.3.2.1. DC loads	34
I.3.2.2. Conversion efficiency	35
I.3.2.3. RES	35
I.3.2.4. Storage	35
I.3.2.5. Data centers	35
I.3.2.6. Plug-in electric vehicles.....	36
I.3.3. Topology/design of DC MG.....	36
I.3.3.1. Single-bus topology	36
I.3.3.2. Multi-bus topology	37
I.3.3.3. Reconfigurable topology	38
I.3.4. Control	39
I.3.4.1. Centralized Control.....	40
I.3.4.2. Decentralized control.....	40

I.3.4.3. Distributed control	41
I.3.5. Stability	41
I.3.6. Protection	42
I.3.7. DC MG developed in AVENUES	43
I.4. Place of the wind power generation in the DC MG.....	46
I.4.1. Historical development of wind turbine	46
I.4.1.1. Vertical axis windmills	46
I.4.1.2. Horizontal axis windmills	48
I.4.2. Current status of wind power generation	50
I.4.3. Classification of wind turbines	52
I.4.3.1. Vertical axis vs. horizontal axis wind turbines	52
I.4.3.2. Fix speed vs. variable speed wind turbine	53
I.4.4. Wind turbine constitution and model	54
I.4.4.1. Wind turbine configuration.....	54
I.4.4.2. Wind turbine mathematical model.....	55
I.4.4.2.1. Power coefficient	55
I.4.4.2.2. Betz' law	56
I.4.4.2.3. Tip speed ratio	58
I.4.5. Need and application of the small-scale wind turbine.....	58
I.4.5.1. Several types of machines	59
I.4.5.1.1. Asynchronous/induction machine	59
I.4.5.1.2. Synchronous generator	60
I.4.5.2. Converters.....	61
I.5. Conclusion	62
Chapitre II. Limited power point tracking for the studied small-scale wind turbine-control analyses	64
II.1. Introduction	64
II.2. Related work.....	66
II.3. Studied wind turbine: MG overview and experimental test bench	68
II.3.1. MG overview.....	68
II.3.2. Experimental setup for the SSWT	69
II.4. LPPT control strategies	72
II.4.1.1. P&O with fixed step size.....	74
II.4.1.2. P&O with variable step size based on Newton's method	75

II.4.1.3. P&O with variable step size based on FL	75
II.5. Experimental results and discussion.....	77
II.5.1. Performance of proposed power control strategies	77
II.5.1.1. P&O with fixed step size.....	77
II.5.1.2. P&O with variable step size based on Newton’s algorithm.....	79
II.5.1.3. P&O based on FL.....	81
II.5.1.4. Comparison of the power control methods	83
II.5.2. Impact of sudden variations on the performance of the WT system.....	85
II.5.2.1. Power variation.....	85
II.5.2.2. Wind speed variation.....	86
II.5.3. Transition between MPPT and LPPT modes	88
II.6. Conclusion.....	90
Chapitre III. Integration of a small-scale wind turbine into the DC microgrid	92
III.1. Introduction.....	92
III.2. Literature review	93
III.3. DC MG modeling with the integration of a SSWT	97
III.3.1. MG system and power balance	97
III.3.2. PV sources.....	99
III.3.3. Wind turbine	99
III.3.4. Public grid connection	99
III.3.5. Storage system	100
III.3.6. DC load	100
III.4. MG supervision overview	100
III.4.1. Energy management.....	101
III.4.2. Power management	104
III.5. Shedding coefficient	106
III.5.1. Alpha coefficient.....	106
III.5.2. Gamma coefficient.....	107
III.6. Simulation results and analysis	107
III.6.1. Power profile.....	107
III.6.2. Simulink parameters	108
III.6.3. Simulation results and analysis	109
III.6.3.1. Simulation scenarios	109
III.6.3.2. Simulation without Optimization (Storage Priority).....	109

III.6.3.2.1. Power flow controlled by the coefficient α for $c_{PVS} > c_{WDS}$ and $c_{PVS} < c_{WDS}$ in the case of Storage Priority	109
III.6.3.2.2. power Flow Controlled by the coefficient γ for $c_{PVS} > c_{WDS}$ and $c_{PVS} < c_{WDS}$ in the case the of Storage Priority	112
III.6.3.3. Simulation with optimization.....	114
III.6.3.3.1. Power flow controlled by the coefficient α for $c_{PVS} > c_{WDS}$ and $c_{PVS} < c_{WDS}$ in the case of Optimization	114
III.6.3.3.2. Power flow controlled by the coefficient γ for $c_{PVS} > c_{WDS}$ and $c_{PVS} < c_{WDS}$ in the case of Optimization.	116
III.6.3.4. Energy cost comparisons	119
III.7. Conclusion	120
General conclusion and perspectives	122
References	125
Appendix 1:.....	139
Appendix 2:.....	141
Appendix 3:.....	145
Appendix 4:.....	148
Appendix 5:.....	149

List of figures

Figure 1. Renewable power generation by technology in the sustainable development scenario (SDS) 2000-2030	23
Figure 2. Thesis structure.....	25
Figure 3. Number of SG keywords in publications	29
Figure 4. Possible topology of SG	30
Figure 5. MG general scheme	31
Figure 6. Structure of an AC-MG with a single power line.....	32
Figure 7. Structure of a DC MG with the single power line.....	33
Figure 8. Structure of an AC/DC hybrid MG	33
Figure 9. Single-bus DC MG with storage: a) directly connected to the common DC-bus; b) connected to the common DC-bus through the dedicated converter	37
Figure 10. Multi-bus DC MG with all components connected through dedicated converter interfaces	38
Figure 11. Reconfigurable DC MG based on a) ring bus [70], b) zonal configuration	39
Figure 12. DC MG control strategies.....	40
Figure 13. Power management interface principle	43
Figure 14. DC MG system overview	45
Figure 15. Some of the world's oldest vertical axis windmills; (a) Ruins of a vertical axis windmill in Afghanistan, approx. 700 AD (picture taken in 1977); (b) Persian windmill; (c) Chinese windmill with flapping sails, approx. 1000 AD; (d) Vertical axis windmills with flapping sails, France 1719 AD; (e) Vertical axis windmills with bodies driven by drag forces, Italy, approx. 1600 AD; All pictures are adapted from [90].....	47
Figure 16. Some of the world's oldest horizontal axis windmills; a) Mediterranean tower mill with sails b) Section of a post mill; c) Section of a wipmolen d) Section of a Dutch smock mill e) Sketch of a gallery windmill [90]	49
Figure 17. Western windmills: a) an American windmill developed by U.S. Wind Engine & Pumping Co [4]; b) The Mid-America Windmill Museum, in Kendallville, Indiana [93].....	49
Figure 18. Evolution of wind power capacity.....	50
Figure 19. New wind power installations growth: a) per year; b) per region	50
Figure 20. New Onshore and Offshore wind installations in 2020: a) in the world, b) in Europe	51
Figure 21. Share of electricity in Eu-27	52

Figure 22. Vertical Axis WTs: a) Straight-blade Darrieus, b) Savonius rotor, and c) Curved-blade Darrieus rotor	53
Figure 23. Siemens HAWT (model: SWT-2.3-82 VS).....	53
Figure 24. Typical configuration of a HAWT	54
Figure 25. Aerodynamic power coefficient as a function of the normalized rotational speed λ ..	57
Figure 26. Fixed-speed WECS, directly connected with the grid.....	59
Figure 27. Variable-speed doubly-fed induction generator with partial scale power converters .	60
Figure 28. Variable-speed, gearless multi-pole PMSG based WECS	60
Figure 29. Variable-speed synchronous generator with full-scale power converter.....	60
Figure 30. Electrical structure of power conversion	61
Figure 31. The MG overview.....	69
Figure 32. a) Wind tunnel; b) pressure transmitters and Pitot tube	70
Figure 33. Electrical scheme and components of the studied SWECS.....	71
Figure 34. a) Electrical power p_{WT} based on the bus voltage v_{WT} ; b) electrical power p_{WT} based on the bus current i_{WT} ; c) electrical power p_{WT} based on mechanical speed Ω	72
Figure 35. Operating cases for: a) LPP1; b) LPP2.....	73
Figure 36. Principle of P&O method for LPPT mode	74
Figure 37. Structure of FLC.....	76
Figure 38. p_{WT} based on v_{WT} for selected wind speed.....	77
Figure 39. Fixed step-size P&O for LPP1: a) evolution of step size Δv ; b) evolution of p_{WT} ; c) evolution of v_{WT} ; d) evolution of i_{WT}	78
Figure 40. Fixed step-size P&O for LPP2: a) evolution of step size Δv ; b) evolution of p_{WT} ; c) evolution of v_{WT} ; d) evolution of i_{WT}	79
Figure 41. Newton's variable step-size P&O for LPP1: a) evolution of step size Δv ; b) evolution of p_{WT} ; c) evolution of v_{WT} ; d) evolution of i_{WT}	80
Figure 42. Newton's variable step-size P&O for LPP2: a) evolution of step size Δv ; b) evolution of p_{WT} ; c) evolution of v_{WT} ; d) evolution of i_{WT}	81
Figure 43. FL variable step-size P&O for LPP1: a) evolution of step size Δv ; b) evolution of p_{WT} ; c) evolution of v_{WT} ; d) evolution of i_{WT}	82
Figure 44. FL variable step-size P&O for LPP2: a) evolution of step size Δv ; b) evolution of p_{WT} ; c) evolution of v_{WT} ; d) evolution of i_{WT}	83
Figure 45. Comparison of experimental results: a) evolution of p_{WT} at LPP1; b) evolution of p_{WT} at LPP2.....	84

Figure 46. Statistical analysis of experimental results: (a) evolution of p_{WT} at LPP1; (b) evolution of p_{WT} at LPP2.....	85
Figure 47. Drop in power: a) sudden increase of p_{WT} ; b) sudden decrease in p_{WT}	86
Figure 48. Wind speed profile.....	87
Figure 49. Drop in wind speed: (a) p_{WT} based on v_{WT} ; (b) evolution of p_{WT} in time	87
Figure 50. Power profile for the selected wind speed.....	88
Figure 51. Evolution of p_{WT} while the transition between LPP2 and MPP for: a) Fixed step-size P&O; b) Newton's variable step-size P&O; c) FL's variable step-size P&O	89
Figure 52. Evolution of v_{WT} while the transition between LPP2 and MPP for: a) Fixed step-size P&O; b) Newton's variable step-size P&O; c) FL's variable step-size P&O	89
Figure 53. Comparison of experimental power results while the transition between LPP2 and MPP.....	90
Figure 54. Proposed classifications of energy management strategies (adapted from [72])	94
Figure 55. DC MG structure	98
Figure 56. The details of the MG multi-layer supervisory concept	101
Figure 57. Flowchart of power management of the DC MG in power management layer	105
Figure 58. Power profile proposed randomly	108
Figure 59. Evolution of k_D , k_{D_real} and soc without optimization by applying α coefficient... ..	111
Figure 60. Power flow curves without optimization by applying α coefficient.....	111
Figure 61. PV and SSWT shedding curves by applying the α coefficient in the case of storage priority.....	111
Figure 62. Evolution of k_D , k_{D_real} , and soc without optimization by applying the γ coefficient in the case of: (a) $c_{PVS} > c_{WDS}$; (b) $c_{PVS} < c_{WDS}$	113
Figure 63. Power flow curves without optimization by applying the γ coefficient in the case of: (a) $c_{PVS} > c_{WDS}$; (b) $c_{PVS} < c_{WDS}$	113
Figure 64. PV and SSWT shedding curves without optimization by applying the γ coefficient in the case of: (a) $c_{PVS} > c_{WDS}$; (b) $c_{PVS} < c_{WDS}$	114
Figure 65. Evolution of k_D , k_{D_real} and soc without optimization by applying α coefficient. .	115
Figure 66. Power flow curves with optimization by applying the α coefficient.	116
Figure 67. The PV and SSWT shedding curves by applying the α coefficient in the case of optimization.	116

Figure 68. Evolution of k_D , k_{D_real} and soc with optimization by applying the γ coefficient in the case of: **(a)** $c_{PVS} > c_{WDS}$; **(b)** $c_{PVS} < c_{WDS}$ 118

Figure 69. Power flow curves with optimization by applying the γ coefficient in the case of: **(a)** $c_{PVS} > c_{WDS}$; **(b)** $c_{PVS} < c_{WDS}$ 118

Figure 70. PV and SSWT shedding curves with optimization by applying the γ coefficient in the case of: **(a)** $c_{PVS} > c_{WDS}$; **(b)** $c_{PVS} < c_{WDS}$ 119

List of tables

Table 1. Rule base for LPPT mode. (N: negative; P: positive; Z: zero; S: small; B: big)	76
Table 2. p_{WT} reached using different control method strategies. SD: standard deviation.....	85
Table 3. Parameters for simulation tests	108
Table 4. Simulation cases.....	109
Table 5. Energy shedding calculation for the α coefficient in the case of storage priority.....	112
Table 6. Energy shedding calculation for the γ coefficient in the case of storage priority.	114
Table 7. Energy shedding calculation for the α coefficient in the case of optimization.	116
Table 8. Energy shedding calculation for coefficient γ in the case of optimization.	119
Table 9. Energy cost calculation for α and γ coefficients.....	120

Abbreviations

RES	Renewable energy source
MG	Microgrid
PV	Photovoltaic
SSWT	Small-scale wind turbine
LPPT	Limited power point tracking
WT	Wind turbine
P&O	Perturb and Observe
LPP	Limited power point
FL	Fuzzy logic
DC	Direct Current
SDS	The Sustainable Development Scenario
DPG	Distributed power generation
SG	Smart grid
PMSG	Permanent magnet synchronous generator
MPPT	Maximum power point tracking
MPP	Maximum Power Point
PE	Power electronic
NIST	The National Institute of Standards and Technologies
EPRI	The Electric Power Research Institute
DECC	The Department of Energy and Climatic Change
DER	Distributed energy resource
AC	Alternating current
CERTS	The Consortium for Electric Reliability Technology Solutions

ESS	Energy storage system
FC	Fuel cell
EV	Electric vehicle
SOC	State of charge
IED	Intelligent electronic devices
CDC	conventional droop control
ADC	adaptive droop control
VSC	Voltage source converter
EKF	Extended Kalman filter
HAWT	Horizontal axis wind turbine
GWEC	The Global Wind Energy Council
VAWT	Vertical axis wind turbine
WECS	Wind energy conversion system
DFIG	Doubly fed induction generator
SWECS	Small wind energy conversion system
DPC	Direct power controller
IPC	Indirect power controller
APC	Advanced power controller
HCS	Hill climb search
IC	Incremental conductance
TSR	Tis speed ratio
PSF	Power signal feedback
OT	Optimal torque
ANN	Artificial neural networks
FLC	Fuzzy logic controller

EMS	Energy management system
SOO	Single objective optimization
MOO	Multi-objective optimization
BS	Battery storage
LP	Linear programming
MILP	Mixed-integer linear programming
MPC	Model predictive control
GA	Genetic algorithm
MAS	Multi-agent system
DG	Diesel generator
CS	Charging station
CPL	constant power loads
CB	Circuit breaker
TW	Traveling wave

Nomenclature

P_{aero}	Aerodynamic power of a wind turbine (W)
ω_r	Angular speed (tr/min)
T_r	Torque (Nm)
ρ	Air density (kg/m ³)
π	Mathematical function
$C_p(\lambda, \beta)$	C_p power coefficient ; λ : tip speed ratio ; β : pitch angle
R	The radius of the rotor blades (m)
v	Wind speed (m/s)
P_{mech}	Mechanical power generated by a wind turbine (W)
$n_{c,1}, n_{c,2}$	Polynomial degree
a_{ij}	Coefficients of the polynomial function
C_{DC}	Capacitor of the DC bus (F)
C_{WT}	Capacitor used to constitute the DC bus of the SWECS (F)
P_{lim}	Limited power or power required by the MG load or the user (W)
v_{WT}	DC bus voltage (V)
p_{WT}	Electrical power available in the DC bus (W)
v_{WT_REF}	DC bus voltage reference or the result provided by the controller (V)
Ω	Mechanical speed (tr/min)
i_{WT}	Current of the DC bus (A)
p_{diff}	The absolute value of the difference between p_{WT} and P_{lim} (W)
X_n	The initial value of X
$F(X_n)$	The value of the X at the point X_n
$F'(X_n)$	The derivative of function at X_n

Δv	Variable step sizes (V)
u_1	The first normalized input of the FLC
u_2	The second normalized input of the FLC
p_{ref}	Compensation power by the public grid and storage
Δt	The time interval between two samples (s)
t	Continues time (s)
t_0	Initial time instant (s)
t_F	Final time instant (s)
p_{PV}	Photovoltaic power (W)
p_{WD}	Wind turbine power (W)
p_L	DC load power (W)
p_P	System dynamic power for P controller
p_S	Battery storage power (W)
p_G	Public grid power (W)
K_p	Proportional gain of DC bus voltage controller
$V_{DC\ ref}$	DC bus voltage control reference (V)
$V_{DC\ bus}$	DC bus voltage (V)
p_{PV_MPPT}	Photovoltaic power by MPPT algorithm (W)
p_{WD_MPPT}	Wind turbine power by MPPT algorithm (W)
p_{PV_S}	Photovoltaic shed power (W)
p_{WD_S}	Wind turbine shed power (W)
p_{G_MAX}	Maximum power that the public grid can buy or sell ($-p_{G_MAX}$)
p_{GI}	Public grid power injection(W)
p_{GI_MAX}	The limit for grid power injection (W)

p_{GS}	Public grid power supply(W)
p_{GS_MAX}	The limit for grid power supply (W)
C_{REF}	Capacitor of battery storage (Ah)
SOC	State of charge of batteries storage (%)
SOC_{MAX}	Upper limit of a state of charge of batteries storage (%)
SOC_{MIN}	Lower limit of a state of charge of batteries storage (%)
v_s	The storage voltage (V)
p_{S_MAX}	Battery storage maximal power limit (W)
p_{L_S}	DC load shed power (W)
p_{L_OPT}	DC load power after the real-time load optimization (W)
p_{L_D}	DC load demand power (W)
p_{AVAIL}	Total available DC microgrid power (W)
C_{PV_S}	Photovoltaic shedding cost (€)
C_{WD_S}	Wind turbine shedding cost
C_{L_S}	DC load shedding cost (€)
C_G	Public grid cost (€)
C_S	Storage cost (€)
C_{TOTAL}	Total energy cost (€)
c_G	Public grid energy tariff (€/kWh)
c_{NH}	Public grid tariff in normal hours (€/kWh)
c_{PH}	Public grid tariff in peak hours (€/kWh)
c_s	Battery storage energy tariff (€/kWh)
c_{PV_S}	Photovoltaic shedding energy tariff (€/kWh)
c_{WD_S}	Wind turbine shedding energy tariff (€/kWh)

c_{L_S}	DC load shedding tariff (€/kWh)
k_D	Power distribution coefficient between the public grid and battery storage
P_{REN_SHEDD}	The total renewable power to be shed (W)
α_{PV}	Shedding coefficient for PV source without taking into account the cost
α_{WD}	Shedding coefficient for wind turbine without taking into account the cost
γ_{PV}	Shedding coefficient for PV source with taking into account the cost
γ_{WD}	Shedding coefficient for a wind turbine with taking into account the cost
ξ_{PV}	Shedding coefficient cost for PV source
ξ_{WD}	Shedding coefficient cost for wind turbine source
N_{PV}	Number of the PV panel
P_{PV_STC}	PV at standard test condition (W)

Publications associated with this PhD thesis

The works presented in this thesis are validated by several publications which have been published in journals. The details of them are listed as below:

Publication in journals with review committees and indexed in Scopus and WoS

1. **Aourir, J.** Locment, F. “Limited Power Point Tracking for a Small-Scale Wind Turbine Intended to Be Integrated in a DC Microgrid”. *Applied Sciences*. vol. 10, no.22, pp 8030, 2020; Impact Factor 2.679, Scopus, WoS, <https://doi.org/10.3390/app10228030> [1].
2. **Aourir J.** Locment F, Sechilariu M. “Power and Energy Management of a DC Microgrid for a Renewable Curtailment Case Due to the Integration of a Small-Scale Wind Turbine”. *Energies*, vol. 15, no.09, pp 3421, 2022; Impact Factor 3.252, Scopus, WoS, <https://doi.org/10.3390/en15093421>.

General introduction

Electric energy is a determining element for any socio-economic growth and development. It has become essential in the daily lives of populations in many countries worldwide. It is also increasingly demanded due to the fast development of the industry, the widespread introduction of new energy-efficient technologies, such as electric vehicles and heat pumps, the proliferation of household appliances, the increase in demand for digitally connected devices, and air conditioning systems [2]. These developments pose significant challenges to the power system, in which supply should fully follow demand. Faced with the extensive rise in electricity demand and the decrease in world hydrocarbon reserves, including the fear of increasing destruction of ecosystems, industrialized countries have resorted massively to nuclear power plants. This source of energy has the undeniable advantage of not causing atmospheric pollution, unlike traditional thermal power stations, but the risk of a nuclear accident (such as the Chernobyl disaster of April 26, 1986, and the recent nuclear accident at the Fukushima plant in Japan), the treatment and waste burial are very real problems that make this energy unattractive for future generations.

Nowadays, with the increasingly serious problems of fossil energy depletion and awareness of environmental issues, RESs has received more and more attention. Indeed, RESs such as wind electric conversion systems, PV systems, biomass resources, and tidal energy have many advantages in terms of their efficient production of electrical energy, reliability, ease of installation, and less environmental impact. According to the international energy agency, renewable power capacity rises annually associated with dropping costs and investment growth. For example, the amount of renewable-based generated

electrical energy will be increased from 5525 TWh in 2015 to 14979 TWh in 2030 (Figure 1). This increase will present almost two-thirds of global electricity generation (including hydropower) [3].

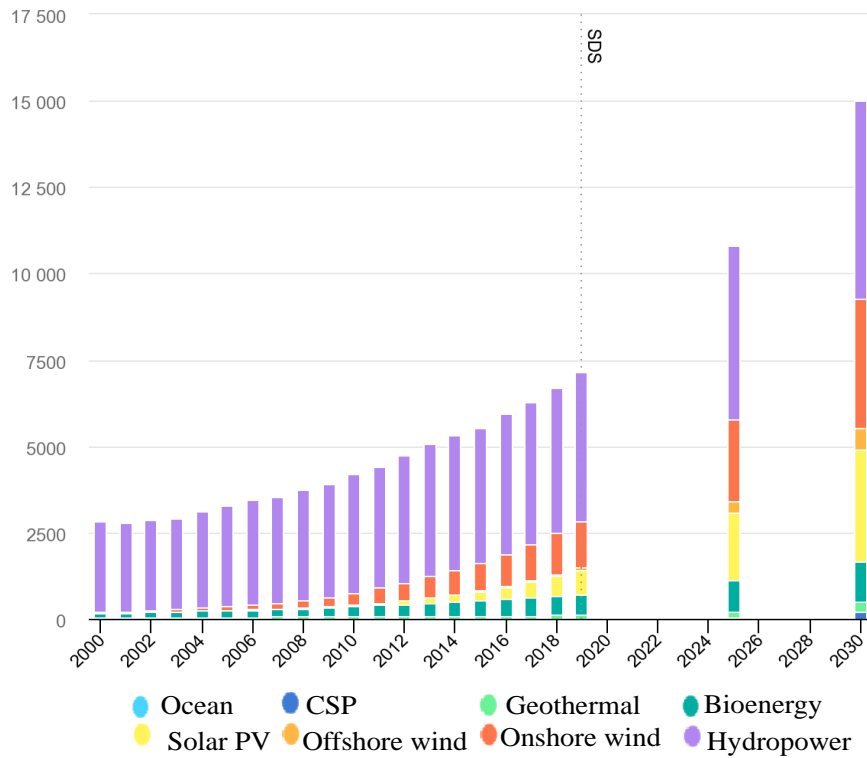


Figure 1. Renewable power generation by technology in the sustainable development scenario (SDS) 2000-2030

As producing energy from RESs is becoming the priority of electricity production, their integration into the existing utility grid gives rise to distributed power generation (DPG). This latter has attracted wide attention and contributed to alleviating the pressure of energy shortage and reducing environmental pollution [4]. Thus, the DPG is evolving as an emerging power scenario for electric power generation and a promising approach to relieving existing power systems from today's stress on transmission and distribution systems [5]. These motivations are changing the power generation concept worldwide with the appearance of new challenges in the generation and distribution markets. The political encouragement and the purchase of renewable energy production, which is qualifying for advantageous rates, make the DPG develop significantly through the PV plants, wind farms, and small power production points such as small plants PV integrated into building or urban WTs, etc. [6]. Hence, the DPG is then based on systems that can work in grid-tied conditions, for a total and permanent power injection into the utility grid, islanded conditions, especially in rural areas or remotes sites, or as a combination of grid-connected / off-grid conditions [7]. This means that the urban and rural areas are going to have the ability to control DPG as well as to produce and consume the power locally. However, systems based on DPG are changing the manner of transmission of energy through the utility power grid. Their increased development leads to serious connection issues with a public grid, which constitutes true scientific and technical constraints. Consequently, the power system architecture must be reformed into a more flexible, scalable, and

powerful management topology. This request results in the appearance of the smart grid (SG) concept, which is an advanced framework based on new electricity transport and distribution network that allows bidirectional communication between suppliers and consumers to adjust the flow of electricity in real-time and enables more efficient management of the electricity grid [8]. The main components of the SG are MGs. Indeed, the MG is known as an electrical energy distribution network consisting of multiple generations, storage, and load managed from the grid more extensive transportation. The interest in MG has grown significantly due to its benefits in providing efficient, secure, reliable, environmentally friendly, and sustainable power from RESs. However, the generation and integration of DPG into the MG system remain a challenge because many important parameters must be considered. The complex structures of MG due to the extensive integration of distributed RESs and their intermittent behavior may influence the power system stability and security. It should be known that the MG has more issues than conventional power grids. These issues depend on different aspects such as power converter (components and power quality), power balancing, protection, and power and energy management. This latter is the center part of MG. Its main objective is to well manage the power flow in real-time and give a long-term energy schedule in order to satisfy load demand, increase the integration of the RESs, and minimize the overall cost. It consists of two approaches: i) the rule-based approach, which is easy and robust but does not ensure optimal performance in some conditions. ii) the optimization-based approach that provides an optimal solution.

One of the most used RES is the wind generation system. This latter can be sorted into three categories depending on the power productivity: small, medium, and large scales. A large wind generation system is widely used for a wind farm, while medium and small-scale WTs can be exploitable in a more flexible environment. A SSWT, for example, is commonly used in the distributed energy system and is more suitable in the urban area. In this work, the integration of a SSWT based on a permanent magnet synchronous generator (PMSG) into a DC urban MG is studied. The work presented in this manuscript is organized into three chapters (Figure 2). After the general introduction, the **first chapter** consists of a bibliographic study on renewable energies, DC MG and wind turbines. Firstly, this part recalls the context of the evolution of the electrical system and the appearance of intelligent grids. The MG as a key element of smart grids is then detailed in different aspects before tackling the wind turbine characteristics that will be studied in this thesis.

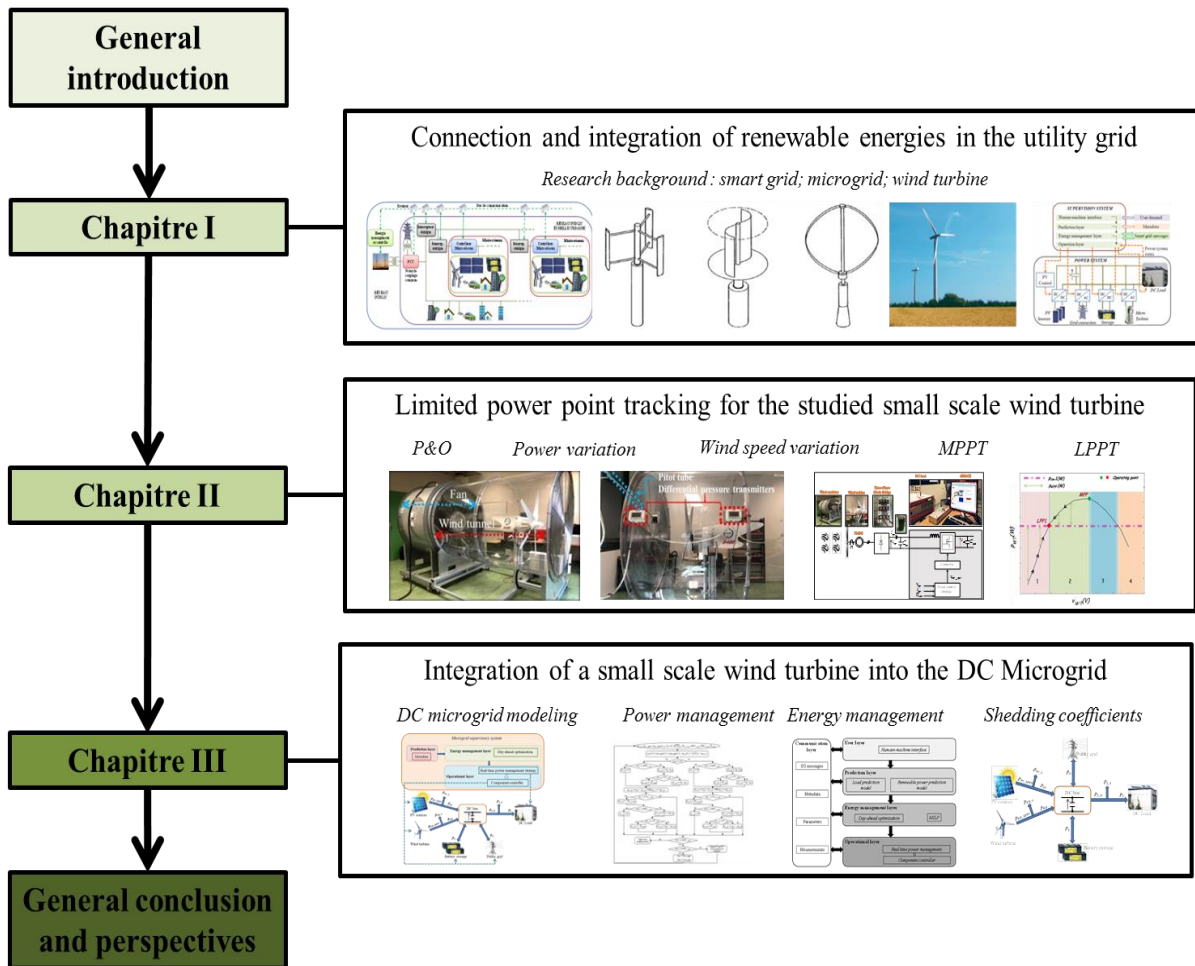


Figure 2. Thesis structure

The **second chapter** suggests a sensorless limited power extraction control for a small-scale wind energy conversion systems (WECS) using a PMSG. Different power control strategies are proposed to produce the required power and meet flexible energy demand. The proposed methods use the output voltage and current of the rectifier and the limited power required by the user to calculate the reference voltage for the controller. Based on the rectifier output power and the difference between the operating point and the limited point, the step size change until the limited point is attained. Three LPPT control strategies for a SSWT are investigated. These methods concern fixed step size, Newton’s method, and FL technique. In addition, the effect of the sudden variation of some conditions, such as power required by the user or climatic changes (wind speed), on the performances of the suggested LPPT methods is examined. Finally, other experiments dealing with the transition between maximum power point tracking (MPPT) mode and LPPT mode are conducted. Performances of the proposed control strategies are evaluated and validated by laboratory experiments using a real SSWT placed in a wind tunnel equipped with ventilation.sensorless controller.

The **third chapter** is dedicated to examining the power and energy management of a DC MG during the integration of a SSWT. It consists firstly of modeling a DC MG connected to the grid. The key MG elements are SSWT, solar PV, battery, DC load, and a connection to the grid. A supervisory system is

also introduced with a formulation of the optimization problem. During the supervision process, some criteria such as the physical limits and tariffs of the components are taken into account. Then, the suggested power management strategy aims to achieve an instantaneous power balance considering a rule-based power flow and depending on the criteria above-mentioned. To better meet the power balance, the current study has explored the constraints related to the control and supervision of the studied DC MG. Performance measures include the overall system cost and renewable curtailment (RESs energy that cannot be utilized and should therefore be limited). For that, a strategy for power limitation is suggested. It consists of using two types of shedding coefficients to calculate the power that should be limited from each renewable source in case of energy surplus. Simulation results are presented and showed that the studied MG can control the power flow at an optimum energy cost. Furthermore, once the limited power will be calculated thanks to the shedding coefficient, it will be able to be generated by the WT thanks to the limitation strategies already set up.in chapter 2.

Finally, general conclusions and perspectives of the research of this thesis are provided at the end.**Equation Chapter (Next) Section 1**

Chapitre I. Connection and integration of renewable energies in utility grid

I.1. Towards the next generation of electricity grid: the emergence of smart grids concept

The power balance between the demand and the supply side of an electrical grid is one of the most important issues in grid operation. These issues are mainly related to fluctuations in energy demand and renewable energy generation. On the one hand, the power balance was historically achievable to a certain level thanks to the conventional power grid that was designed with large centralized generation plants and which assured that the power generation followed the electricity demand [9]. However, this generated power is transferred to consumption on the unidirectional way and over long-distance transmission lines, which causes a certain amount of power loss. On the other hand, the integration of DERs, characterized by bidirectional power flow, is a delicate matter for the utility grid that was not planned for that. The intermittent nature of RESs and the difficulty of forecasting make them very unsettled. In addition, they behaved as passive electric generators, and then did not participate in technical regulation for grid connection. All these problems associated with growing demands and peak loads lead to a rise in the pressure on the electrical structure and affect the power reliability and quality [10]. To cope with these new problems, it is necessary to:

- reinforce the classical power grid, with new devices from power electronics (PEs) and new information technologies like advanced control systems;

- control and improve renewable power injected into the utility grid;
- manage the intermittence and reduce the fluctuations of RES.

One of the avenues to respond to these new constraints is to develop a smarter electrical system through SG technologies [11].

1.1.1. Smart grid characteristics and literature survey

1.1.1.1. Smart grid definition

With the fast development of electric distribution technology, the concept of SG has been developed notably through the electricity market liberalization, the evolution of PE devices, and the enhancement of information and communication technologies [12]. A SG does not have a unique universal definition to be precisely described. Yet, it can be seen as an intelligent automated network that can store, communicate and make its own decisions [13]. US Energy Independence and Security Act 2007 had provided a similar definition for the SG [14]. It is defined as a modernized form of the traditional grid capable of monitoring, increasing grid resilience to disturbances, and automatically optimizing grid operation of interconnected system components (i.e., central generating units, distributed generation, transmission network, and loads).

Furthermore, “a modern grid adapts bi-directional flows of energy” was the definition provided by the US National Institute of Standards and Technologies (NIST) to describe the SG [15]. It guarantees a wide range of functionalities and applications thanks to the utilization of a two-way flow of energy, data, and control strategy. In addition, the Electric Power Research Institute (EPRI) based in the US [16] defines the SG as “the transition from the current grid where the flow of power is permitted from the central generation to load location into a grid where there is a peer to peer consumer interactions, distributed generation, and control centers”.

The Department of Energy and climatic change (DECC) in the UK [17] highlights the role of the SG in achieving power balance and intelligent management of the electrical system. With SG information and communication tools, operators become more aware of supply-demand balance and participate in shifting non-critical demand from peaking periods to off-peaking instants.

Numerous entities and researchers have stated more definitions of SG that could be found for example in [18]–[24]. Indeed, the number of publications dealing with SGs is illustrated in Figure 3. An advanced search in Scopus with a filter for SG technologies in the abstracts, titles, keywords, and text fields of publications from 1999 to 2020 shows an increased interest in SG area.

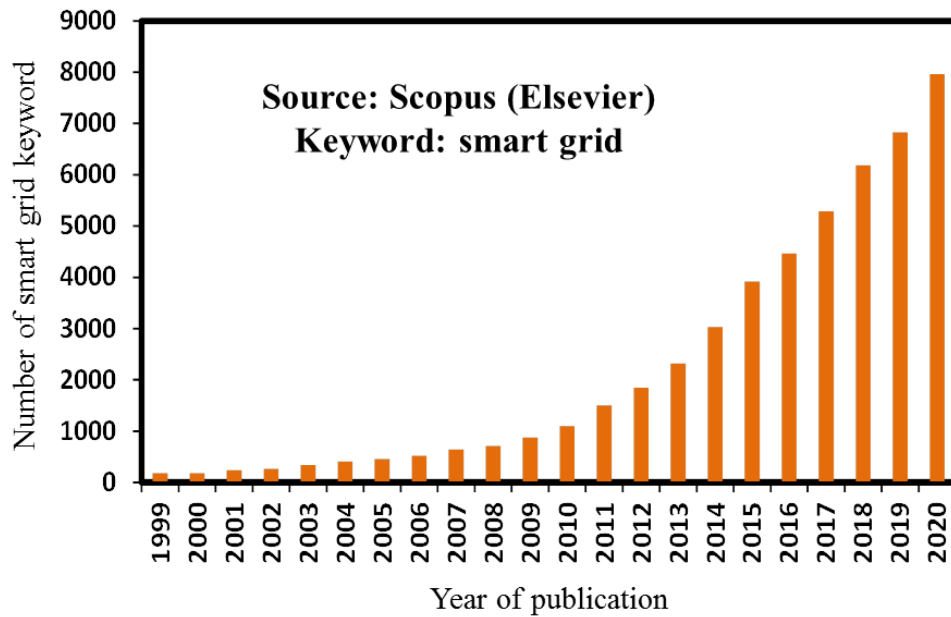


Figure 3. Number of SG keywords in publications

1.1.1.2. Smart grid characteristics

The SG can shift the already existing power system infrastructure into a modernized form with more flexibility and reliability. This new form of the grid permits intelligently the integration of users, generators, and consumers to provide efficient, secure, and economically feasible supplies [21].

The SG integrates distributed energy resources (DERs) that include sustainable energy sources. It is supposed to handle a bidirectional-based structure for energy flow and communications to perform continuously a dynamic optimization of grid operation. Also, it contains demand-side response programs and demand-side resources [25]. Moreover, the SG is a network that digitizes information, enhances the integration of smart appliances, and is fortified against cyber threats. Furthermore, the SG should be equipped with advanced storage devices and peak-shaving technologies.

1.1.1.3. Smart grid advantages

Generation and distribution of electricity with minimal issues is the main goal behind empowering the transition toward the SG [23]. According to [16], [18], [20], it is estimated that, by 2030, applications based on SG can reduce the nation's carbon dioxide emission from 211 to 60 million metric tons annually. The advantages of developing the SG are numerous: increasing the flexibility and the quality of the power grid, reducing power losses and greenhouse gaseous emissions, improving the reliability of electricity supply, facilitating the incorporation of DERs (better penetration of RESs), enabling predictive maintenance and self-healing capacities, and enhancing system security [26]–[28].

Despite the intelligent tools and advanced communication protocols employed in SG, its realization remains complex. Then, the development of this active and intelligent network requires the design of new

structures associated with the existing framework. In this context, SG can be seen as the aggregation of several cells called MGs. This latter was defined by Hatziargyriou in [29] as a “building block of the smart grid”. The possible SG topology evolution facilitated by MG is shown in Figure 4 [7]. MGs are the most promising new structure of grids, and their characteristics will be detailed in the next section.

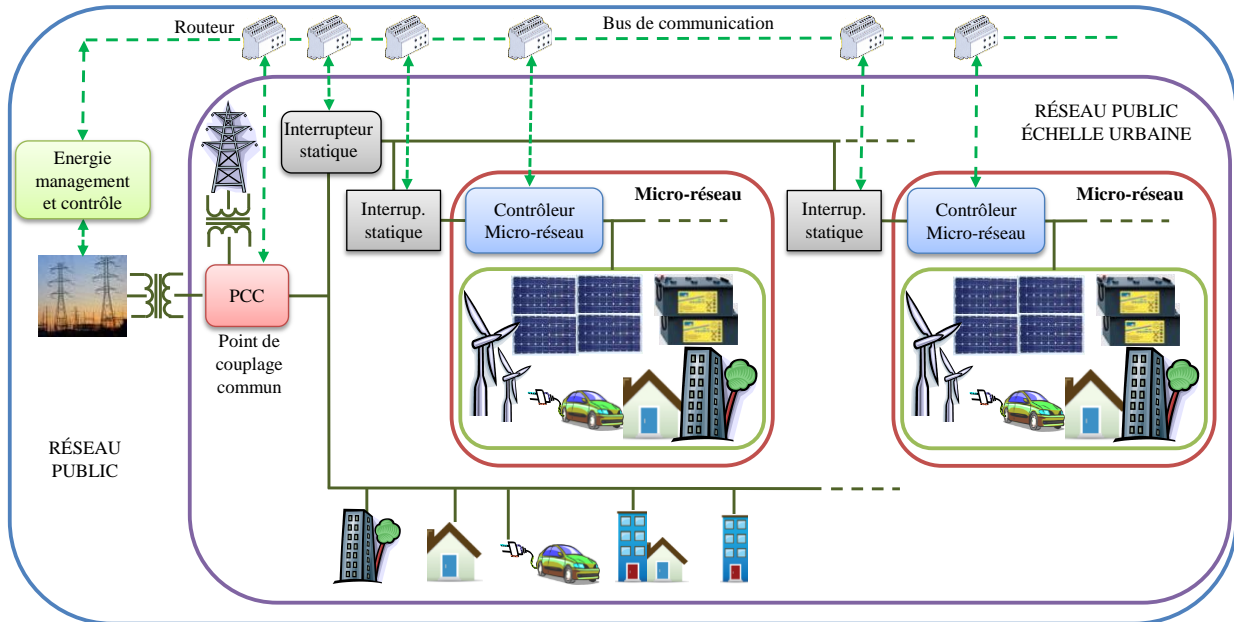


Figure 4. Possible topology of SG

1.2. Microgrid: the backbone of smart grid

1.2.1. Definition

Nowadays, several definitions of MG exist in the literature and are proposed in various journals and reports. A significant one is given by the U.S Department of Energy’s Microgrid Initiative:

Definition.1 “A Microgrid is a group of interconnected loads and distributed energy resources within clearly defined electrical boundaries that acts as a single controllable entity with respect to the grid. A Microgrid can connect and disconnect from the grid to enable it to operate in both grid-connected or island mode” [30].

Another definition that includes components, architecture, and operation of MGs is given by [31]–[33]:

Definition 2: “Microgrids comprise low voltage distribution systems with distributed energy sources, such as micro-turbines, fuel cells, PVs, etc., together with storage devices, i.e., flywheels, energy capacitors and batteries, and controllable loads, that behave as a coordinated entity”. “Such systems can be operated in a non autonomous way, if interconnected to the grid, or in an autonomous way if

disconnected from the main grid. The operation of micro-sources in the network can provide distinct benefits to overall system performance, if managed and coordinated efficiently”.

From these two definitions, the authors concluded that the MG could be considered as a critical component of modern power systems. It includes interconnection and distribution properties that provide the ability to increase and facilitate the integration of RESs and eco-friendly power generation technologies to contribute to zero emissions. Furthermore, MG may be capable of working in two operating modes: grid-connected and islanded mode. During grid-connected mode, a power balance between consumption and generation must be established, and users are then more flexible to supply or consume a specified amount of energy and cost-effectively dispatch their resources. Whereas, independence from the main grid allows providing energy for isolated places. In this context, DPGs and storage devices have to meet the load demand using effective control strategies. The general topology of a MG is shown in Figure 5 [34].

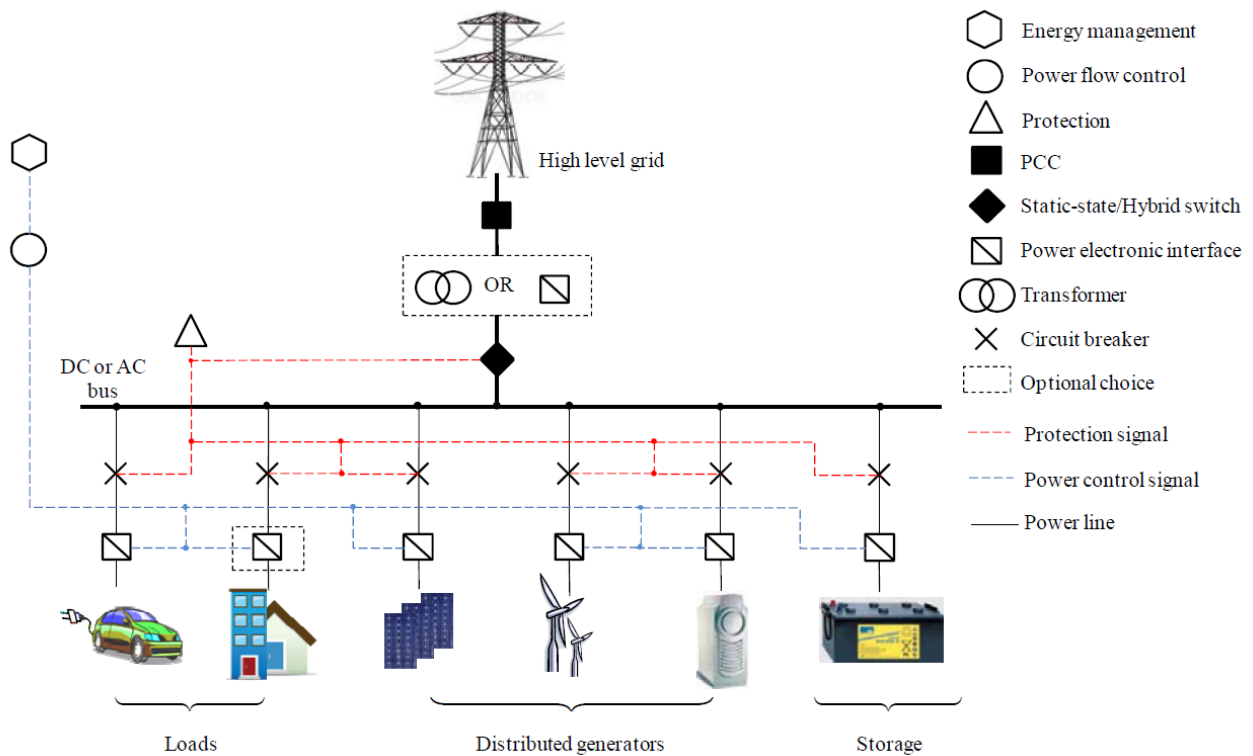


Figure 5. MG general scheme

1.2.2. MG Architecture: AC, DC, and Hybrid

The architecture of MGs is another fundamental parameter to be discussed. MGs can be classified into three types based on how components are connected and the nature of the output voltage fed to the load. There are (i) alternating current (AC)-MG, (ii) DC MG and (iii) hybrid-MG [33].

i) AC-MG

AC-MGs attracted the interest of many researchers and have been tested and discussed in several industrial applications thanks to their easy integration into the existing distribution networks. In an AC-MG, all components are interconnected through AC power lines. Thus, AC loads would be directly supplied [35]. However, DPGs such as PV, storage devices, and most modern loads are inherently DC which requires more integrated inverters [36], (e.g., DC/AC PE devices) as shown in Figure 6. Researchers at the Consortium for Electric Reliability Technology Solutions (CERTS) had proposed and tested this type of MG [37]. They presented a new approach for integrating DERs and studied a radial three-feeder grid with loads, RES-based DERs, and combined heat and power [33]. Their conclusions highlight the robustness, reliability, and economic benefits behind operating this MG in islanded mode.

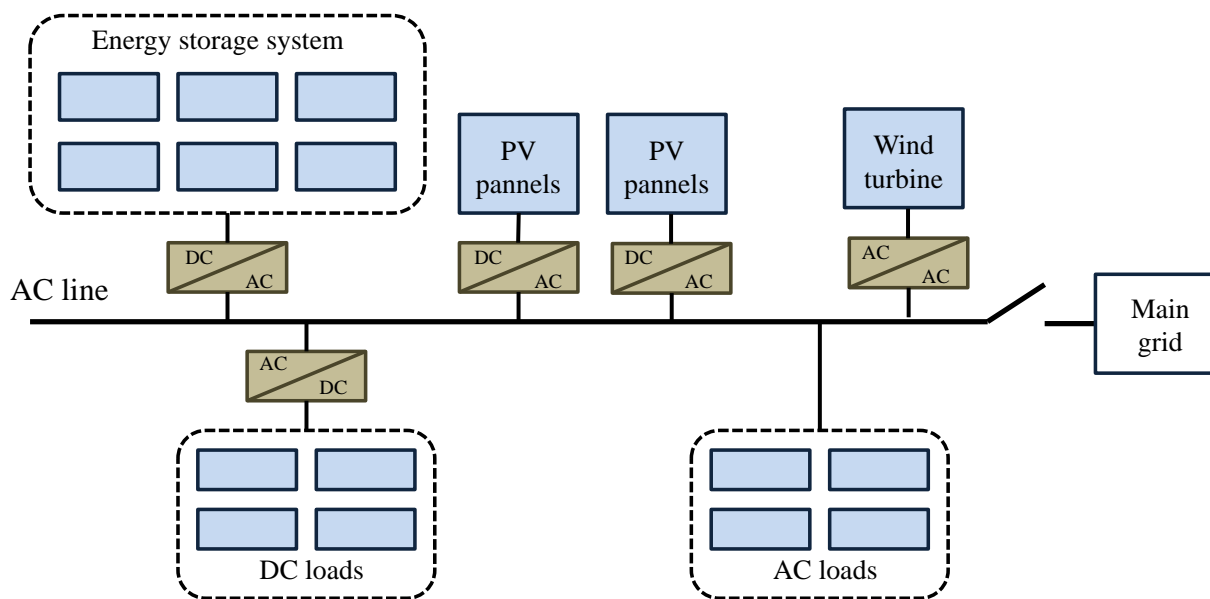


Figure 6. Structure of an AC-MG with a single power line

ii) DC MG

Different authors have tackled the importance of developing DC MGs thanks to their simplicity and wide range of applicability. Indeed, DC MGs generally contain one or more feeders in DC, and the components are interconnected through DC power lines (see Figure 7). They present natural interfaces to many types of RES and energy storage systems (ESSs) (e.g., fewer conversion stages), decreasing then energy losses. Furthermore, they do not allow the circulation of reactive power, which increases the overall efficiency of the configuration [36]. Moreover, this type of configuration does not need synchronization of DERs, which guarantee simple power strategies [33]. For a DC MG operating at low voltage, the CESI RECERCA DER Test Facility is an example of a project involving a well-structured DC MG. It functions at 400V and is connected to the medium voltage (24kV) to perform several tests about energy management strategies for DC configuration and to monitor the power quality of the entire system.[38]. More information about DC MG will be provided in the next section.

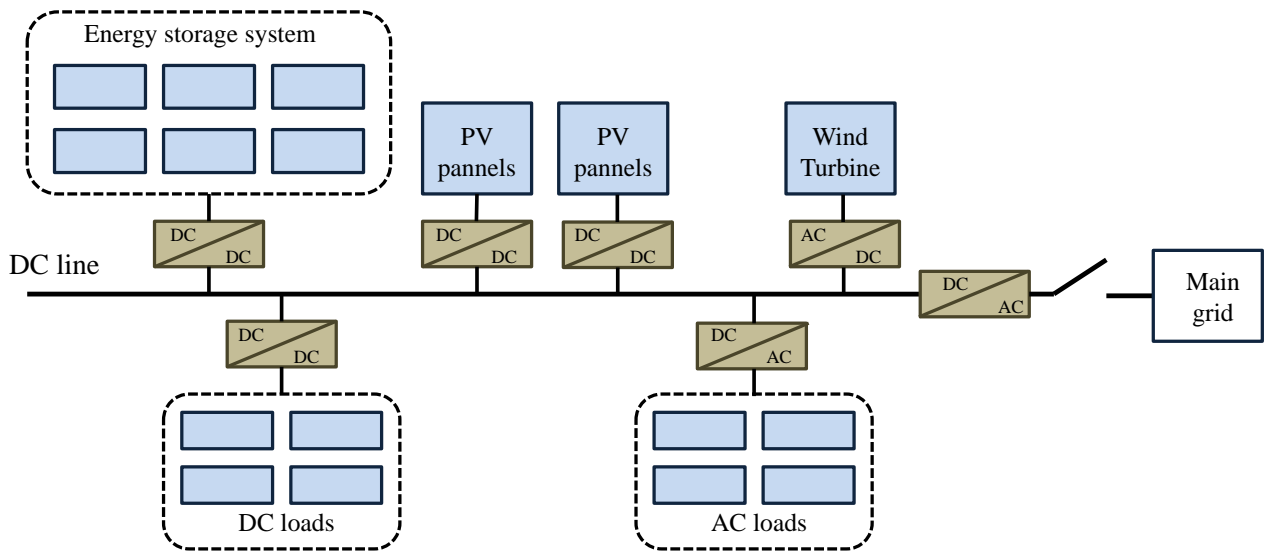


Figure 7. Structure of a DC MG with the single power line

iii) Hybrid-MG

Hybrid-MG is a configuration that combines the characteristics and advantages of both AC and DC MGs presented above. This complex architecture facilitates the insertion of AC and DC-based technologies and allows increasing efficiency by reducing multistage conversions. Furthermore, with the increase of the number of DC components, the hybrid-MG becomes feasible and more economical than AC-MG [38]. However, this configuration still requires complex management strategies to guarantee a simultaneous control of AC and DC components. Figure 8 depicts an example of a hybrid-MG with different AC and DC devices.

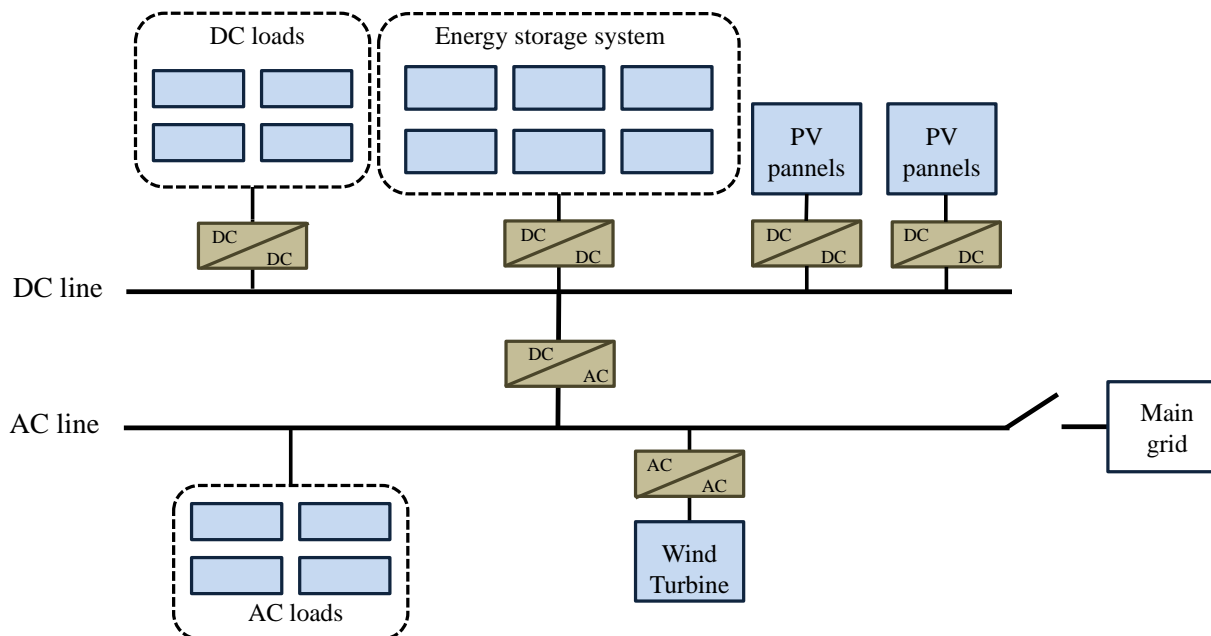


Figure 8. Structure of an AC/DC hybrid MG

1.3. DC MG

1.3.1. Introduction

The current electrical infrastructure was structured and organized based on historical precedence. Consumers find themselves forced to purchase electricity in the form of AC without taking into account the current power needs. However, the shift toward RESs and the remarkable development of the semiconductor industry had changed the power market towards systems based on DC.

The struggle over an adequate electrical power infrastructure dates back to the 19th century that witnessed a fierce battle about introducing electricity to consumers and how it would be generated, transmitted, and utilized. This famous battle was commonly referred to as the “War of Currents” and that was waged between Westinghouse supporting AC, on one side and Edison supporting DC, on the opposite side. This debate was ended by the predominant AC distribution network, which secures the rights to distribute power due to reasons that made much sense at that time. Some of these reasons were: AC power could travel long distances with fewer losses, the invention of transformers which cover a large area of the distribution system, production by large plants was cheaper than many distributed ones, the invention of poly-phase AC machines, etc. However, DC systems were not disappeared completely, and technological advancement was not taken into account by AC systems’ defenders. Indeed, systems were being forced to apt to AC power despite the notable decrease in efficiency. Moreover, all electronics rely on transistor technology depend on DC power to function. Thus, DC voltage regulation becomes a simple task. Furthermore, the increase of loads that could be DC supplied and the penetration of DERs encouraged researchers and industries to revalue DC distribution in today’s power system.

1.3.2. Motivations behind rethinking of DC deployment

Recently, the DC power systems have met standards in a cost-effectively and seamlessly manner thanks to the stunning advent of semiconductors and significant development of PE converters. Also, loads, RESs, and storage devices could be other reasons for reconsideration, and the importance of DC deployment.

1.3.2.1. DC loads

DC power system paradigm paved the way for extensive use of DC loads. Different authors tackled the consummation of electricity in DC form, especially at offices and homes. Various appliances such as laptops, phones, TVs, microwave ovens, etc are DC supplied [39], [40]. In addition, authors of [41] and [42] highlighted the efficiency and low cost of using lighting systems such as LED fixtures and fluorescent in a DC distribution system. Moreover, the use of DC applications in different industrial sectors has attracted the interest of many researchers. As described in [43], an analysis was developed

about the use of DC chopper in the electrochemical industry, while [44] provided a deep study on the use of DC electric arc furnaces in the steel industry.

1.3.2.2. Conversion efficiency

Other authors opted for the analysis of the efficiency of DC systems. For example, nearly 30% of all AC power generated passes through PEs before it is utilized [45]. Another study about wasteful conversions from AC to DC was conducted in [46] and concluded that the among of energy losses varies with types of devices, but generally it lies within the range of 10-25%. Similarly, researchers on in [47] mentioned that the power conversion efficiency decreases by about 8% while using AC-bus instead of the DC one. They concluded that thanks to DC-bus, around 25% of the devices' cost could be saved by removing some components like a rectifier.

1.3.2.3. RES

To respect environmental requirements and economic conditions and overcome power shortages, the proliferation of RESs became a trend all over the world. Some of the RESs, such as PV and fuel cells (FCs), are natively DC, whereas WT still needs a conversion step. However, authors in [48], [49] showed that in the case of offshore WTs with the aims to be integrated to AC grid through DC-bus, converting the distribution system to DC can eliminate a stage of conversion and then decrease losses and increase the efficiency.

1.3.2.4. Storage

DC power systems can also integrate storage elements easier and more efficiently than conventional AC-based systems. Most storage devices such as batteries and ultra-capacitors are already DC. In this context, an advantage of DC MG is its inherited ability to facilitate static storage integration [49]. Besides, [50] and [51] focused on mechanical energy storage a flywheel that is generally coupled to a PMSG integrated into the distribution system through DC-bus.

1.3.2.5. Data centers

Datacenter energy consumption also presents another focus of the discussion. In reality, high reliability is the main feature that must be maintained in data centers power [52]. One way for that is to operate the facility on a DC distribution. Although AC remains the preferred method for distributing power in data centers, almost all of the critical payloads in the data center are DC loads. Thereby, DC distribution offers the ability to eliminate intermediate DC/AC and AC/DC power stages and improve then the efficiency of the entire system [53], [54].

1.3.2.6. Plug-in electric vehicles

As RESs, electric vehicles (EV) also increase in popularity and interact with existing grids. Researchers examine the issues related to the coordination of charging a large number of EVs and work then on developing the concept of smart charging parks. They concluded that these charging parks should operate as DC MG with a common DC-bus at which the EV batteries and any distributed energy units could be integrated [55]–[57].

1.3.3. Topology/design of DC MG

Numerous topologies of DC MG were proposed in the literature and can be classified into three categories: i.e., single-bus topology, multi-bus topology, and reconfigurable topology, respectively. The decision to choose a specific topology of DC MG depends essentially on the application, voltage level, and reliability level [58].

1.3.3.1. Single-bus topology

Single-bus topology (Figure 9) is the most used topology for designing a DC MG. It is based on the singular bus to which storage devices could be directly connected (Figure 9.a) or connected through a dedicated converter interface (Figure 9.b) [59]. For the first configuration, the number of series battery depends mainly on the voltage of the loads. Yet, the state of charge (SOC) and the battery's current make the voltage of the common bus uncontrollable [60]. Thus, the application of such a system is limited to dense and singular bus systems such as telecoms applications that historically operate at 48V [60] or industrial applications that use electrochemical battery stack [60]. For the second configuration and to regulate the low-voltage of the DC-bus, the battery devices are connected to the common bus through adequate converters. Consequently, the system becomes more reliable and easy to be controlled [61]–[66]. However, some technical problems appeared and need to be solved. For example, consumers had only one DC-bus to be powered from and the equivalent capacitance of DC-bus that becomes smaller than the one in case of the battery directly connected to the common bus [59]. To overcome these problems, some alternative configurations, such as the bipolar single regulated bus, are suggested in the literature [60].

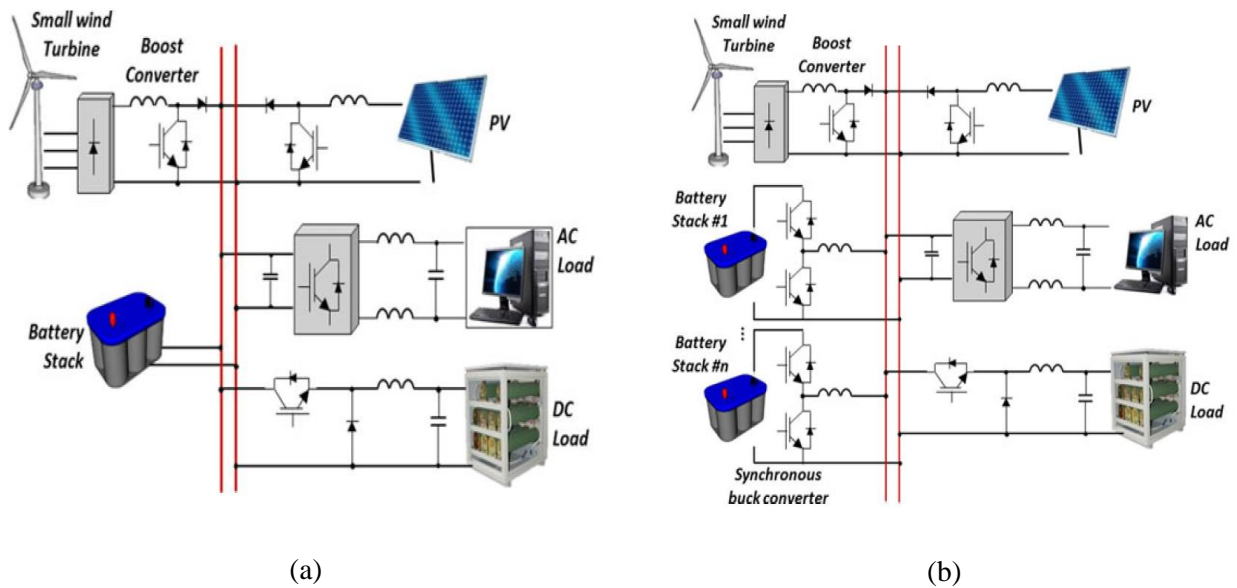


Figure 9. Single-bus DC MG with storage: a) directly connected to the common DC-bus; b) connected to the common DC-bus through the dedicated converter

1.3.3.2. Multi-bus topology

Multi-bus MG, as reported in Figure 10 [59], is extended from the single-bus topology, and it has gained a considerable potential in the industry since recent electronic appliances are operated on distinctive voltage levels [67]. This configuration provides enhanced energy efficiency, reliability, and power density by reducing possibly the global cost [68]. Nonetheless, this complex architecture is difficult to be controlled and evaluate its stability. The line resistances and power flow affect the power management and power-sharing between sources and also deviate the load bus voltage from its nominal value [68]. Control schemes like the FL control method proposed in [69] or the modified control method proposed in [68] are required to overcome these issues and improve the system bus voltage regulation under different operating conditions. Furthermore, stability is another issue of this type of topology. Indeed, the integration of many converters and numerous DC-buses cause different interactions between these components, which lead to the instability of the overall system. Different authors proposed stabilization methods and models such as the multiple droop control sources and loads [68] or even multiple DC voltage control units and constant power loop [68] to maintain stability.

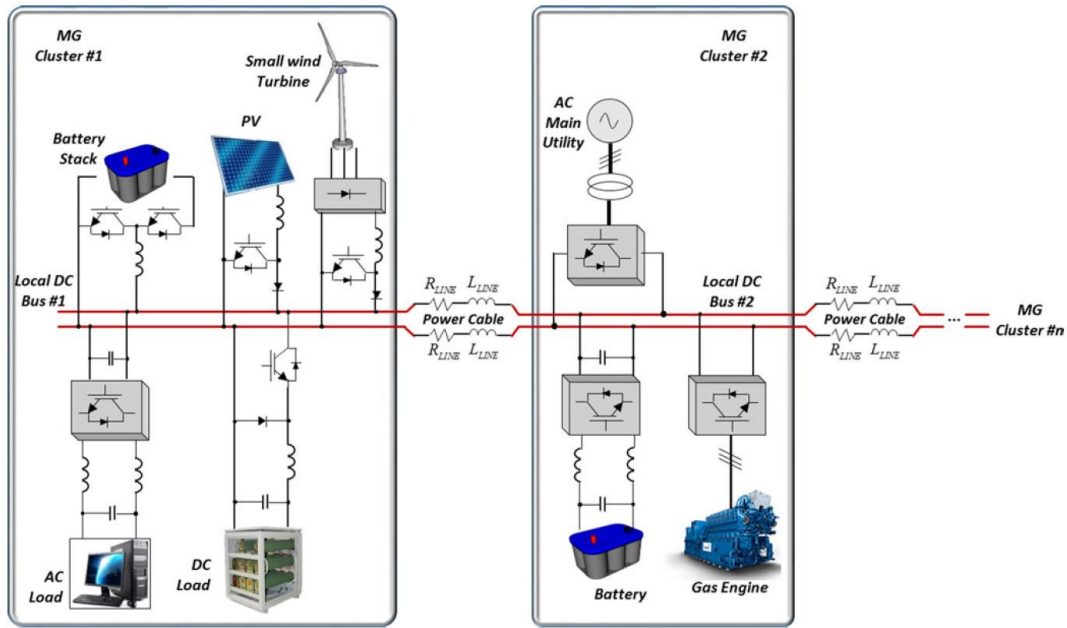


Figure 10. Multi-bus DC MG with all components connected through dedicated converter interfaces

1.3.3.3. Reconfigurable topology

To increase the flexibility of the system, reconfigurable topologies for a DC MG were suggested in different studies. Figure 11.a [70], for example presents a DC ring bus topology that is constituted by overlapping nodes and links controlled by intelligent electronic devices (IEDs). The main goal of this proposed configuration is to ensure high reliability and redundant operation. The faults in this DC MG are detected and isolated without de-energizing the entire system. Also, in this topology, loads could be fed bi-directionally. Then, in case of fault that is firstly located and isolated by the IEDs, loads continue to be supplied by other sources that work in a standard alternative path. Similarly, the authors of [71] employed another DC MG topology based on zonal configuration (Figure 11.b) [71]. This type of DC MG contains multiple DC distributions units connected to each other in series for forming a zonal architecture. All portions or zones have two redundant DC buses and load power could be obtained by one of them. Indeed, when a fault is detected, static switches are used to isolate the system at the end of these buses, and power converters feed the system by de-energizing the defective bus. Then the system could receive power from a voltage source converter (VSC) from the same zone or the converter of another zone via the connection to adjacent buses.

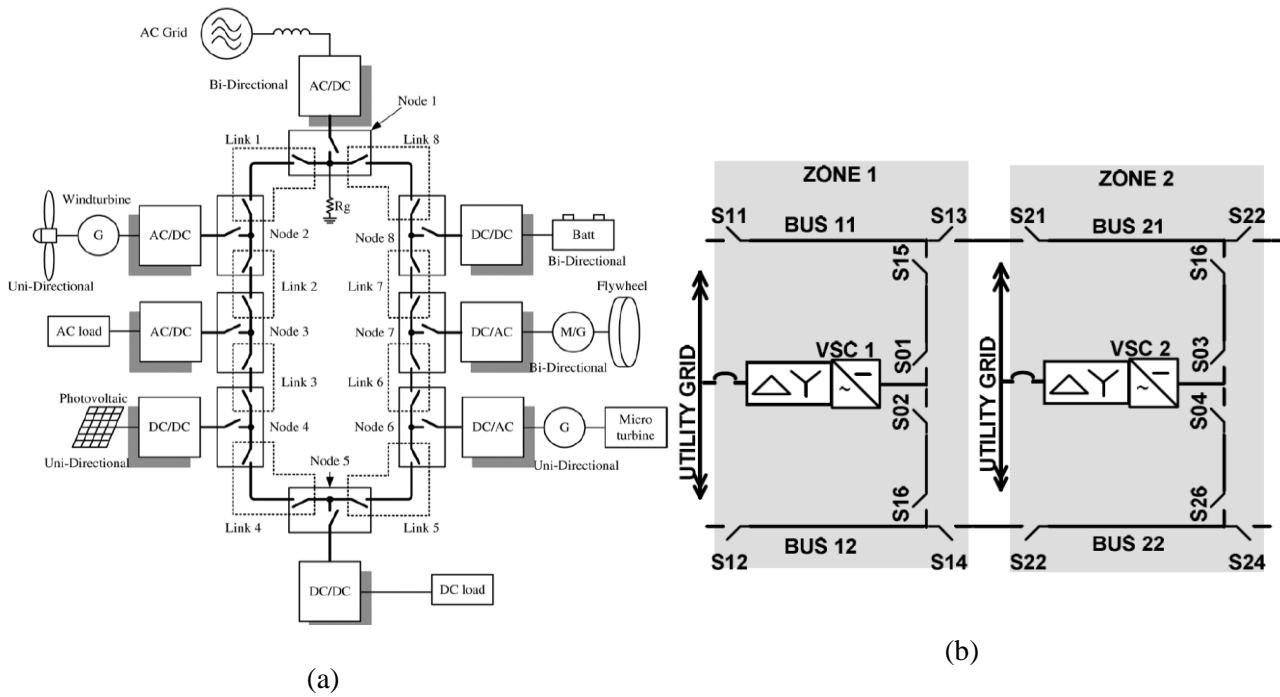


Figure 11. Reconfigurable DC MG based on a) ring bus [70], b) zonal configuration

1.3.4. Control

To ensure the regular operation of DC MG, control topologies (Figure 12 [72]), had to be established. They play a crucial role in the rising stability and efficiency of the overall system. In fact, the PE converters, regarded as voltage sources, are considered as interfaces to control the grid by limiting and regulating the value of DC-bus voltage and also using a strategy for current-sharing. They also facilitate the integration and interconnection of various components that constitute a DC MG. Thus MG control ensures a reliable and economical operation of the MG. Some desirable features and targets of the control system are [73]:

- regulation of voltage and current sharing and ensure their oscillations damping.
- easy transition from grid-connected mode into stand-alone mode.
- accommodation of sudden active power imbalances, (excess or shortage), by keeping frequency and voltage deviations within acceptable ranges.
- Reduction of the operating costs and increase of profit by adopting an appropriate and economic dispatch of DPG units, etc.

Three main and distinctive approaches can be identified: centralized, decentralized, and distributed. Firstly, a fully centralized control relies on the operation of a central controller and determines the control actions of all the units at a single point. Secondly, in the decentralized approach, each unit is controlled by its local controller and interacts within the MG. Finally, the distributed approach combines the advantages of both centralized and decentralized controllers [74].

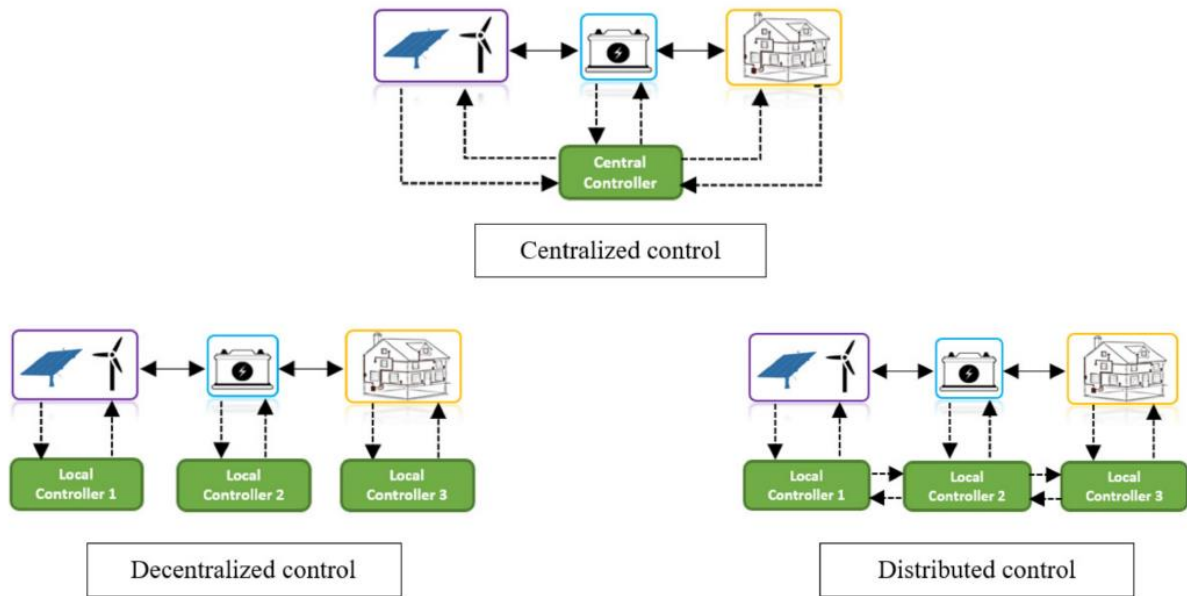


Figure 12. DC MG control strategies

1.3.4.1. Centralized Control

Centralized control architecture consists of gathering the relevant information at a single point, at the same time; which requires the implementation of online optimization routines. The data are firstly collected from units of a DC MG. Then, these collected data are processed and controlled via a communication medium. The central controller can use an online calculation of the optimal or information from an offline calculation to pre-build and continuously updated data. Generally, centralized approaches that are characterized by strong controllability of the entire system are more suitable for remote areas and isolated MGs with fixed infrastructures and critical demand-supply balances [73].

A master-slave control is a well-known centralized control technique to achieve parallel operation of multiple sources. This mechanism uses one converter as master and commands slave units in order to regulate the DC bus. For example, a VSC can act as a master, and the remaining converters act as slaves. These latter feed the system by respecting the instructions provided by the master controller. Also, the master converter has the role in maintaining the grid voltage within an acceptable band while the slaves help it to achieve this goal [74].

1.3.4.2. Decentralized control

The decentralized control is a topology that intends to solve problems related to the energy management of the MG while providing a high level of autonomy for various DPG units. These latter are easily incorporated into a MG without making changes to the controller parameters. Indeed, each DPG unit is controlled by an autonomous local controller via independent local variables without using a communication medium. However, this controller suffers from difficulties in handling MG' operations which require high levels of coordination. Despite these problems, this control strategy is the most

reliable. Its autonomy is achieved using a hierarchical structure with three levels: the first one is the Distribution Network Operator that is responsible for the interaction of the MG with the distribution network and also with neighboring MGs. The second level is the MG Central Controller which is responsible for the coordination between different DPGs units and loads within the MG and the interaction of the overall system with the main grid. The third level contains the Local Controllers that communicate with the Central Controller in order to exchange information, requests, and services [75].

Some of the widely decentralized control schemes are conventional droop control (CDC) and adaptive droop control (ADC).

The role of CDC is minimizing or eliminating the circulatory current between converters without the use of a communication link. Furthermore, this controller participates in the regulation of the MG voltage. Authors of [75] proposed a decentralized droop method for a low-voltage DC MG with the purpose of achieving perfect power-sharing by taking into account the effects of line resistances and also the SOC of the batteries. However, there are tradeoffs between current sharing among distributed resources and DC bus voltage stability while using a CDC for a DC MG. Then, to satisfy both power-sharing and DC bus voltage stability criteria, an ADC strategy for a DC MG is proposed in [76]. This method is based on closed-loop reference adaptive control and uses a time-varying model, a projection algorithm, and a normalization technique. Experimental results showed the capability of this proposed strategy to regulate the current sharing and stabilize the DC bus voltage at 400V.

1.3.4.3. Distributed control

Distributed control is a strategy that was proposed in many types of research studies to combine the advantages of both centralized as well as decentralized control systems. It forms a network of several controllers equipped in each PE source and helps to maintain steady grid voltage by ensuring proper load sharing [74]. This type of control facilitates the increase and integration of DERs contrary to the centralized control scheme. It also ensures the system's function in case of a communication link break.

1.3.5. Stability

One of the main concerns of power system engineers is the stability. Ensuring the dynamic stability of a MG in all its operating states is the crucial key for obtaining safe and reliable performance. In this context, many works have been done to establish the stability criteria of an AC MG while the stability of DC power systems is still under investigation. In a DC MG, instability is mainly caused by impedance mismatch specifications, including the impedance mismatch between damped filters on the source side and regulated power converters on the load side and the impedance ratio calculated by dividing the input impedance representing the load and the output impedance representing the source. Furthermore, many stabilization techniques and strategies were proposed in the literature to overcome these instability issues and smooth the input filter's resonant peak. For this, two types of stabilization are possible: passive

stabilization based on adding damping elements (resistors and inductors) and active stabilization, including small-signal stabilization and large-signal stabilization. More details are provided in Appendix n°1.

It is crucial to note that the broad deployment of DC systems negatively impacts the stability of the utility grid. Indeed, various studies have been done to overcome such an impact. In [77], it was found that DGs in a DC MG are characterized by a low or total absence of inertia dynamics which lead to instability. To handle this problem, researchers of [78] suggested a solution based on the use of synchronverter. The idea behind the use of this type of inverter is to emulate virtual rotor characteristics, particularly synchronous generators [79]. This solution was improved by making necessary changes that such an inverter would be capable of synchronizing with the utility grid without the need of PLL [80].

1.3.6. Protection

DC MG is becoming nowadays a well-known and typical distribution network thanks to its remarkable performances, advantages, and facilities. At present, researchers on DC MGs primarily focus on the topology structure, control methods, and energy control techniques. However, good functioning of this electrical structure requires an appropriate protection system design. The protection of DC systems has presented many challenges, such as the autonomous location of a fault in a MG, improved DC devices, and the absence of standards, guidelines, and enough experiences. Thus, additional efforts and attention should be deployed to have a clear understanding of fault analysis, detection, and isolation and thereby resolve protection issues.

In DC systems, the fault current quickly increases with large peaks because of the low fault impedance. Thus, fault detection and isolation should occur. Appendix n°2 first depicts the DC fault analysis and characteristics. Secondly, the type of grounding that could affect safety, the ability to identify the fault, and the survivability of DC MG under faulty conditions are also investigated. Finally, the current protection systems, including DC fault detection methods, protective devices, and faults location approaches, have been presented in detail.

According to the contents mentioned above and the distinct characteristics of DC MGs during fault scenarios, a proper protection system must be considered. The system design process should take into consideration some systematic aspects, such as grid topology, grounding, and interactions between interconnected converters during fault events. Moreover, the concept of protection is becoming extended thanks to the huge development of DC MGs, which contain many electronic devices. Thus, a coordinated strategy of control and protection could be more effective than considering only traditional protection schemes.

1.3.7. DC MG developed in AVENUES

DC MG developed in AVENUES is an urban MG dedicated to tertiary building. This development allows the establishment of a MG control combined with energy management and SG interaction. The main goal is to improve the penetration of the DERs with respect to end-user demand and local optimization of power flow. As presented in section I.1, the MG is the key element of the SG. In fact, the urban DC MG studied in AVENUES is connected to the SG through a controller that plays the role of an interface between the utility grid and loads. Its main goal is to ensure optimal power management (Figure 13) [81], by creating a power management interface using data exchanged between the MG and the utility grid. Firstly, this controller had to collect different information, such as the availability and dynamic pricing of the public grid. Secondly, the control system sends information about the SG injection intention and power supply forecast. Thirdly, the terminal users' requirements must be satisfied under all physical and technical limits. Finally, all the systems should function with the lowest energy costs.

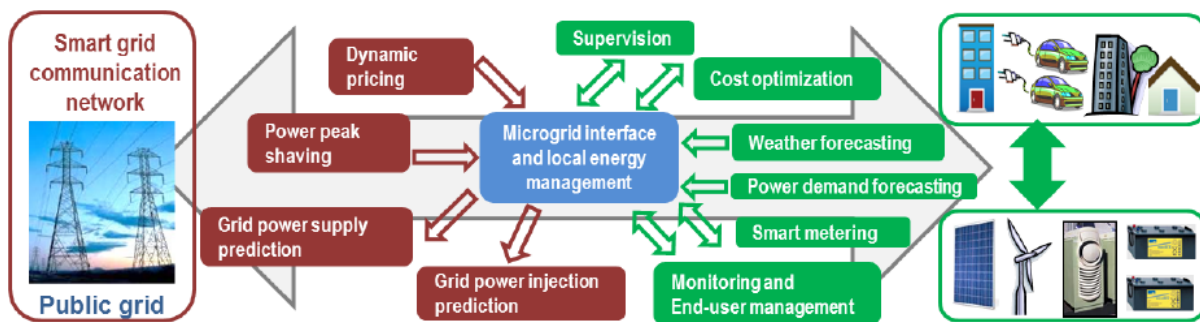


Figure 13. Power management interface principle

The research works in the AVENUES laboratory were started by studying, developing, and analyzing a multisource system belonging to a DC MG with consideration of some aspects for power quality [6]. This DC MG is constituted by PV sources, security system elements, electrochemical storage, and the public grid. This latter was used, in case of a storage shortage, to supply power to the load and to trade back excess energy. The technical feasibility of the multisource system was experimentally validated using the technological platform of AVENUES laboratory called PLER (Production Locale d'Electricité Renouvelable [82]). For energy management, the priority was given to storage that is characterized by its SOC. For this DC MG, hierarchical supervision integrating communication with the SG is feasible and was conducted by our team research in [34].

The control system called “supervision” handles together power balancing, energetic cost optimization, metadata using, and information exchanges from both end-users and the SG. It is proposed in

Figure 14 [7] and classified into four layers with an operating scale time that varies from days to less than seconds.

- **The human-machine interface** is the first layer that contains end-user requirements and some specific criteria such as the critical building loads or load shedding limits.
- **The prediction layer** is the second layer that takes into account two types of information:
 - The end-user options are provided from the first layer.
 - Forecast data for several variables for calculating two power variables: the predictions of RE production and the energy demand.
- **The energy management layer** is the third layer responsible for calculating the energy costs optimization by using the previously calculated power predictions and the operating constraints such as dynamic pricing, grid power limits, peak consumption, storage capacity, etc. The optimization is solved using mixed-integer linear programming under CPLEX [83]. The results obtained by this solver are the evolution of the optimal power of each source that guarantees the minimal total cost for the considered time duration. To transfer these data as an input for the next layer (first output of this layer), it is necessary to translate the power flow into a single interface parameter showing the power balancing control. The second output of this layer concerns information about the injection and supply predictions that should be transmitted to the SG.
- **The operational layer** receives the predictive control parameter from the previous layer, the grid power limits from the SG, and some components limits (storage limits, power states, etc.) from the MG. The algorithm developed in this layer controls the power balancing of the MG system. It provides real-time references of the system powers and the eventual shedding coefficient of loads or renewable sources.

The optimization difficulty is due to the mismatch between the predictions and the real-time operating conditions and the limitation due to the constraints imposed by the utility grid.

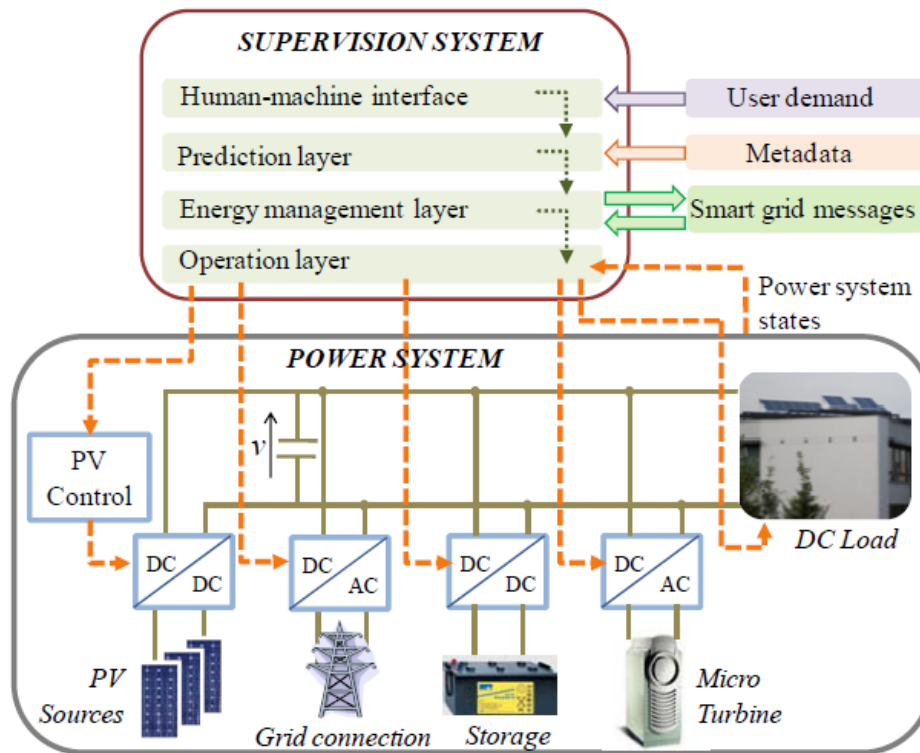


Figure 14. DC MG system overview

The supervision has been validated by experimental tests. Unless there were some uncertainties, the feasibility of implementing optimization in real-time operation was validated. The suggested supervision showed its ability to manage the power flow efficiently while maintaining power balancing. However, the effectiveness of the optimization depends mainly on the accuracy of the prediction. This was carried out in [84] and was based on updating the optimization in real-time. The main objective was to manage the energy power flow while ensuring voltage stability. Other goals concern reducing the energy cost to the end-users and the negative impact on the main grid.

To improve global efficiency and reduce energy cost, other aspects have also been studied by other members of the AVENUES team. The study in [85] investigates the power losses generated by the static power converters in the urban DC MG. The multi-source MG consists of several sources, especially RESs that bring variable power losses and the converter efficiency that is often treated as a constant, but experimental tests showed its variation. Thus, an energy model was developed and applied in real-time to DC/DC and DC/AC converters used in the MG. The proposed energy management strategies were able to shed the powers in the MG in a flexible way. Furthermore, these strategies accelerated the convergence speed of control through the knowledge of power losses of each converter.

The aforementioned research of AVENUES laboratory focused either on the grid-connected or the off-grid mode. Nevertheless, the grid failure in the on-grid mode and the low power supply reliability in the off-grid mode still consist of serious problems that must be solved. The study in [86] proposed a full DC MG combining the advantages of the grid-connected and off-grid modes. It consists of RESs, storage, public grid, and backup sources applied to reduce the load shedding. The suggested supervisory system

consists of real-time power management to ensure power balance. This power is managed using the energy cost or component's tariff, while the load demand optimization is responsible for managing the appliances by the MG and the end-users. The suggested supervisory also considers the dynamic efficiency of the converter to raise the power quality impacted by the instability of the DC bus voltage.

The MG research project of AVENUES laboratory considers not only the PV sources as a RES but also a SSWT that has to be integrated into the described DC MG. The small-scale wind generator is seen as a complementary RES compared with PV source. However, the energy potential and dynamic characteristics of the wind generator are very different from PV generators.

The study of [87] suggests an appropriate approach to minimize the integration cost of a wind generator into DC urban MG. In this case, a SSWT based on a PMSG was studied. As the mechanical sensor for such a structure is expensive, many WECSs were suggested to choose an active structure associated with a sensorless PMSG. The idea is to replace the costly mechanical sensor with a speed/position estimator. Four methods were proposed: rotor flux estimation with a phase-locked loop, sliding mode observer, Luenberger observer of reduced order, and extended Kalman filter (EKF). The latest one was selected as the more appropriate technique that allows sensorless drive control in a wide speed range and estimates the rotation speed with a rapid response. An adaptive EKF was also proposed to overcome the problems related to the tuning parameters of the traditional EKF. This technique tends to decrease the total cost of the studied WECS. In the same context, [88] presents different MPPT for a SSWT, to answer the demand for flexible energy production. Experimental results showed that the lookup table can handle all requirements of MPPT mode, but in more flexible power demand operating mode, a combination of P&O and FL could present the best performance. This was achieved in the actual work characterized by using for the first time a real SSWT placed in a wind tunnel in plateforme PLER. Different control strategies were tested and validated experimentally (see Chapitre II). The second contribution concerns the integration of the SSWT into the studied DC MG. Simulation results are provided in Chapitre III.

1.4. Place of the wind power generation in the DC MG

1.4.1. Historical development of wind turbine

Wind energy is a clean, free, and one of the most abundant renewable energy resources on the earth. It has been targeted mainly with the development of electric power. It is predicted that human beings have been using wind energy to propel boats as early as 5000 BC [89].

1.4.1.1. Vertical axis windmills

King Hammurabi, as early as 1,700 B.C, had to use power provided from wind to irrigate the plains of Mesopotamia [90]. The energy of the wind was also used through windmills to grind cereal grains, such as wheat or corn [89]. Some of these oldest windmills used by early human civilizations are shown

in Figure 15 [90]. It is noticeable that most of the world's primitive windmills had a vertical axis of rotation. Their main advantage is that they were independent of the wind direction. The simplicity of design and construction is displayed in Figure 15(a)-(c) [90]. The braided mats or sails were attached to the central axis that, thanks to the wind; caused drag forces for driving the rotor. Later on, other versions of vertical axis mills were developed in Europe. The windmill with flapping sails, (Figure 15.d), was developed in France. Its millstone is attached directly to the vertical drive shaft without a gear that should redirect the rotational movement. An advanced windmill (Figure 15.e) was created by the Italian Fausto Veranzio. It can be regarded that this windmill was designed to drag-driven rotors with a low tip speed ratio. However, it was equipped with a gearing mechanism that allows millstones to run at a much higher speed [90].

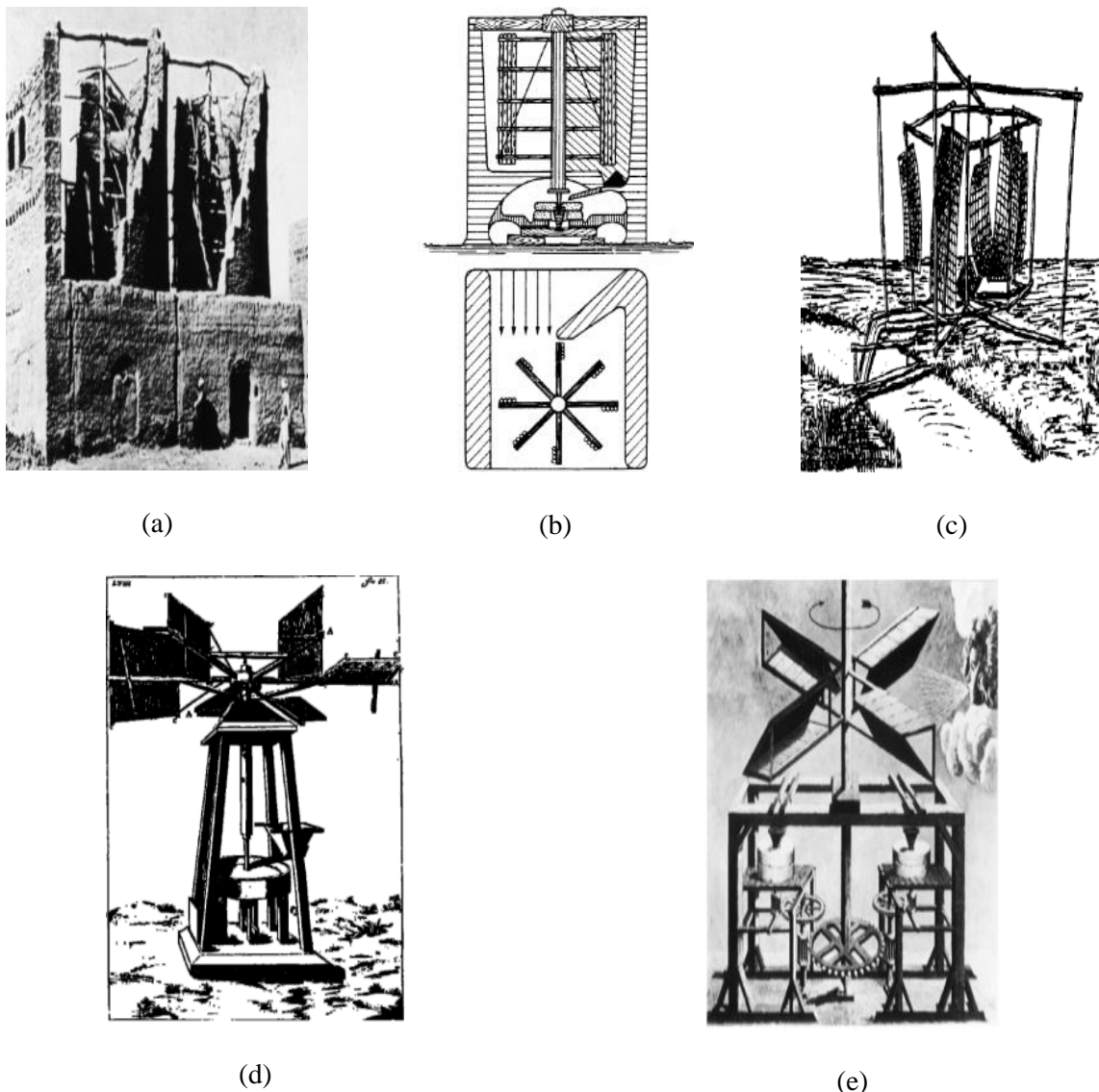
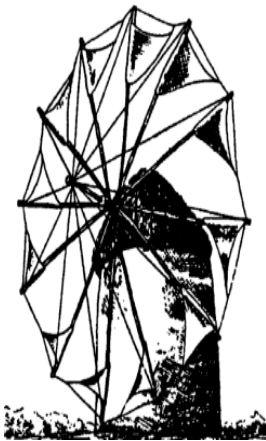


Figure 15. Some of the world's oldest vertical axis windmills; (a) Ruins of a vertical axis windmill in Afghanistan, approx. 700 AD (picture taken in 1977); (b) Persian windmill; (c) Chinese windmill with flapping sails, approx. 1000 AD; (d) Vertical axis windmills with flapping sails, France 1719 AD; (e) Vertical axis windmills with bodies driven by drag forces, Italy, approx. 1600 AD; All pictures are adapted from [90]

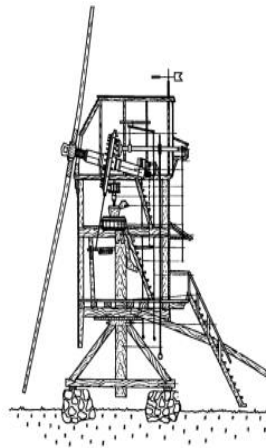
1.4.1.2. Horizontal axis windmills

Albeit much later, the horizontal axis windmills were developed rapidly in the Occident and widely used by the Greeks [91]. Historically, horizontal axis windmills have been found in literature since the 12th century. Indeed, this type of windmills was mentioned in the statutes of the French city of Arles (Provence) and its picture was found in an English prayer book [90]. However, in-depth studies on the use of this type of device were not revealed until the beginning of the 20th century [90].

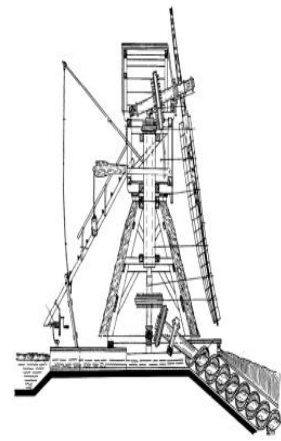
Figure 16.a shows one of the most popular tower mills that existed in southern Europe. It is an early Mediterranean horizontal axis wind turbine (HAWT) equipped with sails and dated back to the 13th century [90]. Moreover, there are some other types of horizontal axis windmills that exist in different parts of the world. The post windmill (Figure 16.b), for example, was exclusively used for grinding grain. Later on, the Wipmolen (Figure 16.c) appeared and was the result of modifying the post windmill to use the wind energy to drive the pumps. Regarding, the Dutch smock mill shown in Figure 16.d, it came into use in the 16th century. It was applied in Europe for grinding grain while it was used for the drainage of the polders in Holland. Figure 16.e showed a special version of the Dutch smock mill called a sketch of a gallery windmill. Due to greater exploitation of wind energy, the use of this type of windmill had known standardization in the Netherlands in the 18th and 19th centuries [90].



(a)



(b)



(c)

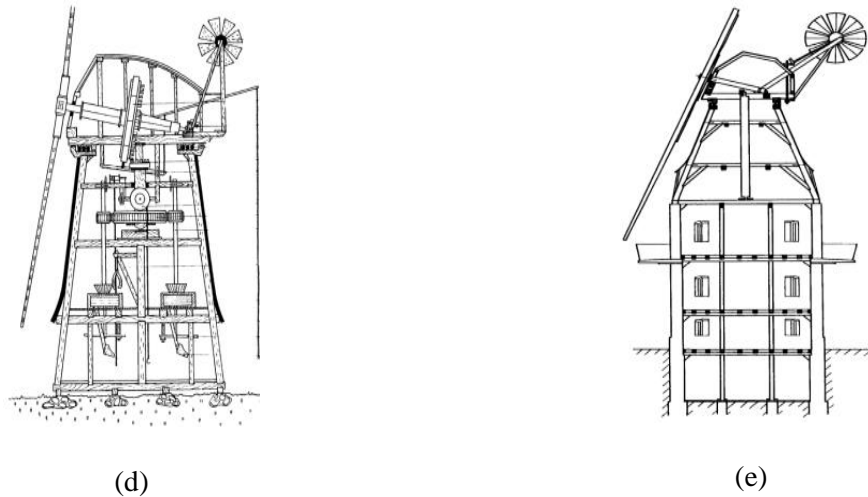
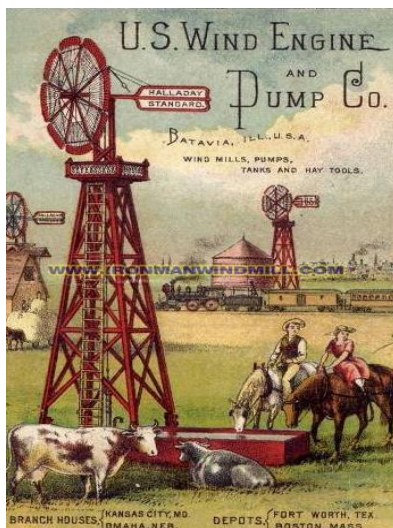


Figure 16. Some of the world's oldest horizontal axis windmills; a) Mediterranean tower mill with sails b) Section of a post mill; c) Section of a wipmolen d) Section of a Dutch smock mill e) Sketch of a gallery windmill [90]

Nevertheless, the American windmill was the most popular HAWT achieving success in the world. It was invented in 1854 by Daniel Halladay and is mainly used to lift drinking water from wells in North America. In addition to that, it was used to assure some tasks such as grinding grain, chopping hay, sawing wood, and providing water supply for the steam locomotives railways [90]. A windmill developed by Halladay's company, the U.S Wind Engine & Pump Co, is shown in Figure 17.a. It has led to improving the quality of life by providing drinking water without pumping it with physical labor [92]. Figure 17.b represents one of such wind farms utilizing the American windpumps for water pumping [93].



(a)



(b)

Figure 17. Western windmills: a) an American windmill developed by U.S. Wind Engine & Pumping Co [4]; b) The Mid-America Windmill Museum, in Kendallville, Indiana [93]

I.4.2. Current status of wind power generation

In recent years, the world has known the fast-growing wind energy development. This innovative electricity generation has reached high levels of installed capacity. This growing trend is evidenced in Figure 18 [94], which shows the evolution of wind power capacity per year, whose total amount reached 743GW in 2020, a growth of 14% compared to 2019.

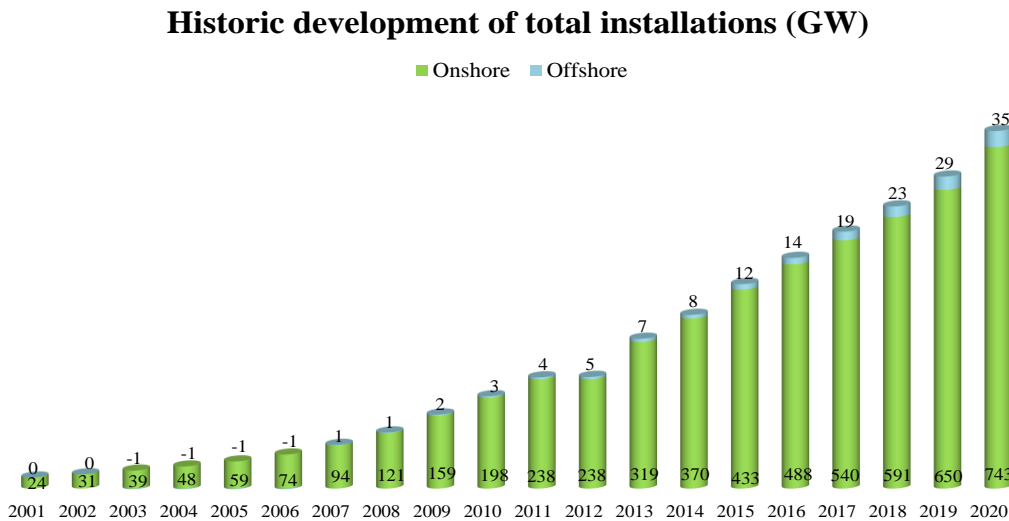


Figure 18. Evolution of wind power capacity

In this context and according to the Global Wind Energy Council (GWEC), 2020 saw global new wind power installation surpass 90GW, a 53% growth compared to 2019 (Figure 19.a). This outstanding increase in 2020 was driven primarily by explosive growth in the world’s two largest wind power markets, China and the United States. China alone holds 56% of the new global worldwide wind power capacity (see Figure 19).

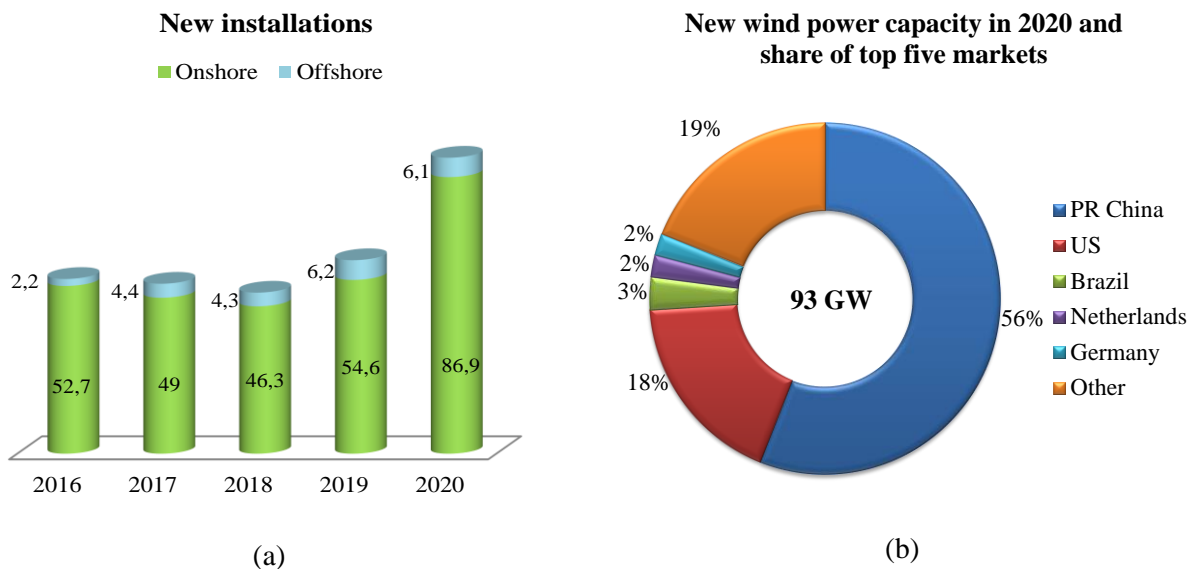


Figure 19. New wind power installations growth: a) per year; b) per region

Moreover, according to WindEurope (Figure 20.a), Europe installed 14.7GW of new wind capacity in 2020. This was 6% less than in 2019 and 19% less than what was expected pre-COVID. 80% of the new wind installations were Onshore with 11.8GW. This was 22% lower than the pre-COVID forecast. However, Offshore wind installations were 2.9GW, in line with what was forecasted before the pandemic. Consequently, Europe now has 220GW of wind capacity. The Netherlands installed the most wind capacity in 2020, most of it Offshore wind. Norway built the most Onshore wind, with Spain and France not far behind. Germany’s new installations were their lowest since 2010 (see Figure 20.b).

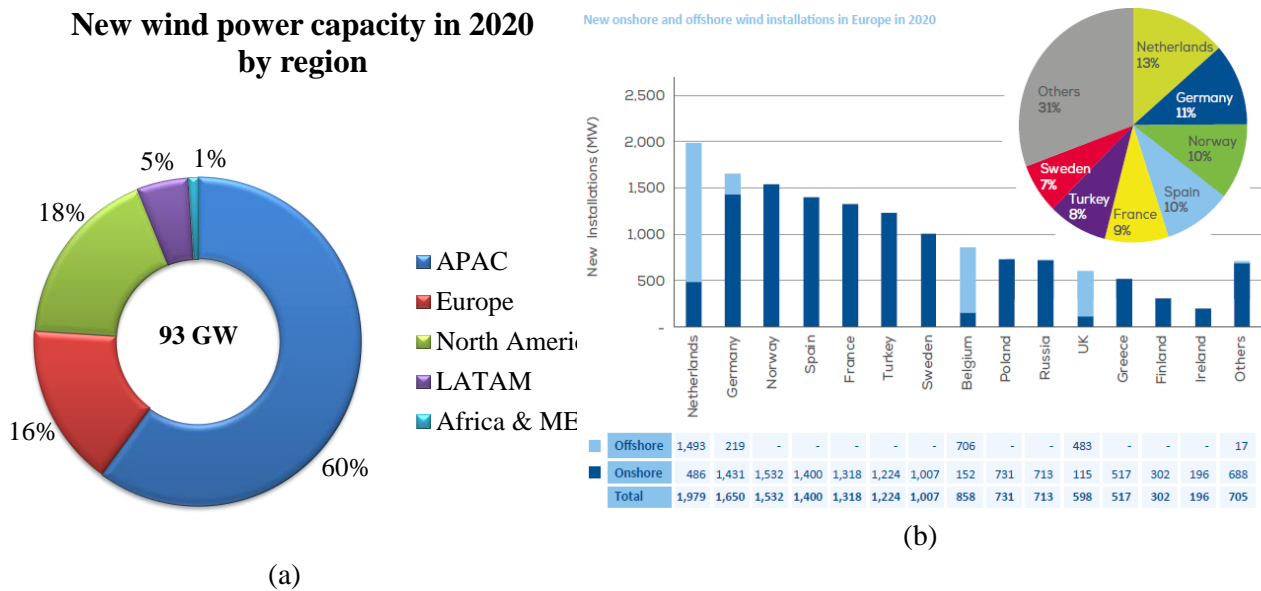


Figure 20. New Onshore and Offshore wind installations in 2020: a) in the world, b) in Europe

Today, wind energy represents one of the leading means of energy generation and plays a key role in the road to net zero. It meets 16% of the EU’s electricity demand, up from 9% in 2015. It overtook coal-based energy generation and then became the second largest form of installed power capacity. In France, for example, wind and solar alone overtook fossils for the first time, marking the next green milestone, which is already met by Denmark and Sweden. Thus, Renewables, in 2020, has overtaken fossil fuels for the first time in the EU (see Figure 21) [95].

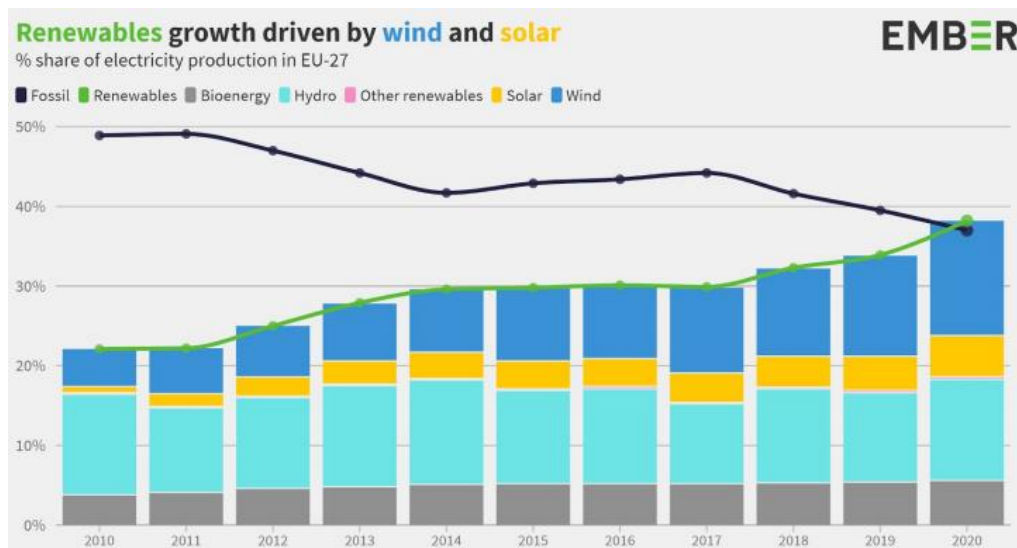


Figure 21. Share of electricity in Eu-27

1.4.3. Classification of wind turbines

1.4.3.1. Vertical axis vs. horizontal axis wind turbines

There are essentially two orientations of WTs: HAWTs and vertical axis wind turbines (VAWT). Each kind of orientation has its advantage and drawbacks.

As the name indicates, the rotor of VAWTs rotates perpendicular to the ground, and they use drag forces to rotate their blades. As mentioned in section I.4.1, the early WTs were VAWT thanks to their simplicity during the construction. Indeed, VAWTs did not require any mechanism to be oriented, and they could accept wind from any direction at any time. Nowadays, they are three famous design of VAWTs. Figure 22(a)-(c) shows Savonius, straight-blade Darrieus VAWT, and curved-blade Darrieus rotors, respectively [96]. This type of WT could be manufactured at a lower cost since the blades are generally straight, without any taper on the long axis. Also, the maintenance costs could be reduced due to the blades that rotate around a vertical axis while the drive train is located near the ground. However, although VAWTs can easily accept wind from any direction, they generally have poor efficiency (less than 25%) and suffer from larger fatigue damage on their blades at the rotor because of the cyclic aerodynamic stresses [97].

In contrast, the rotor of HAWTs is positioned in a horizontal direction i.e. parallel to the ground and they use lift forces to rotate their blades. At present, HAWTs are the most popular among all windmill designs and currently dominate the wind power market. They consist of a rotor, a gearbox, a generator and, a yaw system. Figure 23 shows a HAWT commercialized by SIEMENS (model: SWT-2.3-82 VS) [98]. HAWTs are generally large, which makes the solidity low. Solidity is defined as the ratio of blade area to swept blade area. Then, if the solidity is low, the cost per kilowatt is also decreased. Furthermore, this type of WT is often mounted on top of a larger tower, which minimizes the initial investment cost

[97]. Moreover, HAWTs generally have much higher efficiency than VAWTs. The maximum power coefficient reported for a modern HAWT is up to 45% to 50% whereas the one for an efficient VAWT lies below 40% [99]. Yet, HAWTs, contrary to VAWTs, can't catch the wind from all directions and still need mechanical equipment to turn the rotor to face the wind and they are very sensitive to changes in design, blade profile, and surface roughness.

Consequently, as explained previously, HAWTs dominate the market, but some benefits to the VAWTs rotor may be worth considering for some future applications. Thus, the limitations of each design should be taken into account with a clear understanding of some possible options to overcome those limitations.

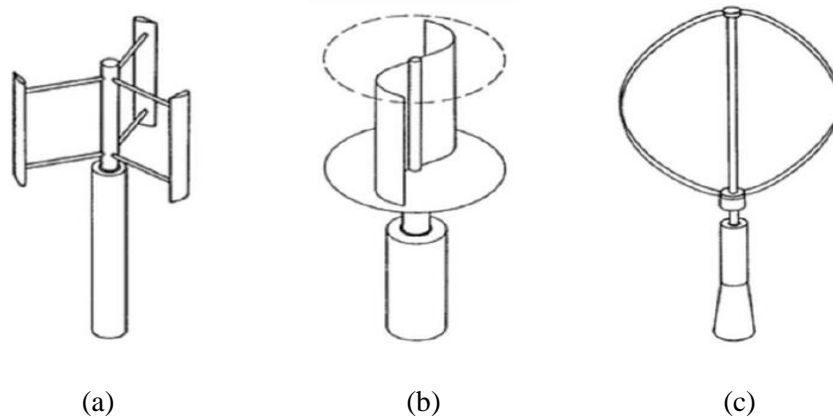


Figure 22. Vertical Axis WTs: a) Straight-blade Darrieus, b) Savonius rotor, and c) Curved-blade Darrieus rotor



Figure 23. Siemens HAWT (model: SWT-2.3-82 VS)

1.4.3.2. Fix speed vs. variable speed wind turbine

There are two types of rotors possible for a WT: fixed speed rotors and variable speed rotors. They are determined depending on the requirements of the electrical generator and the gearbox [100]. The entire design of a fixed speed rotor gains efficiency only when wind speeds are optimal. Even though fixed speed rotors constitute the majority of the WTs currently in use, variable speed rotors are still gaining market share. Indeed, the rotor speed for this field of WT is allowed to vary to capture more

energy from the wind and more flexibility while choosing the generator. Another advantage of such a rotor is the ability to reduce loading on the WT rotor and drive train components. Besides, variable-speed rotors incorporate PE converters so that they became able to adjust the resulting electric power to the voltage and frequency required for transmission on the grid. Thanks to this flexibility in using PE converters, a wind generator could be chosen for a low-speed operation which helps to eliminate the gearbox. However, before designing such a WT, it is imperative to take into account the possible effect of an electrical noise that can be generated due to the PEs in the variable speed turbine [97].

1.4.4. Wind turbine constitution and model

1.4.4.1. Wind turbine configuration

A typical configuration of a HAWT, as shown in Figure 24, is mainly composed of three blades, a rotor, a nacelle, and a tower.

The nacelle is positioned on the top of a wind tower, housing the most turbine components inside and also equipped with an anemometer, for wind measurement, outside. The blades are mounted on the rotor hub, which is connected via the main shaft to the gearbox. The rotor of the wind generator is connected to the output shaft of the gearbox. Thus, the rotational speed of the rotor hub is gradually increasing until the desired rotational speed of the generator rotor is reached.

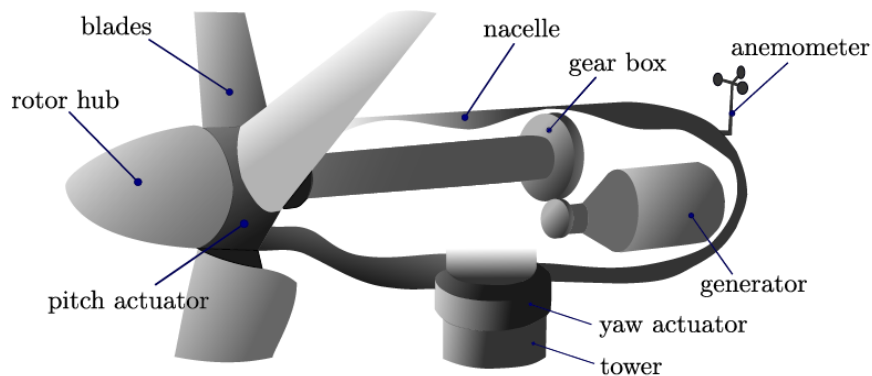


Figure 24. Typical configuration of a HAWT

The mechanism of a WT describes the transformation of wind power into electric power. This transformation can be divided into three types of conversion: each of which describes:

- The conversion from wind power to mechanical power.
- The transmission of the mechanical power to be converted into electrical one.
- The conversion of the mechanical power into electrical one.

Firstly, the conversion of wind power to mechanical power reflects the aerodynamic effect of the system. Indeed, the wind's kinetic energy captured by the turbine is transformed into the mechanical energy of the turbine rotor, which rotates at an angular speed. Secondly, the transmission of the

mechanical power is related to the WT mechanical system. This later is essentially composed of the rotor and can be based on vertical axis technologies or horizontal ones. Finally, the conversion from mechanical power into electrical one is obtained using an electric generator. While there is still existing WT based on fixed-speed technology, the most employed technology recently concerned the variable-speed one, where the rotor can assume angular speed values within a given range. More details about types of WT and generators are given in I.4.5.1.

I.4.4.2. Wind turbine mathematical model

The WT mechanical system is a nonlinear dynamic system, mainly due to the aerodynamic relation describing the conversion from wind to mechanical energy of the turbine rotor that is turning at an angular speed ω_r and subject to a torque T_r . In order to model the power extracted from the wind, it has been shown that considering the wind speed v component in the only longitudinal (axial) direction guarantees sufficient model reliability. Moreover, from the wind field impact on the turbine, the extracted power can be described by the function:

$$P_{aero} = \omega_r T_r = \frac{1}{2} \rho \pi C_p(\lambda, \beta) R^2 v^3 \quad \{1.1\}$$

Where ρ is the air density, R is the radius of the rotor blades, β is the pitch angle, λ is the tip speed ratio.

I.4.4.2.1. Power coefficient

Power coefficient C_p is defined as the amount of mechanical power produced by a WT against the total available wind power. Sometimes, it's also called the coefficient of performance and mathematically, it is calculated using the following expression [101]:

$$C_p = \frac{P_{mech}}{\frac{1}{2} \rho \pi R^2 v^3} \quad \{1.2\}$$

Where P_{mech} is the mechanical power generated by the WT, ρ is the density of the wind, R is the tip radius by the rotor, and v is the free wind speed. The denominator term $(\frac{1}{2} \rho \pi R^2 v^3)$ of the equation{1.2} denotes the total available wind power passing across the swept area of the WT rotor. It also describes the ratio between the extracted and the available wind power as a function of the tip speed ratio and pitch angle. This is typically provided in the turbine specifications as a lookup table. In literature, the expression of C_p is often approximated by an analytic function to be treated for control synthesis purposes. It can be differently described by using a polynomial, a sinusoidal, or even an exponential function.

Typically, C_p can be described firstly by a polynomial function of the form [102]:

$$C_p(\lambda, \beta) \approx \sum_{i=0}^{n_{c,1}} \sum_{j=0}^{n_{c,2}} a_{ij} \lambda^i \beta^j \quad \{1.3\}$$

Where $n_{c,1}$ and $n_{c,2}$ are the polynomial degree and a_{ij} its coefficients. Moreover, it can be simply expressed as [103]:

$$C_p(\lambda) \approx \sum_{i=0}^{n_{c,1}} a_i \lambda^i \quad \{1.4\}$$

Where n_c is the polynomial degree. This regression can be expressed by polynomials of different degrees.

The second form of C_p can be expressed by the following exponential forms as [104], [105]:

$$C_p(\lambda, \beta) = 0,5176 \left(\frac{116}{\lambda_i} - 0,4\beta - 5 \right) e^{-\frac{21}{\lambda_i}} \quad \{1.5\}$$

$$\lambda_i = \frac{1}{\frac{1}{\lambda - 0,08\beta} - \frac{0,035}{\beta^3 + 1}}$$

$$C_p(\lambda, \beta) = 0,5176 \left(\frac{116}{\lambda_i} - 0,4\beta - 5 \right) e^{-\frac{21}{\lambda_i}} + 0,0068\lambda \quad \{1.6\}$$

$$\lambda_i = \frac{1}{\frac{1}{\lambda - 0,08\beta} - \frac{0,035}{\beta^3 + 1}}$$

$$C_p(\lambda, \beta) = 0,53 \left(\frac{151}{\lambda_i} - 0,58\beta - 0,002\beta^{2,14} - 13,2 \right) e^{-\frac{18,4}{\lambda_i}} \quad \{1.7\}$$

$$\lambda_i = \frac{1}{\frac{1}{\lambda - 0,002\beta} - \frac{0,003}{\beta^3 + 1}}$$

The third form of C_p can be expressed by the following sinusoidal forms as [106]:

$$C_p(\lambda, \beta) = (0,44 - 0,0167\beta) \sin\left(\frac{\pi(\lambda - 2)}{13 - 0,3\beta}\right) - 0,00184(\lambda - 2)\beta \quad \{1.8\}$$

It can be concluded that the evolution of C_p is specific data for each WT, and only the experimental tests carried out on each WT can give an approximation of the expression of this coefficient.

1.4.4.2.2. Betz' law

The German physicist BETZ defined through his theorem an upper limit of the power coefficient $C_{p,max}$ [107]. It calculates the maximum mechanical power produced by a WT in an open wind flow.

According to Betz's law, any turbine cannot extract more than 16/27 (59.3%) of the kinetic energy in wind. The factor 16/27 (0.593) is the maximum value of the power coefficient of a WT and it is most commonly known as Betz's coefficient or Betz's limit.

$$C_p = \frac{16}{27} \approx 0.5926 \quad \{1.9\}$$

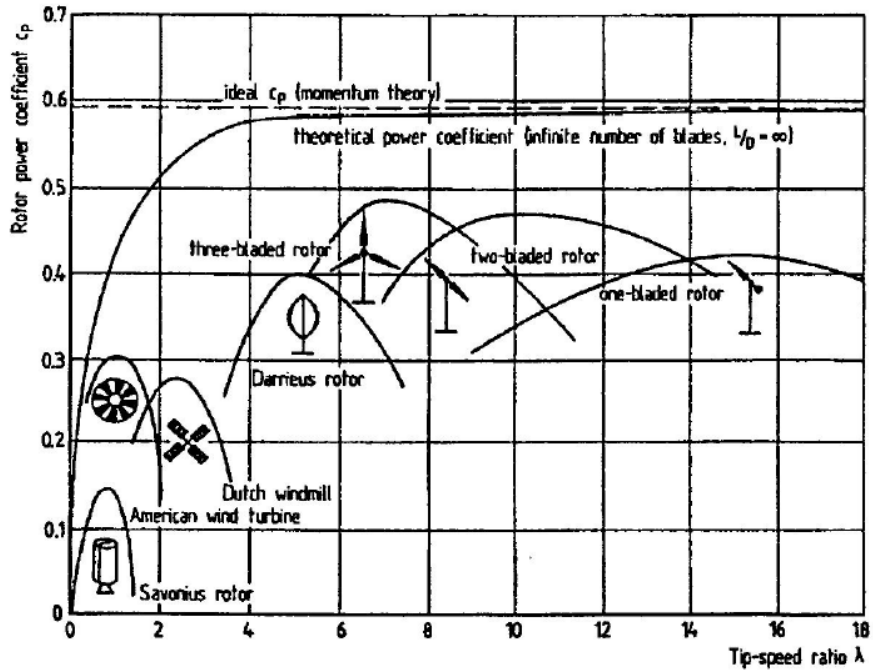


Figure 25. Aerodynamic power coefficient as a function of the normalized rotational speed λ

1.4.4.2.3. Tip speed ratio

The tip speed ratio λ is the most commonly and conveniently used scaling parameter, which integrates the principle aerodynamic effect of the wind speed, rotor size, and rotor's angular speed with the power coefficient of the WT rotor. It evaluates the tangential speed of the turbine's blade concerning the free wind speed and is given as [101]:

$$\lambda = \frac{\omega_r R}{v} \quad \{1.10\}$$

Where ω_r is the angular speed of the WT rotor, v is free wind speed and R is the radius of the rotor blades.

1.4.5. Need and application of the small-scale wind turbine

In the wind energy literature, the definition of "small" and "large" scale WTs remains vague. Indeed, the definition of a WT as "small" comes from its ability to produce enough electrical power to meet the electrical needs of an individual household [108]. However, the consumption of electricity by a household is not constant and changes depending on the place and time. For example, in the United States of America, one household requires around 10kW to meet their full electrical consumption, while in Europe, an average family needs around 4kW. However, a Chinese family needs only 1kW [108]. Thus, there is no standard to generalize the range for the rated power related to each type of WT. In this context, small WTs could be referred to small and medium power turbines (100 watts to 20 kilowatts) mounted on 10 to 35 meter masts, connected to the grid, or stand-alone in remote locations [107]. The European standard EN 61400-2 [109] limits the category of small WTs to machines with a swept area of less than 200 m² and an operating voltage of less than 1000 V AC or 1500 V DC. Consequently, and in order to bring consistency to the analysis, the classification of WTs could be based on the size of the HAWT rotors as follow [110]:

- Micro-scale WT: rotor diameter 10cm,
- SSWT: 10cm < rotor diameter ≤ 100cm,
- Mid-scale WT: 1m < rotor diameter ≤ 5m,
- Large-scale WT: rotor diameter > 5m.

Although large-scale WTs are efficient and have a power coefficient of up to 40%-45% [24], they still require high wind speeds (12m/s-14m/s) to operate. In addition, this category of WT should be installed in wind farms, far from cities and urban areas to ensure human safety and avoid noise emission. In contrast, SSWTs can operate at low wind speed, be placed in urban areas (no known safety hazards), and generate supportable and minimal noise.

1.4.5.1. Several types of machines

The most commonly used generators for WTs, namely synchronous and asynchronous machines, are shown in Figure 26, Figure 27, Figure 28, and Figure 29 and will be discussed in this section [111]–[116]. For SSWTs, various types of electrical machines could be used. Although an induction machine may be useful in that case, a PMSG is still the most used thanks to its efficiency, reliability, small size, and light weight [88].

1.4.5.1.1. Asynchronous/induction machine

- *Squirrel-Cage Induction Generator*

Thanks to their robustness, brushless structure, and lower price, induction generators are widely used in the WECS [117] and most WT manufacturers mainly built constant speed WTs with power levels increasing to 1.5MW [111]. This fixed speed system (Figure 26) consists of a three-stage gearbox and a squirrel-cage induction generator directly connected to the utility grid. While all induction generators draw reactive power from the grid, this electrical structure uses the capacitor bank for compensating for the reactive power and a current limiter to decrease the inrush current during the startup of the induction generator [118]–[120].

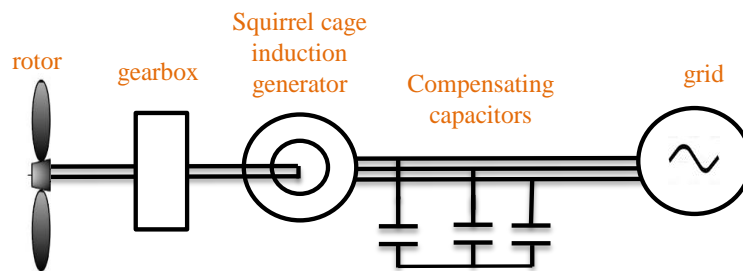


Figure 26. Fixed-speed WECS, directly connected with the grid

- *Doubly Fed Induction Generator*

Recently, many WT manufactures change from fixed to variable speed systems with a doubly fed induction generator (DFIG). This latter occupies near 50% of the wind energy market, and it is recommended for WTs with power levels above roughly 1.5MW [121]. As shown in Figure 27, the WECS consists of a gearbox, a relatively low-cost standard DFIG, and a partly rated PE converter feeding the rotor winding. DFIG with low-rated power converters (usually 25-30% of the rated power of the system) leads to improve efficiency [122], [123]. Pitch control also helps to limit the output power to rated power at high wind speed (wind speeds above rated).

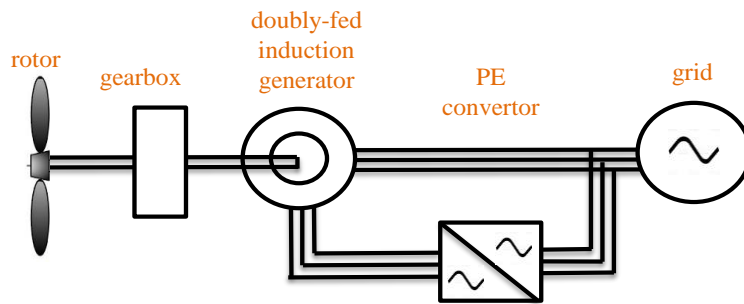


Figure 27. Variable-speed doubly-fed induction generator with partial scale power converters

1.4.5.1.2. Synchronous generator

Generating power at low wind speeds is one of the critical issues of WECS. The salient pole machines are characterized by having a high number of poles which facilitates generating power even for low wind speeds [124]. Recently, the PMSG based on a PE system (Figure 28) is a promising and interesting approach to generate power without the need of the gear-box [125]–[127]. The absence of slip rings in PMSG reduces the necessity of higher technical maintenance and increases then the efficiency of the overall system. Furthermore, PMSG is known for its lower weight and has its own reactive power controlling capability which helps to stabilize it more than other types of generators [128]. As shown in Figure 28 and Figure 29, the synchronous generators can be connected with or without gear.

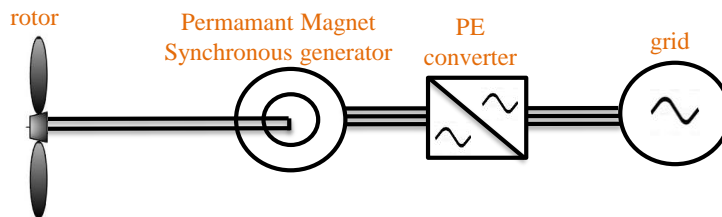


Figure 28. Variable-speed, gearless multi-pole PMSG based WECS

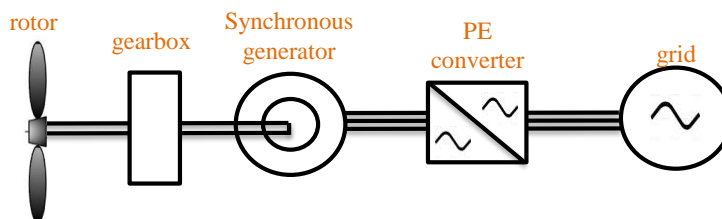


Figure 29. Variable-speed synchronous generator with full-scale power converter

To conclude, several architectures can be used for the SSWT. Yet, a PMSG with a high number of pole pairs seems to be the most convenient for such an application. It can operate at low speed without decreasing efficiency and by avoiding the use of a gearbox. It can also be adapted for variable-frequency operations induced by wind-speed variations.

1.4.5.2. Converters

The WT, as PV source, is operated to increase the energy benefits. This is ensured through extracting the maximum power by using suitable algorithms, i.e. MPPT algorithm. The study through this thesis focuses not only on extracting the maximum power but also the limited power under all operating conditions. As explained in I.4.3.2, the WT could function with fixed or variable speed. Yet, extracting the maximum power is only possible with variable speed WTs. In this context, the PE converter is a key element of the WECS and has the role to convert either the variable voltage/frequency of the generator into a fixed voltage /frequency suitable for the load [88]. In the case of a SSWT, there are two types of structures aiming to convert mechanical energy into electrical one: passive and active structures (see Figure 30).

Passive structure, as shown in Figure 30.a, uses a no controllable three-phase AC-DC converter like a three-phase diode bridge and it is characterized by its robustness and low cost. Nonetheless, active structure, as its name indicates, is based on a controllable three-phase AC-DC converter (see Figure 30.b).

Another active structure is possible by adding a controllable DC-DC converter to a passive structure (Figure 30.c) [87].

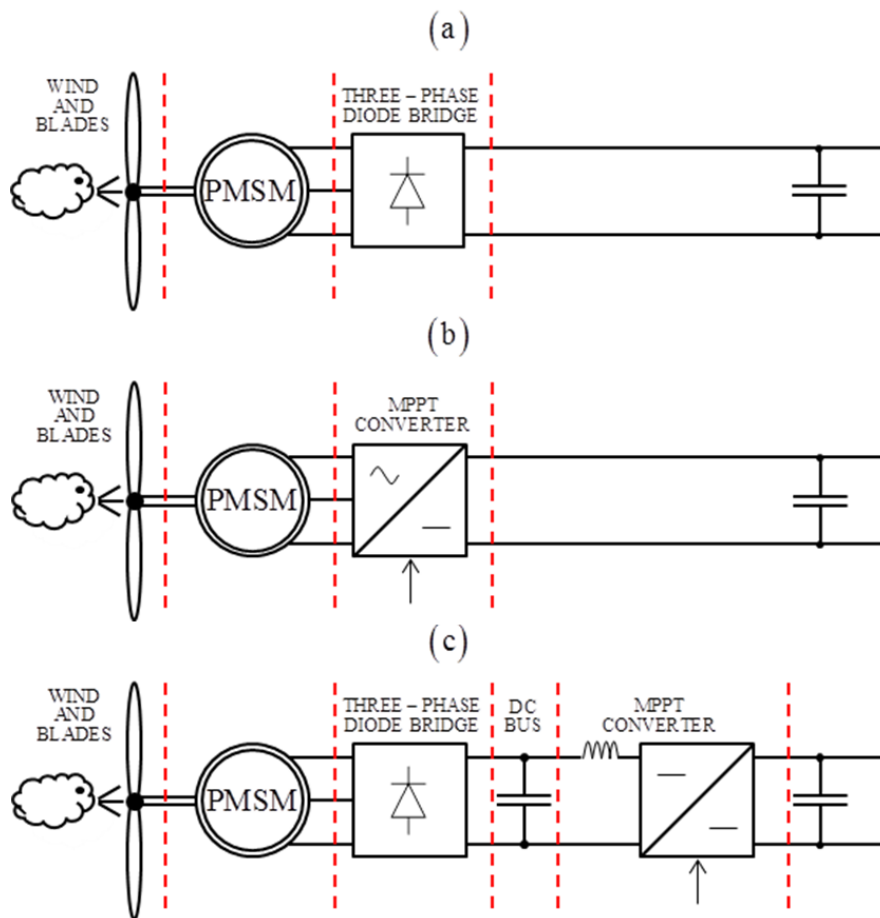


Figure 30. Electrical structure of power conversion

It is necessary to consider different requirements during the design and the choice of a convenient topology of converters. All topologies of static requirements could be applied for medium or high power scales applications. However, it is necessary to take into consideration the global cost while choosing suitable converters for small-scale applications, i.e. SSWTs. In that case, a wholly controlled structure could be too expensive. Indeed, it is reasonable to select a passive structure such as the diode bridge since it reduces the cost and provides acceptable energy performances. Thus, the three-phase diode bridge rectifies the voltage provided from the PMSG, and the output of the rectifier is continuous. However, it is crucial to use additional PE devices to meet the load requirements. The key element of the WECS with variable speed that allows extracting the maximum power produced by the WT is the static converter. Then, using a controlled PWM rectifier as presented in Figure 30.b or a rectifier of three-phase diode bridge associated with a controlled converter as shown in Figure 30.c allows the system operating at variable speed to extract the maximum power provided by the WT.

Since the fully controlled rectifier seems to be an expensive and complex structure to control the output power and it requires a solid background and experience, this research is based on using a passive structure associated with a DC/DC converter as displayed in Figure 30.c. The control of this structure remains simple and robust and guarantees fewer power losses than the controlled one [88] [87].

1.5. Conclusion

Nowadays, pollution has reached record levels since the world still heavily relies on fossil fuels and continues subsidizing them. The recent consideration of environmental and economic factors is forcing researchers and manufacturers to encourage the use of clean energy even if replacing fossil-fuel infrastructure will take time and require consistent support from the states and communities.

Since 2011, renewable energy has grown faster than all other energy forms. Like all other energy sources, renewable energies have their trade-offs. However, they guarantee several benefits over the devastating impacts of fossil fuels, namely lower greenhouse gas emissions, less air and water pollution, and reduction of water and land use.

This chapter is started with a description of the electrical system evolution through the integration of renewable energies in the utility grid. For that, the SG concept was introduced as a solution to favorite the DPG use and answers the requirement of both the utility grid and end-user. The SG can be described as a power grid equipped with communication and information technology that can solve peak consumption, optimal energy, and energy demand problems.

Since this thesis focuses on the control of a SSWT that will be integrated into an urban DC MG. a literature review about DC MGs was firstly detailed in this chapter. It concerns the essential concepts of a DC MG, namely:

- Motivations: DC deployment;

- Topologies: single-bus, multi-bus, and reconfigurable topologies;
- Control: centralized, decentralized, and distributed controls;
- Stability: impedance specifications and stabilization strategies;
- Protection: DC faults analysis and detection, grounding, protective devices, and fault location.

Secondly, the importance of wind power generation was given attention by describing the historical and current evolution of RESs. Moreover, some key concepts about wind technology were given, starting with a description of the turbine types (horizontal and vertical axis) and constitution (blades, rotor, generator, etc.). A particular interest in a SSWT with a horizontal axis dedicated to the urban environment was mentioned. Need and applications of this set of RESs are presented. Furthermore, types of machines useful for this category of a WT were presented and the PMSG was chosen thanks to its multiple benefits and suitability in this study. For performing the control, several architectures were suggested and studied.

The next chapter will present a study concerning the control power strategies using the system composed of the chosen architecture (generator and power conversion structure). The study used for the first time a SSWT located in the experimental platform of AVENUES. The principle of the power control strategies such as LPPT and MPPT will be proposed and detailed. These algorithms are studied and implemented, and experimental results show the efficiency of each method. Other experiments are carried out to reveal the system's flexibility and applicability of the studied power control strategies.

Equation Chapter (Next) Section 1

Chapitre II. Limited power point tracking for the studied small-scale wind turbine-control analyses

II.1. Introduction

The research community is still exploring all possibilities to provide an alternative to traditional energy resources based on fossil fuels in order to reduce environmental issues such as greenhouse gas emissions and global warming [129]. In this context, the use of renewable energy resources has significantly increased in recent decades with more intention to integrate them into the utility grid [8]. For this reason, the SG has been created and developed to manage renewable energy resources in the utility grid. The SG is a new electricity transport and distribution network that allows bidirectional communication between suppliers and consumers in order to adjust the flow of electricity in real-time and enables more efficient management of the electricity grid [8]. The main components of the SG are MGs. Indeed, an MG is based on the idea of providing electrical energy in a decentralized form: it combines loads, storage and multiple energy sources (traditional and renewable) in one unique entity. The MG can operate on-grid and off-grid. Thus, it is suggested to facilitate the realization of the SG, supply isolated areas, ensure power balancing and promote local energy consumption and production [130], [131]. There are three different structures of MGs depending on the common bus, i.e., DC or AC, of its various components: AC MG, DC MG, and hybrid AC/DC MG [132]. While the AC MG has been the subject of remarkable dynamic research for enhancing its performance, several works have presented the attractive uses of the DC MG thanks to its high efficiency to integrate DC native renewable energies.

In this perspective, wind energy is forming part of DC MG's distributed energies, and it fits well into this paradigm of using renewable energy resources for responding to environmental issues. Wind energy is earning more interest thanks to its lower space occupancy, significant power cost reduction, and zero carbon emissions during operation [133]. This is true not only for high-power WTs but also for small ones. According to the market reports of the World Wind Energy Association, the small wind capacity installed worldwide increases annually with a growth rate of 12%. Approximately 270MW of new capacity is forecasted to be installed in 2020 and then 1.9GW of cumulative installed capacity will be achieved by 2020 [134]. SSWTs provide electric energy, supply off-grid consumers like remote villages, and can be used as distributed resources in MG systems [133]. Although the implementation of SSWTs has grown worldwide, the efficiency of wind energy systems is still impacted by many factors. For instance, the empirical extraction capacity of wind power makes the stability between supply and demand for energy very difficult to maintain.

For a small wind energy conversion system (SWECS), several generators could be used to transform wind energy into electrical power. The most used amongst them are AC generators, particularly induction generators and PMSGs. These latter are mostly used thanks to their high efficiency, low cost, and low-priced maintenance [132]–[135]. To apply the power control strategies to the WT, the PMSG is connected to PE converters. There are three types of converters, i.e., diode bridge rectifiers, boost converters, and inverters, that can be classified into two kinds of electrical structure: passive and active [136]. A three-phase diode bridge, as a passive structure, is an uncontrollable structure, robust, and less expensive. An AC/DC converter (inverter) is an active structure fully controlled that may either require rotation speed or torque. The active converter's topology that is based on a three-phase diode rectifier with a boost converter is more suitable for SWECS applications, due to its low cost and high reliability [137]. Indeed, a three-phase diode bridge guarantees less power loss and the DC/DC converter is still more robust and simpler compared to the controlled rectifier.

When the WT system is connected to the grid, it generally operates at MPPT which allows for extracting the maximum power from the wind energy system in all environmental conditions [138]. However, for distributed generation systems, there may be constraints where WT systems are not supposed to generate maximum power. Indeed, taking into account some constraints in terms of economy and system security of the MG, e.g., when the storage device is fully charged or there is low demand, a technique able to function below MPPT must be used instead. This technique, called limited LPPT, allows for more flexible operation of the system [135]. Consequently, a general control strategy that can deal with both MPPT and LPPT is very important for WT systems. Several power control strategies, especially MPPT algorithms, have been suggested in the literature with the main objective of extracting the desired power, reducing power oscillation, using excess power and improving the quality of the power injected into the grid. They are classified into three categories: direct power controllers (DPCs) [139][140], indirect power controllers (IPCs) [141]–[143] and advanced power controllers (APCs) [141][142][144]. The main DPC methods are the P&O method or its derived version called hill-climb

search (HCS) and the incremental conductance (IC). Regarding IPCs, three algorithm methods are mostly considered: the tip speed ratio (TSR), the power signal feedback (PSF) and the optimal torque (OT). APCs are characterized by using soft computing techniques like FL and artificial neural networks (ANNs). These techniques could work independently or combined with other methods to reach the operating point [144]. An overview and details about these techniques are provided in Section 2. Some of these algorithms have already been modified to allow the possibility of operating in LPPT mode. However, the change from one operating point to another still represents the most critical situation for the system's stability. In addition, the sudden variation of some conditions, such as power required by the user or climatic changes, e.g., wind speed, can have an impact on power output [145].

Therefore, the purpose of this work is split into three objectives:

- To propose a strategy to limit the power provided from a SSWT that will be integrated into a DC MG.
- To propose two LPPT algorithms based on the P&O principle to overcome drawbacks of the conventional P&O method.
- To test the impact of a sudden variation of the power and the wind speed on the performances of the selected LPPT methods.

Firstly, this chapter presents an overview of control power strategies found in the literature. Secondly, a description of the MG, the experimental test bench, and the proposed power control strategies are given in Section II.3. Finally, the strategies are validated by experimental tests, and the performances of the proposed methods are investigated in section II.4.

II.2. Related work

The enhancement of monitoring, management and control of WTs has become an essential key to guarantee better quality of the grid injected power. In recent years, many studies have been carried out to improve the control of the WECS and develop power extraction techniques. These techniques could be evaluated depending on the requirements of each method, such as wind speed information, turbine parameters, use of sensors, simplicity of implementation and robustness. The majority of studies found in the literature [141], [142], [146] mainly deal with MPPT strategies. Each method has its specific advantages and drawbacks. For example, the TSR algorithm is a simple control method that requires keeping the TSR at the optimum value by regulating the rotational speed of the generator. It provides efficient results and a quick response. Nevertheless, its robustness decreases when the wind speed suddenly changes. In addition, this method requires previous knowledge of power coefficient (TSR characteristic curve) and also the use of an accurate sensor for wind and turbine speeds, which increases the cost of the system, especially for SSWTs. Concerning the MPPT based on OT, the PMSG torque is controlled and set to its optimal value [141]–[143]. This optimal reference is obtained according to the

WT's maximum power at a given wind speed. This strategy provides a smooth output power with slow transient responses. Despite its robustness and effectiveness, it can not be generalized to all turbines because it requires specific characteristics of each WT.

Contrary to the previous techniques, some enhanced methods are developed with no need to know the turbine characteristics, wind measurement or mechanical speed sensors [141][142][144]. The fuzzy logic controller (FLC) is one of those methods that can be used independently or along with other methods. According to the results reported in [147], [148], the FLC can provide a fast response and a quick change in parameters when climatic conditions change. Despite the robustness and effectiveness of this method, it requires a large memory for resolution during fuzzification and defuzzification stages and prior knowledge of the results in order to choose the rule base, the levels of membership function and the appropriate error. With the development of soft computing technologies, MPPTs based on ANNs are becoming more and more popular. ANN techniques offer three types of layers: input, hidden and output layers. The ANN's architecture (number of neurons in each layer, number of layers, etc.) is chosen depending on the task to learn. For a WT system, the input variables can be wind speed, rotor speed, output torque, etc. The output can be a reference signal such as reference power, reference torque, etc. This output is used to operate the converter at the maximum power point (MPP). The authors of [149], [150] show sensorless MPPT algorithms based on ANN techniques. The inputs are the rotor speed and the output power of the turbine while the output is the optimal rotor speed. The latter is used to control the generator and then to obtain the optimum power. This ANN-based controller decreased the response time with the ability to provide a smooth power transition during wind speed variations.

Furthermore, the most used MPPT methods to target the MPP for SSWTs are PSF and P&O. Regarding MPPT-PSF, this method is based on an optimum relationship. It requires parameters of a specific WT such as mechanical power equation or maximum power curve [8]. In these work [151], [152], an example of controllers based on optimum relationships was reported, such as the output power with the rotational speed or the torque with the rotor speed. These relationships make the system more expensive (by using mechanical speed sensors) and complex (by using estimators for rotor speed). However, some studies highlight that the use of the DC bus's parameter in SWECS, equipped with a PMSG and a diode rectifier, makes the system more reliable with no need to use a mechanical sensor. This method remains simple and allows for a fast response of tracking the MPP, but defining an accurate relationship for a real WT system is still difficult.

Concerning MPPT-P&O, this technique is the most used for power extraction. It is a simple technique that allows for reaching the MPP without knowledge of the WT system parameters. It consists of perturbing the system, observing and analyzing the output electrical power and then deciding the direction of the next perturbation based on that outcome. Several variables could be perturbed in this method, such as the DC bus voltage, the DC current and the rotational speed, or the duty cycle of the boost converter could be adjusted [139][140]. However, it is not preferable to perturb the rotor speed in order to avoid the use of a mechanical sensor. Moreover, the choice of the appropriate perturbation step

size is not obvious. Indeed, according to the chosen step size, the performances of the WT (response time, oscillation around the MPP and high mechanical vibration) change. For this reason, many authors suggested an adaptive P&O method with a variable step size. Belhadji et al. [153] suggested an adaptive P&O method where the variable step size was calculated by multiplying the fixed step size by a variable gain. Harrag et al. [154] proposed an adaptive duty cycle step using proportional–integral–derivative controller based on a genetic algorithm. In [155], an ANN approach is proposed to provide the power converter duty cycle under different atmospheric conditions.

Besides the MPPT method presented above, other control strategies, such as pitch control, could be added to increase the performances of the WT system. These control strategies are mostly used to protect WTs, especially when the rated power is reached while the wind speed is still increasing. SSWTs are not concerned by this type of control since their pitch angle is always set at 0° . Even though small-scale wind energy production should ideally operate to extract the maximum power, its exploitation can require the use of an additional strategy to limit the generated power. Only a few studies have been interested in limiting the generated power of SSWTs. Hui et al. [156] proposed an intelligent power management controller for a small standalone off-grid wind energy system equipped with a PMSG. It consists of two methods: a slope-assisted MPPT algorithm, which tracks the MPP and minimizes the logical errors by identifying the changes in atmospheric conditions, and a power-limited search (PLS) algorithm which minimizes the surplus generated power and avoids energy dissipation.

In this chapter, three LPPT-P&O algorithms for the SWECS are proposed. The SSWT used in this work will be integrated into a DC MG. It should respect the MG constraints and requirements. In this case, the SSWT should not always extract the maximum power but rather provide the power depending on the needs of the MG. The proposed algorithms are P&O with fixed step size, P&O based on Newton's method, and P&O based on the FL technique. All proposed methods should have the ability to perform at two operating points. They ensure an easy transition from one point to another depending on the user's requirements and the turbine's characteristics (less power loss, low generator speed, etc.).

II.3. Studied wind turbine: MG overview and experimental test bench

II.3.1. MG overview

The SSWT studied in this work is intended to be integrated in a DC MG applied to tertiary buildings. Figure 31 illustrates the topology of a DC MG. This MG consists of a small WT and PV panels as RESs. Storage is added to deal with the intermittence of power generated by this type of energy. A utility grid is also connected to the MG in order to ensure the exchange of power. All these components are connected to a common DC bus through their appropriate converters. The power system of this MG supplies a DC load (the building's electrical appliances) which is directly connected to the DC bus through a capacitor

C_{DC} in order to stabilize its voltage. In this context, the DC power system is chosen thanks to its many advantages. Examples of these benefits are the fact that the DC MG could efficiently integrate many DC native power generators (PV or FCs), and that the majority of tertiary buildings' electrical appliances can be DC supplied [130].

The MG is supervised by an energy management strategy which controls each physical element by an independent controller. This strategy aims to ensure the power balance between power production and power consumption [157]. Therefore, the SSWT must be driven to provide the maximum power and ensure more benefits. However, when the power provided by the WT source exceeds the needs of the MG, this could destabilize the entire system and risk damaging components, especially when they reach their physical limits. Thus, limiting the power provided by the WT source is a solution to keep the power balance and prevent any critical operating situations. In this case, LPPT mode is activated by the SSWT.

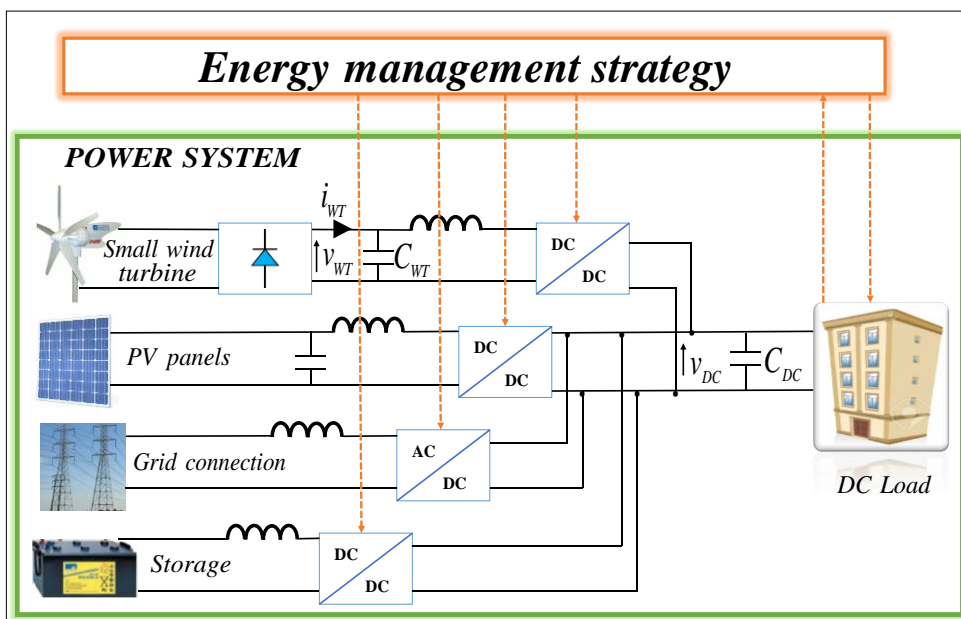


Figure 31. The MG overview

II.3.2. Experimental setup for the SSWT

The WT rotor converts the kinetic energy of wind into mechanical energy. The aim of this study is to integrate a SSWT in the DC MG already developed in a research testing platform in the AVENUES laboratory of the Université de Technologie de Compiègne (UTC), France. The experiment was conducted in a wind tunnel, as shown in Figure 32.a.

The SSWT is installed in a ventilation tunnel with an axial fan. It is placed downstream of the WT to reduce aeraulic disturbance. This wind tunnel is also equipped with two differential pressure transmitters (KIMO CP210) (red lines in Figure 32.b). One of them is combined with a Pitot tube (blue lines in Figure 32.b) that is used as a flow transmitter. This Pitot tube measures the dynamic pressure of the air produced by the fan in the wind tunnel and then can deduct the wind speed in m/s (see Appendix n°3).

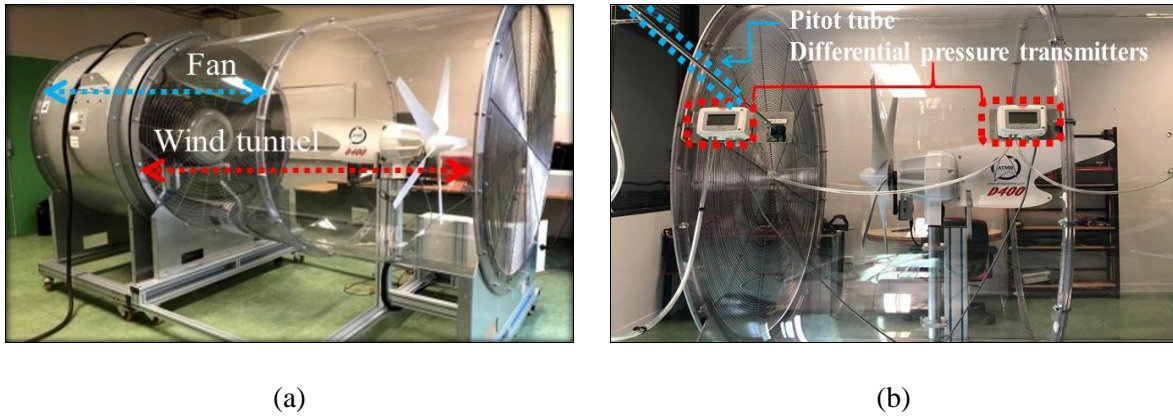


Figure 32. a) Wind tunnel; b) pressure transmitters and Pitot tube

In this study, the SSWT used is a horizontal axis WT produced by ATMB Marine (Appendix n°4). It is constructed of five blades and the diameter of the turbine is 1.1m. This SSWT is designed by the manufacturer to operate at a rated power of about 400W at 11m/s while the maximum power is 600W. The maximal rotational speed is estimated to be 1250rpm at 11.5m/s.

The SWECS investigated in this study is based on a three-phase diode rectifier to convert AC voltage obtained from the PMSG to DC voltage (Figure 33). A smoothing capacitor C_{WT} is used to constitute the DC bus of the SWECS. Then, a controllable DC/DC converter with a controller bloc, where the algorithms are implemented and which is driven by dSPACE, is designed to adjust the desired power and reach the operating point. Finally, to emulate the MG load demand, a programmable DC electronic load is used. Thus, the power required by the MG load or the user, P_{lim} , and the DC bus voltage, v_{WT} , are used as parameters for algorithms which aim to manage the electrical power available in the DC bus (p_{WT}). The result provided by the controller is v_{WT_REF} .

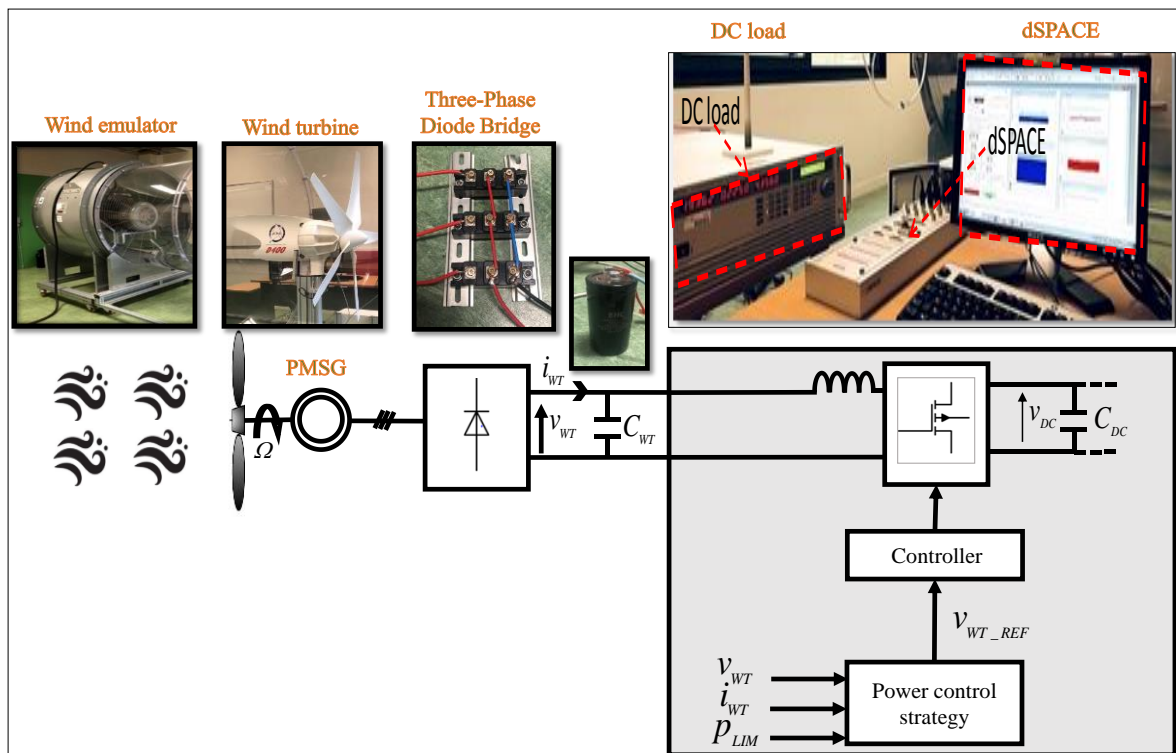
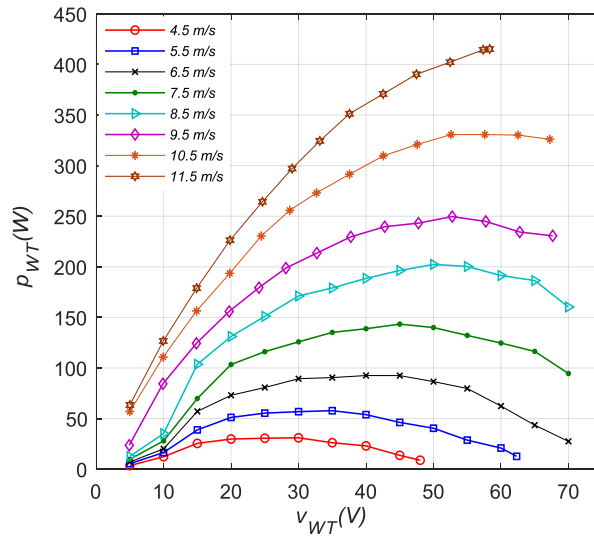


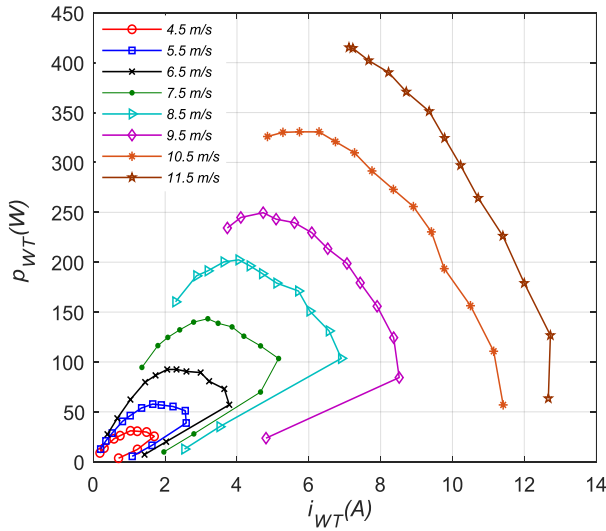
Figure 33. Electrical scheme and components of the studied SWECS

Prior to investigating different power control strategies, several tests are carried out within the wind tunnel by changing the load and the wind speed. The voltage, the current and the electrical power in the DC bus are then measured. In addition, the mechanical speed (Ω) of the PMSG is observed and measured in order to not exceed the maximum value recommended for this WT. Collected experimental data are given in Figure 34.

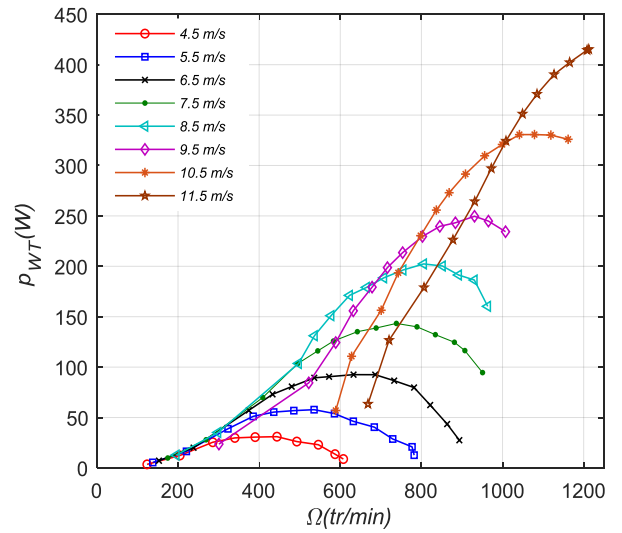
As can be seen in Figure 34.a,c, all power curves reach a maximum point and then decrease as v_{WT} and Ω rise. Additionally, it is noticed that each value of v_{WT} corresponds to one value of p_{WT} . However, one value of i_{WT} is attributed to two values of p_{WT} (Figure 34.b). Thus, v_{WT} is used as the controlled parameter.



(a)



(b)



(c)

Figure 34. a) Electrical power p_{WT} based on the bus voltage v_{WT} ; b) electrical power p_{WT} based on the bus current i_{WT} ; c) electrical power p_{WT} based on mechanical speed Ω

II.4. LPPT control strategies

The use of power control strategies to maximize the efficiency of the WT system is still relevant. MPPT control is a well-known mechanism developed to keep the power output of the WT system at the MPP [138] (green point in Figure 35). However, some power limitations can be associated with this tracking method and then the WT is supposed to provide less power [156]. Thus, the LPPT mode is chosen and activated (pink line in Figure 35). The suggested control power strategies presented in this

study focus on LPPT characteristics and evolution. The principle of LPPT control for the WT system is explained with the help of the $p_{WT} - v_{WT}$ curve shown in Figure 35.

When the SSWT converter operates in LPPT mode, the P_{lim} is under maximal value, which means that the user or loads ask for less power. Therefore, to function correctly in LPPT mode, the absolute value of the difference between p_{WT} and P_{lim} should be calculated as $p_{diff} = |p_{WT} - P_{lim}|$. This p_{diff} must be low in order to reach the operating point. For this reason, algorithms used in the LPPT control strategies aim to decrease the value of p_{diff} as much as possible. Overall, in LPPT mode, two limited power points (LPP1 and LPP2) could be achieved by reducing p_{diff} . Consequently, the $p_{WT} - v_{WT}$ curve is divided into four regions, which are characterized by different conditions (see Figure 35), allowing the transition from one operating point to another according to the needs of the user and the constraints of the used equipment. Thus, it is crucial to make a wise choice based on the advantages and disadvantages of each point. To avoid the generator's over-speeding and minimize the mechanical stress, the proposed power control strategies should seek LPP1, whereas LPP2 ensures less power loss and low currents. In this study, the limits of the test bench equipment restrict the WT system to operate at a specific point. In this context, the characteristics of the SSWT used in this study (Figure 33.a,c) show that for high wind speeds, the system can operate only in LPP1. Indeed, the rotor maximum rotation speed estimated at 1250rpm can be exceeded while trying to reach the second point LPP2, which can damage the WT.

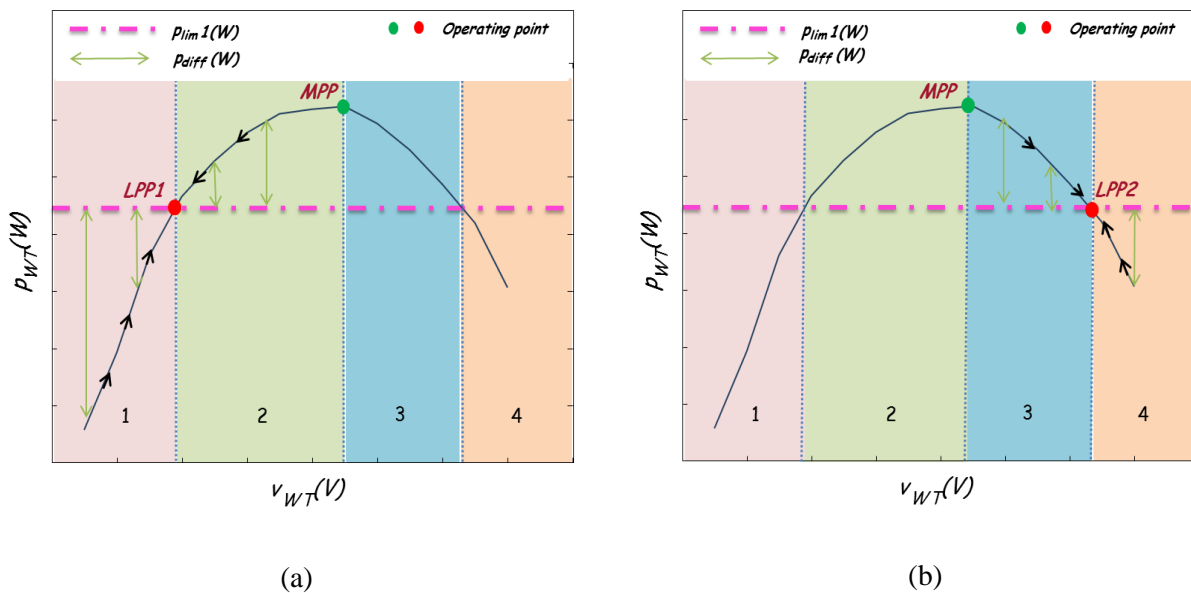


Figure 35. Operating cases for: a) LPP1; b) LPP2

The selected controller in this present study is P&O, which is very simple and allows for a fast dynamic in tracking the operating power points. It does not require knowledge of SWECs components. It consists of perturbing the operating voltage of the system and analyzing the resulting change of power to decide the direction of the next perturbation. The P&O principle is used and presented in Figure 6. It is different from the flowchart for classical P&O [138] because it takes into account two operating points.

Thus, several conditions were analyzed in order to identify the four regions (r) presented in Figure 35. The value of v_{WT_REF} is calculated following the conditions in Figure 36. This flowchart measures at each k instant the variables $v_{WT}(k)$ and $i_{WT}(k)$, calculates $p_{WT}(k)$ and $p_{diff}(k)$, and then compares them with powers calculated at the k-1 instant: $p_{WT}(k-1)$ and $p_{diff}(k-1)$. Three LPPT control strategies based on P&O are presented below.

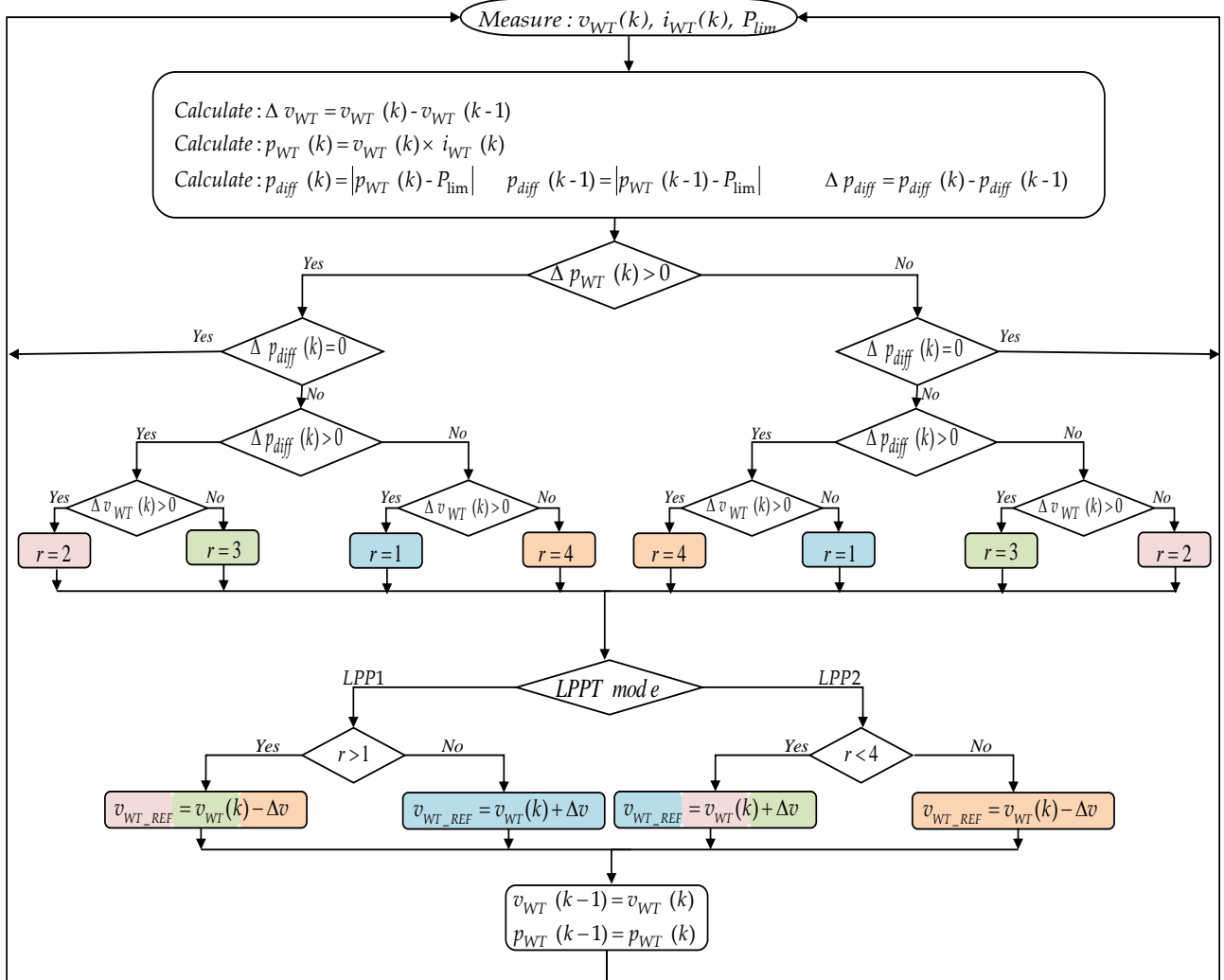


Figure 36. Principle of P&O method for LPPT mode

II.4.1.1. P&O with fixed step size

The P&O with fixed step size is the conventional algorithm that is widely used for the MPPT method. Some direct methods focus on perturbing the converter's variables (input voltage [140], input current [138] or duty cycle [158]) or the inverter input voltage [159], whilst others observe the mechanical power while perturbing the mechanical speed [130].

In this study, the P&O with fixed step size method is used to perturb the DC-bus voltage $v_{WT}(k)$ to track LPP1 and LPP2. Three different perturbation step size Δv (2V, 4V, and 6V) were applied to the system to analyze the stability and the speed tracking.

II.4.1.2. P&O with variable step size based on Newton's method

The second method used in this work is Newton's method. It was developed to improve the efficiency and rapidity of the traditional P&O. This method allows for calculating the variable perturbation step size according to the operating point [135]. Indeed, if the operating point is far away from the LPP, the step size increases rapidly to approach the LPP. Conversely, if the operating point is close to the LPP, the step size decreases. In this method, the root value is calculated through the following equation [160]:

$$X_{n+1} = X_n - \frac{F(X_n)}{F'(X_n)} \quad \{2.1\}$$

where X_n is the initial value of X , $F(X_n)$ represents the value of the X at the point X_n and $F'(X_n)$ is the derivative of function at X_n . The Newton's method applied in this study depends on the evolution of p_{diff} as a function of v_{WT} . The calculation of step size following this technique is based on the iterative method mentioned in {2.2}-{2.7} for each k instant as shown below:

$$X_n = v_{WT}(k) \quad \{2.2\}$$

$$X_{n+1} = v_{WT}(k+1) = v_{WT_REF}(k) \quad \{2.3\}$$

$$F(X_n) = F(v_{WT}(k)) = p_{diff}(k) \quad \{2.4\}$$

$$F'(X_n) = F'(v_{WT}(k)) = \frac{\Delta p_{diff}(k)}{\Delta v_{WT}(k)} = \frac{p_{diff}(k) - p_{diff}(k-1)}{v_{WT}(k) - v_{WT}(k-1)} \quad \{2.5\}$$

$$v_{WT_REF}(k) = v_{WT}(k) + \Delta v \quad \{2.6\}$$

$$\Delta v = \frac{p_{diff}(k)}{\Delta p_{diff}(k) / \Delta v_{WT}(k)} \quad \{2.7\}$$

The variable step sizes provided by this method were limited for protection and saturated to 2V, 4V and 6V in order to compare their performances with the ones provided by the method with the fixed step sizes.

II.4.1.3. P&O with variable step size based on FL

The variable step size based on the FL method is gaining popularity as a method for the MPPT technique. It was used by many authors [144] to extract the maximum power thanks to its fast convergence and handling of the non-linearity of the system. However, few studies have been carried out using this method to investigate the WT's performances when limited power is required [161]. The FL method consists of mapping the input space and the output space through logical operations. This method's realization process is divided into three steps: fuzzification, fuzzy reasoning and defuzzification [135] (Figure 37). In order to calculate the variable step size, the inputs here are the slope

$(\Delta p_{WT}(k) / \Delta v_{WT}(k))$ and $p_{diff}(k)$. They are converted, during the fuzzification process, into fuzzy linguistic sets using the Mamdani method [8] and the universe of discourse of the inputs and the output is normalized into $[-1, 1]$. Thus, u_1 is the first normalized input corresponding to $(\Delta p_{WT}(k) / \Delta v_{WT}(k))$ and u_2 is the second normalized input corresponding to $p_{diff}(k)$. These fuzzy sets are then analyzed by the fuzzy reasoning surface where a fuzzy output s is obtained by using fuzzy rules. To simplify the study, forms of membership function were selected as triangular and trapezoidal. Furthermore, the defuzzification process converts this fuzzy output to the desired output value Δv and the operator used in this study is the center of gravity. The FL controller presented in this study allows for examining the first input and, if this value is greater than zero, the step size increases until the LPP is reached. If it is less than zero, the opposite occurs until the operating point is reached. The second input is then used to adjust the value of the step size and determine the region of the operating point.

The fuzzy subsets corresponding to the first input $(\Delta p_{WT}(k) / \Delta v_{WT}(k))$ are divided into five values: negative big (NB), negative small (NS), zero (ZE), positive small (PS) and positive big (PB), while the second input $p_{diff}(k)$ is divided into three values: negative (N), zero (Z) and positive (P). For example, if the value of $p_{diff}(k)$ is zero, whatever the value of the slope is, the predefined value assigned to the output s is zero, which means that the LPP is reached. All rules are provided in Table 1. As in the previous method, the variable step sizes provided by this controller were limited to 2V, 4V and 6V.

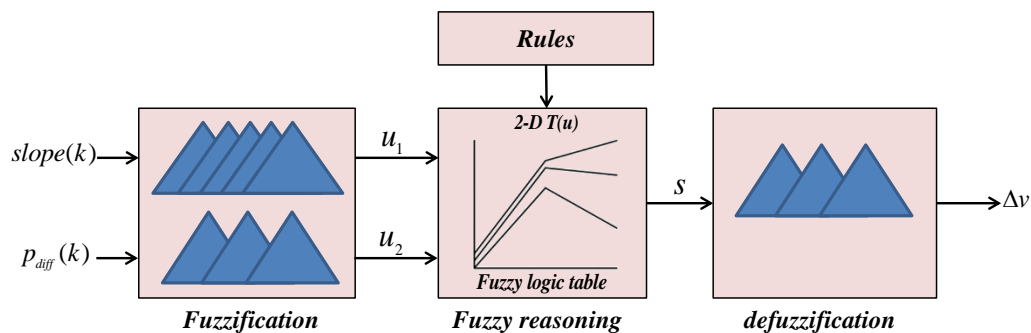


Figure 37. Structure of FLC

Table 1. Rule base for LPPT mode. (N: negative; P: positive; Z: zero; S: small; B: big)

$\frac{\Delta p_{WT}(k)}{\Delta v_{WT}(k)}$	$p_{diff}(k)$		
	N	Z	P
NB	z	z	z
NS	p	z	n
ZE	p	z	n
PS	p	z	n
PB	z	z	z

II.5. Experimental results and discussion

II.5.1. Performance of proposed power control strategies

In order to demonstrate the effectiveness and applicability of the proposed power control strategies, algorithms were performed using MATLAB Simulink. At first, the simulations were carried out to investigate the performances of the WT under varying step sizes for each algorithm. Due to the constraints linked to the characteristics of the WT studied in this work, two points, LPP1 and LPP2, allow for reaching the same power for a specific wind speed. They are examined in Figure 38. Thus, the wind speed is fixed at 6.5m/s and the limited power (P_{lim}) at 50W, which is under the maximal power provided in this case. After studying the performances of each proposed control strategy, a comparison of the results with a specific step size is carried out.

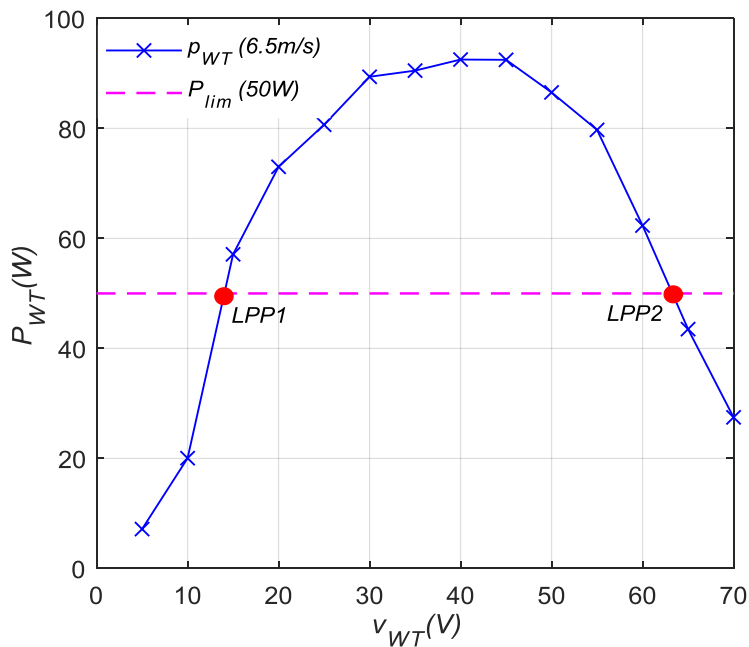


Figure 38. p_{WT} based on v_{WT} for selected wind speed

II.5.1.1. P&O with fixed step size

Figure 39 and Figure 40 present the experimental results of P&O with three different fixed step sizes (2, 4, and 6V) to target LPP1 and LPP2 for a wind speed of 6.5m/s. As can be seen in these figures, the power generated (p_{WT}) for different fixed step sizes is oscillating at around 50W for both LPP1 and LPP2, whereas the voltage (v_{WT}) varies close to 15V and 60V for LPP1 and LPP2, respectively. This corresponds to the selected case (see Figure 38). In addition, during the transition from LPP1 to LPP2, the current decreases approximately from 3.5A to 1.5A (Figure 39.d and Figure 40.d).

It can be obviously observed in the figures that according to the voltage perturbation step size, the results are not similar. Indeed, increasing the step size leads to a faster response with more power oscillations around the P_{lim} and, hence, less efficiency. In contrast, a smaller step size enhances efficiency, but reduces the convergence speed. This is in agreement with the results found in the literature [162][163]. In addition, comparing LPP1 and LPP2 reveals that working in LPP2 point leads to more power oscillations around the P_{lim} . This could be related to the rotor speed, which is less braked in LPP2, inducing an increase in the voltage and the rotor speed and thus generating more power oscillations compared to LPP1.

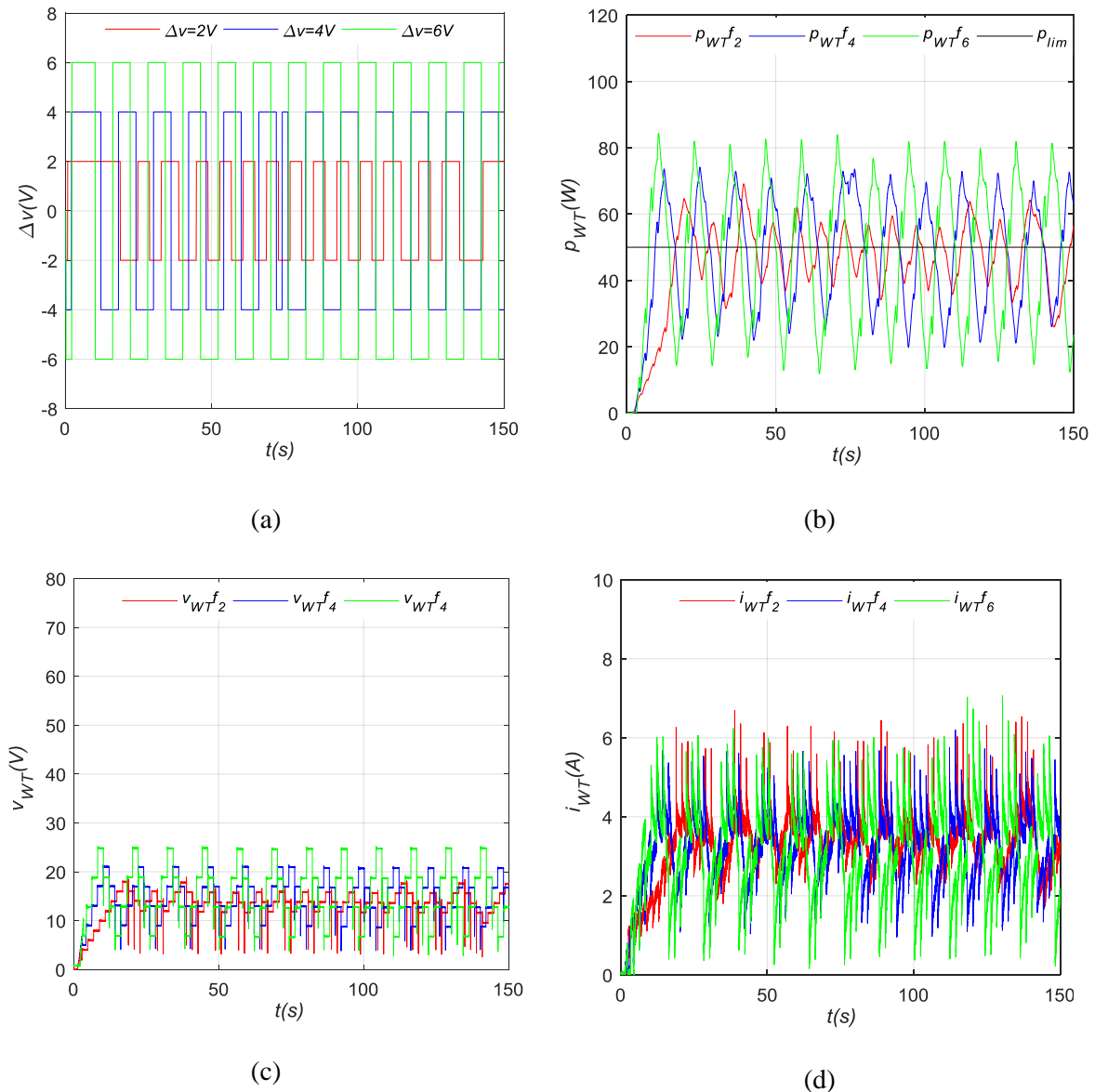


Figure 39. Fixed step-size P&O for LPP1: a) evolution of step size Δv ; b) evolution of p_{WT} ; c) evolution of v_{WT} ; d) evolution of i_{WT}

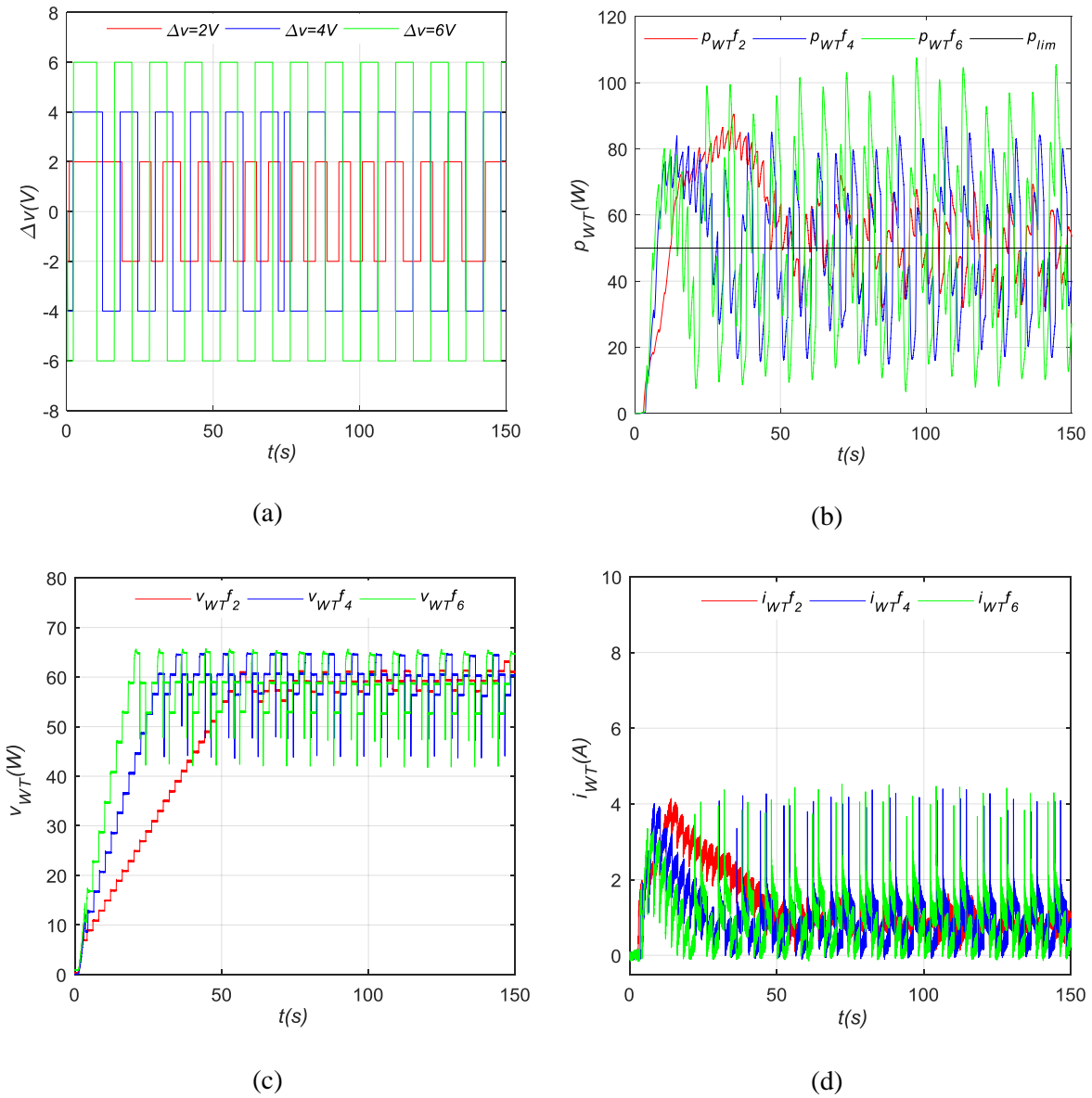


Figure 40. Fixed step-size P&O for LPP2: a) evolution of step size Δv ; b) evolution of p_{WT} ; c) evolution of v_{WT} ; d) evolution of i_{WT}

II.5.1.2. P&O with variable step size based on Newton's algorithm

Figure 41 and Figure 42 present the experimental results of P&O with three different variable step sizes, which are limited to 2, 4, and 6V, in order to target LPP1 and LPP2 for a wind speed of 6.5m/s. The power generated (p_{WT}), for different varied step sizes, follows the user recommendation well. It oscillates at around 50W for both LPP1 and LPP2, whereas the voltage (v_{WT}) varies close to 15V and 60V for LPP1 and LPP2, respectively. In addition, concerning the current, it varies from 3.5A to 1.5A for LPP1 and LPP2, respectively.

As for the P&O with a fixed step size method, the performances differ according to the selected step size. A larger step size leads to a faster transient response with more power oscillations around the P_{lim}

and, hence, less efficiency. Contrariwise, a smaller step size enhances efficiency, but reduces the convergence speed. These results mean that with the variable step size method, a compromise must be chosen between the state of dynamic transient response and the oscillation state. In addition, working in LPP2 point leads to more power oscillations around P_{lim} for all variable step sizes compared to LPP1 point.

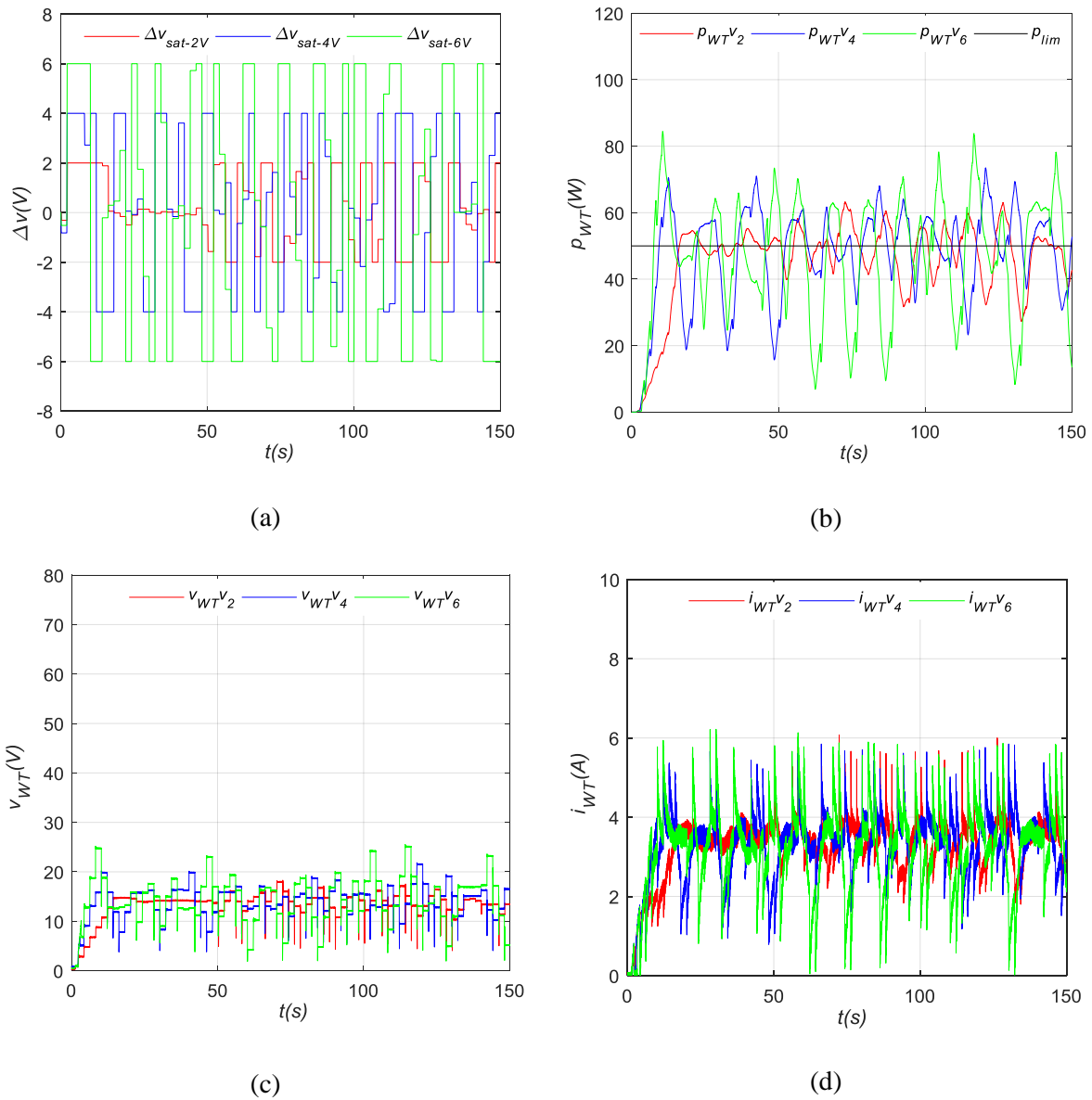


Figure 41. Newton's variable step-size P&O for LPP1: a) evolution of step size Δv ; b) evolution of p_{WT} ; c) evolution of v_{WT} ; d) evolution of i_{WT}

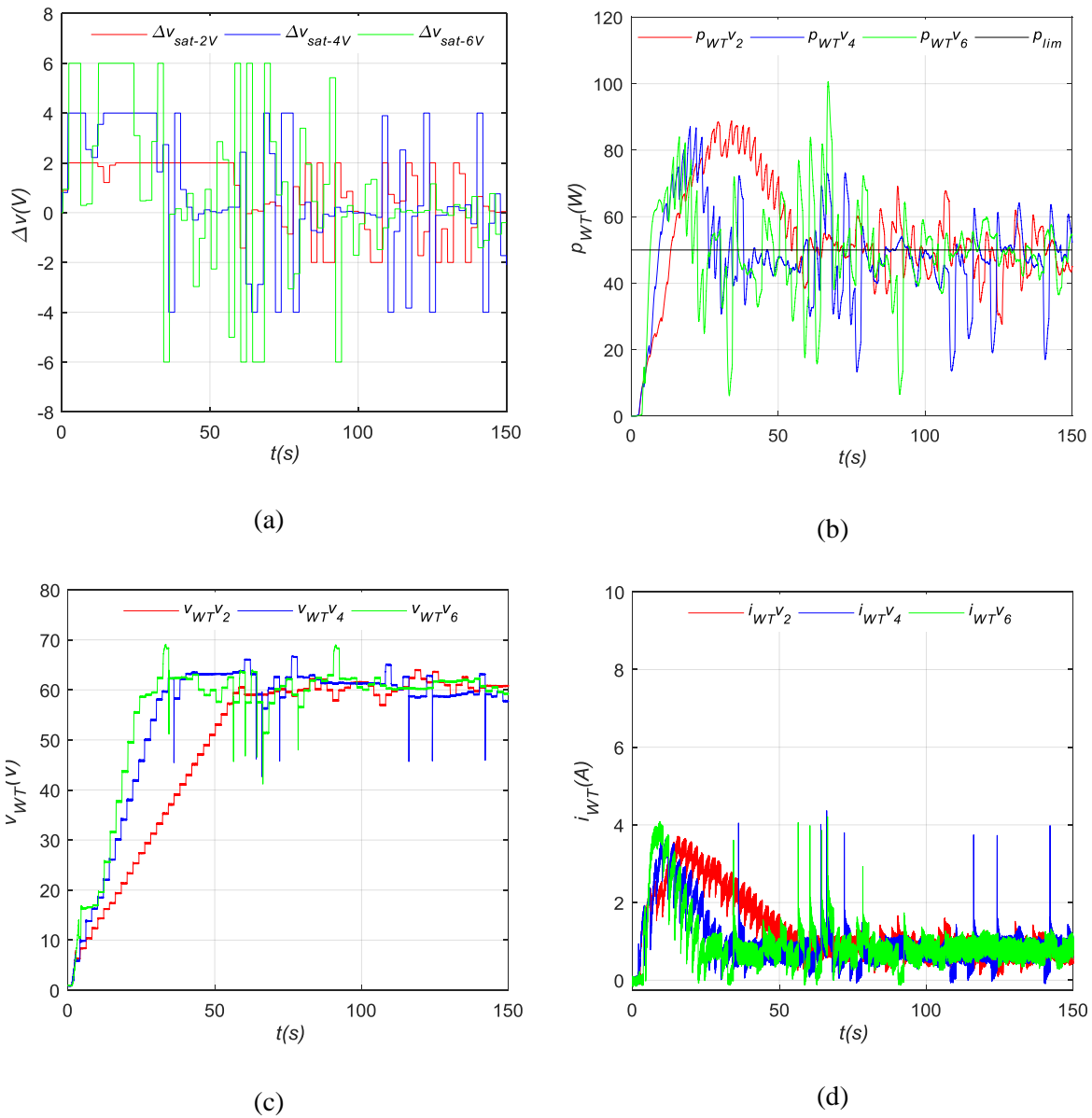


Figure 42. Newton's variable step-size P&O for LPP2: a) evolution of step size Δv ; b) evolution of p_{WT} ; c) evolution of v_{WT} ; d) evolution of i_{WT}

II.5.1.3. P&O based on FL

Figure 43 and Figure 44 illustrate the experimental results of P&O based on the FL method. In the same way as previous methods, the voltage perturbation step sizes were limited to 2, 4, and 6V to be tested and to achieve LPP1 and LPP2 points, for the same wind speed (6.5m/s). The results show that the p_{WT} for different step sizes oscillates near to 50W for both LPP1 and LPP2, whereas the v_{WT} varies close to 15V and 60V for LPP1 and LPP2, respectively. The current (i_{WT}) evolves inversely with the voltage and decreases during the transition from LPP1 to LPP2.

Whatever the step size is used, the FL method allows fewer power oscillations around P_{lim} which leads to more efficiency. However, the response timeliness differs depending on the step size. Indeed, increasing the step size leads to reaching P_{lim} quickly. Moreover, the results also reveal that there are

more power oscillations for LPP2 compared to LPP1. This confirms what was observed in the fixed step size and Newton's methods while comparing between LPP1 and LPP2.

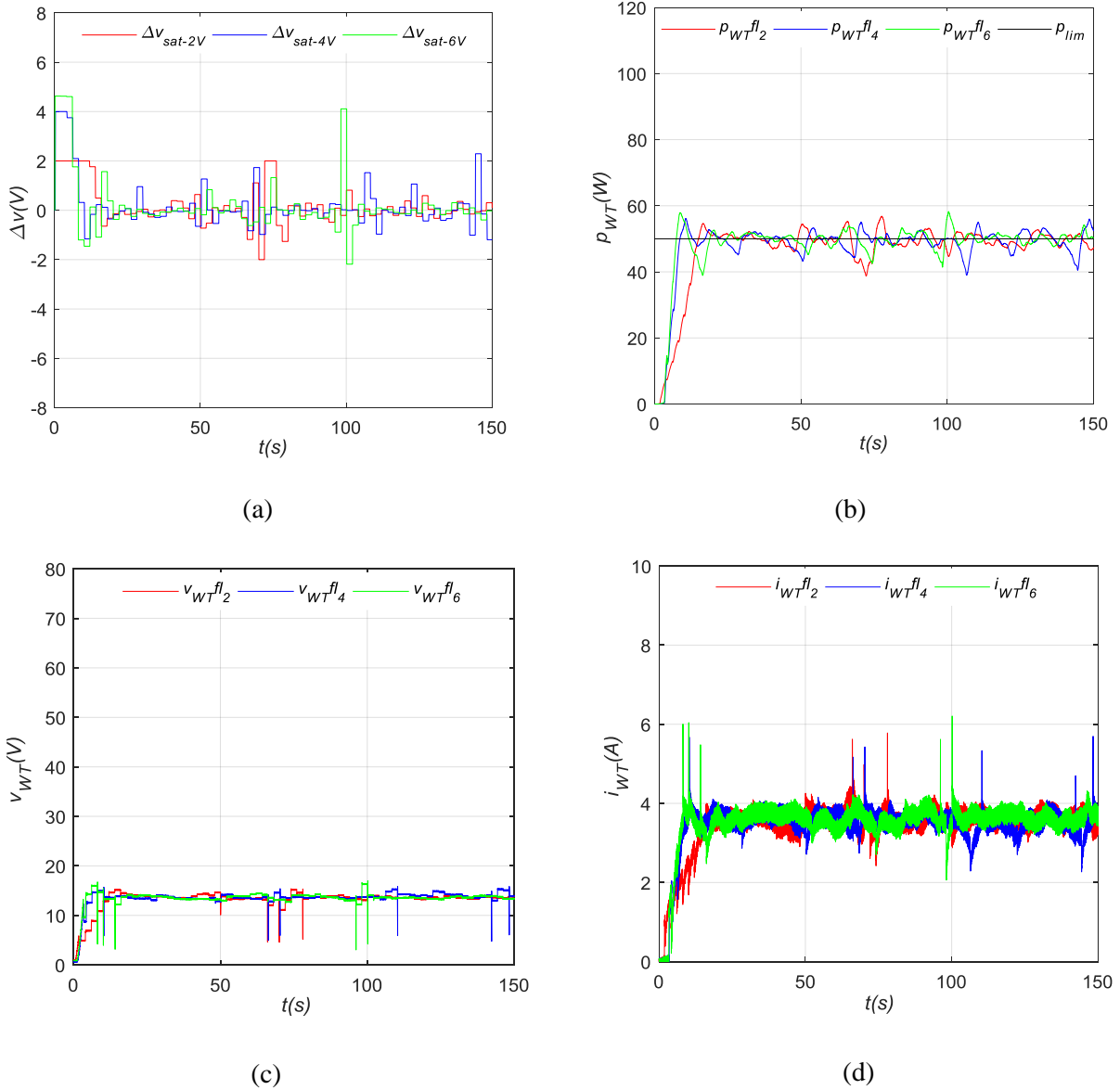


Figure 43. FL variable step-size P&O for LPP1: a) evolution of step size Δv ; b) evolution of p_{WT} ; c) evolution of v_{WT} ; d) evolution of i_{WT}

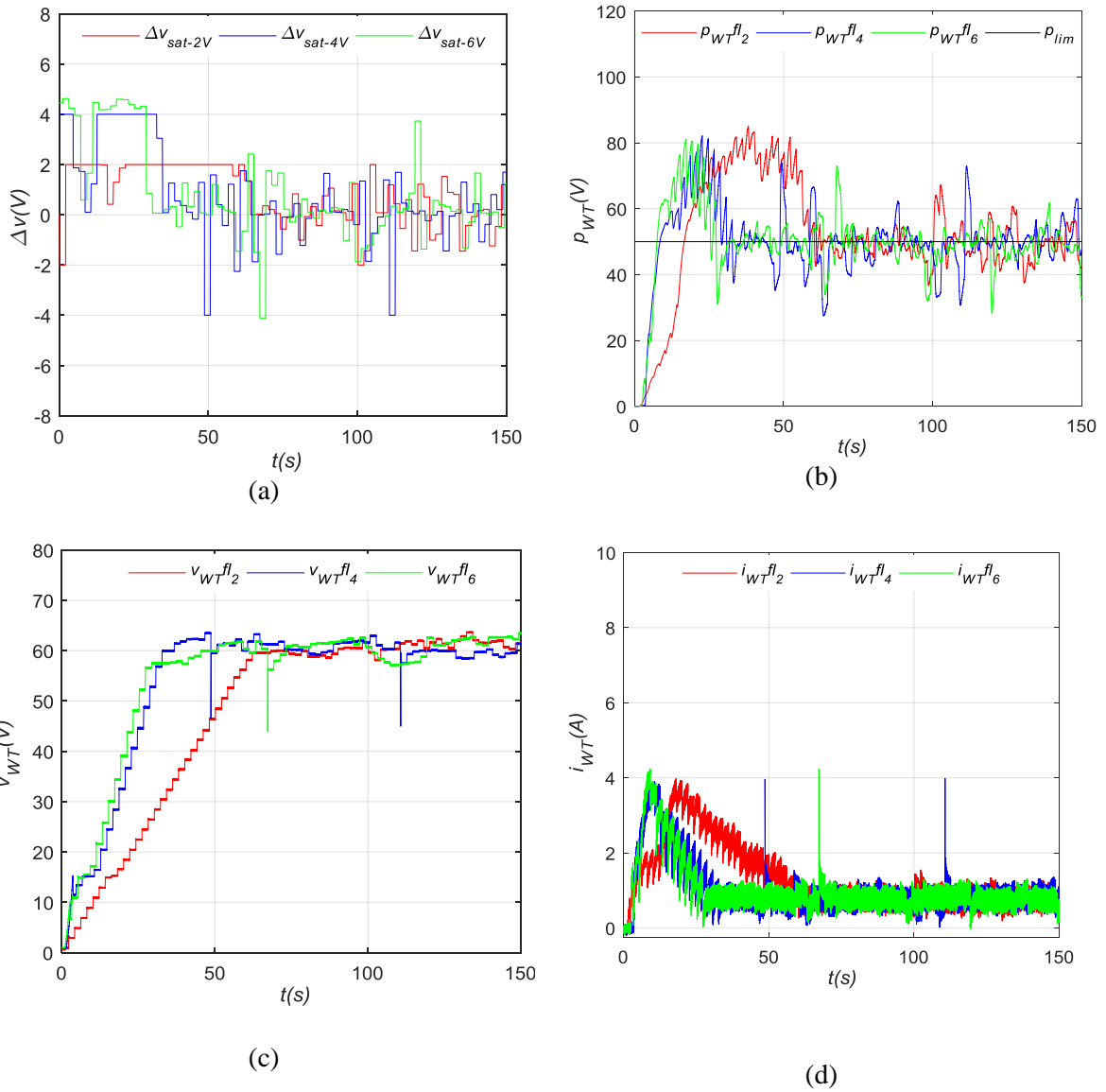


Figure 44. FL variable step-size P&O for LPP2: a) evolution of step size Δv ; b) evolution of p_{WT} ; c) evolution of v_{WT} ; d) evolution of i_{WT}

II.5.1.4. Comparison of the power control methods

In order to compare the performances of the proposed power control methods previously mentioned, the voltage perturbation step size of 4V is selected.

Figure 45.a,b depicts the effectiveness and the system response for LPP1 and LPP2. It can be observed that the response timeliness is identical whatever the algorithm method used. In contrast, the oscillation state differs according to the power control method. The FL method's power control has better dynamic performances with more steady oscillations compared to the fixed step size and Newton's methods.

Figure 46.a, b represents the descriptive statistical analysis (called a boxplot) of these three selected methods. The boxplot is a standardized way of displaying the dataset based on a five-number summary i.e., the minimum, the maximum, the sample median, the first quartile (25th percentile) and the third

quartile (75th percentile). The results clearly show a huge power variation of the fixed step size and Newton's methods compared to the FL technique, despite having roughly the same mean and median (around 49–50W) (Table 2). The variability could be calculated by measuring the interquartile range (IQR) which means the difference between the third and first quartiles (the distance covering 50% of the data). Regarding LPP1 (Figure 46.a), the IQR values are 29, 11 and 3W for the fixed step size, Newton's and FL methods, respectively, whereas for LPP2 (Figure 46.b), the IQR values are 32, 12 and 5W for the fixed step size, Newton's and FL methods, respectively. These values reflect the power oscillations' variations for each technique. In addition, when comparing boxplot results between LPP1 and LPP2 for the same method, it is obvious that the power oscillations around LPP2 are larger than those around LPP1. However, if there is a possibility to work in both LPP1 and LPP2, the priority should be given to LPP2. Indeed, as losses are mainly related to the current, LPP2 is placed in the high voltage and low current side, which insures less power loss. Yet, sometimes the system should operate in the low voltage and high current side (LPP1) to respect the equipment's physical limits (to avoid reaching the maximal generator speed and minimize the mechanical stress).

Summarizing all presented results, it can be concluded that all proposed LPPT control strategies are able to work properly, reach operating points and identify the direction of the next perturbation. However, the performances of the FL method are better, despite its complexity when implemented. FL enhances the overall efficiency and eradicates the limitations of the fixed step size and Newton's methods

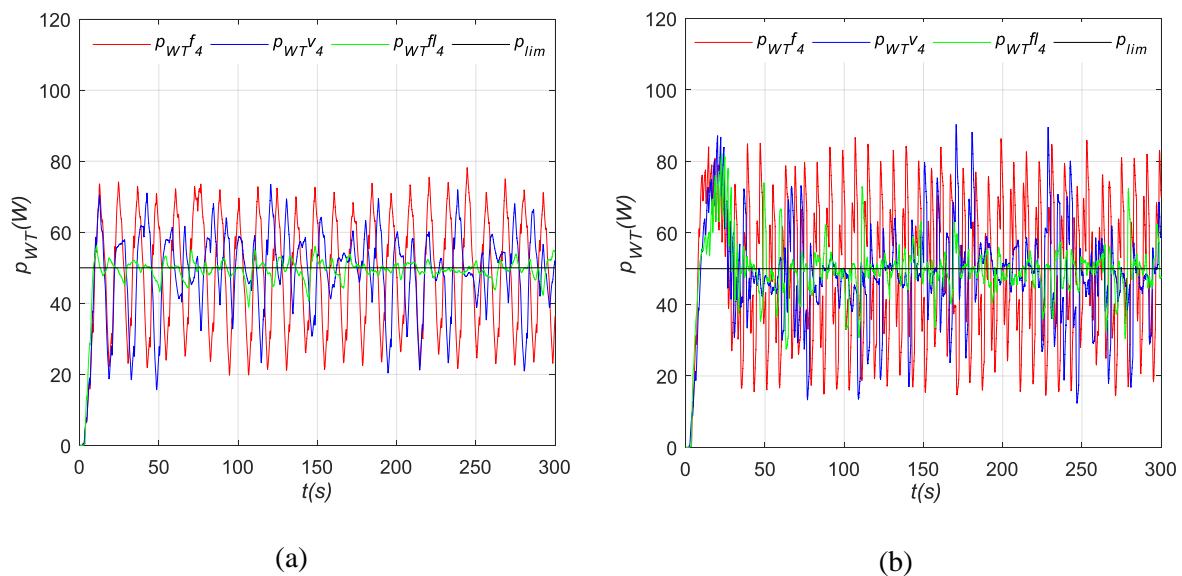


Figure 45. Comparison of experimental results: a) evolution of p_{WT} at LPP1; b) evolution of p_{WT} at LPP2

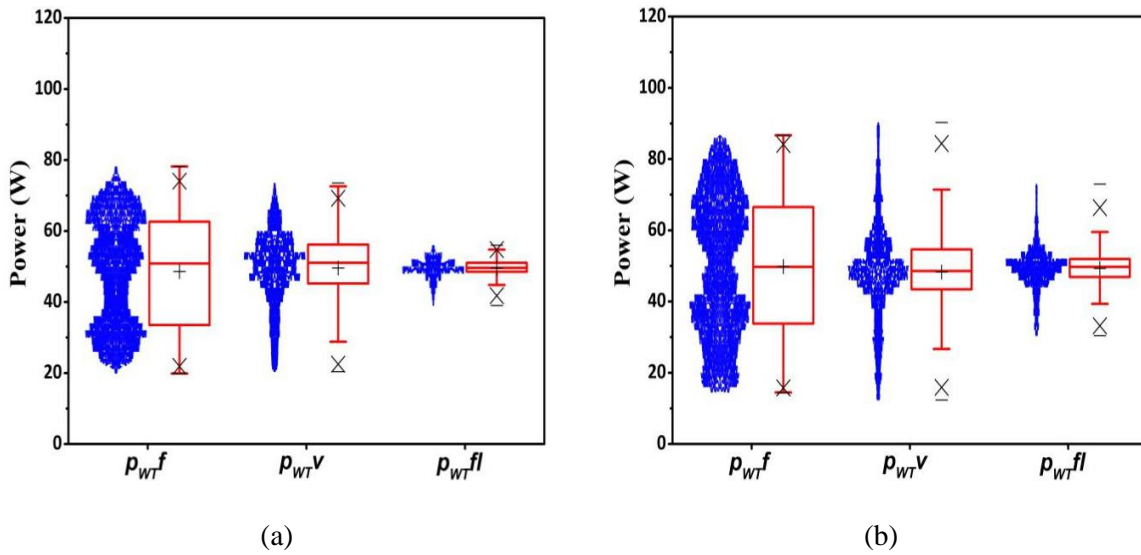


Figure 46. Statistical analysis of experimental results: (a) evolution of p_{WT} at LPP1; (b) evolution of p_{WT} at LPP2

Table 2. p_{WT} reached using different control method strategies. SD: standard deviation

Control Strategy Method	p_{WT} (W)	
	LPP1 (Mean \pm SD)	LPP2 (Mean \pm SD)
Fix step size	48.6 \pm 15.4	49.8 \pm 19.3
Newton's method	49.5 \pm 10.0	48.3 \pm 12.7
FL	49.6 \pm 2.4	49.3 \pm 5.6

II.5.2. Impact of sudden variations on the performance of the WT system

The impact of a sudden increase and decrease in limited power and the variation of wind speed on the SSWT's performances by using the proposed power control strategies is investigated. The LPP2 is selected as the operating point since it allows the system to work in the low current and high voltage side.

II.5.2.1. Power variation

The change of power represents a frequent situation in LPPT mode. Figure 47.a,b depicts two cases of a sudden variation of power, i.e., the sudden increase and decrease in power. The selected P_{lim1} and P_{lim2} correspond to 50W and 82W, respectively. For both cases, the wind speed is maintained constant at 6.5m/s. It can be clearly observed in the case of a sudden increase and decrease in power that all power control strategies operate successfully with a difference in terms of oscillation as described previously. The required time to make a transition to the new operating point is almost the same for all power control strategies. However, the decrease in power requires more time than the increase in power. It means that the increase in power from P_{lim1} to P_{lim2} needs 13s, while it takes place within 20s in the opposite case. It is important to also note that the FL technique stabilizes quickly compared to the fixed step size and Newton's methods in the case of an increase and decrease in power.

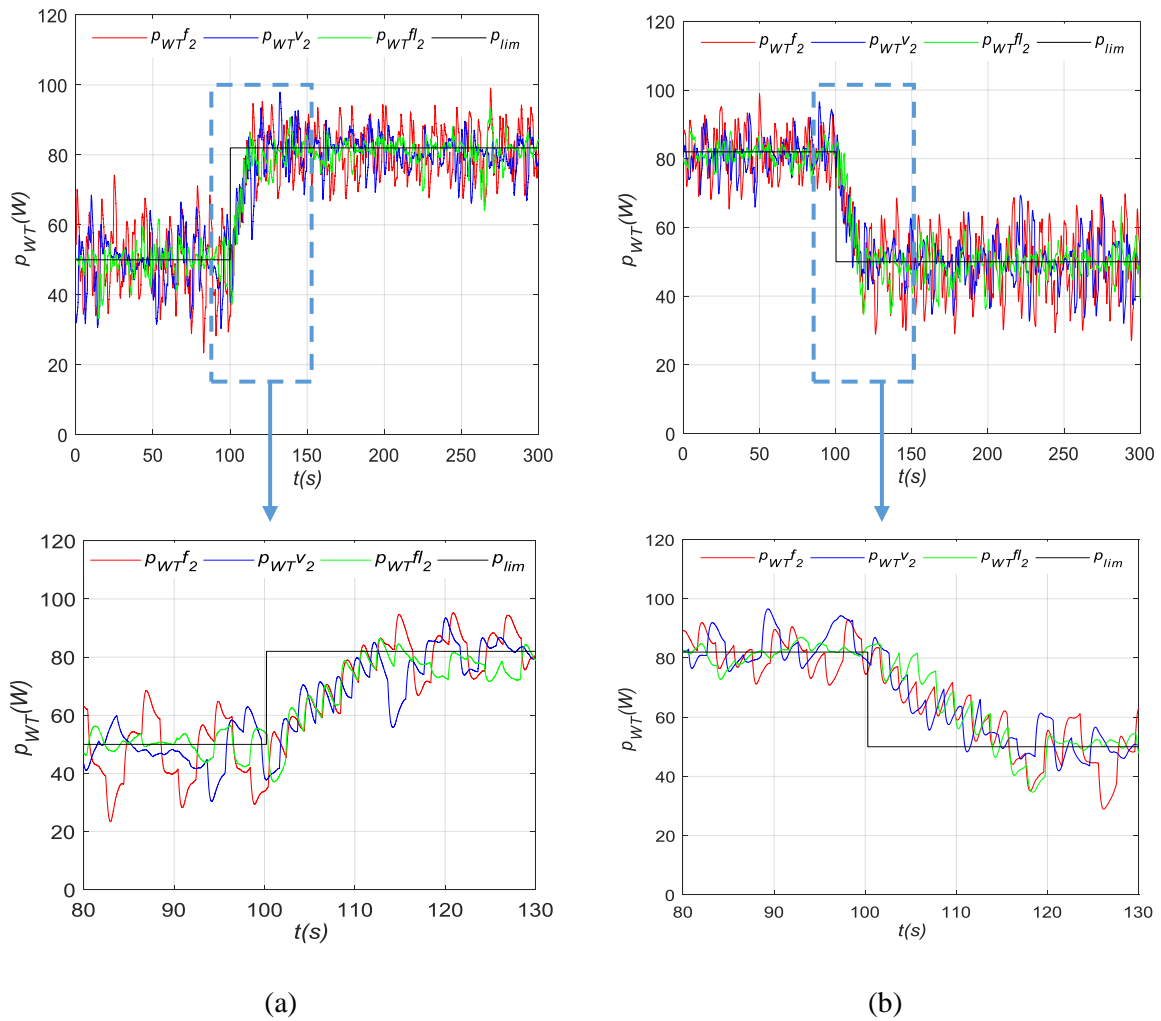


Figure 47. Drop in power: a) sudden increase of p_{WT} ; b) sudden decrease in p_{WT}

II.5.2.2. Wind speed variation

The sudden change of wind speed represents the most critical situation for the wind system stability. Despite the variation of wind speed, the p_{WT} must reach the P_{lim} recommended by the user. A wind speed profile varying from 6.5, 5.5 to 4.5m/s and a limited power of 50W are selected (

Figure 48). Based on different tests performed to characterize the WT for the selected wind speeds, a presentation of $p_{WT} - v_{WT}$ and $p_{WT} - t$ curves are illustrated in Figure 49.

As can be clearly observed, all proposed power control strategies have an identical behavior during wind speed variation. At the start, the wind speed is 6.5m/s and the system is following the P_{lim} of 50W which is situated at point 1 with a voltage of 63V. With the weather's variation, the wind speed drops to 5.5m/s, but the P_{lim} is maintained at 50W. Indeed, prior to reach point 2, the power decreases to 12W and is then raised to reach the P_{lim} . In this case, the WT is still able to deliver that power since $P_{lim} \in p_{WT} - v_{WT}$ curve. Later on, the wind speed drops to 4.5m/s and, thus, the power drops to 20W. Since the P_{lim} has become higher than the maximum power that can be generated for this wind speed, the

system is unable to deliver it. In such case, the algorithms of the proposed power control strategies are adapted to avoid the drop in power to 0W if the P_{lim} cannot be reached. Therefore, as can be seen in Figure 49.a, when the P_{lim} is not found, the system searches for the MPP (point 3) delivered under this wind speed. In addition, it is also important to notice that the time required to make the transition to the new operating point is almost similar for all proposed power control strategies. However, what changes is the oscillations' state around P_{lim} . Overall, there are very large oscillations around P_{lim} when the wind speed is high, which could be related to the increase in machine vibrations. Furthermore, it is evident that the FL technique allows for getting better performances around P_{lim} even with a sudden change of wind speed compared to the fixed step size and Newton's methods.

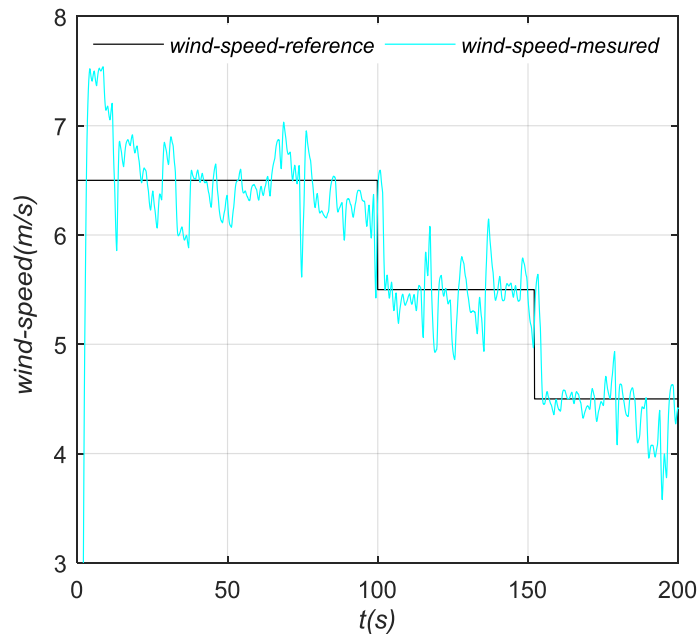


Figure 48. Wind speed profile

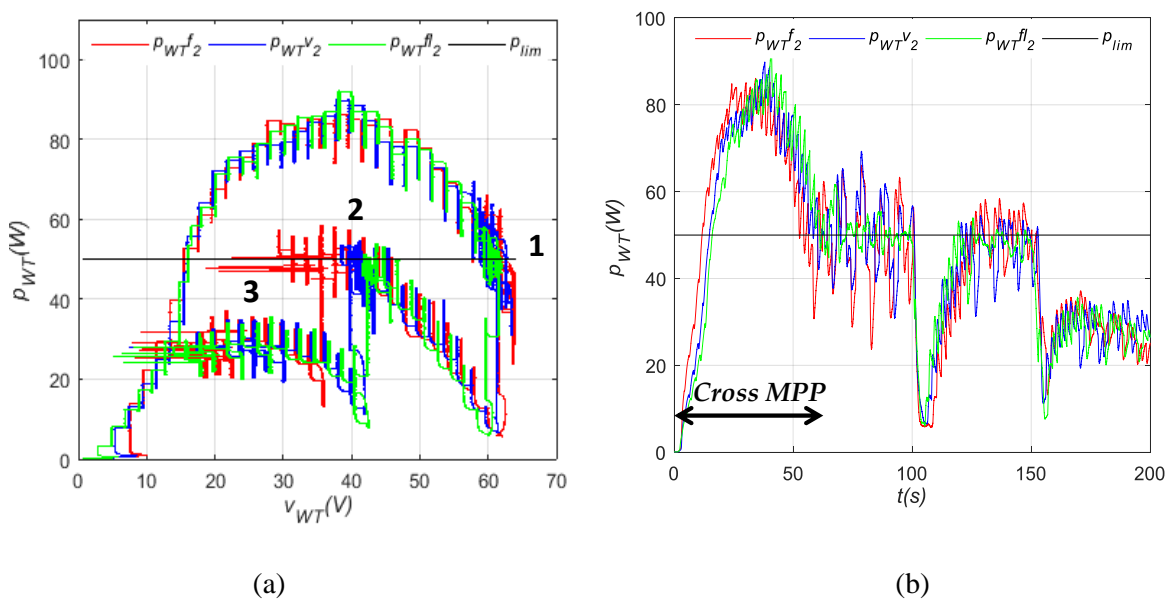


Figure 49. Drop in wind speed: (a) p_{WT} based on v_{WT} ; (b) evolution of p_{WT} in time

II.5.3. Transition between MPPT and LPPT modes

By integrating the SSWT in the DC MG, LPPT mode will not be the only mode that would be carried out. Indeed, when the power produced by the WT is totally consumed by the loads, the MPPT mode is activated. Once there is an excess of power production, MPPT mode switches to the LPPT one in order to decrease this power. Thus, it is crucial to test the transition between these two modes to demonstrate the effectiveness and applicability of the proposed power control strategies. The power profile displayed for these tests is presented in the

Figure 50. The wind speed is fixed at 7.5m/s, the limited power (P_{lim}) at 90W, and the maximum power (P_{max}) is around 125W. LPP2 was chosen as the limited point in the case of LPPT mode (see green arrow).

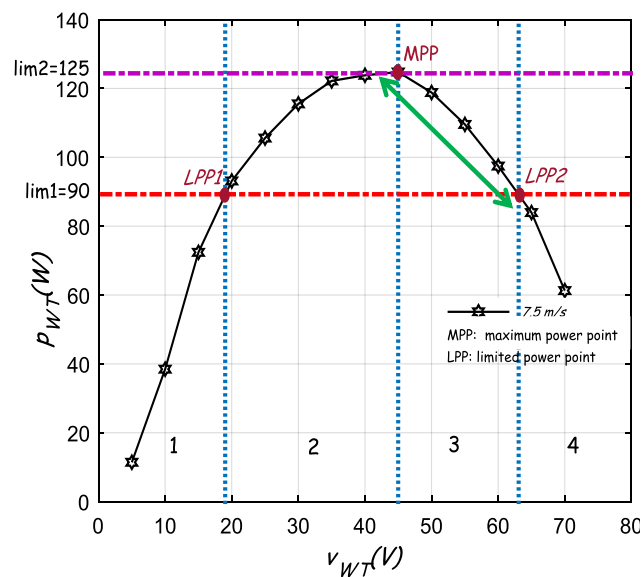


Figure 50. Power profile for the selected wind speed

The tests with a variation of step-sizes perturbation for each method were performed during the transition between LPP2 and MPP (Figure 51 and Figure 52). The performances (power p_{WT} and voltage v_{WT}) of all methodes differ according to the selected step size. In general, a larger step size induce a faster transient response with more power oscillations around the target and, hence, less efficiency. In constrast, a smaller step size enhances efficiency but reduces the convergence speed.

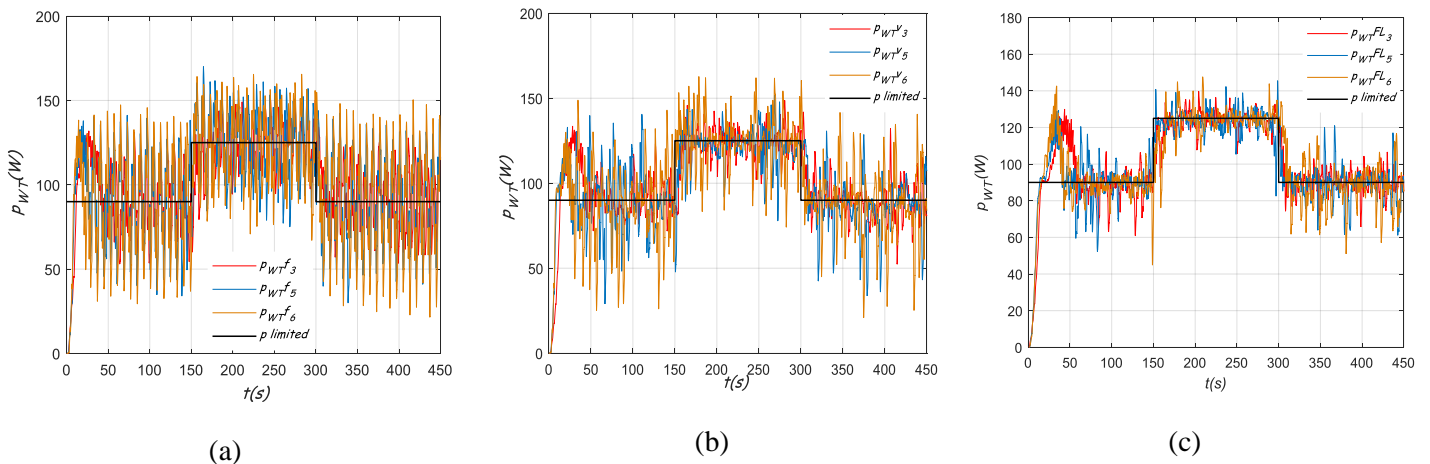


Figure 51. Evolution of p_{WT} while the transition between LPP2 and MPP for: a) Fixed step-size P&O; b) Newton's variable step-size P&O; c) FL's variable step-size P&O

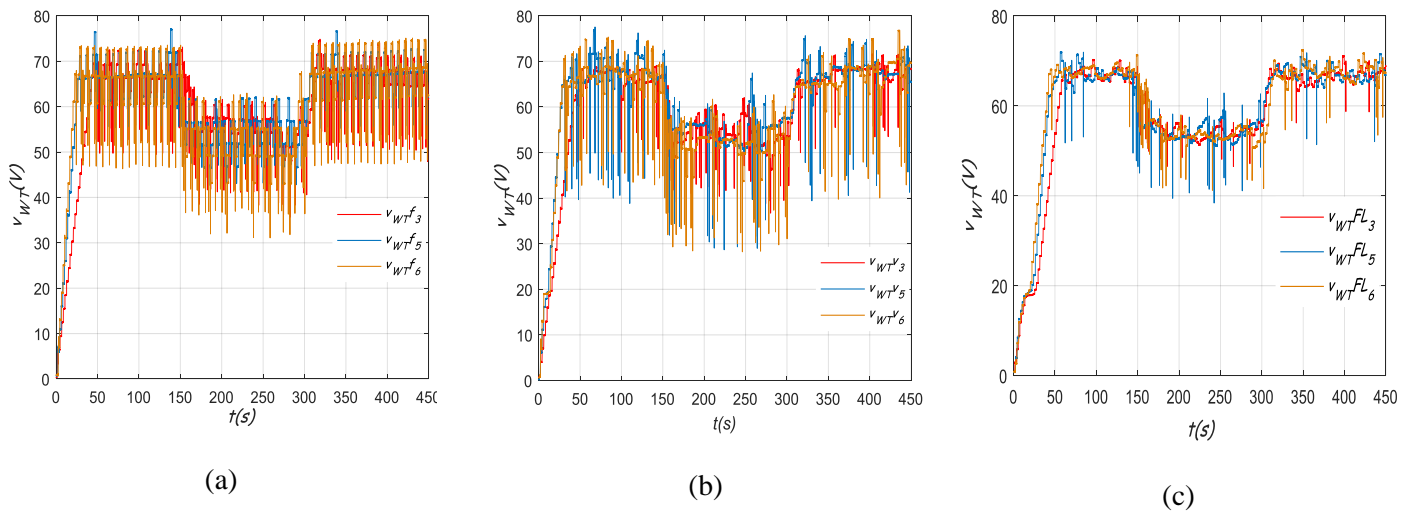


Figure 52. Evolution of v_{WT} while the transition between LPP2 and MPP for: a) Fixed step-size P&O; b) Newton's variable step-size P&O; c) FL's variable step-size P&O

Figure 53 shows the comparison of performances of these methods. The selected voltage perturbation step size for this example is 6V. Firstly, it can be observed in the Figure 53, that the system with all methods operates correctly during the transition between MPPT and LPPT. As remarked previously, the oscillation state differs according to the power control method. The FL method's power control (green line) has better dynamic performances with more steady oscillations during MPPT and LPPT transition compared to the fixed step size and Newton's methods. It means that the results of the fixed step size and Newton's methods show a huge power variation compared to the FL technique. This is in agreement with the results obtained during the tests of proposed methods for LPPT modes.

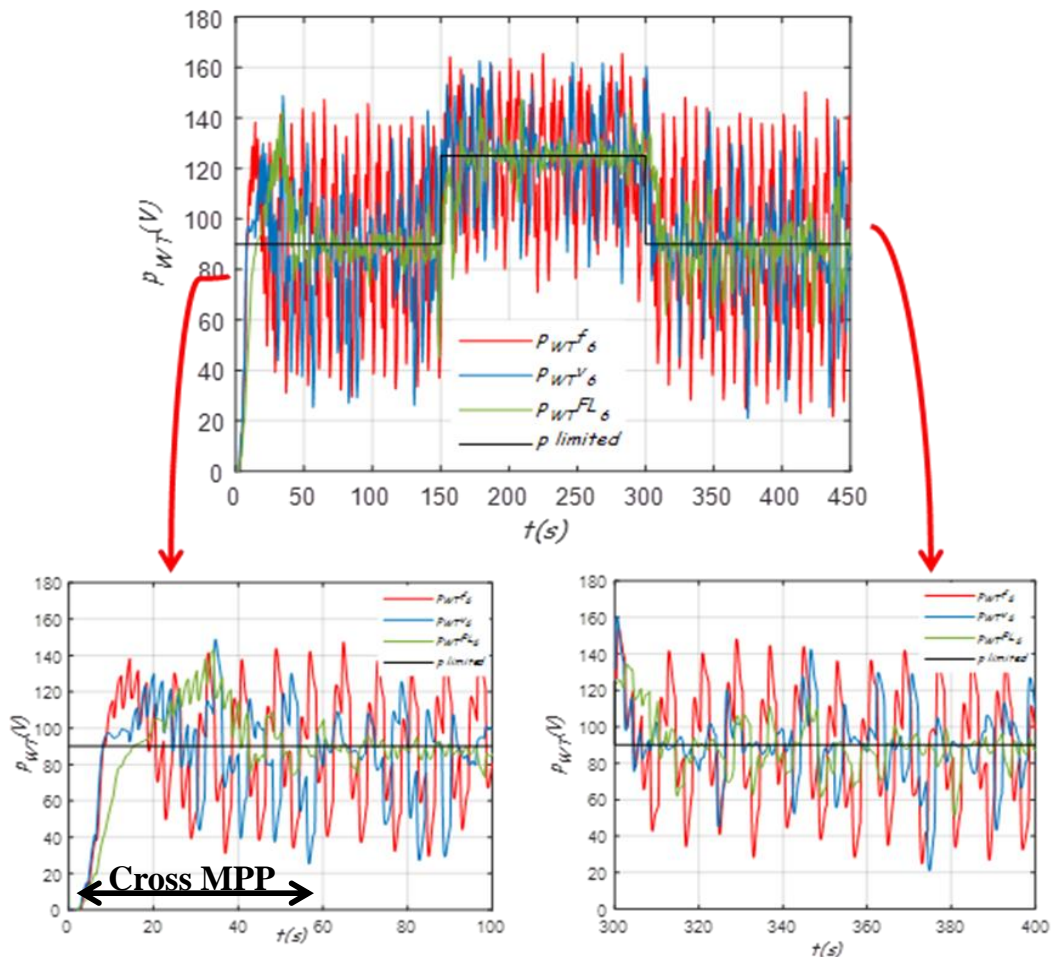


Figure 53. Comparison of experimental power results while the transition between LPP2 and MPP

II.6. Conclusion

In this study, the performances of LPPT control for a SSWT were investigated. Three different LPPT control power strategies for a SSWT were proposed and tested in order to compare their characteristics and study the effect of some sudden variations (i.e., power variation and weather condition change) on their performances. The proposed methods are the fixed step size, Newton's method and the FL technique. All these methods are based on the P&O principle. The results show that whatever method is used, the system operates correctly, reaches LPPs, and identifies the direction of the next perturbation. However, what changes are the performances of each method. At first, the results differ according to the perturbation step size used. Indeed, for the fixed step size and Newton's methods, a large step size contributes to a faster dynamic response but excessive steady-state oscillations, which result in a low efficiency. This situation is reversed when the LPPT is running with a smaller step size. Thus, the LPPT with a fixed step size and variable step size based on Newton's methods should make a satisfactory tradeoff between the dynamics and oscillations. Regarding the FL method, it has better dynamic performances with more steady oscillations compared to the fixed step size and Newton's methods. In addition, it is also clearly demonstrated that all methods react correctly during a sudden change of power

and wind speed. They change identically in terms of the response time. The FL technique stabilizes quickly compared to the fixed step size and Newton's methods, both in power increase or decrease and in rapid change of wind speed. This method is also interesting for the control of a SSWT in a DC MG. Indeed, it will guarantee less fluctuation in the generated power that can be injected into the public grid.

The next chapter will concern the integration of the SSWT in a DC MG with the adaptation of the proposed control strategies to the constraints linked to power and energy management. The main objective is to apply a supervisory system that can take into account the impact of adding a second RES, namely a SSWT, into the MG. The study focuses on the case of RESs excess power production by suggesting coefficients helping to well manage the energy and power flow and reducing the overall cost. **Equation Chapter (Next) Section 1**

Chapitre III. Integration of a small-scale wind turbine into the DC microgrid

III.1. Introduction

In recent years, providing energy by using fossil fuels has rapidly increased environmental pollution and global warming. In addition, a lack of pure and inexpensive energy is still felt due to the rising fuel cost and energy demand. In this context, RESs such as PV and WT have been introduced and developed to partially solve issues related to energy. Besides, to increase power supply efficiency and save costs, DERs based on RESs have also been proposed and studied. Nonetheless, increasing RESs power' cannot be directly exploited or entirely stored due to the intermitted power generation. This makes the management of the electrical network a critical issue. Therefore, the deployment of conventional and RESs alongside local loads in small-scale networks such as a MG is one of the newest aspects of electrical networks as well as a solution to solve the intermittency problem [164].

MG can be described as an integrated power system that functions in a small power range compared to the public grid. This electrical structure offers many benefits, such as stability, independence, and flexibility. It also guarantees economic advantages by reducing costs owing to the liberalized electricity market and decentralized power management [157]. Thanks to these MG characteristics, the power supply systems in the form of MG have been very studied in recent years. The research in the MG field has tackled different aspects such as power balance, and energy management by investigating defects and advantages [165]. The main objectives of all these research works are related to

the power flow distribution and the achievement of the lowest MG operating cost by keeping the power balance among every component, meeting load demand, and encouraging the use of RESs.

This chapter studies the impact of integrating a SSWT into a DC MG connected to the grid. Three points were approached. Firstly, an algorithm for both power control and power management for the studied DC MG considering the grid-connected mode is suggested. The constraints of all physical components of this MG have been taken into account. Secondly, in case of an excess in power produced by PV panels and WT, two types of coefficients called “shedding coefficients” are proposed to calculate the amount of power that should be limited from each RESs. Finally, two strategies for energy management, i.e, optimization, and storage priority (without optimization), are considered during the simulation.

This chapter is organized as follows: a literature review about power and energy management is provided in section 2. The DC MG modeling is presented in section 3. The supervision overview, including power control and energy management, is described in section 4. Shedding coefficients are proposed and detailed in section 5. The performance of the proposed coefficients is verified using simulation, and the results and analysis are discussed in section 6. The conclusions are given in section 7.

III.2. Literature review

Researchers have made remarkable efforts to increase environmental protection to overcome the fast depletion of fossil fuels and the energy crisis. In this context, RESs have been deployed in the power system to meet the energy demand and respond to environmental issues. Thus, MGs are introduced as a new electrical structure to combine DERs, ESSs, and loads. However, despite the significant growth of the MG concept, its architectures and control system are still novel and under continuous development.

Some problems such as the intermittence of PV and WT power generation, the physical constraints related to the components, the uncertainty of the power prediction, the overall operating cost, etc have to be considered while designing a MG. In this regard, a supervisory system including a power and energy management system is crucial for the optimal exploitation of DERs in secure, reliable, and intelligent ways. It is based on the collection and communication of the information, a system for power prediction, an economic dispatch system, and the needs of the end-users. The main goal is to meet load demand at the lowest operating cost by managing the power flow in real-time, improving power quality, optimizing a long-term energy schedule, raising the use of renewable energy, and smoothing power fluctuations from RESs.

In aMG, economic dispatch optimization and power management systems are always considered to minimize power losses and simplify the control process. The energy management system (EMS) for a MG can be described as a multi-objective system that optimizes the economic dispatch, operation, energy scheduling, system reliability, and the global cost of the system for both grid-connected and islanded

modes [166]. Several studies in the literature suggest different energy management strategies to achieve an optimal and efficient operation of the MG. Many classifications may exist for the common methods used for the EMS. Strategies such as rule-based and optimization-based EMS have been suggested. Yet, a combination of different methods could be a practical solution for EMS. In general, EMS techniques can be classified into two major categories, i.e., classical and artificial intelligence (AI) methods, as shown in Figure 54.

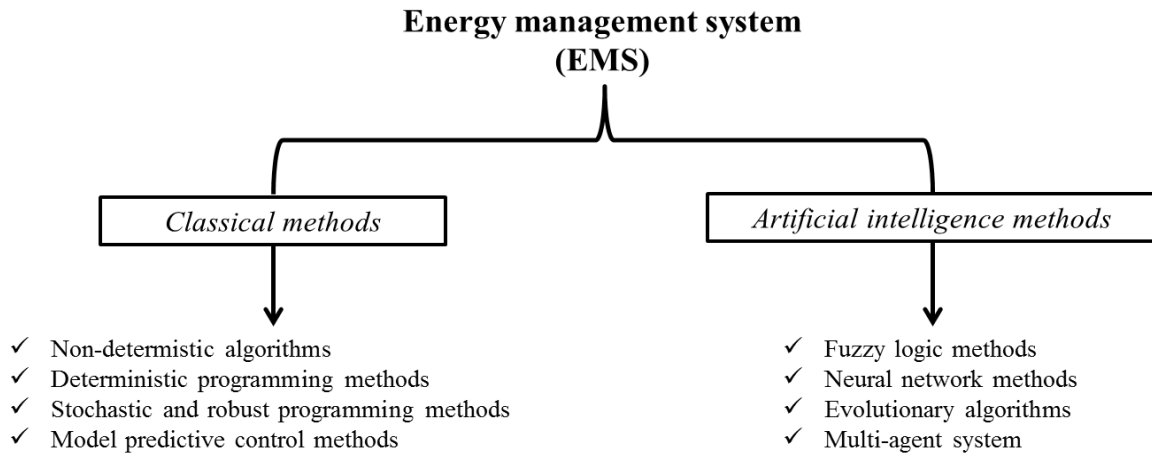


Figure 54. Proposed classifications of energy management strategies (adapted from [72])

The iterative non-deterministic algorithm is one of the classical methods used for executing the EMS. It can be utilized to realize several design objective functions, such as the single objective optimization (SOO) or the multi-objective optimization (MOO), which can be optimized. If a SOO approach was adopted by the designer, it means that a single-objective is optimized during the process of the optimization and can also be extended to many non-conflicting objectives. However, once multiple, conflicting objectives need to be optimized simultaneously, SOO deteriorates some objectives to achieve only one. In such a case, MOO makes a trade-off and provides the best values of all objectives. Many works of using iterative algorithms for the exploitation of RESs were found in the literature [167]–[169]. The authors of [170] proposed an SO optimal sizing algorithm for an islanded MG. This approach performs energy management in terms of determining the optimal components sizing for the studied MG. Some criteria such as the battery SOC and the power balance between demand and supply were analyzed to evaluate the system reliability. The authors of [171] highlighted another example of the SOO algorithm, applied to study the techno-economical feasibility of a stand-alone hybrid PV-WT-FC–battery storage (BS) system. The main interest is reducing the system’s total cost in four regions in Iran with a steady demand of 10kW.

Most studies about deterministic optimization in the literature employ a forecasting algorithm to predict future energy pricing, load profile and power generation from RESs. Authors of [172] proposed an optimization technique based on linear programming (LP) for sizing and simulating a stand-alone hybrid PV-WT-BS system located in rural areas in favor of reducing the total cost by measuring power supply probability losses. A novel optimization methodology that also used LP was suggested in [173]. It aims to

solve the optimal scheduling problem of DERs containing BS systems to ensure economic benefits and peak-shaving. Mixed-integer linear programming (MILP) is another deterministic method that is used by several authors for MG EMS. It takes advantage of its ability to use integer and binary variables to decide on the operation system. In [174], researchers highlighted and designed an EMS model through a MILP optimization for residential MG system. It is constituted by PV panels, which its power was forecasted by NN method, thermal storage, and batteries, which were realized by load management. The conclusion placed the batteries as an uncompetitive element in the case of residential applications because of their high investment and replacement cost in the residential market.

As mentioned before, most EMS dispatch algorithms based on deterministic methods depend on forecasting algorithms and are assumed to be 100% accurate over the future dispatching interval [175]–[179]. Nonetheless, these deterministic approaches did not take into account the effects of forecasting errors which can provide a sub-optimal dispatch solution. In the wind energy market, for example, it has been found that even some of the best forecasting algorithms available on the market are subject to standard deviations ranging from 10 to 20% [180], [181]. To overcome these errors, some solutions were suggested in the literature. In this work, the authors [182] proposed to solve the problem by implementing a second dispatching algorithm to the ideal forecast scheduler to adjust the real-time dispatch and take into consideration the forecasting errors.

Many authors have suggested stochastic economic dispatch techniques to deal with constrained optimization with uncertainty in the MG system. The MG is characterized by an increasing number of variable and volatile generation sources under fluctuating energy markets. A two-stage stochastic optimization model was presented by several authors. In [183] an optimization built on two stages for the MG operation, with consideration of load demand and uncertainties of RESs, was presented. The first stage performs the optimization based on the investment cost of the MG and the second stage attempts to deal with the energy management operation of the MG. Another two-stage stochastic optimization was proposed in [184], where the economic dispatch in the first stage was associated with the expected forecast, and the second stage attempts to mitigate any discrepancies by reacting to the deviations as they occur. Although many stochastic methods perform favorably compared to deterministic approaches, their solutions still require a high level of complexity in the formulation.

Model predictive control (MPC) is very suitable for defining EMS and is widely used to decrease the daily cost and emission of the MG by taking into account the physical limits and technical constraints in real operation cases. Many authors tackle the EMS strategies based on the MPC approach [185], [186]. [187], for example, presents an MPC approach that considers the uncertainties associated with renewables and electricity demand. Smart loads were used to perform an efficient operation and a supervised NN was applied to estimate the controllable residential load. In another study presented in [186], the MPC-based EMS was suggested to ensure better utilization of the battery during peak load demand. Moreover, this study aims to maximize the use of wind power generation to meet the local demand and then reduce the cost induced by the energy trading with the public grid. The authors concluded that this power-sharing

helps to establish a fault-tolerant scheme that facilitates the MG operation during sudden failures of WTs or power supply shortages. The most remarkable about this method is the ability to predict the deterioration of the grid elements, mainly storage systems.

Several recent studies have focused on utilizing AI methods for performing the EMS for the MGs. These approaches could be applied to solve both SOO and MOO problems. Firstly, the FL technique is an artificial method commonly used for EMS in both grid-connected and stand-alone energy systems. Researchers in [188] discuss an EMS based on fuzzy control for a DC MG. The study focuses firstly on modeling MG components, i.e., the DERs and storage devices. Secondly, the FLC supervises the SOC of the battery to guarantee its long life and reduce the global system cost. In [188], the authors enumerate the advantages of the FL-based EMS over other methods by comparing the response capability and the ease to be adapted to sudden changes during the period of operation. The study was about a FL-based EMS that was used for a residential system and contained PV, WTs, a FC system, and batteries. The FLC was responsible for regulating the power flow while keeping the battery SOC at the desired value. Secondly, the NN in another intelligent approach widely used for control and energy management in MG systems. It is able to handle complex–non linear system in a reliable way. [188] presents a control strategy for a multi-energy common DC hybrid power system. The model developed by the authors is about an hourly forecast of PV and wind renewable energy systems, and to accelerate the convergence and to prevent oscillation, the control strategy is based on a NN approach. Results showed that this strategy can keep the voltage stable and continuous during the maximum use of RESs, which can be satisfied to consumers' electricity needs. Other studies based on NN approaches to optimize the economic dispatch could be found in [189], [190]. Thirdly, evolutionary algorithms, inspired initially by biological evolution, constituted another subfield of AI. Genetic algorithm (GA) is one of the popular algorithms in this category. In several studies [191]–[193], GA was used thanks to its powerful optimization capacity. An interesting study was conducted in [191] where authors applied a GA algorithm in four different residential zones in India for an optimal sizing of RESs associated with ESS. Results showed that a combination of PV, WT, and BSs guarantee the most cost-effective solution for residential applications. Other algorithms such as fruit fly optimization [194], ant colony optimization [195], and particle swarm optimization [196] are also used to solve the non-linear optimization problems. Finally, a multi-agent system (MAS) is composed of several intelligent agents designed and integrated into different sources and loads. They cooperated to solve the problem of controlling energy consumption and reach an optimal operating strategy for the EMS. [197] and [198] suggested a MAS-based EMS for monitoring and efficient operation of a grid-connected residential (home/buildings) MG system with various RESs, controllable loads, and ESS. The purposes of the proposed method were to minimize the operational cost while satisfying the consumer's comfort and meeting the system's objectives and related constraints.

Therefore for control purposes, it is necessary within a MG, that an EMS has a connection with a power management strategy to achieve the goals of the supervision.

The power in a MG should be well distributed to keep the power balanced among every component. For this purpose, power management, including source, storage, and load management, should be considered. The intermittency related to power generated by RESs makes its usage and control necessary and more difficult. Thus, the authors of [199] suggested an optimal power scheduling of PV-WT-FC-diesel generator (DG)-battery-based MG to stable the frequency and overcome voltage fluctuations that may occur in the system. Therefore, storage devices can be the most viable option to handle the intermittent issues of RESs. In this context, batteries with different ratings used for storage and connected to the grid (to sell/buy power from the MG) are termed as a distributed energy storage system. The optimal power management of this MG emphasizes the control of the charging and discharging rates of the individual battery by using a droop-based controller. The power in the MG is distributed among the various charging stations (CSs) that distribute in their turn the power among the individual batteries by using a droop participation factor. Thus, the batteries' charging and discharging rates are controlled to reach the desired power flow between the CSs and MG. Another control and power management system for PV-battery-based hybrid MGs is suggested in [200] to regulate the DC and AC bus voltages and frequency under different operating circumstances. Yet, the battery here is considered limited in terms of capacity, charging, and discharging current. Then, the public grid is presented as an important power exchanges interface to complete the battery functions and provide a low-cost operation. In [201], the authors propose a new control algorithm for effective power management in DC MG with RESs and ESS. The purpose is to overcome the average power-sharing and bus voltage regulation problems and maximize the utilization of source power. The control scheme treats the additional power available beyond its average rated value as a virtual generation. Thus, new references are generated considering virtual generation. This proposed algorithm allows using the virtual generation in operation to reduce the charging/discharging cycles of ESS. Hence, it increases the life span of the ESS, reduces power fluctuations, and regulates the system bus voltage. Reference [202] presents a battery energy management system for a MG, in which PVs and DG are the primary sources of electricity; the novelty of the proposed battery EMS lies within the energy management of multiple types of batteries' characteristics and the reduction of the DGs' operating hours simultaneously. In this work [203], a distributed robust energy management scheme for multiple interconnected MGs is developed. It aims to optimize the total operational cost of the MGs through energy trading with neighboring MGs and the main grid in the real-time energy market. To keep consistent with the distributed nature of the multiple MGs, a distributed adjustable robust optimal scheduling algorithm is suggested. Each MG energy management system determines its own selling price and operation schedule via distributed communication of noncritical information with its neighboring MGs. Robust optimal scheduling and fair energy trading can be collectively achieved.

III.3. DC MG modeling with the integration of a SSWT

III.3.1. MG system and power balance

A MG consists of multiple sources and storages, and a real-time power controller that achieves different users' load demands and controls the instantaneous power balance.

The proposed DC MG (Figure 55) is composed of its supervisory system, which consists mainly of an energy management layer and a power management layer. The aim of power management is to control the real-time power flow for reaching power balance, while the objective of energy management is to optimize the energy cost by dispatching power sources according to the PV, WT and load power predictions and measurement data under the constraints of every physical component.

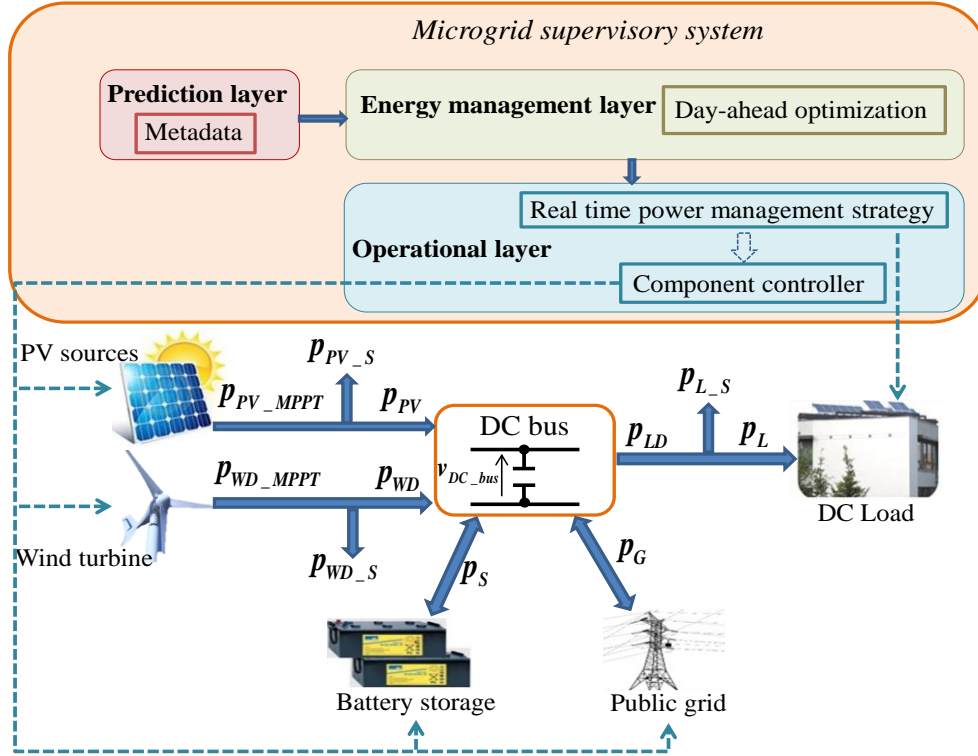


Figure 55. DC MG structure

In order to keep the power balance and to stabilize the DC-bus voltage, a proportional (P) controller is used to calculate the amount of power that should be compensated by the public grid and storage. This power balance neglects the power loss in the conversion and is expressed in the steady-state as:

$$P_{ref} = P_{PV} + P_{WD} - P_L - P_P = P_S + P_G \quad \{3.1\}$$

Where p_{ref} is the compensation power, p_{PV} is the power of PV sources, p_{WD} is the power of the WT, p_L is the DC load power, p_P is the system dynamic power for the P controller, p_G is the public grid power, and p_S is the storage power. p_P can be expressed as follows:

$$p_P = K_P (V_{DC_{ref}} - v_{DC_{bus}}) \quad \{3.2\}$$

Where K_P is the proportional gain of the P controller and $v_{DC_{bus}}$ is the common DC-bus voltage that should be kept at the reference voltage noted by $V_{DC_{ref}}$.

III.3.2. PV sources

Many approaches for modeling PV arrays have been suggested in the literature [204][205]. In this study, a mathematical model based on an experimental comparison of PV panel operating cell temperature was used [206]. To maximize the economic and energetic benefits, the PV model should generate maximal power by using an MPPT method. When the PV power is greater than the needs of the MG, a limited control [207] should occur to operate PV shedding and protect MG devices. The PV power is expressed by {3.3}:

$$P_{PV} = P_{PV_MPPT} - P_{PV_S} \quad \{3.3\}$$

Where P_{PV_MPPT} is the MPPT PV power and P_{PV_S} is the shedding power of PV.

III.3.3. Wind turbine

The WT power is calculated at maximal value (P_{WD_MPPT}) by using the MPPT strategy. Parameters of the mathematical model can be defined by using experimental tests for the studied WT (see I.4.4.2.1). P_{WD_S} is the power that should be subtracted in case of a surplus of production. Many limited power control strategies were suggested in Chapitre II. The WT power is then expressed by {3.4}:

$$P_{WD} = P_{WD_MPPT} - P_{WD_S} \quad \{3.4\}$$

Where P_{WD_MPPT} is the MPPT WT power and P_{WD_S} is the shedding power of the WT.

III.3.4. Public grid connection

The public grid is a complex and larger electricity delivery system. It can be connected to a MG in order to be used as a source that can supply and absorb power. For that, some power limitations must be taken into account for protection reasons. Thus, the public grid power P_G is limited as in {3.5}:

$$-P_{G_MAX} \leq P_G(t) \leq P_{G_MAX} \quad \{3.5\}$$

Where P_{G_MAX} is the maximum power that the public grid can buy or the limit for grid power injection P_{GI_MAX} , $-P_{G_MAX}$ is the maximum power that the public can sell or the limit for grid power supply P_{GS_MAX} . These limits are imposed by SG messages in order to solve some problems such as performing peak shaving and avoiding undesired injection, etc.

During DC MG operation, the grid should be controlled as:

$$0 \leq p_{G_I}(t) \leq P_{GI_MAX} \quad \{3.6\}$$

$$0 \leq p_{G_S}(t) \leq P_{GS_MAX} \quad \{3.7\}$$

III.3.5. Storage system

The battery storage can charge and discharge power to keep the MG power balance. The soc is calculated according to {3.8}, where soc_0 is the initial state of charge of the storage, C_{REF} is the battery capacity, v_s is the storage voltage, and soc is limited between SOC_{MIN} and SOC_{MAX} in {3.9}. The storage charging and discharging powers are limited by P_{S_MAX} and $-P_{S_MAX}$ respectively, as in {3.10}.

$$soc(t) = soc_0 + \frac{100\%}{3600C_{REF}v_s} \int_{t_0}^{t_f} p_s(t)dt = soc_0 + \frac{100\%}{3600C_{REF}v_s} \int_{t_0}^{t_f} (p_{s_c}(t) - p_{s_d}(t))dt \quad \{3.8\}$$

$$SOC_{MIN} \leq soc(t) \leq SOC_{MAX} \quad \{3.9\}$$

$$-P_{S_MAX} \leq p_s(t) \leq P_{S_MAX} \quad \{3.10\}$$

III.3.6. DC load

The DC load is the electrical appliances of a building, in which a load shedding real-time optimization [208], [209] is applied. The problem is formulated and solved by MILP in IBM CPLEX [20]. The load power defined the needs of the end-users that have to be satisfied. However, if the load power cannot be fully met, the load must be partially shed. The load power p_L and the load shedding power p_{L_S} are given respectively by {3.11} and {3.12}, where p_{L_OPT} is the load power after the load real-time optimization, p_{AVAIL} is the total available DC MG power, and p_{L_D} is the load demand power.

$$p_L = \begin{cases} p_{L_OPT} & \text{if } p_{AVAIL} < p_{L_D} \\ p_{L_D} & \text{if } p_{AVAIL} \geq p_{L_D} \end{cases} \quad \{3.11\}$$

$$p_{L_S} = p_{L_D} - p_L \quad \{3.12\}$$

III.4. MG supervision overview

The proposed multi-layer supervisory system (Figure 56) [86] is structured into four main layers that interact between them and operate in different scale time. The aim of the MG supervisory is to interact with the SG and the end-user. It is able to receive metadata from external sources, and keep the

instantaneous power balance in the MG. Several works carried out in the AVENUES laboratory have been based on this structure [6], [84]–[86], [210], [211].

Parameters refer to a group of parameters related to the MG and their physical limitations. The metadata receives the forecast data. The SG is responsible of exchanging messages and communication with the public grid. Characteristics of each layer have been explained in details in I.3.7.

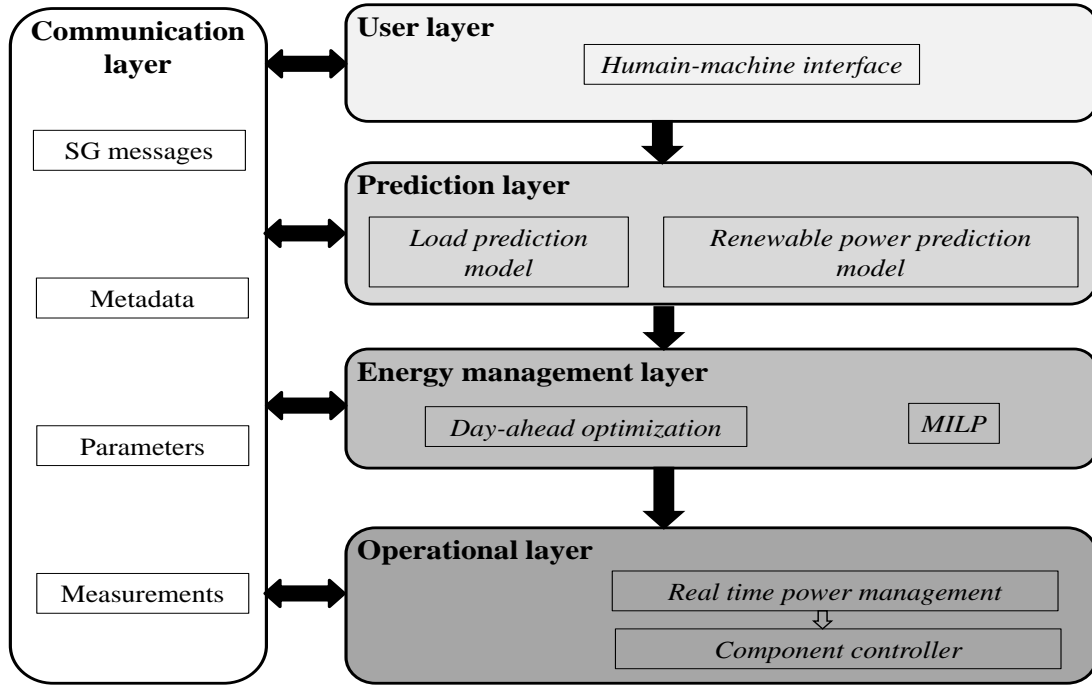


Figure 56. The details of the MG multi-layer supervisory concept

III.4.1. Energy management

The energy management layer aims to optimize and minimize the total energy cost by dispatching power flow according to the power prediction, SG messages, and measurement data under the constraints of the modeling. In this section, optimization for a grid-connected mode is studied.

MILP is chosen as a solver for the formulated problem, and the optimization is performed day-ahead by using prediction data. The optimization results are the power flows of sources and load translated into a distribution coefficient. This latter is regarded as a predictive control variable responsible for communication with the operational layer to ensure an optimal operation.

The proposed problem formulation is based on the components characteristics and constraints already presented on {3.2} {3.3} {3.4} {3.5} {3.6} {3.7} {3.8} {3.9} {3.10} {3.11} {3.12}. The stability of the DC bus voltage is then ensured by the power balance constraint presented in {3.13}. The controller dynamic considered for the MG is not used in this study.

$$p_{PV}(t) + p_{WD}(t) - p_L(t) = p_S(t) + p_G(t) \quad \{3.13\}$$

The total cost result of the optimization is expressed in {3.14}:

$$C_{TOTAL} = C_{PV_S} + C_{WD_S} + C_{L_S} + C_S + C_G \quad \{3.14\}$$

Where C_{PV_S} is the PV shedding energy cost, C_{WD_S} is the WT shedding energy cost, C_{L_S} is the load shedding energy cost, and C_S is the storage energy cost, C_G is the public grid energy cost.

The tariffs C_{PV_S} and C_{WD_S} are calculated in {3.15} and {3.16} according to the amount of PV and WT shedding power.

$$C_{PV_S} = \frac{1}{3.6 \times 10^6} \sum_{t_i=t_0}^{t_F} c_{PVS}(t_i) \cdot \Delta t \cdot p_{PV_S}(t_i) \quad \{3.15\}$$

$$C_{WD_S} = \frac{1}{3.6 \times 10^6} \sum_{t_i=t_0}^{t_F} c_{WDS}(t_i) \cdot \Delta t \cdot p_{WD_S}(t_i) \quad \{3.16\}$$

The cost of load shedding is defined in {3.17}, and it introduces inconvenience for end-users:

$$C_{LS} = \frac{1}{3.6 \times 10^6} \sum_{t_i=t_0}^{t_F} c_{LS}(t_i) \cdot \Delta t \cdot p_{L_S}(t_i) \quad \{3.17\}$$

The grid cost is defined in {3.18}, and it shows that the grid power could be bought or sold at the same price

$$C_G = \frac{1}{3.6 \times 10^6} \sum_{t_i=t_0}^{t_F} c_G(t_i) \cdot \Delta t \cdot (-p_{G_I}(t_i) + p_{G_S}(t_i)) \quad \{3.18\}$$

Where p_{G_I} and p_{G_S} are respectively the power grid and supply.

This study takes into consideration a single rate for energy purchased or sold and the grid energy tariff is defined according to peak hour (c_{PH}) or normal hour (c_{NH}).

The storage cost is provided in {3.19}, and it is based on storage aging:

$$C_S = \frac{1}{3.6 \times 10^6} \sum_{t_i=t_0}^{t_F} c_S(t_i) \cdot \Delta t \cdot (p_{S_C}(t_i) + p_{S_D}(t_i)) \quad \{3.19\}$$

Where p_{S_C} and p_{S_D} are respectively the storage power charge and discharge.

This optimization is considered under the following constraints:

Minimize:

$$C_{TOTAL} = C_{PV_S} + C_{WD_S} + C_{L_S} + C_S + C_G \quad \{3.20\}$$

With respect to:

$$\left\{ \begin{array}{l}
p_{PV}(t_i) + p_{WD}(t_i) + p_{S_D}(t_i) + p_{G_S}(t_i) = p_L(t_i) + p_{S_C}(t_i) + p_{G_I}(t_i) \\
p_S(t_i) = p_{S_C}(t_i) + p_{S_D}(t_i) \\
p_{PV} = p_{PV_MPPT} - p_{PV_S} \\
p_{WD} = p_{WD_MPPT} - p_{WD_S} \\
p_L = p_{LD} - p_{L_S} \\
\text{if } p_{PV_MPPT}(t_i) + p_{WD_MPPT}(t_i) > p_{LD} \text{ then } p_{L_S}(t_i) = 0 \\
\text{if } p_{PV_MPPT}(t_i) + p_{WD_MPPT}(t_i) = 0 \text{ then } \begin{cases} p_{L_S}(t_i) = 0 \\ p_{PV_S}(t_i) = 0 \\ p_{WD_S}(t_i) = 0 \end{cases} \\
\text{if } p_{PV_MPPT}(t_i) + p_{WD_MPPT}(t_i) < 0 \text{ then } \begin{cases} p_{PV_S}(t_i) = 0 \\ p_{WD_S}(t_i) = 0 \end{cases} \\
SOC_{MIN} \leq soc(t_i) \leq SOC_{MAX} \\
soc(t_i) = soc_0 + \frac{100\%}{3600C_{REF}V_S} \int_{t_0}^{t_f} p_S(t) dt \\
SOC(t_f) > SOC_f \\
p_{PV}(t_i) \geq 0 \\
p_{WD}(t_i) \geq 0 \\
p_L(t_i) \geq 0 \\
p_{PV_S}(t_i) \geq 0 \\
p_{WD_S}(t_i) \geq 0 \\
p_{L_S}(t_i) \geq 0 \\
-P_{S_MAX} \leq p_S(t) \leq P_{S_MAX} \\
0 \leq p_{G_I}(t) \leq P_{GI_MAX} \\
0 \leq p_{G_S}(t) \leq P_{GS_MAX} \\
t_i = \{t_0, t_0 + \Delta t, t_0 + 2\Delta t, \dots, t_F\}
\end{array} \right. \quad \{3.21\}$$

All these constraints have been explained in section III.3.1. The three constraints preceded by “if” show that no load shedding power is allowed when the load can be fully supplied, while no PV and WT shedding power could occur when the PV and WT power can be fully consumed. Moreover, neither load shedding nor RESs power shedding could happen when there is no production from PV and WT.

Additional constraints are given in {3.22}:

$$\left\{ \begin{array}{l}
\text{if } p_{PV_MPPT}(t_i) + p_{WD_MPPT}(t_i) \geq p_{L_D}(t_i) \text{ then } \begin{cases} p_G(t_i) \geq 0 \\ p_S(t_i) \geq 0 \end{cases} \\
\text{if } p_{PV_MPPT}(t_i) + p_{WD_MPPT}(t_i) < p_{L_D}(t_i) \text{ and then } \begin{cases} p_G(t_i) < 0 \\ p_S(t_i) < 0 \end{cases}
\end{array} \right. \quad \{3.22\}$$

The additional constraints show that the storage and the grid cannot directly exchange power. The coefficient k_D is given to introduce the day-ahead optimization results into the power management layer and to decouple the system operation between the power management layer and the energy management layer. It is calculated according to {3.23}:

$$k_D = \frac{P_s}{P_s + P_G}, k_D \in [0, 1] \quad \{3.23\}$$

Where k_D is the power distribution rate between storage and public grid.

III.4.2. Power management

The power management is performed in the operational layer that is responsible for keeping the instant power balance and ensuring the DC bus voltage stabilization concerning the system's constraints and physical limits. The applied algorithm started first by reading the fixed parameters, the real measurements, and the updated parameter value provided from the optimization. Secondly, the compensation power is calculated according to the {3.1}. Using the resulting power and the distribution parameter, the power that should be exchanged with the public grid and the storage is calculated to ensure power balance and voltage stability. The suggested power management strategy is a rule-based method. It is presented in the flow chart given in Figure 57

The k_D is calculated in the energy management and introduced in the real-time power management strategy. As illustrated in the flow chart, the storage reference is updated two times: the first one is for power balancing before that the grid reaches its limits. Once this latter occurs a second update of the storage reference is happened to perform load shedding or PV and WT constrained production.

Furthermore, the proposed power management strategy consists of two extreme cases: i) if there is shortage energy for supplying load, which means that PV panels and WT produce an insufficient power, the grid reaches its limit and the storage is empty. In this case load shedding happened. ii) if the PV panels and WT power production cannot be totally consumed, which means that the grid reaches its injection limit, the storage achieves the *SoC* upper limit, and the load is fully supplied or cannot consume enough, the PV and WT energy should be limited.

To separate and calculate the power which must be limited from each source, two coefficients called "shedding coefficients" have been proposed. The idea is to first calculate the total power which must be shed from the two sources and multiply it respectively by the shedding coefficients in order to define the power which must be shed by each source.

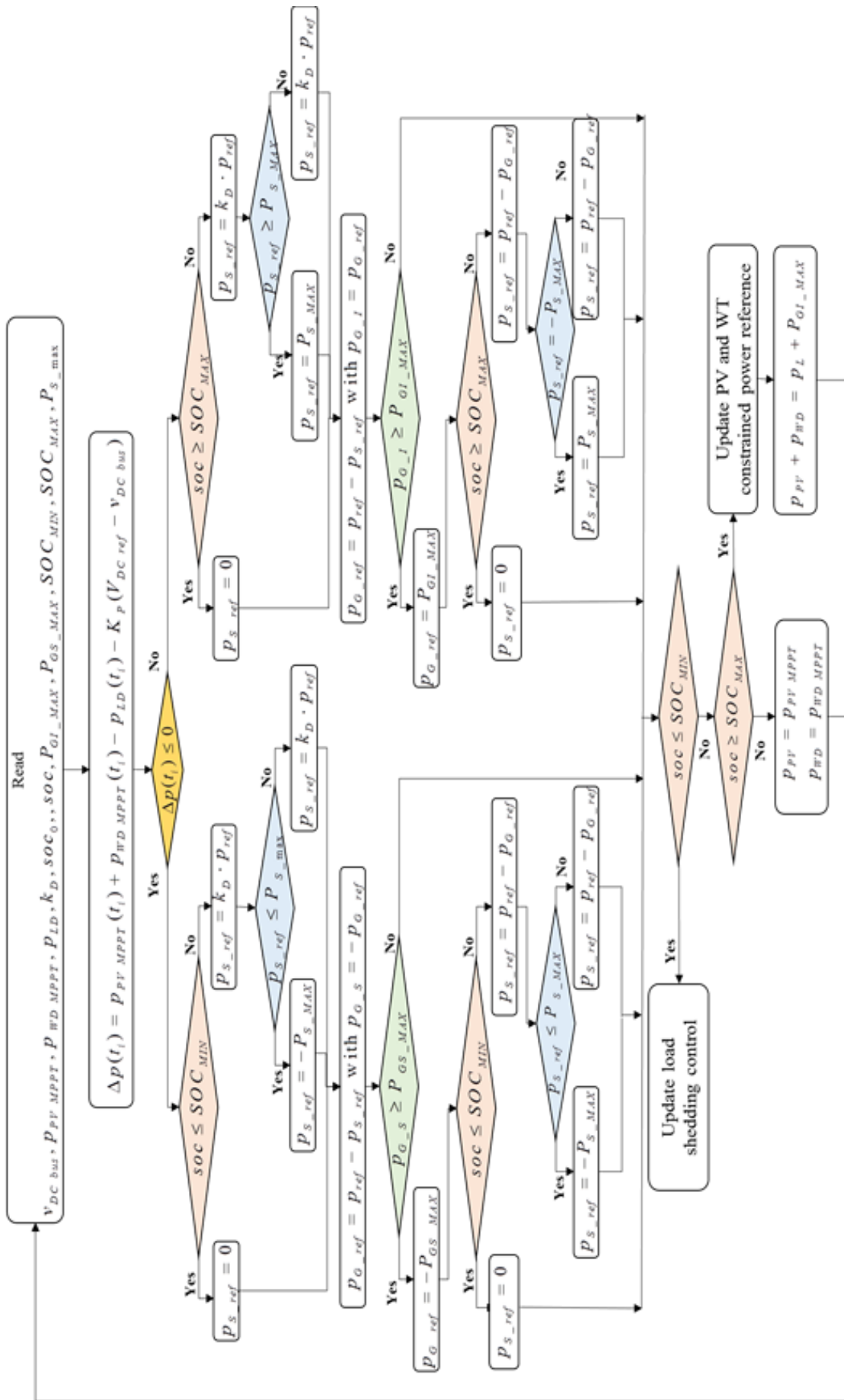


Figure 57. Flowchart of power management of the DC MG in power management layer

III.5. Shedding coefficient

After installation of PV sources and WT, only the maintenance involves costs while the production does not need extra fees. However, shedding PV and WT power represent that the assets are not fully used. So the PV sources and WT powers shedding are penalized in the optimization and their costs are already defined in {3.15} and {3.16}.

The total renewable power to be shed is defined as follows:

$$P_{REN_SHEDD} = P_{PV_S} + P_{WD_S} = P_{PV_MPPT} + P_{WD_MPPT} - (P_{L_D} + P_S + P_G) \quad \{3.24\}$$

The role of the shedding coefficients related to the RESs was not emphasized or even noticed in the case where the renewable production was completely consumed. In this case, the two renewable sources (PV sources and WT) were considered as one renewable source and their production was mainly destined to feed the load and the rest to be stored in batteries or injected into the public grid (depending on the adopted power management strategy). Once the production of these RESs exceeds the needs of the MG, namely the limit of injection into the grid, limits of storage, and the load that is fully supplied, the power generation from PV sources and WT must be limited. The shedding coefficients embody the principle of separation of the two sources and the calculation of the power that must be limited from each source by taking into account different criteria such as the share of each source in this excess generation and the shedding cost attributed to each source.

III.5.1. Alpha coefficient

Alpha coefficients are proposed in order to calculate p_{PV_S} and p_{WD_S} . They are based on the contribution of each renewable source in generating P_{REN_SHEDD} without taking into account the PV sources and WT shedding costs. Thus, the source that generates more and is responsible for the excess of power should be more limited. Here, the penalization cost associated with each source is not considered. Their expressions showed the percentage of the contribution of each source in generating the total power that should be shed and they are calculated as follows:

$$\alpha_{PV} = \frac{P_{PV_MPPT}}{P_{PV_MPPT} + P_{WD_MPPT}}, \alpha_{PV} \in [0, 1] \quad \{3.25\}$$

$$\alpha_{WD} = \frac{P_{WD_MPPT}}{P_{PV_MPPT} + P_{WD_MPPT}}, \alpha_{WD} \in [0, 1] \quad \{3.26\}$$

$$\alpha_{PV} + \alpha_{WD} = 1 \quad \{3.27\}$$

The PV and WT shed powers are then given in {3.28} and {3.29} respectively:

$$P_{PV_S} = \alpha_{PV} \cdot P_{REN_SHEDD} \quad \{3.28\}$$

$$P_{WD_S} = \alpha_{WD} \cdot P_{REN_SHEDD} \quad \{3.29\}$$

III.5.2. Gamma coefficient

Gamma coefficients are proposed in order to calculate p_{PV_S} and p_{WD_S} . They are based not only on the contribution of each RESs in generating p_{REN_SHEDD} but also on the PV sources and WT shedding costs. In fact, the percentage already calculated based on the coefficient α is added to another coefficient called ξ . This latter reflects the impact of the shedding cost of each RESs on the global contribution of each source in generating the total power that should be shed. They are calculated as follows:

$$\gamma_{PV} = \alpha_{PV} + \xi_{PV} = \frac{P_{PV_MPPT}}{P_{PV_MPPT} + P_{WD_MPPT}} + \frac{c_{WD_S} - c_{PV_S}}{\max(c_{PV_S}, c_{WD_S})} \quad \{3.30\}$$

$$\gamma_{WD} = \alpha_{WD} + \xi_{WD} = \frac{P_{WD_MPPT}}{P_{PV_MPPT} + P_{WD_MPPT}} + \frac{c_{PV_S} - c_{WD_S}}{\max(c_{PV_S}, c_{WD_S})} \quad \{3.31\}$$

$$\gamma_{PV} + \gamma_{WD} = 1 \quad \{3.32\}$$

Where $\xi_{PV} = \frac{c_{WD_S} - c_{PV_S}}{\max(c_{PV_S}, c_{WD_S})}$ and $\xi_{WD} = \frac{c_{PV_S} - c_{WD_S}}{\max(c_{PV_S}, c_{WD_S})}$ are two coefficients that take into

account the costs of shedding PV and WT powers respectively.

III.6. Simulation results and analysis

III.6.1. Power profile

In order to study the shedding coefficients, arbitrary power curves were selected (Figure 58). As it can be seen, the maximum power provided by the WT was limited and fixed to 500W, which is the maximal limit of the studied SSWT. The load power curve was fixed at 1000W. The PV power curve is calculated according to the weather data recorded on the 29th of June 2019 in Compiègne. In addition, the selected simulation time horizon is from 07:00 until 20:00. During this period, the DC MG operates only in on-grid mode.

It should know that the choice of such power profiles is to analyze the optimization of the DC MG in the case of production excess. In the opposite case, PV sources and WT are considered as a single source of renewable energy since the amount of power that they produce is completely consumed.

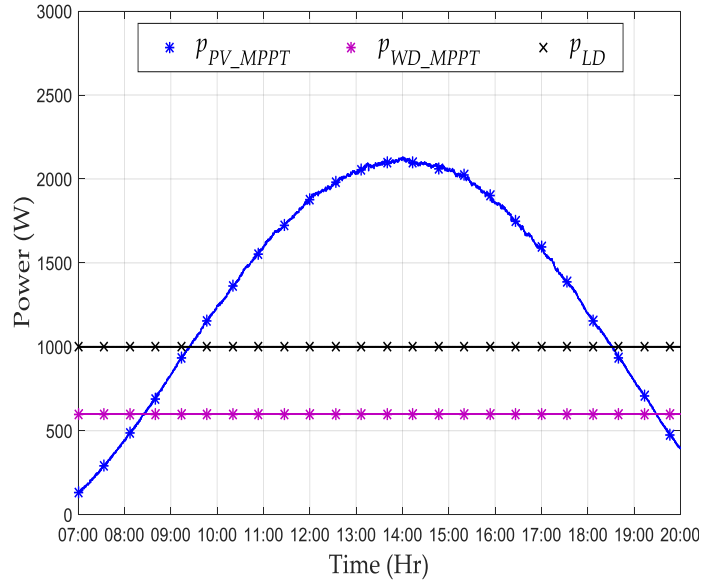


Figure 58. Power profile proposed randomly

III.6.2. Simulink parameters

Table 3 shows the simulation parameters values which are tested during the simulation. The grid tariff proposed in normal hour c_{NH} is close to the ones proposed by most energy providers, while for peak hours, c_{PH} a penalized purchase tariff that was chosen to perform power peak shaving. Other tariffs were chosen arbitrary but they respect the logic of management strategy, which is an energy trend for the next 20 years. Thus, the energy tariffs are considered in the order given by {3.33}:

$$c_{PVS,WDS,LS} \gg c_{G_PH} > c_{G_NH} > c_S \quad \{3.33\}$$

Table 3. Parameters for simulation tests

	Parameters	Values
Grid	$P_{GI_MAX} = P_{G_MAX}$	500W
	$P_{GS_MAX} = -P_{G_MAX}$	-500W
Storage	P_{S_MAX}	1300W
	SOC_{MIN}	20%
	SOC_{MAX}	80%
	soc_0	50%
	C_{REF}	130Ah
	v_s	48V (4×12)
DC bus	$V_{DC\ ref}$	400V
PV sources (Appendix n°5)	N_{PV}	18
	P_{PV_STC}	25W
WT	P_{WD_MPPT}	600W

DC load	P_{LD}	1000W
Tarrifs	c_G	0.1€/kWh
	c_{NH}	0.7€/kWh
	c_{PH} (11:00-13:00 and 18:00 20:00)	
	c_S	0.01€/kWh
	c_{PVS}	1.5€/kWh
c_{WDS}	1.2€/kWh	
	c_{LS}	1.8€/kWh

III.6.3. Simulation results and analysis

The DC MG supervisory control for grid-connected mode is simulated based on the power profile presented in Figure 58. The system is put in a situation of energy excess produced by renewable sources and the power flow in two instances depending on the value of k_D was analyzed. The first instance is based on a constant value of k_D which is equal to 1. In this case, the simulation is carried out without optimization, and the power balanced is ensured by the storage firstly and the grid intervenes only when the storage has reached its limits. This is called “storage priority”. The second instance is about a power flow simulation controlled by a variable $k_{D,p}$ provided from the optimization calculation under CPLEX. This case is called “optimization”. Shedding coefficients mentioned in III.5 are applied for these two power management strategies. The power management of the DC MG is verified in MATLAB/Simulink, and the optimization is performed using CPLEX [212].

III.6.3.1. Simulation scenarios

The power balancing control in the operational layer is an independent function that can work with any value of $k_D(t)$. Thus, two scenarios’ cases presented in Table 4 are applied to show the influence of shedding coefficients on the operation cost of the DC MG.

Table 4. Simulation cases

Cases	Shedding coefficients	
	α coefficient	γ coefficient
Storage priority ($k_D=1$)	YES	YES
Optimization ($k_D=k_D(t)$)	YES	YES

III.6.3.2. Simulation without Optimization (Storage Priority)

III.6.3.2.1. Power flow controlled by the coefficient α for $c_{PVS} > c_{WDS}$ and $c_{PVS} < c_{WDS}$ in the case of Storage Priority

The power management strategy mentioned in the flowchart of Figure 57 was implemented using the MATLAB/Simulink environment. k_D (cyan bleu curve) and k_{D_real} (blue curve) represent the same variable. In fact, $k_D = 1$ was selected to show that the storage had a higher priority than the public grid to supply the DC MG while k_{D_real} represented the real value of k_D during the simulation depending on the use or not of the storage.

First, in Figure 59, the k_D was set to 1 during the period of 07:00–11:05, meaning that only the storage was used. In the period 07:00–08:00, the soc decreased first which indicated that the storage was discharging. After that, in the period 08:10–11:05, the storage started recharging, which is explained by the increase in the soc . At 11:05, k_D should switched to 0 (k_{D_real}) and soc stabilize at the upper limit (80%). It is crucial to mention that the evolution of k_D is the same whatever the value of PV or SSWT shedding tariff.

Regarding the power flow provided in Figure 60, the period 07:00–07:55 was characterized by supplying DC load (red line) using the total power produced by PV sources (blue line) and the SSWT (purple line) and also discharging the storage (magenta curve). From 07:55 until 11:05, the power produced by renewable sources was enough to supply the DC load and contribute to charging the storage. At 11:05, the storage was full, and turned into 0, allowing the public grid (cyan bleu curve) to ensure the power balance. After at 11:05, the load was fully fed, the storage was completely charged, and the grid reached its limit of injection, the PV and SSWT shedding happened. The blue and purple curves are, respectively, the p_{PV_MPPT} and p_{WD_MPPT} that are usually provided to meet the power balance and should be limited. The green and the brown curves show the new powers that should be provided. At 18:40, the power balance was again ensured by the public grid that was injected until 20:00.

Figure 61 presents the period where the PV and SSWT shedding occurred in the case of storage priority. As can be seen in this figure, the amount of power that each renewable source should shed was calculated using the α coefficient. The duration of shedding lasted for 7 h and 45 min (11:05–18:40). Therefore, in order to compare shedding powers of PV source and the SSWT (black square and blue star markers, respectively), percentages (black and blue dashes lines) were calculated depending on the total power that should be shed p_{REN_SHEDD} (red triangle marker) and the α coefficient. The results (Figure 5Table 5) clearly show that these power percentages were identical whatever the used tariffs ($c_{PVS} > c_{WDS}$ or $c_{PVS} < c_{WDS}$). In fact, p_{PV_S} constituted around 75.8% of p_{REN_SHEDD} , while p_{WD_S} was about 24.2% of this power. Thus, applying coefficient α provided the same distribution of power that should be shed from each source without taking into account the shedding tariffs.

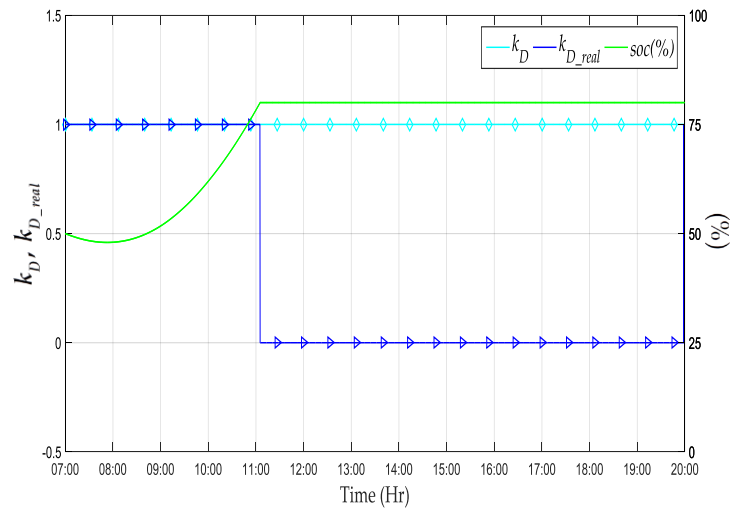


Figure 59. Evolution of k_D , k_{D_real} and soc without optimization by applying α coefficient

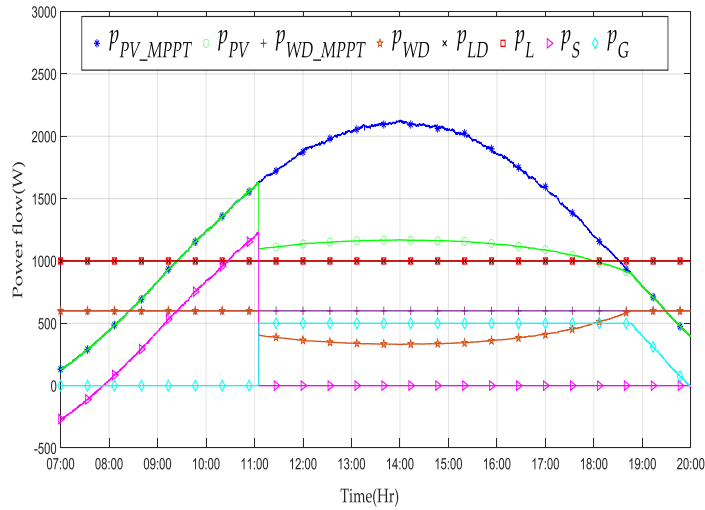


Figure 60. Power flow curves without optimization by applying α coefficient

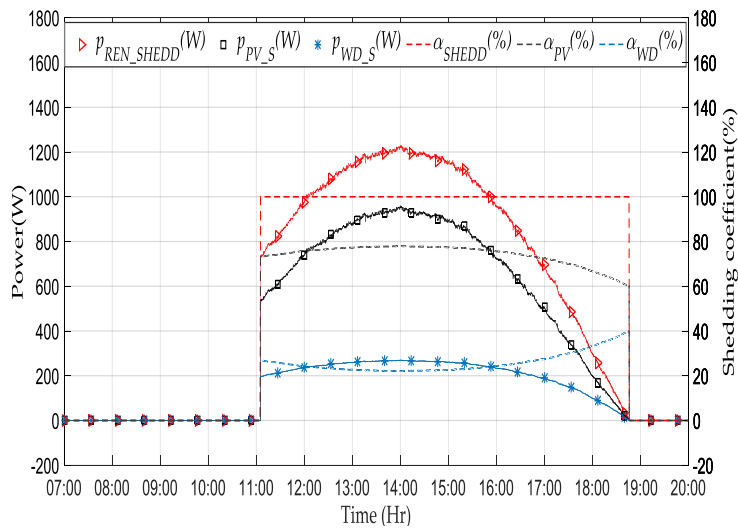


Figure 61. PV and SSWT shedding curves by applying the α coefficient in the case of storage priority

Table 5. Energy shedding calculation for the α coefficient in the case of storage priority.

	Storage Priority	
	α	
	$c_{PVS} > c_{WDS}$ ($2 > 1$ (€/kWh)) or	$c_{PVS} < c_{WDS}$ ($1 < 2$ (€/kWh))
	PV	SSWT
Total energy shedding (kWh)	6.74	
Energy shedding per source (kWh)	5.1	1.64
Contribution of each source (%)	75.8	24.2

III.6.3.2.2. power Flow Controlled by the coefficient γ for $c_{PVS} > c_{WDS}$ and $c_{PVS} < c_{WDS}$ in the case the of Storage Priority

The The evolution of k_D , k_{D_real} , and soc in the simulation without optimization by applying the γ coefficient are shown in Figure 62a,b. During the period from 07:00 to 11:05 the k_D was set to 1, which indicated that only the storage was used, while k_{D_real} represents the real value of k_D during the simulation depending on the use or not of the storage. In the period between 07:00 and 07:55, the soc decreased, which means that the storage was discharging, while in the period from 07:55 to 11:05, the soc increased until reaching the upper limit. At 11:05, k_D switched to 0 (k_{D_real}) and the soc stabilized at 80%.

Concerning the power flow provided in Figure 63a,b, the period from 07:00 to 11:05 was characterized by using the total power produced by PV sources (blue line) and the SSWT (purple line) to supply the DC load (red line) and recharge the storage (magenta curve). At 11:05, the storage was full, and turned into 0, letting the public grid (cyan bleu curve) ensure the power balance. At 11:05, the load was fully fed (1000 W), the storage was completely charged (1300 W), and the grid had reached its limit of injection (500 W). Then, the excess of power from PV and SSWT should be limited. Since γ takes into account the shedding tariff of each source, a difference in the amount of power that should be limited from each source was then noticed. The blue and purple curves are, respectively, the p_{PV_MPPT} and the p_{WD_MPPT} that are normally provided and the green and the brown curves, (p_{PV} and p_{WD} , respectively) show the limited powers that should be provided to meet the power balance. It can be noticed in Figure 63a ($c_{PVS} > c_{WDS}$) that the SSWT power was totally limited (the SSWT turned off) in the period from 11:05 to 16:40, while the rest of the power was limited from the PV source. However, when $c_{PVS} < c_{WDS}$ (Figure 63b) and since an important amount of power was produced by PV sources, only these later were limited and the SSWT continued to produce at its maximum power. At 18:40, the power balance was again ensured by the public grid that was injected until 20:00.

Figure 64a,b presents periods where the shedding occurred for PV and SSWT in the case of storage priority by applying γ for $c_{PVS} > c_{WDS}$ and $c_{PVS} < c_{WDS}$, respectively. As can be seen in these figures, the amount of power that should be shed by each renewable source was calculated using the γ coefficient

and different shedding tariffs. Durations of shedding were identical (7 h 45 min). Nevertheless, in the case of $c_{PVS} > c_{WDS}$, both PV sources and the SSWT (black square and blue star markers, respectively) were contributing to limiting the p_{REN_SHEDD} (red triangle marker), while in the case of $c_{PVS} < c_{WDS}$, only PV sources were responsible for the power balance (p_{REN_SHEDD} and p_{PV_S} lines are combined). Thus, in order to compare shedding powers of PV sources and the SSWT, respectively, percentages (black and blue dashes lines) were calculated depending on p_{REN_SHEDD} and the γ coefficient. Table 6 provides these percentages according to the simulation cases. The results clearly showed that in the case of $c_{PVS} > c_{WDS}$, p_{PV_S} and p_{WD_S} constituted 40.2% and 59.8% of p_{REN_SHEDD} , respectively. Otherwise, when $c_{PVS} < c_{WDS}$, only PV sources were limited (100% of p_{REN_SHEDD}).

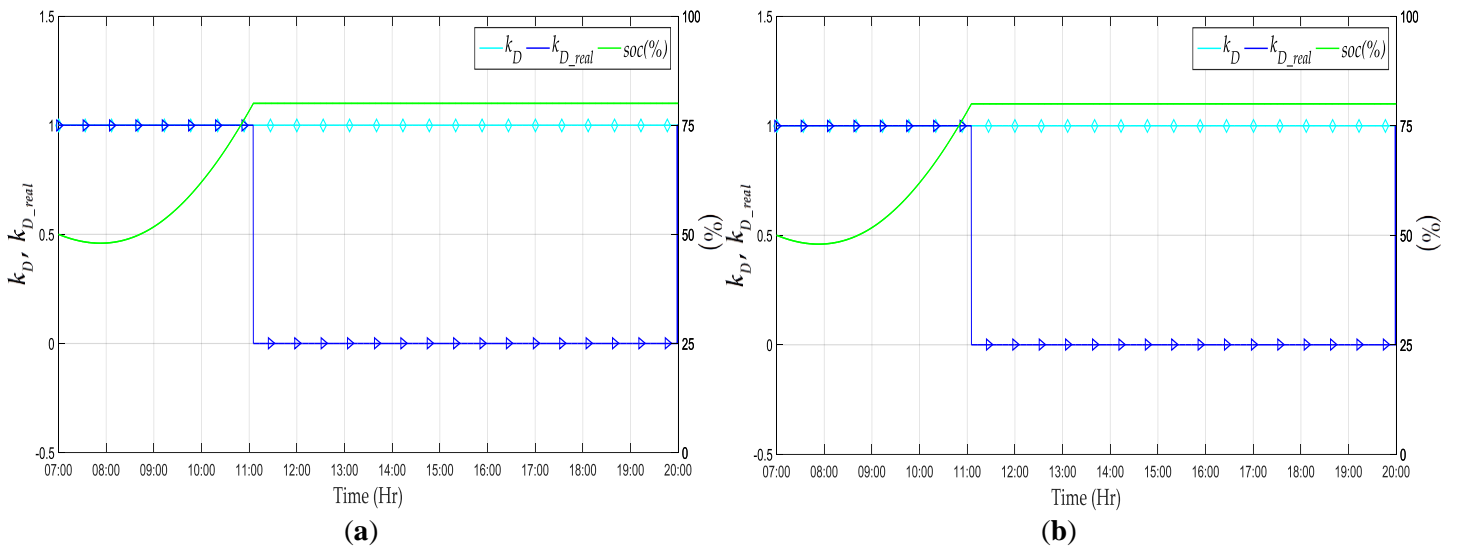


Figure 62. Evolution of k_D , k_{D_real} , and soc without optimization by applying the γ coefficient in the case of: (a) $c_{PVS} > c_{WDS}$; (b) $c_{PVS} < c_{WDS}$.

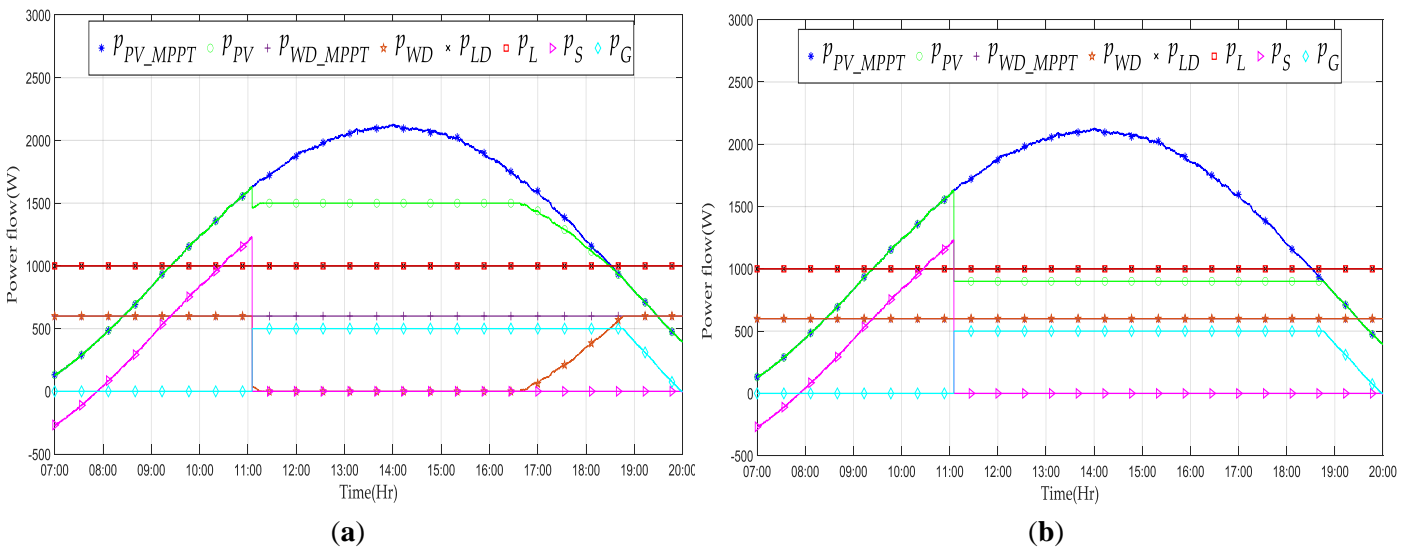


Figure 63. Power flow curves without optimization by applying the γ coefficient in the case of: (a) $c_{PVS} > c_{WDS}$; (b) $c_{PVS} < c_{WDS}$

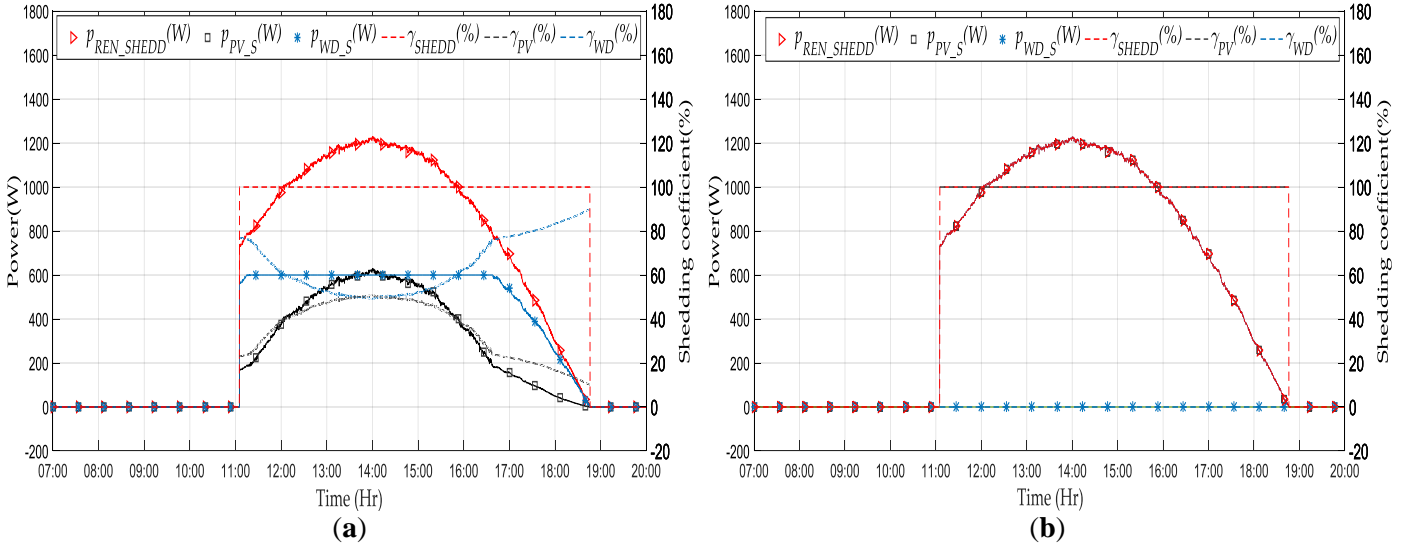


Figure 64. PV and SSWT shedding curves without optimization by applying the γ coefficient in the case of: (a) $c_{PVS} > c_{WDS}$; (b) $c_{PVS} < c_{WDS}$

Table 6. Energy shedding calculation for the γ coefficient in the case of storage priority.

	Storage Priority			
	γ			
	$c_{PVS} > c_{WDS}$ (2 > 1 (€/kWh))		$c_{PVS} < c_{WDS}$ (1 < 2 (€/kWh))	
	PV	SSWT	PV	SSWT
Total energy shedding (kWh)	6.74		6.74	
Energy shedding per source (kWh)	2.71	4.03	6.74	0
Contribution of each source (%)	40.2	59.8	100	0

III.6.3.3. Simulation with optimization

III.6.3.3.1. Power flow controlled by the coefficient α for $c_{PVS} > c_{WDS}$ and $c_{PVS} < c_{WDS}$ in the case of Optimization

The optimization issue was solved by CPLEX in the energy management layer. Indeed, this latter provided the optimum energy flow management that helped to calculate $k_D(t)$. The distribution coefficient was then transmitted to the operational layer to run the power system.

As can be observed in Figure 65, k_D (cyan bleu curve) and k_{D_real} (blue curve) were confused since k_D was the result of the optimization. During the period between 07:00 and 07:55, the k_D was set to 1, which indicated that only the storage was used. In addition, the soc decreased during this period, meaning that the storage was discharging. In the period from 09:10 to 12:30, the value of k_D evolved between 0 and 1, indicating that both the public grid and storage supported the MG. It can be notice that, despite the difference in the value of PV or SSWT shedding tariff, the evolution of k_D still remained the same.

Concerning the power flow provided in Figure 66, the power balance in the period from 07:00 to 07:55 was ensured by discharging the storage and using the production of PV sources and the SSWT. From 07:55 to 12:30, the total power produced by PV sources (blue line) and the SSWT (purple line) was used to supply the DC load (red line), recharged the storage (magenta curve), and was injected into the public grid (cyan bleu curve). After 12:30, the load was fully fed, the storage was completely charged, and the grid reached its limit of injection, therefore, PV and SSWT shedding happened. The blue and purple curves are, respectively, the p_{PV_MPPT} and p_{WD_MPPT} that are normally provided but to meet the power balance, these powers should be limited. The new powers that should be provided are shown by the green and the brown curves. At 18:40, the power balance was again ensured by the public grid that was injected until 20:00.

Figure 67 presents the period where the PV and SSWT shedding occurred in the case of optimization. As can be seen in this figure, the amount of power that should be shed by each renewable source was calculated using the α coefficient. The duration of shedding lasted for 6 h and 10 min (12:30–18:40). Therefore, in order to compare shedding powers of PV source and the SSWT (black square and blue star markers, respectively), percentages (black and blue dashes lines) were calculated depending on the total power that should be shed p_{REN_SHEDD} (red triangle marker) and the α coefficient. The results in Table 7 were identical whatever the used tariffs ($c_{PVS} > c_{WDS}$ or $c_{PVS} < c_{WDS}$). In fact, p_{PV_S} constituted around 76% of p_{REN_SHEDD} , while p_{WD_S} reached 24% of this power. Thus, applying coefficient α provided the same distribution of power that should be shed from each source without taking into account the shedding tariffs.

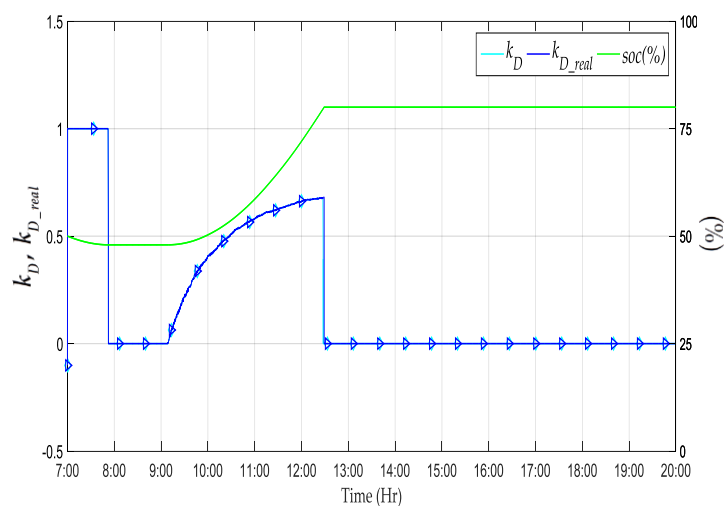


Figure 65. Evolution of k_D , k_{D_real} and soc without optimization by applying α coefficient.

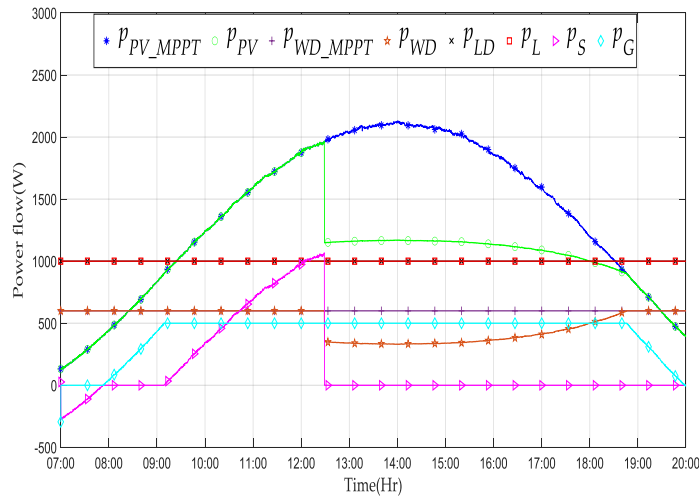


Figure 66. Power flow curves with optimization by applying the α coefficient.

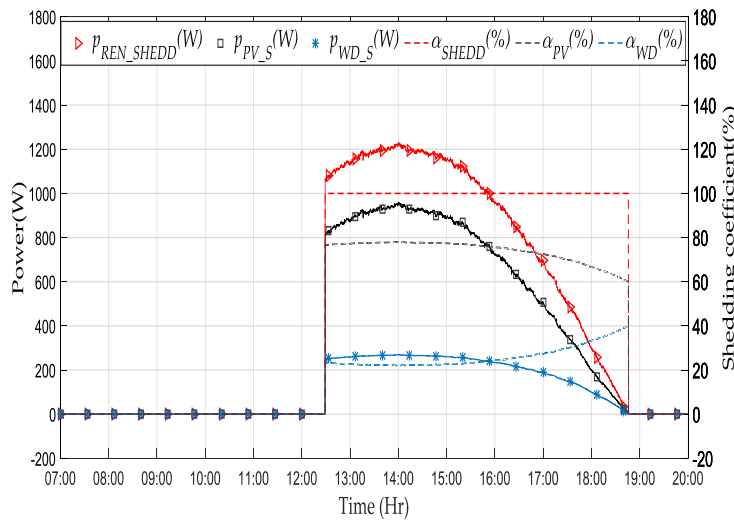


Figure 67. The PV and SSWT shedding curves by applying the α coefficient in the case of optimization.

Table 7. Energy shedding calculation for the α coefficient in the case of optimization.

	Optimization	
	α	
	$c_{PVS} > c_{WDS}$ ($2 > 1$ (€/kWh)) or $c_{PVS} < c_{WDS}$ ($1 < 2$ (€/kWh))	
	PV	SSWT
Total energy shedding (kWh)		5.46
Energy shedding per source (kWh)	4.15	1.31
Contribution of each source (%)	76	24

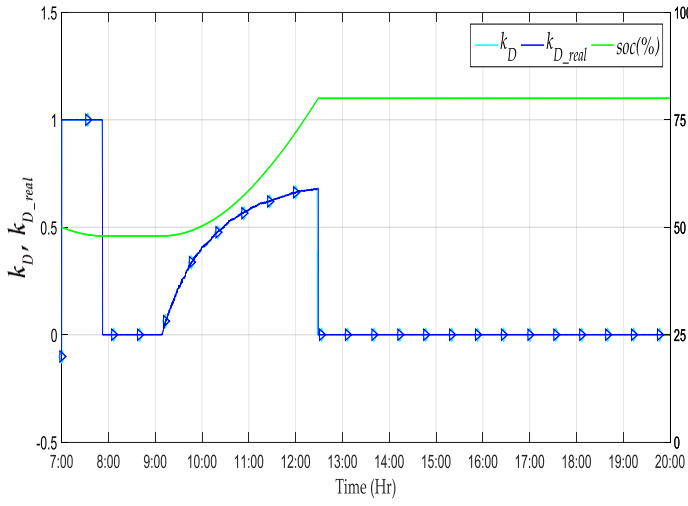
III.6.3.3.2. Power flow controlled by the coefficient γ for $c_{PVS} > c_{WDS}$ and $c_{PVS} < c_{WDS}$ in the case of Optimization.

Figure 68a,b shows that k_D and k_{D_real} were confused since k_D is the result of the optimization. In the period between 07:00 and 07:55, k_D was set to 1 and the soc also decreased, which means that the

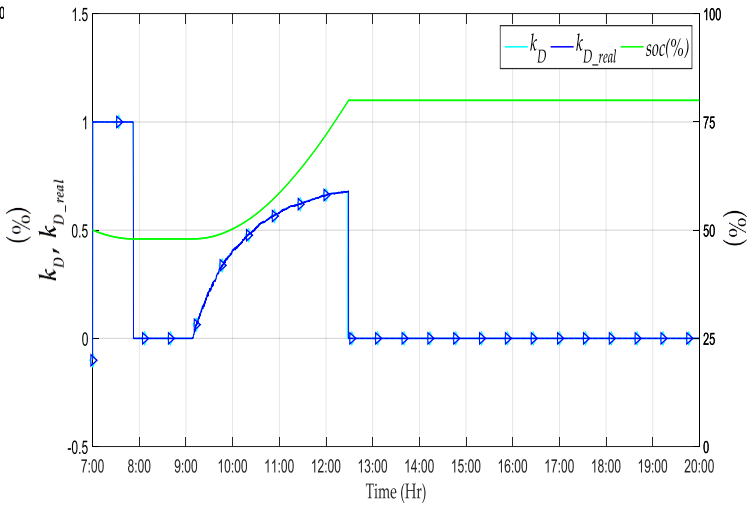
storage was discharging, while in the period 09:10–12:30 the value of k_D varied between 0 and 1, indicating that both the public grid and storage supported the MG.

Regarding the power flow provided in Figure 69a,b, the period 07:00–12:30 was first characterized by using the power produced by PV sources (blue line) and the SSWT (purple line) and discharging the storage (magenta curve) to supply the DC load (red line) (07:00–07:55) and second, by using the total renewable power to feed the DC load, recharge the storage and to be injected into the public grid (cyan blue curve) (07:55:12:30). The PV and SSWT shedding happened at 12:30 since the load was fully fed, the storage was completely charged, and the grid had reached its limit of injection. The blue and purple curves are, respectively, the P_{PV_MPPT} and P_{WD_MPPT} that are normally provided to meet the power balance, these powers should be limited (green and the brown curves). Thus, in Figure 69a, where $c_{PVS} > c_{WDS}$, the SSWT was turned off in the period from 12:30 to 16:40 and the rest of the power that should be limited was subtracted from the production of the PV sources. Nonetheless, when $c_{PVS} < c_{WDS}$ (Figure 69b) only PV sources were limited and the SSWT continued to produce at its maximum power. At 18:40, the power balance was again ensured by the public grid that was injected until 20:00.

Figure 70a,b present periods where the shedding occurred for PV sources and the SSWT in the case of optimization by applying γ for $c_{PVS} > c_{WDS}$ and $c_{PVS} < c_{WDS}$, respectively. The durations of shedding were identical (6 h 10 min) and calculated depending on the γ coefficient and different shedding tariffs. It was noticed that in the case of $c_{PVS} > c_{WDS}$, both PV sources and SSWT (blue star marker) powers were limited. Yet, when $c_{PVS} < c_{WDS}$, P_{REN_SHEDD} (red triangle marker) and P_{PV_S} (black square marker) were combined, which means that only PV sources power was limited. Consequently, percentages (black and blue dashes lines) were calculated depending on P_{REN_SHEDD} and the γ coefficient with the aim to compare shedding powers of PV sources and the SSWT, respectively. Table 8 provides these percentages according to simulation cases. The results clearly showed that in the case of $c_{PVS} > c_{WDS}$, P_{PV_S} and P_{WD_S} constituted 41.5% and 58.5% of P_{REN_SHEDD} , respectively. Otherwise, when $c_{PVS} < c_{WDS}$ only PV sources were limited (P_{PV_S} 100% of P_{REN_SHEDD}).

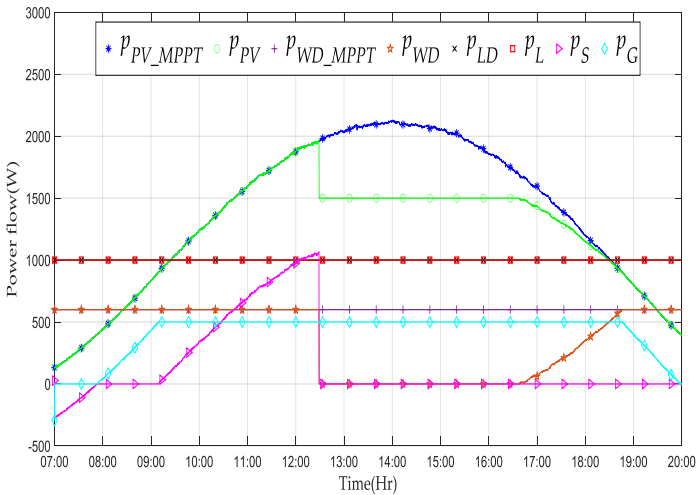


(a)

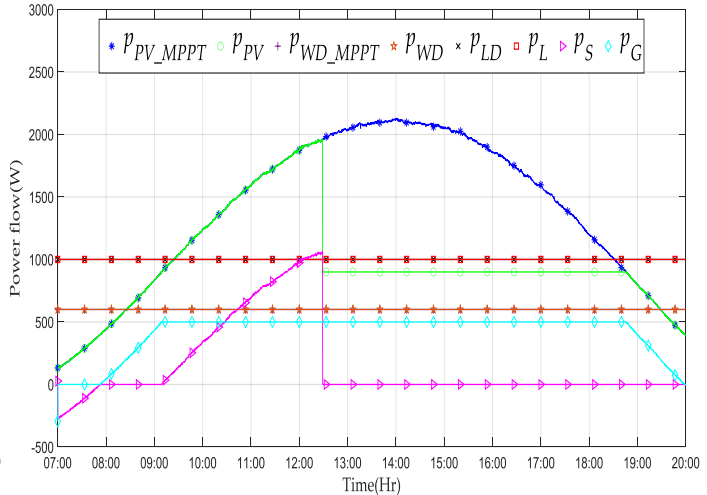


(b)

Figure 68. Evolution of k_D , k_{D_real} and soc with optimization by applying the γ coefficient in the case of: (a) $c_{PVS} > c_{WDS}$; (b) $c_{PVS} < c_{WDS}$.



(a)



(b)

Figure 69. Power flow curves with optimization by applying the γ coefficient in the case of: (a) $c_{PVS} > c_{WDS}$; (b) $c_{PVS} < c_{WDS}$.

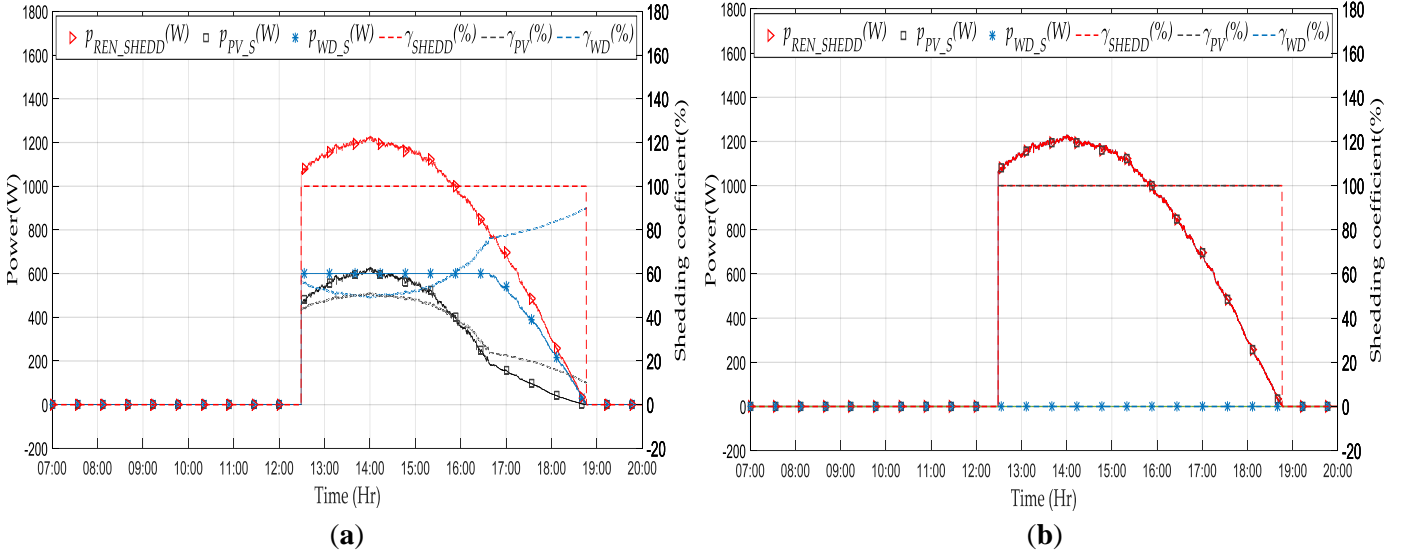


Figure 70. PV and SSWT shedding curves with optimization by applying the γ coefficient in the case of:

(a) $c_{PVS} > c_{WDS}$; (b) $c_{PVS} < c_{WDS}$.

Table 8. Energy shedding calculation for coefficient γ in the case of optimization.

	Optimization			
	γ			
	$c_{PVS} > c_{WDS}$ (2 > 1 (€/kWh))		$c_{PVS} < c_{WDS}$ (1 < 2 (€/kWh))	
	PV	SSWT	PV	SSWT
Total energy shedding (kWh)	5.46		5.46	
Energy shedding per source (kWh)	2.26	3.2	5.46	0
Contribution of each source (%)	41.5	58.5	100	0

III.6.3.4. Energy cost comparisons

In order to make cost comparisons of energy calculated using shedding coefficients, the case where $c_{PVS} > c_{WDS}$ was selected. The energy costs calculated by α and γ coefficients are listed in Table 9. The results showed that the cost of PV energy shedding (C_{PV_S}), SSWT energy shedding (C_{WD_S}), load shedding energy (C_{L_S}), storage energy (C_S), and public grid energy (C_G) differed according to the performed simulation. The total cost of the α coefficient calculated for priority storage was higher (10.46€) compared to that obtained after optimization (8.08€) It means that the total cost was decreased by about 22.8%. In addition, the total energy cost of the γ coefficient calculated after the simulation without and with optimization was 8.06€ and 6.21€, respectively. This indicates that the optimization allowed minimizing the energy cost. Indeed, the optimization favored the exchange of power between the public grid and the storage in order to establish the power balance. It can be also noticed that for the same simulation case, the total energy cost obtained by using the γ coefficient was significantly lower than the one obtained by applying the α coefficient.

Table 9. Energy cost calculation for α and γ coefficients

Cost (€)	α			γ		
	Storage Priority	Optimization	Cost Decrease (%)	Storage Priority	Optimization	Cost Decrease(%)
C_{PV_S}	10.21	8.3		5.41	4.54	
C_{WD_S}	1.63	1.31		4.03	3.20	
C_{L_S}	0	0		0	0	
C_G	-1.4	-1.55		-1.4	-1.55	
C_S	0.02	0.02		0.02	0.02	
C_{TOTAL}	10.46	8.08	22.8	8.06	6.21	23

III.7. Conclusion

The integration of a SSWT into a DC MG connected to the grid requires a deep understanding of many parameters, including factors related to energy and power management. In this article, the supervision control design was described. In this context, a strategy for optimizing the MG that permits transactions with the main distribution network and the participation of the end-user customers has been suggested. The optimization and minimization of the total operating cost were investigated by dispatching power flow according to the power profiles and measurement data under the constraints of the modeling. Indeed, in the case of the power excess produced by PV sources and the SSWT, it is crucial to perform the power limitation to ensure power balancing, which is the main goal of the supervision. For that, two approaches were suggested:

The first one was based on applying a shedding coefficient called α that was based on limiting power depending on the percentage of contribution of each source in generating the excess of power. This coefficient was performed in two different cases: storage priority and optimization.

The second one was about using a second shedding coefficient called γ . This latter principle was limiting the excess of power by taking into account not only the production of each RESs but also the shedding cost related to each source. This coefficient was tested in scenarios with and without optimization.

The results highlighted that the coefficient γ provides good performances in terms of the cost compared to α since the coefficient γ takes into account the RESs' tariff in the case of renewable power shedding. In addition, the results also revealed that whatever the scenario used, the simulation with optimization conditions leads to reduce the costs compared to the simulation without optimization. The optimization permits minimizing the cost by favoring the exchange of power between the public grid and

the storage (selling power to the grid). This study showed the importance of the optimization method and the impact of the shedding coefficients in obtaining the best energy performances with the lowest cost. Moreover, the optimization gave better energy performance while minimizing PV and SSWT power shedding.

To conclude, simulation results showed that the supervision control can maintain power balancing while performing optimized control, even by using an arbitrary power profile and arbitrary energy tariffs. The optimized power control handles several constraints, such as storage and grid power limitations.

Further work will focus on experimental validation of the studied DC MG by taking into account the dynamic efficiency of the converters and real-life random trends. The supervisory system should be also improved to be able to manage and decrease power losses in the converters and contribute to the stabilization of the bus voltage.

General conclusion and perspectives

The fast development of the industry and the widespread introduction of new energy technologies induce a continuous increase in energy demand and the incessant growth of global electricity consumption. To meet these energy needs, it necessitates finding new methods for energy production. In the last years, the growing awareness of environmental factors, sustainability, industrial ecology, and eco-efficiency is applied to the development of a new generation of energy issued from renewable energies. The depletion of fossil fuels, combined with increasingly restrictive regulations, acts in synergy to encourage the development of RES. In this context, the cost of wind power energy knows an annual decrease, conducting to the establishment of large-scale wind power plants. However, large-scale wind power is more suitable in remote areas since it takes up ample space. Therefore, in recent years, the research has been interested in the SSWT installed in urban/rural areas and locally consumed, which minimizes the use and pressure of public grid energy. This interest in small-scale RESs leads to the appearance of a microgrid, which reduces the power grid's operating pressure and provides efficient, secure, reliable, environmentally friendly, and sustainable power from RESs.

The presented thesis makes a contribution in the field of RESs, mainly in the SSWT sector. At first, the main objectives were proposing and performing power control strategies for the SSWT and then analyzing the integration of this renewable source into a DC urban MG.

In the first chapter, a state of art focused on renewable energies is presented. Firstly, a description of the electrical system evolution through integrating renewable energies in the utility grid is introduced. Since the thesis concerns controlling a SSWT integrated into an urban DC MG. A literature review about DC MGs was first detailed in this chapter. It concerns the important concepts of a DC MG, namely

topologies, control, stability, protection, etc. Secondly, the importance of wind power generation has been given attention. It concerns the historical and current evolution of this field of RESs with a description of the turbine types and constitution. A particular interest in a SSWT with a horizontal axis was mentioned. The types of machines useful for this category of WTs were presented such as the PMSG that was selected thanks to its multiple benefits and suitability in this study. For performing the control, several architectures were suggested and studied. The active structure based on a three-phase diode bridge and a boost DC-DC convertor was chosen.

In the second chapter, different power control strategies to produce energy as much as possible and meet flexible energy demand for SSWTs intended to be integrated into a DC urban MG were suggested and compared. These methods concern P&O with fixed step size, P&O based on Newton's approach, and P&O based on FL technique. A test bench constituted of a ventilation tunnel, where the SSWT is installed, was used to perform this study. The SWECS is based on a three-phase diode rectifier to convert AC voltage obtained from the PMSG to DC voltage, a controllable DC/DC, and a programmable DC electronic load. The experimental results highlighted that all the methods worked correctly, identified the direction of the next perturbation and reached the LPPs. However, the performances of each method are different. Indeed, for the fixed step-size and Newton's methods, large step sizes provided faster dynamic responses with excessive steady-state oscillations, which decreased the system's efficiency. Hence, these methods should make an acceptable compromise between the dynamics and oscillations. In addition, compared to fixed step size and Newton's methods, the FL method showed better dynamic performances with more steady oscillations around LPP. During a sudden change of power and wind speed, all the suggested methods reacted correctly and changed identically in terms of response time. The FL technique stabilized quickly compared to other methods, both in power increase or decrease and in the sudden change of wind speed. This technique could also be interesting for controlling a SSWT during its integration in a DC MG. It is able to guarantee less fluctuation in power that can be injected into the public grid. Thus, the FL method stabilized quickly and ensured a good balance between reducing oscillation of WT output power around the operating point and convergence of rising time toward LPP.

The third chapter focused on studying the impact of the integration of a SSWT into a DC MG and investigated the constraints that can intervene in the system control and supervision. The studied DC MG is constituted by RESs, which were assumed to produce an amount of power based on weather data and mathematical modeling, battery storage, and connection to the public grid. To ensure that the load was met, a dispatch algorithm was proposed to distribute the RES's energy to the load firstly, then to the storage or the grid depending on the selected power management strategies. Minimizing the system cost with constraints on renewable curtailment was given particular attention. In this case, the RESs (PV and WT) produced a surplus of power, and a strategy for renewable energy limitation was proposed. It consisted of suggesting two types of coefficients, called "shedding coefficients", to calculate the power that should be limited from each source. To perform these coefficients, namely coefficient α and coefficient γ ., two types of scenarios were used during simulations (optimization and priority storage).

The obtained results showed that the proposed coefficient γ provides good performances in terms of the cost compared to α since the coefficient γ takes into account the RESs' tariff related to the power shedding of each renewable source. Moreover, the simulation with optimization leads to reduce costs compared to the simulation without optimization whatever the used coefficient. The optimization permits minimizing the cost by favoring selling the excess of power to the grid and the exchange of power between the public grid and the storage. To conclude, this study showed the importance of the optimization method and the impact of the shedding coefficients in getting the best energy performances at a low cost.

This thesis opens multiple perspectives that need to be treated and improved:

- effective integration of the studied SSWT into the DC MG already developed in the experimental platform of AVENUES laboratory;
- the WT power is very dependent on the wind speed. Thus, an accurate measure of wind speed is the key for calculating the accuracy of WT prediction power. Nowadays, it is easy to get the wind speed from Meteo France, but it is still difficult to get an accurate prediction of wind speed because of the intermitted of the WT generation. Thus, suggesting and comparing wind speed prediction models could be important and can impact the DC MG cost positively;
- the dynamic efficiency of the converters is an important aspect that should be considered while building a DC MG. Thus, the supervisory system should be improved in order to be able to manage and decrease power losses in the converters and contribute to the stabilization of the bus voltage;
- as renewable energy from a PV source and WT is dispatched to the load or is stored for later use, evaluating the MG performances by measuring both the renewable energy penetration and the renewable curtailment could be interesting in calculating the system cost over time;
- built a supervisory system that can operate in 24 hours.

References

- [1] J. Aourir and F. Locment, "Limited power point tracking for a small-scale wind turbine intended to be integrated in a DC microgrid," *Appl. Sci.*, vol. 10, no. 22, pp. 1–23, 2020.
- [2] A. Elmouatamid, R. Ouladsine, M. Bakhouya, N. El Kamoun, M. Khaidar, and K. Zine-Dine, "Review of Control and Energy Management Approaches in Micro-Grid Systems," *Energies*, vol. 14, no. 1, p. 168, 2020.
- [3] P. IEA, "IEA, Renewable power generation by technology in the Sustainable Development Scenario, 2000-2030." [Online]. Available: <https://www.iea.org/data-and-statistics/charts/renewable-power-generation-by-technology-in-the-sustainable-development-scenario-2000-2030>.
- [4] Z. H. Jian, Z. Y. He, J. Jia, and Y. Xie, "A review of control strategies for DC micro-grid," *Proc. 2013 Int. Conf. Intell. Control Inf. Process. ICICIP 2013*, pp. 666–671, 2013.
- [5] P. Basak, S. Chowdhury, S. Halder Nee Dey, and S. P. Chowdhury, "A literature review on integration of distributed energy resources in the perspective of control, protection and stability of microgrid," *Renew. Sustain. Energy Rev.*, vol. 16, no. 8, pp. 5545–5556, 2012.
- [6] I. HOUSSAMO and Contribution, "Contribution à l'étude théorique, à la modélisation et à la mise en œuvre d'un système multisource appartenant à un micro-réseau électrique. Considérations sur la qualité de l'énergie," 2015.
- [7] Baochao WANG, "Intelligent control and power flow optimization of microgrid: energy management strategies," 2010.
- [8] H. Fathabadi, "Novel high efficient speed sensorless controller for maximum power extraction from wind energy conversion systems," *Energy Convers. Manag.*, vol. 123, pp. 392–401, 2016.
- [9] A. Aoun, M. Ghandour, A. Ilinca, and H. Ibrahim, "Demand-side management," in *Hybrid Renewable Energy Systems and Microgrids*, Elsevier, 2021, pp. 463–490.
- [10] A. Singh and M. Badoni, "Power quality issues, modeling, and control techniques," *Adv. Smart Grid Power Syst.*, no. i, pp. 299–329, 2021.
- [11] B. To and H. A. L. Id, "Contribution des Smart Grids ` a la transition evaluation dans des sc ` enarios long terme ephanie Bouckaert l ` École nationale supérieure des mines de Paris Contribution des Smart Grids à la transition énergétique : évaluation dans des scénarios long te," 2013.
- [12] J. Dulout, "Optimal sizing and energy management of storage systems for renewable sources deployment, design of a LVDC microgrid," 2017.
- [13] M. E. El-hawary, "The Smart Grid—State-of-the-art and Future Trends," *Electr. Power Components Syst.*, vol. 42, no. 3–4, pp. 239–250, Mar. 2014.
- [14] Independence Energy. Security act of 2007., "Publiclaw 110-140.," 2007, vol. 153, no. 110–140.
- [15] P. . Bryson, J.; Gallagher, "NIST framework and roadmap for smart grid interoperability standards. Natl. Inst. Stand. Technol. NIST US Dep. Commer.," vol. 227, 2012.
- [16] K. P. O Siddiqui, P Hurtado, "The Green Grid Energy Savings and Carbon Emissions Reductions Enabled by a Smart Grid.," *Electr. Power Res. Inst. EPRI Palo Alto, CA, USA*, p. 64, 2008.
- [17] DECC. Smarter grids: The Opportunity, "Department of Energy & Climate Change: London, UK," p. 18, 2009.
- [18] G. Betis, C. G. Cassandras, and C. A. Nucci, "Smart Cities [Scanning the Issue]," *Proc. IEEE*, vol. 106, no. 4, pp. 513–517, 2018.
- [19] S. Bi and Y. J. A. Zhang, "Graph-based cyber security analysis of state estimation in smart power grid," *IEEE Commun. Mag.*, vol. 55, no. 4, pp. 176–183, 2017.

- [20] M. L. Tuballa and M. L. Abundo, "A review of the development of Smart Grid technologies," *Renew. Sustain. Energy Rev.*, vol. 59, pp. 710–725, 2016.
- [21] L. Ardito, G. Procaccianti, G. Menga, and M. Morisio, "Smart grid technologies in Europe: An overview," *Energies*, vol. 6, no. 1, pp. 251–281, 2013.
- [22] H. Farhangi, "The path of the smart grid," *IEEE Power Energy Mag.*, vol. 8, no. 1, pp. 18–28, 2010.
- [23] Y. Cunjiang, Z. Huaxun, and Z. Lei, "Architecture Design For Smart Grid," *Energy Procedia*, vol. 17, pp. 1524–1528, 2012.
- [24] M. Irfan, J. Iqbal, A. Iqbal, Z. Iqbal, R. A. Riaz, and A. Mehmood, "Opportunities and challenges in control of smart grids – Pakistani perspective," *Renew. Sustain. Energy Rev.*, vol. 71, no. December 2014, pp. 652–674, 2017.
- [25] I. Alotaibi, M. A. Abido, M. Khalid, and A. V. Savkin, "A comprehensive review of recent advances in smart grids: A sustainable future with renewable energy resources," *Energies*, vol. 13, no. 23, pp. 1–41, 2020.
- [26] N. S. Wade, P. C. Taylor, P. D. Lang, and P. R. Jones, "Evaluating the benefits of an electrical energy storage system in a future smart grid," *Energy Policy*, vol. 38, no. 11, pp. 7180–7188, 2010.
- [27] B. Hamilton and M. Summy, "Benefits of the smart grid: Part of a long-term economic strategy," *IEEE Power Energy Mag.*, vol. 9, no. 1, pp. 102–104, 2011.
- [28] K. Moslehi and R. Kumar, "A reliability perspective of the smart grid," *IEEE Trans. Smart Grid*, vol. 1, no. 1, pp. 57–64, 2010.
- [29] N. Hatziargyriou, "Microgrids control issues," *Microgrids Archit. Control*, pp. 25–80, 2014.
- [30] D. T. Ton and M. A. Smith, "The U.S. Department of Energy's Microgrid Initiative," *Electr. J.*, vol. 25, no. 8, pp. 84–94, 2012.
- [31] C. Schwaegerl, "Advanced Architectures and Control Concepts for More Microgrids," *More Microgrids, Siemens AG, STREP Proj. funded by EC under 6FP, SES6-019864, TG2. Anal. Tech. benefits, TG3. Anal. Soc. Econ. Environ. benefits*, no. January 2006, pp. 1–145, 2009.
- [32] N. Hatziargyriou *et al.*, "Microgrids - Large scale integration of microgeneration to low voltage grids," *41st Int. Conf. Large High Volt. Electr. Syst. 2006, CIGRE 2006*, no. Lv, 2006.
- [33] E. Amicarelli and E. Amicarelli, "Control and management strategies of smart grids with high penetration of renewable energy To cite this version : HAL Id : tel-01712034 Stratégie de gestion des réseaux électriques à fort taux de production renouvelable distribuée," 2018.
- [34] B. WANG, "Thèse présentée pour l'obtention du grade de Docteur de l'UTC Contributions by Vision Systems to," 2013.
- [35] A. Hirsch, Y. Parag, and J. Guerrero, "Microgrids: A review of technologies, key drivers, and outstanding issues," *Renew. Sustain. Energy Rev.*, vol. 90, pp. 402–411, Jul. 2018.
- [36] J. Kumar, A. Agarwal, and V. Agarwal, "A review on overall control of DC microgrids," *J. Energy Storage*, vol. 21, pp. 113–138, Feb. 2019.
- [37] R. Lasseter, A. Akhil, C. Marnay, and J. Ste, "Consortium for Electric Reliability Technology Solutions White Paper on Integration of Distributed Energy Resources The MicroGrid Concept," no. April, 2002.
- [38] CESI RICERCA DER Test Facility, "Pilot Microgrids - CESI RICERCA DER Test Facility." [Online]. Available: <http://www.microgrids.eu/index.php?page=kythnos&id=6>.
- [39] C. H. Tsai, Y. W. Bai, M. B. Lin, R. J. Jhang, and C. Y. Chung, "Reduce the standby power consumption of a microwave oven," *IEEE Trans. Consum. Electron.*, vol. 59, no. 1, pp. 54–61, 2013.

- [40] S. H. Ryu, J. H. Ahn, K. S. Cho, and B. K. Lee, "Single-switch ZVZCS quasi-resonant CLL isolated DC-DC converter for 32" LCD TV," *J. Electr. Eng. Technol.*, vol. 10, no. 4, pp. 1646–1654, 2015.
- [41] B. A. Thomas, "Edison revisited: Impact of DC distribution on the cost of LED lighting and distributed generation," *Conf. Proc. - IEEE Appl. Power Electron. Conf. Expo. - APEC*, pp. 588–593, 2010.
- [42] W. Yu, J. S. Lai, H. Ma, and C. Zheng, "High-efficiency dc-dc converter with twin bus for dimmable LED lighting," *IEEE Trans. Power Electron.*, vol. 26, no. 8, pp. 2095–2100, 2011.
- [43] P. S. Maniscalco, V. Scaini, and W. E. Veerkamp, "Specifying DC chopper systems for electrochemical applications," *IEEE Trans. Ind. Appl.*, vol. 37, no. 3, pp. 941–948, 2001.
- [44] G. C. Lazaroiu and D. Zaninelli, "A control system for dc arc furnaces for power quality improvements," *Electr. Power Syst. Res.*, vol. 80, no. 12, pp. 1498–1505, 2010.
- [45] G. F. Reed, "DC technologies: Solutions to electric power system advancements," *IEEE Power Energy Mag.*, vol. 10, no. 6, pp. 10–17, 2012.
- [46] B. T. Patterson, "DC, Come Home: DC Microgrids and the Birth of the 'Enernet,'" *IEEE Power Energy Mag.*, vol. 10, no. 6, pp. 60–69, 2012.
- [47] T. F. Wu, C. H. Chang, L. C. Lin, G. R. Yu, and Y. R. Chang, "DC-bus voltage control with a three-phase bidirectional inverter for DC distribution systems," *IEEE Trans. Power Electron.*, vol. 28, no. 4, pp. 1890–1899, 2013.
- [48] C. Dierckxsens, K. Srivastava, M. Reza, S. Cole, J. Beerten, and R. Belmans, "A distributed DC voltage control method for VSC MTDC systems," *Electr. Power Syst. Res.*, vol. 82, no. 1, pp. 54–58, 2012.
- [49] M. Aragüés-Peñalba, A. Egea-Álvarez, S. G. Arellano, and O. Gomis-Bellmunt, "Droop control for loss minimization in HVDC multi-terminal transmission systems for large offshore wind farms," *Electr. Power Syst. Res.*, vol. 112, pp. 48–55, 2014.
- [50] B. Han, "Integrated power and single axis attitude control system with two flywheels," *Chinese J. Mech. Eng. (English Ed.)*, vol. 25, no. 3, pp. 564–575, 2012.
- [51] A. Al-Diab and C. Sourkounis, "Integration of flywheel energy storage system in production lines for voltage drop compensation," *IECON Proc. (Industrial Electron. Conf.)*, pp. 3882–3887, 2011.
- [52] D. J. Becker and B. J. Sonnenberg, "DC microgrids in buildings and data centers," *INTELEC, Int. Telecommun. Energy Conf.*, 2011.
- [53] P. Gross, "Today's Data Centres Typical Configuration," pp. 125–130.
- [54] S. Rajagopalan, B. Fortenbery, and D. Symanski, "Power quality disturbances within DC data centers," *INTELEC, Int. Telecommun. Energy Conf.*, 2010.
- [55] A. Mohamed, V. Salehi, T. Ma, and O. Mohammed, "Real-time energy management algorithm for plug-in hybrid electric vehicle charging parks involving sustainable energy," *IEEE Trans. Sustain. Energy*, vol. 5, no. 2, pp. 577–586, 2014.
- [56] M. Tabari and A. Yazdani, "Stability of a dc distribution system for power system integration of plug-in hybrid electric vehicles," *IEEE Trans. Smart Grid*, vol. 5, no. 5, pp. 2564–2573, 2014.
- [57] B. E. Noriega, R. T. Pinto, and P. Bauer, "Sustainable DC-Microgrid Control System for Electric-Vehicle Charging Stations Delft University of Technology Overview of planned dc-microgrid," *Power Electron. Appl. (EPE), 2013 15th Eur. Conf.*, 2013.
- [58] S. Beheshtaein, R. M. Cuzner, M. Forouzesh, M. Savaghebi, and J. M. Guerrero, "DC Microgrid Protection: A Comprehensive Review," *IEEE J. Emerg. Sel. Top. Power Electron.*, vol. 6777, no. c, pp. 1–1, 2019.
- [59] T. Dragičević, X. Lu, J. C. Vasquez, and J. M. Guerrero, "DC Microgrids - Part II: A Review of Power Architectures, Applications, and Standardization Issues," *IEEE Trans. Power Electron.*,

vol. 31, no. 5, pp. 3528–3549, 2016.

- [60] T. Dragicevic, “Hierarchical control of a direct current microgrid with energy storage systems in a distributed topology,” Faculty Elect. Eng. Comput., Zagreb Univ., Zagreb, Croatia, 2013.
- [61] R. Deenadayalan, K. Parkavi Kathirvelu, R. Balasubramanian, and R. Amirtharajan, “A distributed control strategy for coordination of an autonomous LVDC system,” *Int. J. Appl. Eng. Res.*, vol. 10, no. 9, pp. 22489–22502, 2015.
- [62] T. Dragicevic, J. M. Guerrero, J. C. Vasquez, and D. Skrlec, “Supervisory control of an adaptive-droop regulated DC microgrid with battery management capability,” *IEEE Trans. Power Electron.*, vol. 29, no. 2, pp. 695–706, 2014.
- [63] P. Liutanakul, A. B. Awan, S. Pierfederici, B. Nahid-Mobarakeh, and F. Meibody-Tabar, “Linear stabilization of a dc bus supplying a constant power load: A general design approach,” *IEEE Trans. Power Electron.*, vol. 25, no. 2, pp. 475–488, 2010.
- [64] A. Kwasinski and C. N. Onwuchekwa, “Dynamic behavior and stabilization of DC microgrids with instantaneous constant-power loads,” *IEEE Trans. Power Electron.*, vol. 26, no. 3, pp. 822–834, 2011.
- [65] P. Karlsson and J. Svensson, “DC Bus Voltage Control for a Distributed Power System,” *IEEE Trans. Power Electron.*, vol. 18, no. 6, pp. 1405–1412, 2003.
- [66] K. Sun, L. Zhang, Y. Xing, and J. M. Guerrero, “A distributed control strategy based on DC bus signaling for modular photovoltaic generation systems with battery energy storage,” *IEEE Trans. Power Electron.*, vol. 26, no. 10, pp. 3032–3045, 2011.
- [67] M. Leng, G. Zhou, H. Li, G. Xu, F. Blaabjerg, and T. G. Dragicevic, “Impedance-Based Stability Evaluation for Multibus DC Microgrid Without constraints on Subsystems,” *IEEE Trans. Power Electron.*, vol. 8993, no. c, pp. 1–1, 2021.
- [68] R. R. Deshmukh and M. S. Ballal, “A Supervisory Modified Control Scheme for Power Management in Multi Bus DC Microgrid,” *IECON Proc. (Industrial Electron. Conf.)*, vol. 2019-Octob, pp. 2282–2287, 2019.
- [69] R. R. Deshmukh, M. S. Ballal, and H. M. Suryawanshi, “A Fuzzy Logic Based Supervisory Control for Power Management in Multibus DC Microgrid,” *IEEE Trans. Ind. Appl.*, vol. 56, no. 6, pp. 6174–6185, 2020.
- [70] J. Do Park, J. Candelaria, L. Ma, and K. Dunn, “DC ring-bus microgrid fault protection and identification of fault location,” *IEEE Trans. Power Deliv.*, vol. 28, no. 4, pp. 2574–2584, 2013.
- [71] R. M. Cuzner and G. Venkataramanan, “The status of DC micro-grid protection,” *Conf. Rec. - IAS Annu. Meet. (IEEE Ind. Appl. Soc.)*, pp. 1–8, 2008.
- [72] S. Ali, Z. Zheng, M. Aillerie, J. P. Sawicki, M. C. Péra, and D. Hissel, “A review of dc microgrid energy management systems dedicated to residential applications,” *Energies*, vol. 14, no. 14, pp. 1–26, 2021.
- [73] D. E. Olivares *et al.*, “Trends in microgrid control,” *IEEE Trans. Smart Grid*, vol. 5, no. 4, pp. 1905–1919, 2014.
- [74] K. R. Bharath, M. Krishnan Mithun, and P. Kanakasabapathy, “A review on DC microgrid control techniques, applications and trends,” *Int. J. Renew. Energy Res.*, vol. 9, no. 3, pp. 1328–1338, 2019.
- [75] T. H. E. Environmentaleconomical, B. Of, and T. H. E. Microgrid, “IEEE may/june 2008,” no. june, pp. 54–65, 2008.
- [76] T. V. Vu, D. Perkins, F. Diaz, D. Gonsoulin, C. S. Edrington, and T. El-Mezyani, “Robust adaptive droop control for DC microgrids,” *Electr. Power Syst. Res.*, vol. 146, pp. 95–106, 2017.
- [77] M. Benidris, S. Elsaiah, S. Sulaeman, and J. Mitra, “Transient stability of distributed generators in the presence of energy storage devices,” *2012 North Am. Power Symp. NAPS 2012*, 2012.

- [78] Q. C. Zhong and G. Weiss, "Synchronverters: Inverters that mimic synchronous generators," *IEEE Trans. Ind. Electron.*, vol. 58, no. 4, pp. 1259–1267, 2011.
- [79] Q. C. Zhong, P. L. Nguyen, Z. Ma, and W. Sheng, "Self-synchronized synchronverters: Inverters without a dedicated synchronization unit," *IEEE Trans. Power Electron.*, vol. 29, no. 2, pp. 617–630, 2014.
- [80] S. M. Ashabani and Y. A. R. I. Mohamed, "A flexible control strategy for grid-connected and islanded microgrids with enhanced stability using nonlinear microgrid stabilizer," *IEEE Trans. Smart Grid*, vol. 3, no. 3, pp. 1291–1301, 2012.
- [81] M. Sechilariu, "Urban dc microgrids for advanced local energy management with smart grid communication," in *3rd International Congress on Energy Efficiency and Energy Related Materials (ENEFM2015)*, 2015, pp. 19–23.
- [82] M. Sechilariu, F. Locment, and I. Houssamo, "Production Locale d'électricité Renouvelable. Réseau Semi-Isole et Sécurise pour Bâtiments," in *EF09*.
- [83] M. Sechilariu, B. C. Wang, F. Locment, and A. Jouglet, "DC microgrid power flow optimization by multi-layer supervision control. Design and experimental validation," *Energy Convers. Manag.*, vol. 82, pp. 1–10, 2014.
- [84] Leonardo TRIGUEIRO DOS SANTOS, "Contribution on the day-ahead and operational optimization for DC microgrid building-Integrated," 2017.
- [85] H. WU, "Étude et analyse globale de l'efficacité énergétique d'un micro-réseau urbain à courant continu," 2018.
- [86] W. Bai, "DC Microgrid optimized energy management and real-time control of power systems for grid-connected and off-," 2021.
- [87] H. Al-Ghossini, "Contributions to the study of control for small-scale wind turbine connected to electrical microgrid with and without sensor," 2016.
- [88] H. Liu, "Contribution for integrating urban wind turbine into electrical microgrid: modeling and control," 2017.
- [89] 1, "Wind energy foundation." [Online]. Available: <https://windenergyfoundation.org/about-wind-energy/history/>.
- [90] R. Gasch and J. Twele, Eds., *Wind Power Plants*, vol. 44, no. 8. Berlin, Heidelberg: Springer Berlin Heidelberg, 2012.
- [91] power.solapv.com, "HISTORY OF WINDMILLS," *An Autom. Irrig. Syst. Using Arduino Microcontroller*, vol. 1908, no. January, pp. 2–6, 2011.
- [92] 2, "water pumping windmills."
- [93] 3, "The Iconic Windmills That Made the American West."
- [94] the Global Wind Energy Council, "Evolution of power wind power capacity," 2020. [Online]. Available: <https://gwec.net>.
- [95] "<https://ember-climate.org/about/>."
- [96] "<http://www.elite.tugraz.at/Jungbauer/3.htm>."
- [97] A. R. Reitz, C. R. Yan, J. Ogle, and P. Seel, "COMPUTATIONAL MODELING OF WIND TURBINE WAKE INTERACTIONS Submitted," 2012.
- [98] "http://www.energy.siemens.com/us/pool/hq/power-generation/wind-power/E50001-W310-A123-X-4A00_WS_SWT-2.3-82%20VS_US.pdf."
- [99] J. V. Akwa, H. A. Vielmo, and A. P. Petry, "A review on the performance of Savonius wind turbines," *Renew. Sustain. Energy Rev.*, vol. 16, no. 5, pp. 3054–3064, 2012.
- [100] J. G. McGowan and S. R. Connors, "Windpower: A turn of the century review," *Annu. Rev. Energy Environ.*, vol. 25, pp. 147–197, 2000.

- [101] R. A. Kishore, “Small-scale Wind energy portable turbine (SWPT),” 2013.
- [102] N. Gionfra, “Stratégies de commande distribuée pour l’optimisation de la production des fermes éoliennes To cite this version: Stratégies de commande distribuée pour l’optimisation de la production des fermes éoliennes,” 2018.
- [103] D. H. Tran, B. Sareni, X. Roboam, and C. Espanet, “Integrated optimal design of a passive wind turbine system: An experimental validation,” *IEEE Trans. Sustain. Energy*, vol. 1, no. 1, pp. 48–56, 2010.
- [104] M. A. Abdullah, A. H. M. Yatim, C. W. Tan, and R. Saidur, “A review of maximum power point tracking algorithms for wind energy systems,” *Renew. Sustain. Energy Rev.*, vol. 16, no. 5, pp. 3220–3227, 2012.
- [105] V. Courtecuisse, “Supervision d’une centrale multisources à base d’éoliennes et de stockage d’énergie connectée au réseau électrique,” 2009.
- [106] S. K. Kim and E. S. Kim, “PSCAD/EMTDC-based modeling and analysis of a gearless variable speed wind turbine,” *IEEE Trans. Energy Convers.*, vol. 22, no. 2, pp. 421–430, 2007.
- [107] A. Abdelli, “Optimisation multicritère d’une chaîne éolienne passive,” 2007.
- [108] Z. P., “Small Wind World Report,” Germany, 2012.
- [109] International Electrotechnical Commission, “Iec 61400-2,” *Test*, vol. 3, 2013.
- [110] R. A. Kishore, T. Coudron, and S. Priya, “Small-scale wind energy portable turbine (SWEPT),” *J. Wind Eng. Ind. Aerodyn.*, vol. 116, pp. 21–31, 2013.
- [111] H. Polinder, J. A. Ferreira, B. B. Jensen, A. B. Abrahamsen, K. Atallah, and R. A. McMahon, “Trends in wind turbine generator systems,” *IEEE J. Emerg. Sel. Top. Power Electron.*, vol. 1, no. 3, pp. 174–185, 2013.
- [112] A. D. Hansen, F. Lov, F. Blaabjerg, and L. H. Hansen, “Review of contemporary wind turbine concepts and their market penetration,” *Wind Eng.*, vol. 28, no. 3, pp. 247–263, 2004.
- [113] M. Liserre, R. Cárdenas, M. Molinas, and J. Rodríguez, “Overview of multi-MW wind turbines and wind parks,” *IEEE Trans. Ind. Electron.*, vol. 58, no. 4, pp. 1081–1095, 2011.
- [114] H. Polinder, F. F. A. Van Der Pijl, G. J. De Vilder, and P. J. Tavner, “Comparison of direct-drive and geared generator concepts for wind turbines,” *IEEE Trans. Energy Convers.*, vol. 21, no. 3, pp. 725–733, 2006.
- [115] H. Polinder, S. W. H. De Haan, M. R. Dubois, and J. G. Slootweg, “Basic operation principles and electrical conversion systems of wind turbines,” *EPE J. (European Power Electron. Drives Journal)*, vol. 15, no. 4, pp. 43–50, 2005.
- [116] E. De Vries, *Wind turbine drive systems: A commercial overview*. Woodhead Publishing Limited, 2013.
- [117] F. Blaabjerg, R. Teodorescu, M. Liserre, and A. V. Timbus, “Overview of control and grid synchronization for distributed power generation systems,” *IEEE Trans. Ind. Electron.*, vol. 53, no. 5, pp. 1398–1409, 2006.
- [118] Z. Chen, J. M. Guerrero, and F. Blaabjerg, “A review of the state of the art of power electronics for wind turbines,” *IEEE Trans. Power Electron.*, vol. 24, no. 8, pp. 1859–1875, 2009.
- [119] A. Mesemanolis, C. Mademlis, and I. Kioskeridis, “Conversion System With Induction Generator,” vol. 1, no. 4, pp. 238–246, 2013.
- [120] L. Gertmar, L. Liljestränd, and H. Lendenmann, “Wind energy powers-that-be successor generation in globalization,” *IEEE Trans. Energy Convers.*, vol. 22, no. 1, pp. 13–28, 2007.
- [121] M. M. Hossain and M. H. Ali, “Future research directions for the wind turbine generator system,” *Renew. Sustain. Energy Rev.*, vol. 49, pp. 481–489, 2015.
- [122] W. Rik, “The Aim of Wind Turbine Sys-,” *Converter*, pp. 26–33, 2002.

- [123] L. Xu, L. Yao, and C. Sasse, "Grid integration of large DFIG-based wind farms using VSC transmission," *IEEE Trans. Power Syst.*, vol. 22, no. 3, pp. 976–984, 2007.
- [124] A. Mirecki, X. Roboam, and F. Richardeau, "Architecture complexity and energy efficiency of small wind turbines," *IEEE Trans. Ind. Electron.*, vol. 54, no. 1, pp. 660–670, 2007.
- [125] M. Chinchilla, S. Arnaltes, and J. C. Burgos, "Control of permanent-magnet generators applied to variable-speed wind-energy systems connected to the grid," *IEEE Trans. Energy Convers.*, vol. 21, no. 1, pp. 130–135, 2006.
- [126] B. J. Chalmers, W. Wu, and E. Spooner, "An axial-flux permanent-magnet generator for a gearless wind energy system," *IEEE Trans. Energy Convers.*, vol. 14, no. 2, pp. 251–256, 1999.
- [127] F. Blaabjerg, M. Liserre, and K. Ma, "Power electronics converters for wind turbine systems," *IEEE Trans. Ind. Appl.*, vol. 48, no. 2, pp. 708–719, 2012.
- [128] A. S. Abdel-Khalik, S. Ahmed, A. M. Massoud, and A. A. Elserougi, "An improved performance direct-drive permanent magnet wind generator using a novel single-layer winding layout," *IEEE Trans. Magn.*, vol. 49, no. 9, pp. 5124–5134, 2013.
- [129] P. A. Owusu and S. Asumadu-Sarkodie, "A review of renewable energy sources, sustainability issues and climate change mitigation," *Cogent Eng.*, vol. 3, no. 1, pp. 1–14, 2016.
- [130] M. Sechilariu, B. C. Wang, F. Locment, and A. Joulet, "DC microgrid power flow optimization by multi-layer supervision control. Design and experimental validation," *Energy Convers. Manag.*, 2014.
- [131] T. Dragicevic, X. Lu, J. C. Vasquez, and J. M. Guerrero, "DC Microgrids - Part I: A Review of Control Strategies and Stabilization Techniques," *IEEE Trans. Power Electron.*, vol. 31, no. 7, pp. 4876–4891, 2016.
- [132] H. Al-Ghossini, F. Locment, M. Sechilariu, L. Gagneur, and C. Forgez, "Adaptive-tuning of extended Kalman filter used for small scale wind generator control," *Renew. Energy*, 2016.
- [133] J. Hussain and M. K. Mishra, "Adaptive Maximum Power Point Tracking Control Algorithm for Wind Energy Conversion Systems," *IEEE Trans. Energy Convers.*, vol. 31, no. 2, pp. 697–705, 2016.
- [134] Y. Daili, J. P. Gaubert, and L. Rahmani, "New control strategy for fast-efficient maximum power point tracking without mechanical sensors applied to small wind energy conversion system," *J. Renew. Sustain. Energy*, vol. 7, no. 4, 2015.
- [135] H. Liu, F. Locment, and M. Sechilariu, "Integrated control for small power wind generator," *Energies*, vol. 11, no. 5, 2018.
- [136] N. A. Orlando, M. Liserre, R. A. Mastromauro, and A. Dell'Aquila, "A survey of control issues in pmsg-based small wind-turbine systems," *IEEE Trans. Ind. Informatics*, vol. 9, no. 3, pp. 1211–1221, 2013.
- [137] Y. Daili, J. P. Gaubert, and L. Rahmani, "Implementation of a new maximum power point tracking control strategy for small wind energy conversion systems without mechanical sensors," *Energy Convers. Manag.*, vol. 97, pp. 298–306, 2015.
- [138] R. Syahputra and I. Soesanti, "Performance improvement for small-scale wind turbine system based on maximum power point tracking control," *Energies*, vol. 12, no. 20, 2019.
- [139] A. R. Vijay Babu, K. Suresh, C. Umamaheswara Rao, and C. Saida Reddy, "Design and implementation of high gain power converter for wind energy conversion system," *J. Adv. Res. Dyn. Control Syst.*, vol. 10, no. 1, pp. 307–317, 2018.
- [140] H. Liu, F. Locment, and M. Sechilariu, "Maximum Power Point Tracking Method for Small Scale Wind Generator Experimental validation," *SICE Annu. Conf. 2015 July 28-30, 2015, Hangzhou, China*, pp. 87–101, 2015.
- [141] D. Kumar and K. Chatterjee, "A review of conventional and advanced MPPT algorithms for wind

energy systems,” *Renew. Sustain. Energy Rev.*, vol. 55, pp. 957–970, 2016.

- [142] A. Amir, A. Amir, J. Selvaraj, and N. A. Rahim, “Study of the MPP tracking algorithms: Focusing the numerical method techniques,” *Renew. Sustain. Energy Rev.*, vol. 62, pp. 350–371, 2016.
- [143] M. Nasiri, J. Milimonfared, and S. H. Fathi, “Modeling, analysis and comparison of TSR and OTC methods for MPPT and power smoothing in permanent magnet synchronous generator-based wind turbines,” *Energy Convers. Manag.*, vol. 86, pp. 892–900, 2014.
- [144] R. Tiwari and N. R. Babu, “Fuzzy logic based MPPT for permanent magnet synchronous generator in wind energy conversion system,” *IFAC-PapersOnLine*, vol. 49, no. 1, pp. 462–467, 2016.
- [145] A. Urtasun, P. Sanchis, and L. Marroyo, “Limiting the power generated by a photovoltaic system,” *2013 10th Int. Multi-Conference Syst. Signals Devices, SSD 2013*, pp. 1–6, 2013.
- [146] H. Rezk and A. M. Eltamaly, “A comprehensive comparison of different MPPT techniques for photovoltaic systems,” *Sol. Energy*, vol. 112, pp. 1–11, 2015.
- [147] K. Belmokhtar, M. L. Doumbia, and K. Agbossou, “Novel fuzzy logic based sensorless maximum power point tracking strategy for wind turbine systems driven DFIG (doubly-fed induction generator),” *Energy*, vol. 76, pp. 679–693, 2014.
- [148] B. Meghni, D. Dib, and A. T. Azar, “A second-order sliding mode and fuzzy logic control to optimal energy management in wind turbine with battery storage,” *Neural Comput. Appl.*, vol. 28, no. 6, pp. 1417–1434, 2017.
- [149] D. Calabrese, G. Tricarico, E. Brescia, G. L. Cascella, V. G. Monopoli, and F. Cupertino, “Variable structure control of a small ducted wind turbine in the whole wind speed range using a luenberger observer,” *Energies*, vol. 13, no. 18, pp. 14–20, 2020.
- [150] C.-H. Lin, “Wind Turbine Driving a PM Synchronous Generator Using Novel Recurrent Chebyshev Neural Network Control with the Ideal Learning Rate,” *Energies*, vol. 9, no. 6, p. 441, 2016.
- [151] Y. Zhang, L. Zhang, and Y. Liu, “Implementation of maximum power point tracking based on variable speed forecasting for wind energy systems,” *Processes*, vol. 7, no. 3, 2019.
- [152] C. H. Liu and Y. Y. Hsu, “Effect of rotor excitation voltage on steady-state stability and maximum output power of a doubly fed induction generator,” *IEEE Trans. Ind. Electron.*, vol. 58, no. 4, pp. 1096–1109, 2011.
- [153] L. Belhadji, S. Bacha, I. Munteanu, A. Rumeau, and D. Roze, “Adaptive MPPT applied to variable-speed microhydropower plant,” *IEEE Trans. Energy Convers.*, vol. 28, no. 1, pp. 34–43, 2013.
- [154] A. Harrag and S. Messalti, “Variable step size modified P&O MPPT algorithm using GA-based hybrid offline/online PID controller,” *Renew. Sustain. Energy Rev.*, vol. 49, pp. 1247–1260, 2015.
- [155] S. Messalti, A. Harrag, and A. Loukriz, “A new variable step size neural networks MPPT controller: Review, simulation and hardware implementation,” *Renew. Sustain. Energy Rev.*, vol. 68, no. October 2016, pp. 221–233, 2017.
- [156] J. C. Y. Hui, A. Bakhshai, and P. K. Jain, “An Energy Management Scheme with Power Limit Capability and an Adaptive Maximum Power Point Tracking for Small Standalone PMSG Wind Energy Systems,” *IEEE Trans. Power Electron.*, vol. 31, no. 7, pp. 4861–4875, 2016.
- [157] W. Bai and M. Sechilariu, “applied sciences DC Microgrid System Modeling and Simulation Based on a Specific Algorithm for Grid-Connected and Islanded Modes with Real-Time Demand-Side Management Optimization,” 2020.
- [158] T. L. Tiang and D. Ishak, “Novel MPPT Control in Permanent Magnet Synchronous Generator System for Battery Energy Storage,” *Appl. Mech. Mater.*, vol. 110–116, pp. 5179–5183, Oct. 2011.

- [159] T. Papadopoulos, E. Tatakis, and E. Koukoulis, "Improved active and reactive control of a small wind turbine system connected to the grid," *Resources*, vol. 8, no. 1, 2019.
- [160] M. Kesraoui, N. Korichi, and A. Belkadi, "Maximum power point tracker of wind energy conversion system," *Renew. Energy*, vol. 36, no. 10, pp. 2655–2662, 2011.
- [161] V. Lazarov, D. Roye, D. Spirov, and Z. Zarkov, "Study of control strategies for variable speed wind turbine under limited power conditions," *Proc. EPE-PEMC 2010 - 14th Int. Power Electron. Motion Control Conf.*, pp. 125–130, 2010.
- [162] R. M. Linus and P. Damodharan, "Maximum power point tracking method using a modified perturb and observe algorithm for grid connected wind energy conversion systems," *IET Renew. Power Gener.*, vol. 9, no. 6, pp. 682–689, 2015.
- [163] K. Vijayakumar, N. Kumaresan, and N. Ammasaigounden, "Speed sensor-less maximum power point tracking and constant output power operation of wind-driven wound rotor induction generators," *IET Power Electron.*, vol. 8, no. 1, pp. 33–46, 2015.
- [164] M. Sechilariu, N. Molines, G. Richard, H. Martell-Flores, F. Locment, and J. Baert, "Electromobility framework study: Infrastructure and urban planning for EV charging station empowered by PV-based microgrid," *IET Electr. Syst. Transp.*, vol. 9, no. 4, pp. 176–185, 2019.
- [165] M. A. Jirdehi, V. S. Tabar, S. Ghassemzadeh, and S. Tohidi, "Different aspects of microgrid management: A comprehensive review," *J. Energy Storage*, vol. 30, no. June 2019, p. 101457, 2020.
- [166] M. Ross, C. Abbey, F. Bouffard, and G. Joos, "Microgrid Economic Dispatch with Energy Storage Systems," *IEEE Trans. Smart Grid*, vol. 9, no. 4, pp. 3039–3047, 2018.
- [167] A. Alarcon-Rodriguez, G. Ault, and S. Galloway, "Multi-objective planning of distributed energy resources: A review of the state-of-the-art," *Renew. Sustain. Energy Rev.*, vol. 14, no. 5, pp. 1353–1366, 2010.
- [168] J. J. Wang, Y. Y. Jing, C. F. Zhang, and J. H. Zhao, "Review on multi-criteria decision analysis aid in sustainable energy decision-making," *Renew. Sustain. Energy Rev.*, vol. 13, no. 9, pp. 2263–2278, 2009.
- [169] S. D. Pohekar and M. Ramachandran, "Application of multi-criteria decision making to sustainable energy planning - A review," *Renew. Sustain. Energy Rev.*, vol. 8, no. 4, pp. 365–381, 2004.
- [170] F. A. Bhuiyan, A. Yazdani, and S. L. Primak, "Optimal sizing approach for islanded microgrids," *IET Renew. Power Gener.*, vol. 9, no. 2, pp. 166–175, 2015.
- [171] R. Hosseinalizadeh, H. Shakouri G, M. S. Amalnick, and P. Taghipour, "Economic sizing of a hybrid (PV-WT-FC) renewable energy system (HRES) for stand-alone usages by an optimization-simulation model: Case study of Iran," *Renew. Sustain. Energy Rev.*, vol. 54, pp. 139–150, 2016.
- [172] C. E. C. Nogueira *et al.*, "Sizing and simulation of a photovoltaic-wind energy system using batteries, applied for a small rural property located in the south of Brazil," *Renew. Sustain. Energy Rev.*, vol. 29, pp. 151–157, 2014.
- [173] S. Chouhan, D. Tiwari, H. Inan, S. Khushalani-Solanki, and A. Feliachi, "DER optimization to determine optimum BESS charge/discharge schedule using Linear Programming," *IEEE Power Energy Soc. Gen. Meet.*, vol. 2016-Novem, 2016.
- [174] G. Comodi *et al.*, "Multi-apartment residential microgrid with electrical and thermal storage devices: Experimental analysis and simulation of energy management strategies," *Appl. Energy*, vol. 137, pp. 854–866, 2015.
- [175] H. Karami, M. J. Sanjari, S. H. Hosseinian, and G. B. Gharehpetian, "An optimal dispatch algorithm for managing residential distributed energy resources," *IEEE Trans. Smart Grid*, vol. 5, no. 5, pp. 2360–2367, 2014.
- [176] H. Kanchev, D. Lu, F. Colas, V. Lazarov, and B. Francois, "Energy management and operational

- planning of a microgrid with a PV-based active generator for smart grid applications,” *IEEE Trans. Ind. Electron.*, vol. 58, no. 10, pp. 4583–4592, 2011.
- [177] R. Sioshansi, P. Denholm, T. Jenkin, and J. Weiss, “Estimating the value of electricity storage in PJM: Arbitrage and some welfare effects,” *Energy Econ.*, vol. 31, no. 2, pp. 269–277, 2009.
- [178] T. Gabriel, “Renewable resources,” *Technol. Guid. Princ. - Appl. - Trends*, vol. 3, no. 2, pp. 30–33, 2009.
- [179] M. Parvania, M. Fotuhi-Firuzabad, and M. Shahidehpour, “Comparative hourly scheduling of centralized and distributed storage in day-ahead markets,” *IEEE Trans. Sustain. Energy*, vol. 5, no. 3, pp. 729–737, 2014.
- [180] D. Lew, M. Milligan, G. Jordan, and R. Piwko, “The Value of Wind Power Forecasting,” *Proc. 91st Am. Meteorol. Soc. Annu. Meet. Second Conf. Weather. Clim. New Energy Econ.*, no. April, 2011.
- [181] C. Chen, S. Duan, T. Cai, B. Liu, and G. Hu, “Smart energy management system for optimal microgrid economic operation,” *IET Renew. Power Gener.*, vol. 5, no. 3, pp. 258–267, 2011.
- [182] S. Modes, Q. Jiang, M. Xue, G. Geng, and S. Member, “Energy Management of Microgrid,” vol. 28, no. 3, pp. 3380–3389, 2013.
- [183] M. C. Hu, S. Y. Lu, and Y. H. Chen, “Stochastic programming and market equilibrium analysis of microgrids energy management systems,” *Energy*, vol. 113, pp. 662–670, 2016.
- [184] Y. Liu and N. K. C. Nair, “A Two-Stage Stochastic Dynamic Economic Dispatch Model Considering Wind Uncertainty,” *IEEE Trans. Sustain. Energy*, vol. 7, no. 2, pp. 819–829, 2016.
- [185] M. N. Akter, M. A. Mahmud, and A. M. T. Oo, “A hierarchical transactive energy management system for energy sharing in residential microgrids,” *Energies*, vol. 10, no. 12, 2017.
- [186] I. Prodan and E. Zio, “A model predictive control framework for reliable microgrid energy management,” *Int. J. Electr. Power Energy Syst.*, vol. 61, pp. 399–409, 2014.
- [187] B. V. Solanki, A. Raghurajan, K. Bhattacharya, and C. A. Canizares, “Including Smart Loads for Optimal Demand Response in Integrated Energy Management Systems for Isolated Microgrids,” *IEEE Trans. Smart Grid*, vol. 8, no. 4, pp. 1739–1748, 2017.
- [188] G. Saveen, P. Prudhvi Raju, D. V. Manikanta, and M. Satya Praveen, “Design and implementation of energy management system with fuzzy control for multiple microgrid,” *Proc. 2nd Int. Conf. Inven. Syst. Control. ICISC 2018*, vol. 28, no. 4, pp. 1239–1244, 2018.
- [189] S. Standard, “iTeh STANDARD PREVIEW iTeh STANDARD PREVIEW,” vol. 1, no. I, pp. 2–5, 2020.
- [190] T. Wang, X. He, and T. Deng, “Neural networks for power management optimal strategy in hybrid microgrid,” *Neural Comput. Appl.*, vol. 31, no. 7, pp. 2635–2647, 2019.
- [191] S. Rajanna and R. P. Saini, “Development of optimal integrated renewable energy model with battery storage for a remote Indian area,” *Energy*, vol. 111, pp. 803–817, 2016.
- [192] A. S. O. Ogunjuyigbe, T. R. Ayodele, and O. A. Akinola, “Optimal allocation and sizing of PV/Wind/Split-diesel/Battery hybrid energy system for minimizing life cycle cost, carbon emission and dump energy of remote residential building,” *Appl. Energy*, vol. 171, pp. 153–171, 2016.
- [193] O. Erdinc *et al.*, “Experimental performance assessment of an online energy management strategy for varying renewable power production suppression,” *Int. J. Hydrogen Energy*, vol. 37, no. 6, pp. 4737–4748, 2012.
- [194] J. Zhao and X. Yuan, “Multi-objective optimization of stand-alone hybrid PV-wind-diesel-battery system using improved fruit fly optimization algorithm,” *Soft Comput.*, vol. 20, no. 7, pp. 2841–2853, 2016.
- [195] P. Suhane, S. Rangnekar, A. Mittal, and A. Khare, “Sizing and performance analysis of standalone

wind-photovoltaic based hybrid energy system using ant colony optimization,” *IET Renew. Power Gener.*, vol. 10, no. 7, pp. 964–972, 2016.

- [196] M. Manas, “Optimization of Distributed Generation Based Hybrid Renewable Energy System for a DC Micro-Grid Using Particle Swarm Optimization,” *Distrib. Gener. Altern. Energy J.*, vol. 33, no. 4, pp. 7–25, 2018.
- [197] M. K. Perera *et al.*, “Multi agent based energy management system for microgrids,” *PHICON 2020 - 9th IEEE Power India Int. Conf.*, 2020.
- [198] A. Anvari-Moghaddam, A. Rahimi-Kian, M. S. Mirian, and J. M. Guerrero, “A multi-agent based energy management solution for integrated buildings and microgrid system,” *Appl. Energy*, vol. 203, pp. 41–56, 2017.
- [199] S. Singh, M. Singh, and S. C. Kaushik, “Optimal power scheduling of renewable energy systems in microgrids using distributed energy storage system,” *IET Renew. Power Gener.*, vol. 10, no. 9, pp. 1328–1339, 2016.
- [200] Z. Yi, W. Dong, and A. H. Etemadi, “A unified control and power management scheme for PV-Battery-based hybrid microgrids for both grid-connected and islanded modes,” *IEEE Trans. Smart Grid*, vol. 9, no. 6, pp. 5975–5985, 2018.
- [201] R. R. Deshmukh, M. S. Ballal, H. M. Suryawanshi, and M. K. Mishra, “An adaptive approach for effective power management in DC microgrid based on virtual generation in distributed energy sources,” *IEEE Trans. Ind. Informatics*, vol. 16, no. 1, pp. 362–372, 2020.
- [202] K. Thirugnanam, S. K. Kerk, C. Yuen, N. Liu, and M. Zhang, “Energy Management for Renewable Microgrid in Reducing Diesel Generators Usage with Multiple Types of Battery,” *IEEE Trans. Ind. Electron.*, vol. 65, no. 8, pp. 6772–6786, 2018.
- [203] Y. Liu *et al.*, “Distributed Robust Energy Management of a Multimicrogrid System in the Real-Time Energy Market,” *IEEE Trans. Sustain. Energy*, vol. 10, no. 1, pp. 396–406, 2019.
- [204] M. G. Villalva, J. R. Gazoli, and E. R. Filho, “Comprehensive approach to modeling and simulation of photovoltaic arrays,” *IEEE Trans. Power Electron.*, vol. 24, no. 5, pp. 1198–1208, 2009.
- [205] A. Dev and S. B. Jeyaprabha, “Modeling and Simulation of Photovoltaic Module in MATLAB,” *Proc. Int. Conf. Appl. Math. Theor. Comput. Sci.*, no. figure 1, pp. 268–273, 2013.
- [206] T. Denoix, M. Sechilariu, and F. Locment, “Experimental comparison of photovoltaic panel operating cell temperature models,” *IECON Proc. (Industrial Electron. Conf.)*, pp. 2089–2095, 2014.
- [207] M. Sechilariu; F. Locment, *Urban DC Microgrid*, Elsevier. 2016.
- [208] L. T. Dos Santos, M. Sechilariu, and F. Locment, “Optimized load shedding approach for grid-connected DC microgrid systems under realistic constraints,” *Buildings*, vol. 6, no. 4, 2016.
- [209] T. D. Khoa, L. T. Dos Santos, M. Sechilariu, and F. Locment, “Load shedding and restoration real-time optimization for DC microgrid power balancing,” *2016 IEEE Int. Energy Conf. ENERGYCON 2016*, 2016.
- [210] B. Wang, “Thèse présentée pour l’obtention du grade de Docteur de l’UTC par,” 2013.
- [211] L. Avenues, “Impact of diesel generator operating modes on standalone DC microgrid and control strategies implying supercapacitor,” 2018.
- [212] IBM ilog cplex optimizer. Available from: “<http://ibm.com>,” 2010. .
- [213] E. R. C. da Silva and M. E. Elbuluk, *Fundamentals of Power Electronics*, vol. 59. 2013.
- [214] N. O. Sokal, “System Oscillations From Negative Input Resistance At Power Input,” *PESC Rec. - IEEE Annu. Power Electron. Spec. Conf.*, pp. 1–3, 1973.
- [215] R.D. Middlebrook, “Input filter considerations in design and application of switching regulators,”

IEEE Ind. Appl. Soc. Annu. Meet., 1976.

- [216] R.D. Middlebrook, "Design techniques for preventing input-filter oscillations in switched-mode regulators," *roceedings Fifth Natl. Solid State Power Convers. Conf.*, 1978.
- [217] T. Dragicevic, X. Lu, J. C. Vasquez, and J. M. Guerrero, "DC Microgrids - Part I: A Review of Control Strategies and Stabilization Techniques," *IEEE Transactions on Power Electronics*, vol. 31, no. 7. Institute of Electrical and Electronics Engineers Inc., pp. 4876–4891, 01-Jul-2016.
- [218] X. Feng, J. Liu, and F. C. Lee, "Impedance specifications for stable DC distributed power systems," *IEEE Trans. Power Electron.*, vol. 17, no. 2, pp. 157–162, 2002.
- [219] X. Feng, Z. Ye, K. Xing, F. C. Lee, and D. Borrojevic, "Impedance specification and impedance improvement for DC distributed power system," *PESC Rec. - IEEE Annu. Power Electron. Spec. Conf.*, vol. 2, pp. 889–894, 1999.
- [220] J. Sun, "Impedance-Based Stability Criterion for," *IEEE Trans Power Appar. Syst.*, vol. 26, no. 11, pp. 1–10, 2011.
- [221] M. Cespedes, L. Xing, and J. Sun, "Constant-power load system stabilization by passive damping," *IEEE Trans. Power Electron.*, vol. 26, no. 7, pp. 1832–1836, 2011.
- [222] A. M. Rahimi and A. Emadi, "An analytical investigation of DC/DC power electronic converters with constant power loads in vehicular power systems," *IEEE Trans. Veh. Technol.*, vol. 58, no. 6, pp. 2689–2702, 2009.
- [223] W. J. Lee and S. K. Sul, "DC-link voltage stabilization for reduced DC-link capacitor inverter," *IEEE Trans. Ind. Appl.*, vol. 50, no. 1, pp. 404–414, 2014.
- [224] R. K. Maheshwari, S. Munk-Nielsen, and K. Lu, "An active damping technique for small DC-link capacitor based drive system," *IEEE Trans. Ind. Informatics*, vol. 9, no. 2, pp. 848–858, 2013.
- [225] X. Liu, A. J. Forsyth, and A. M. Cross, "Negative input-resistance compensator for a constant power load," *IEEE Trans. Ind. Electron.*, vol. 54, no. 6, pp. 3188–3196, 2007.
- [226] C. N. Onwuchekwa and A. Kwasinski, "Analysis of boundary control for buck converters with instantaneous constant-power loads," *IEEE Trans. Power Electron.*, vol. 25, no. 8, pp. 2018–2032, 2010.
- [227] M. Vsc, D. Multiterminal, M. Davari, S. Member, Y. A. I. Mohamed, and S. Member, "Variable-Structure-Based Nonlinear Control for the," vol. 29, no. 11, pp. 6196–6213, 2014.
- [228] S. Beheshtaein, R. M. Cuzner, M. Forouzesh, M. Savaghebi, and J. M. Guerrero, "DC Microgrid Protection: A Comprehensive Review," *IEEE J. Emerg. Sel. Top. Power Electron.*, vol. 6777, no. c, pp. 1–1, 2019.
- [229] D. Salomonsson, L. Söder, and A. Sannino, "Protection of low-voltage DC microgrids," *IEEE Trans. Power Deliv.*, vol. 24, no. 3, pp. 1045–1053, 2009.
- [230] L. Zhang, N. Tai, W. Huang, J. Liu, and Y. Wang, "A review on protection of DC microgrids," *J. Mod. Power Syst. Clean Energy*, vol. 6, no. 6, pp. 1113–1127, 2018.
- [231] J. Do Park and J. Candelaria, "Fault detection and isolation in low-voltage dc-bus microgrid system," *IEEE Trans. Power Deliv.*, vol. 28, no. 2, pp. 779–787, 2013.
- [232] M. Mobarrez, D. Fregosi, S. Bhattacharya, and M. A. Bahmani, "Grounding architectures for enabling ground fault ride-through capability in DC microgrids," *2017 IEEE 2nd Int. Conf. Direct Curr. Microgrids, ICDCM 2017*, pp. 81–87, 2017.
- [233] M. Mobarrez, M. G. Kashani, S. Bhattacharya, and R. Adapa, "Comparative study of DC circuit breakers using realtime simulations," *IECON Proc. (Industrial Electron. Conf.)*, pp. 3736–3742, 2014.
- [234] R. M. Cuzner, K. Palaniappan, W. Sedano, N. Hoeft, and M. Qi, "Fault characterization and protective system design for a residential DC microgrid," *2017 6th Int. Conf. Renew. Energy Res. Appl. ICRERA 2017*, vol. 2017-Janua, pp. 642–647, 2017.

- [235] K. Palaniappan, W. Sedano, N. Hoefft, R. Cuzner, and Z. J. Shen, "Fault discrimination using SiC JFET based self-powered solid state circuit breakers in a residential DC community microgrid," *2017 IEEE Energy Convers. Congr. Expo. ECCE 2017*, vol. 2017-Janua, pp. 3747–3753, 2017.
- [236] M. Monadi, C. Koch-Ciobotaru, A. Luna, J. I. Candela, and P. Rodriguez, "A protection strategy for fault detection and location for multi-terminal MVDC distribution systems with renewable energy systems," *3rd Int. Conf. Renew. Energy Res. Appl. ICRERA 2014*, pp. 496–501, 2014.
- [237] A. Meghwani, S. C. Srivastava, and S. Chakrabarti, "A Non-unit Protection Scheme for DC Microgrid Based on Local Measurements," *IEEE Trans. Power Deliv.*, vol. 32, no. 1, pp. 172–181, 2017.
- [238] A. A. S. Emhemed, K. Fong, S. Fletcher, and G. M. Burt, "Validation of fast and selective protection scheme for an LVDC distribution network," *IEEE Trans. Power Deliv.*, vol. 32, no. 3, pp. 1432–1440, 2017.
- [239] A. A. S. Emhemed and G. M. Burt, "An advanced protection scheme for enabling an LVDC last mile distribution network," *IEEE Trans. Smart Grid*, vol. 5, no. 5, pp. 2602–2609, 2014.
- [240] J. Yang, J. E. Fletcher, and J. O'Reilly, "Short-circuit and ground fault analyses and location in VSC-based DC network cables," *IEEE Trans. Ind. Electron.*, vol. 59, no. 10, pp. 3827–3837, 2012.
- [241] P. Cairoli and R. A. Dougal, "Fault detection and isolation in medium-voltage DC microgrids: Coordination between supply power converters and bus contactors," *IEEE Trans. Power Electron.*, vol. 33, no. 5, pp. 4535–4546, 2018.
- [242] S. D. A. Fletcher, P. J. Norman, K. Fong, S. J. Galloway, and G. M. Burt, "High-speed differential protection for smart DC distribution systems," *IEEE Trans. Smart Grid*, vol. 5, no. 5, pp. 2610–2617, 2014.
- [243] C. Yuan, M. A. Haj-Ahmed, and M. S. Illindala, "Protection Strategies for Medium-Voltage Direct-Current Microgrid at a Remote Area Mine Site," *IEEE Trans. Ind. Appl.*, vol. 51, no. 4, pp. 2846–2853, 2015.
- [244] J. P. Brozek, "DC overcurrent protection—where we stand," *IEEE Trans. Ind. Appl.*, vol. 29, no. 5, pp. 1029–1032, 1993.
- [245] G. D. Gregory, "Applying Low-Voltage Circuit Breakers in Direct Current Systems," *IEEE Trans. Ind. Appl.*, vol. 31, no. 4, pp. 650–657, 1995.
- [246] Z. Zhou, J. Jiang, S. Ye, C. Liu, and D. Zhang, "A Γ -Source Circuit Breaker for DC Microgrid Protection," *IEEE Trans. Ind. Electron.*, vol. 68, no. 3, pp. 2310–2320, 2021.
- [247] C. Meyer, S. Schröder, and R. W. De Doncker, "Solid-state circuit breakers and current limiters for medium-voltage systems having distributed power systems," *IEEE Trans. Power Electron.*, vol. 19, no. 5, pp. 1333–1340, 2004.
- [248] D. Lawes, L. Ran, and Z. Xu, "Design of a solid-state D.C. Circuit breaker for light rail transit power supply network," *2014 IEEE Energy Convers. Congr. Expo. ECCE 2014*, pp. 350–357, 2014.
- [249] W. Wen, Y. Huang, Y. Sun, J. Wu, M. Al-Dweikat, and W. Liu, "Research on Current Commutation Measures for Hybrid DC Circuit Breakers," *IEEE Trans. Power Deliv.*, vol. 31, no. 4, pp. 1456–1463, 2016.
- [250] H. Zheng, H. Lin, and Y. Du, "Designing and research of a novel current limiting DC hybrid circuit breaker with the combinatorial electronic switch," *Proc. 2015 IEEE Innov. Smart Grid Technol. - Asia, ISGT ASIA 2015*, 2016.
- [251] D. M. Bui, S. L. Chen, C. H. Wu, K. Y. Lien, C. H. Huang, and K. K. Jen, "Review on protection coordination strategies and development of an effective protection coordination system for DC microgrid," *Asia-Pacific Power Energy Eng. Conf. APPEEC*, vol. 2015-March, no. March, 2014.
- [252] Z. Xu, B. Zhang, S. Sirisukprasert, X. Zhou, and A. Q. Huang, "The emitter turn-off thyristor-

based DC circuit breaker,” *Proc. IEEE Power Eng. Soc. Transm. Distrib. Conf.*, vol. 1, pp. 288–293, 2002.

- [253] J. M. Haefliger, “Radio-oncology: current status and future trends,” *Rev. Med. Suisse Romande*, vol. 108, no. 12, pp. 1011–106, 1988.
- [254] A. Kazakov, K. Janson, and T. Vaimann, “DC Microgrid Protection Means,” no. May, pp. 58–64, 2016.
- [255] E. Christopher, M. Sumner, D. W. P. Thomas, X. Wang, and F. De Wildt, “Fault location in a zonal DC marine power system using active impedance estimation,” *IEEE Trans. Ind. Appl.*, vol. 49, no. 2, pp. 860–865, 2013.
- [256] K. Jia, T. Bi, B. Liu, E. Christopher, D. W. P. Thomas, and M. Sumner, “Marine Power Distribution System Fault Location Using a Portable Injection Unit,” *IEEE Trans. Power Deliv.*, vol. 30, no. 2, pp. 818–826, 2015.
- [257] K. Jia, E. Christopher, D. Thomas, M. Sumner, and T. Bi, “Advanced DC zonal marine power system protection,” *IET Gener. Transm. Distrib.*, vol. 8, no. 2, pp. 301–309, 2014.
- [258] R. Mohanty, U. S. M. Balaji, and A. K. Pradhan, “An Accurate Noniterative Fault-Location Technique for Low-Voltage DC Microgrid,” *IEEE Trans. Power Deliv.*, vol. 31, no. 2, pp. 475–481, 2016.
- [259] M. B. Dewe, “References To HvdC Fault Location,” vol. 8, no. 3, pp. 1295–1302, 1993.
- [260] O. M. K. K. Nanayakkara, A. D. Rajapakse, and R. Wachal, “Location of DC line faults in conventional HVDC systems with segments of cables and overhead lines using terminal measurements,” *IEEE Trans. Power Deliv.*, vol. 27, no. 1, pp. 279–288, 2012.
- [261] X. Feng, L. Qi, and J. Pan, “A Novel Fault Location Method and Algorithm for DC Distribution Protection,” *IEEE Trans. Ind. Appl.*, vol. 53, no. 3, pp. 1834–1840, 2017.

Appendix 1:

Impedance specifications

One of the typical sources of instability in DC power systems, particularly DC MG, is the impedance mismatch between damped filters on the source side and regulated power converters on the load side. These converters are modeled as the constant power loads (CPLs) [213]. It was shown in [214] that the negative input resistance of the equipment can exceed the positive output resistance of the LC filter and the power source. Thus, the whole system can oscillate causing instability. The author of [215] and [216] investigated the problem of the negative impedance characteristics in low frequency. A switch-mode converter was the solution proposed by the author and it was based on providing the input filter of this switch-mode converter and keeping the output of the filter smaller than the input impedance of the converter.

Another solution to deal with the instability in a DC MG was based on the Nyquist stability criterion. This solution is based on dividing the full system into two subsystems, i.e., a load subsystem modeled by an input impedance and a source subsystem modeled with an output impedance [217]. The impedance analysis consists then of calculating the impedance ratio and defining a forbidden region. The impedance ratio is the ratio between the output ratio and the input ratio and it expressed the interaction of these two impedances and is often referred to as the minor loop gain [218]. The forbidden region is a region already defined by the Nyquist criterion. In order to preserve the stability, the impedance ratio must meet the stability condition by keeping the minor loop gain outside the forbidden region [219].

It is worth noting that the proposed impedance-based approach was all established for voltage source systems. Indeed, studies about current source systems showed opposite characteristics for stability requirements [220]. Authors of [220] analyzed the stability for a DC-DC converter with its input filter using the Routh-Hurwitz criterion. They concluded that for current source systems, the system is stable if the impedance ratio is less than unity while for voltage source systems, this ratio should be more than unity.

Stabilization strategies

The presence of resonant conditions because of the virtual inductance provided by the operation of CPLs harms the stability of the system. Thus, the common way to meet impedance criteria and stability is to smooth the resonant peak of the input filter. For this, two types of stabilization are possible: passive stabilization and active stabilization.

Passive stabilization consists of adding physical resistors in series and /or parallel with inductors and capacitors, respectively [215], [221], [222]. Yet, adding these damping elements introduces and increases

dissipative and transmission losses [213]. Consequently, a tradeoff must be considered between the system stability and transmission losses.

Active stabilization or active damping consists of modifying control loops of load converter or source converter. For that, two strategies are deployed by researchers to achieve stability, i.e. small-signal stabilization and large-signal stabilization.

Small-signal stabilization is a strategy that is based on a linear feedback control loop. Its objective is to produce the same damping effects as the real damping elements by modifying the loop gain of the system. Thus, the efficiency of the overall system is conserved. This active damping can shape the closed-loop impedance related either to the point of the load converter or the output impedance of the power supply. One example of this active compensation method was presented in [63]. This study aims to overcome the instabilities caused by the negative incremental input admittance in DC systems feeding PMSGs. For that, and to shape the input impedance, the stabilization block was made of a proportional compensator followed by a bandpass filter. This later takes the DC link voltage as a reference and input and adds its output to the current reference calculated by the speed control. Similar algorithms were adopted for speed drives DC voltage [223], [224] and also for brushless DC motors drive as in [225]. However, large-signal stability is ensured by using nonlinear controllers. Authors of [64] and [226] present an example of a nonlinear method based on a geometric principle. This study proposed a boundary control that consists of driving the source converter, which feeds CPLs, to a specific operating point. This approach allows tracking every state variable of the source converter and the switching occurs when the boundary is crossed by the trajectories of selected state variables. Another nonlinear controller was proposed in [227] with the aim to regulate DC voltage in DC distribution systems. It was designed for a VSC and used a sigma-delta modulation scheme. Results showed good stabilization achievement of all system states.

Appendix 2:

DC fault analysis and characteristics

In a DC MG, DC fault could usually arise either in the DC bus or at the DC cables that connect all the components that make up the MG. Furthermore, DC bus and DC interconnections are also responsible for the energy transfer between DERs, ESSs, and loads through the single point of energy interface. Thus, an adequate protection system is crucial to provide a fatal impact of any single fault in the system [228]. The battery, for example, might be placed far away from DC bus and transmission lines, but if the fault occurs, the fault current could be calculated based not only on line resistance and inductance but also on internal resistance and inductance of the battery. Similarly, for loads, the fault current could be measured depending on the type of load that can be categorized into a constant impedance, constant power, and constant current [229]. Consequently, the fault type can be bus fault or feeder fault depending on the fault location.

Other possible faults could exist in DC systems: pole to pole faults and pole to ground faults. A pole-to-pole fault also named line to line fault, happened when a path between the positive and negative line is created, short-circuiting them together. It is characterized by low fault impedance. However, the impedance of a pole to a ground fault could be either low or high. This type of fault occurs when either the positive or the negative pole is short-circuited with to ground. It is the most common fault in industrial systems. The line-to-line fault is the most typical type in a DC MG. A response for such a fault could be depicted in three different stages including capacitor-discharge stage, diode free wheel stage, and grid-side current stage [230].

Since the MG systems need to be multi-terminal, these latter take advantage of the VSC that must be used to interface different subsystems to the bus, i.e. the AC side through an inductor and the DC side through a capacitor. Internal switch faults can occur at the VSCs, causing a line-to-line short circuit fault. This is considered as terminal faults that generally cannot be cleared. In such a case, the devices have to be replaced, and using fuses could be an appropriate protection measure in this case [231].

Different types of grounding system for DC MG

Grounding is a serious issue for DC MG protection and it relates to different design objectives and system considerations that include essential safety of equipment and personnel, grid reliability, ground fault detection, and minimization of leakage current [232]. Thus, the main purposes of grounding designs are to ease the ground fault detection, minimize DC stray current, and reduce the common-mode voltage (CMV) [233]. The latter are related to each other by the grounding resistance. A DC MG could be grounded with high resistance, low resistance, or even ungrounded. High resistance ground results in very

low stray current and high CMV while a low grounding resistance leads to low CMV and high stray current [59].

According to IEC 60364-1, there are three grounding strategies including Terre-Neutre (TN), Isolated-Terre (IT), and Terre-Terre (TT). The first letter, T or I, refers respectively to the direct connection of the earth and no connection to the earth while the second letter, T or N, denotes respectively direct earthing of the exposed conductive parts and connection of the exposed parts to the earth neutral.

Different types of DC fault detection methods

Considering serious problems that can cause DC fault current and to avoid any damage to equipment, the fault must be located reliably. Yet, the coordination between different protective devices is still very difficult because of the fast rate of change of sudden inception of DC fault [234], [235].

Until now, the methods to detect and identify the faulty section could be subdivided into five main categories including overcurrent, directional overcurrent, current derivative, differential, and distance-based strategies have been proposed.

- The overcurrent method is based on defining a threshold current for the fault occurrence. The current is measured using an overcurrent relay. Once the value of that current reached the predefined threshold, a signal is sent to the circuit breaker (CB). This type of protection is implemented for simple DC MGs. Indeed, complex DC MG architecture may cause some problems related to time response or disconnecting some essential parts of the network responsible to solve the problem [236].
- The current derivative is a protection method where the current derivative increases from 0 to a high value to detect the fault quickly. The value of that current depends essentially on the fault impedance and the cable length [237].
- Directional overcurrent protection is proposed for DC MG. In that case, the direction of the current could be from either side and a communication system exists to help identify the direction of all branches. Thus, when the fault occurs, the direction and the magnitude of fault current change, and the location of the faulty line become easier [238], [239].
- Distance protection is a method that functions by measuring the impedance from the first point of measuring until the fault point. The protection is then ensured by sending a tripping signal to the CB based on the distance related to the measured impedance. Nonetheless, this technique loses its performance especially in the case of high impedance faults and short cable section [240], [241].
- Differential protection is a technique based on measuring the value of the current from each side for a specific element. Then, a current transducer is used to verify if there is any difference between the measured currents. Any difference in these values shows that a fault has occurred. Nevertheless, using this method for a DC MG is susceptible to current transducer errors and will require a robust communication system and backup protection [242], [243].

Protective devices

In a DC MG, components, size, and configuration are the essential parameters to be taken into account for the selection of appropriate protective devices. At the moment, fuses [244] and CBs [245] are the commercially available approaches designed for the protection of DC distribution systems. They are the components in the power system that can open the circuit during a fault. In the case of an over-current with an arc, both of these protection devices begin the process of opening a current flow path.

- Fuses are the most traditional protection devices and could be applicable for both AC and DC systems. For DC systems, that have low inductance, fuses are useful for traction, battery protection, auxiliary low voltage power supplies, and power circuit protection [71], etc. However, fuses are not a good solution to protect DC MG. Indeed, many constraints may appear on the length of the distribution cable and the difficulty of predicting transient effects on the MG voltage due to fuse opening [244].
- CB is one of the most important pieces in a DC system and it can replace fuses and enhance the operating conditions of a system. However, conventional CB still suffers from some obstacles because of the lack of a natural zero crossing in DC fault currents. Indeed, these traditional breakers cause arcs during the interruption and cannot meet fault cleaning time requirements [246]. To overcome these drawbacks and improve the protection, PE switches have been proposed and developed. These commonly refer to solid-state CBs [247], [248] and Hybrid CBs [249], [250] with less/no arcing and minimum fault clearing time. Different types of semiconductors determine the characteristics of these protection devices and are available for DC MG systems [251]–[254]. They are: gate turn off thyristors, insulated gate bipolar transistor and insulated gate commutated thyristors. Yet, the economic feasibility of these breakers must be analyzed before designing the protection system for DC MG. Furthermore, despite the increase of power losses while using this new protection equipment, they guarantee to meet the strict protection requirements.

Faults location approaches

As highlighted at the beginning of this section, the fault must be located quickly and precisely to repair the faulty segment without impacting the MG reliability. For that, two types of fault location approaches were proposed in the literature: active methods and passive methods.

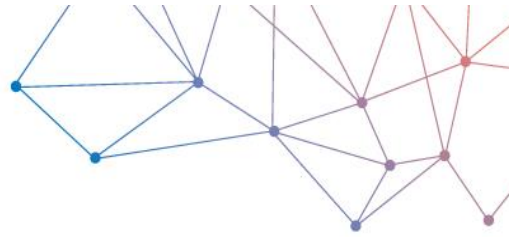
On the one hand, active methods are characterized by their high accuracy and no requirement of communication devices. They are using external equipment for injecting a signal which is responsible to locate the fault. Active impedance estimation (AIE) [255]–[257] and power probe unit (PPU) [70], [258] are the two well-known injection-based active methods. The first one uses a triangle current waveform signal injected by a power converter with the aim to calculate the impedance at the coupling point. The second one creates a second-order RLC circuit in to calculating the fault distance by analyzing the probe

current response. However, these active methods require more equipment to function and then increase their implementation cost.

On the other hand, passive methods, contrary to active ones, are using existing signals to identify the location of the fault without the need for extra devices. The main inactive approaches are including Traveling Wave (TW) and the local measurement. TWs are the voltage and current signals that propagate through a DC MG once the fault occurs. The location of that fault is identified by analyzing some characteristics of the TWs such as the measurement of first arrival times of the waves at the converter station [259] or the interval times at different locations [260]. Yet, these techniques are not applied for MG applications since they require accurate data acquisition using high-performance equipment. Local measurement is another passive method that does not use communication but focuses on exploiting local electrical variables to calculate the fault distance. For example, the location of the fault could be estimated either by using an iterative method based on measuring the voltage across a length of the line [240] or by calculating the equivalent inductance between protective devices and a fault [261]. However, this method cannot be applied to DC MG in which the capacitor is not connected to only one end of the cable, unlike AC MG.

To conclude, in DC MGs, these fault location methods are an even much more demanding issue because the DC line resistance and reactance are considerably lower than in AC systems.

Appendix 3:



DATA SHEET

PITOT TUBE

NPL type (L / straight)



Large range of type L Pitot tubes



High quality and accuracy



Better than 1% for an alignment in relation to the flow axis of the fluid of $\pm 10^\circ$




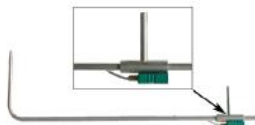

Made according to AFNOR NFX 10-112

KIMO offers a broad range of Pitot tubes of great quality and accuracy realised according to the NF X 10-112 norm.

The KIMO Pitot tubes, connected to a differential column of liquid manometer, with needle or electronic, enable to measure the dynamic pressure of a fluid in movement in a pipe and determine its speed in m/s and its flow in m³/h.

The Pitot tubes are used in climatic engineering, ventilation, dust-removal and pneumatic transport. They are particularly adapted for measurement in warm air, charged with particles and for high speed.

References

Reference	Description
 <p>Pitot tube L type</p>	<p>Pitot tubes with ellipsoidal top. A total pressure port and six holes of static pressure. Body in full stainless steel.</p>
 <p>Pitot tube L type with K thermocouple</p>	<p>Pitot tubes with ellipsoidal top. A total pressure port and six holes of static pressure. K thermocouple probe lined integrated with connecting cable of 1.5 meter long. Body in full stainless steel.</p>
 <p>Pitot tube straight type & straight type with K thermocouple</p>	<p>It enables to carry out measurement directly by immersing the tube in the air-diffusing equipment. Diameter and dimensions: same as the NPL curved Pitot.</p>

Technical features

Model	AFNOR NF
Coefficient	1.0015 ±0.01
Material	Inox 316 L
Measuring range	3 to 85 m/s
Operating temperature	From 0 to 600°C in standard and up to 1000°C in option
Static pressure	2 bar maximum in static Hereafter on request
Global accuracy of the measurement system	Better than 1% for an alignment in relation to the flow axis of the fluid of ±10°
Standards	AFNOR NFX10-112, Annex of the 77.09.14 This standard is in accordance with the international standard ISO 3966.

Presentation of the range

• Pitot tubes L type and straight type

Diameter	Reference L type	Reference straight type	Length
Ø3 mm	TPL-03-100	TPL-D-03-100	100 mm
	TPL-03-200	TPL-D-03-200	200 mm
	TPL-03-300	TPL-D-03-300	300 mm
Ø6 mm	TPL-06-300	TPL-D-06-300	300mm
	TPL-06-500	TPL-D-06-500	500 mm
	TPL-06-800	TPL-D-06-800	800 mm
Ø8 mm	TPL-08-1000	TPL-D-08-1000	1000 mm
	TPL-08-1250	TPL-D-08-1250	1250 mm
Ø12 mm	TPL-12-1500	TPL-D-12-1500	1500 mm
	TPL-12-2000	TPL-D-12-2000	2000 mm
Ø14 mm	TPL-14-2500	-	2500 mm
	TPL-14-3000	TPL-D-14-3000	3000 mm

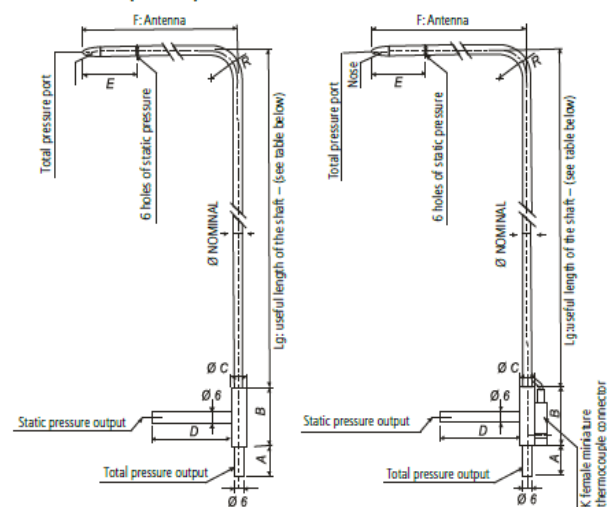
• Pitot tubes L type and straight type with K thermocouple

Diameter	Reference L type	Reference straight type	Length
Ø3 mm	TPL-03-100-T	TPL-D-03-100-T	100 mm
	TPL-03-200-T	TPL-D-03-200-T	200 mm
	TPL-03-300-T	TPL-D-03-300-T	300 mm
Ø6 mm	TPL-06-300-T	TPL-D-06-300-T	300mm
	TPL-06-500-T	TPL-D-06-500-T	500 mm
	TPL-06-800-T	TPL-D-06-800-T	800 mm
Ø8 mm	TPL-08-1000-T	TPL-D-08-1000-T	1000 mm
	TPL-08-1250-T	TPL-D-08-1250-T	1250 mm
Ø12 mm	TPL-12-1500-T	TPL-D-12-1500-T	1500 mm
	TPL-12-2000-T	TPL-D-12-2000-T	2000 mm
Ø14 mm	TPL-14-2500-T	-	2500 mm
	TPL-14-3000-T	-	3000 mm

Options

- Graduation (mm) with red mark on the shaft, on request
- TIG Welding for a use up to 1000°C (except Pitot tube Ø3)

Dimensions (in mm)



Pitot tube L type Pitot tube L type with K thermocouple

	A	B	ØC	D	E	F	R
Pitot tube Ø3 mm	17	32	10	30	25	48	9
Pitot tube Ø6 mm	25	40	10	40	48	96	18
Pitot tube Ø8 mm	25	40	10	50	64	128	24
Pitot tube Ø12 mm	25	50	16	70	96	192	36
Pitot tube Ø14 mm	25	50	16	70	112	224	42



All dimensions and ratings of this document are specified in mm.

Accessories

Name	Reference
Gland in plated brass for the installation of Pitot tubes for fixed station	x
Mounting flange stainless steel and cast iron	x
Sliding connections with stainless steel turn or PTFE	x
Extension cable for K thermocouple class 1	x
Stopper cap in caoutchouc: bag of 10 pieces	x
Caps: bag of 10 pieces	x
Black silicone tube (4 x 7 mm)	SN-47-1
Transparent silicone tube (4 x 7mm)	SB-47-1
Crystal tube (5 x 8 mm)	C-58-1
Transport case VTP type for Pitot tubes: - 1210 X 320 mm, length 1000mm, max. Ø8 - 810 X 100mm, length 500mm, max. Ø6	x/x
Spherical ball valve female / female	555 FF
Junctions in Y for a tube Ø5 x 8 mm (bag of 10)	JYC
Junctions in T for a tube Ø5 x 8 mm (bag of 10)	JTC



For every other cases, KIMO offers special realisations. Consult us, we intervene on plans study, machining.

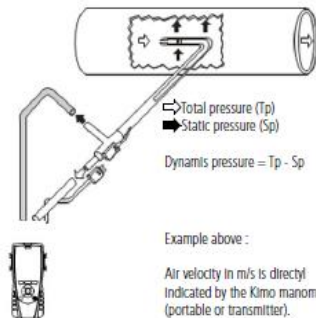
Operating principle

The Pitot tube is introduced perpendicularly in the pipe by pre-determined points (cf. "Measurement").
 The antenna composed of an ellipsoidal nose (bow) maintained in parallel and in front of the flow to control.
 The total pressure (+) is picked up by the bow and is connected to the + sign of the manometer.
 The static pressure (-) picked up by the small holes located around the antenna is connected to the - sign of the manometer.
 The connecting cable of the K thermocouple is connected to the input K of the manometer (for the Pitot tube type L with K thermocouple).

The device then indicates the dynamic pressure, sometimes called speed pressure.

The dynamic pressure corresponds to the difference between total pressure and static pressure: $Dp = Tp - Sp$

Application



- GTC Record
- GTC Analyze

Low differential pressure transmitter sensor CP210 and SQR/3



- Alarm
- Visualize
- Operate
- GTC Record
- GTC Analyze
- Live monitoring

Low differential pressure transmitter sensor with digital display C310 or CA 310 with SPI 2 - 100, 500, 1000, 10000 and SQR/3



- Alarm
- Visualize
- Reocord
- Analyze
- Live monitoring

Multifunction intelligent portable AMI 310

Measurement

- Punctual velocity measurement

$$V = C_F \sqrt{\frac{2 \Delta P}{\rho}} \quad \rho = \frac{P_o}{287.1 \times (\Theta + 273.15)}$$

With:
 C_F : coefficient of the flow device element
 Pitot tube L: $C_F = 1.0015$
 Θ : given temperature (°C)
 P_o : given atmospheric pressure (Pa)

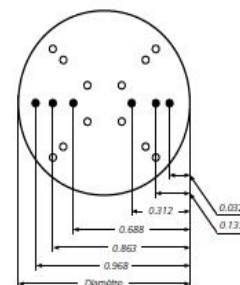
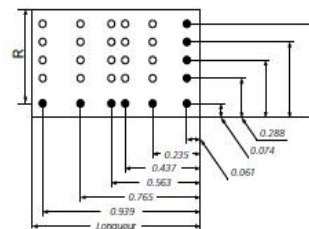
- Air flow measurement

Average (A) of several measurements of punctual velocity according to Log-Tchebychev (see measurement scheme above).

Air flow calculation

Flow = Velocity_A x Surface x 3600
 Surface: surface of the circular or rectangular sheath in m²
 N.B: in the electronic devices, the surface is automatically adjustable.

With:
 Flow: in m³/h
 Surface: in m²
 V_A : in m/s



Log-Tchebychev in 3 points

Flang - Pitot L - 27/05/19 - RCS (24)Périgueux 349 282 095 - Non-contractual document - We reserve the right to modify the characteristics of our products without prior notice.

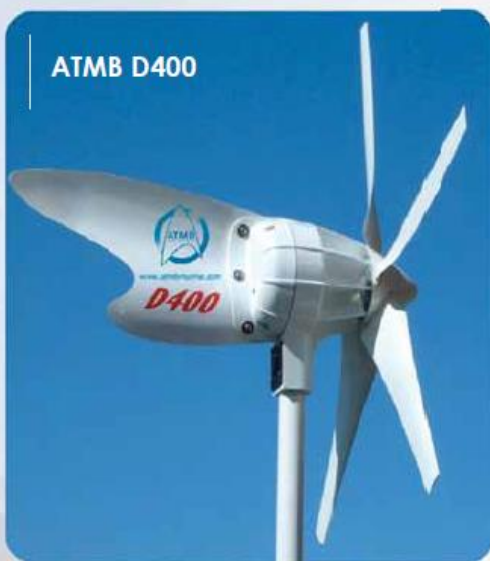
Appendix 4:



ENERGIE

ÉOLIENNE FORTE PUISSANCE ATMB D400

L'éolienne ATMB D400 est l'auxiliaire idéale pour charger les batteries des bateaux de voyage. Sa puissance lui permet de pallier à tous les consommateurs du bord. Elle peut fournir 91 Ampères par jour avec 9 nœuds de vent seulement, sa courbe est unique dans sa catégorie. L'éolienne marine ATMB D400 est la plus puissante actuellement produite. L'éolienne ATMB D400 est actuellement la référence retenue par la majorité des constructeurs de bateaux de voyage.

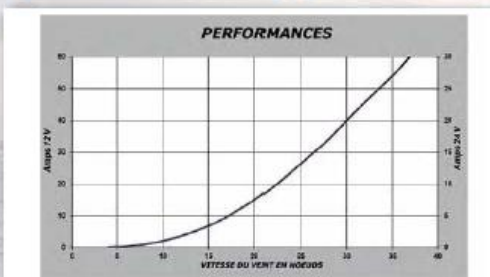


ATMB D400 : Conception et Avantages

- L'éolienne ATMB D400 a été conçue pour délivrer un ampérage élevé avec de faibles vitesses de vent, elle est extrêmement silencieuse et fonctionne sans vibrations.
- L'empennage a un profil spécial anti-turbulences.
- L'alternateur haut rendement, le profil des pâles permettent de fonctionner à régime lent.
- Les avantages de la D400 sont ses hautes performances, la production dépasse 500 Watts à 40 Nœuds.
- Cette éolienne innove de part sa qualité de fabrication et son design. Elle est un gage de fiabilité à long terme.
- Régulateur conseillé 6TB / Arrêt par inter bipolaire.

- Référence en 12V : **D400-12**
- Référence en 24V : **D400-24**
- Référence régulateur : **LVM6TB12** pour D400-12
- Référence régulateur : **LVM6TB24** pour D400-24
- Référence Switch d'arrêt 12V-50A : **SW1250**
- Référence Switch d'arrêt 24V-30A : **SW2430**
- Référence Mât inox : **K12**
- Référence Mât inox 2.60m articulé : **K8**

Régulateurs et accessoires : page 10



Courbe indicative issues de tests en laboratoire. Les valeurs peuvent varier en fonction de la force et la constance du vent, ainsi que l'état et la condition du parc batterie.



1 mètre/seconde = 1,94 Nœud = 3,6 km/h

CARACTÉRISTIQUES TECHNIQUES

- Puissance 235W @ 11 m/s (22 Nœuds) – 420W @ 14 m/s (28 Nœuds)
- Puissance maximale + de 600W - Amorçage : 2,5 m/s (5 Nœuds)
- Vitesse de rotation : 1100 tours à 14 m/s, (28 Nœuds)
- Disponible pour Tensions : 12 – 24 – 48 VDC
- Rotor 5 pâles Diamètre 1.10m
- Niveau sonore à 7 m. : 2-6 Db/A
- Diamètre de rotation : 700 mm – Embase fixation Mâle : 42 mm
- Alternateur Triphasé 12 pôles avec redresseur sortie DC – Continu
- Carter Aluminium revêtu de peinture époxy
- Poids : 17 Kg
- Garantie : 2 ans.

Kits de fixation : page 10



Mât Articulé K8



Régulateur 6TB

ATMB Marine 8, Bis rue de la Source 92000 NANTERRE - FRANCE

6

☎ : +33 (0) 141 187 518 - 📠 : + 33 (0) 141 187 573 - ✉ atmbmarine@atmbmarine.com - 🌐 www.atmbmarine.com

Appendix 5:

Module Photovoltaïque Solar-Fabrik Série SF 130/2



Une qualité optimale de série:

- Stabilité dans le temps grâce au verre solaire spécial transparent, équipé de filtre UV
- Présélection et tri des cellules à 100 %
- Rendement énergétique élevé grâce à l'utilisation de composants de qualité appariés avec précision (cf. l'étude « Power Check » de l'institut Fraunhofer ISE)
- Techniques de production de pointe et système de gestion de la qualité certifié (ISO 9001), pour la garantie d'une qualité produit « made in Germany »
- Cadre de module en aluminium spécialement développé en option; montage rapide et facile avec le système de fixation breveté Profilink; esthétique avantageuse grâce aux fixations intégrées
- Charge du panneau jusqu'à: 5400 Pa selon la norme IEC 61215
- Critères de tri très sélectifs de seulement +/- 2,5 W (= 1,9 %) pour éviter une première sélection des modules.
- Contrôles réguliers des modules de calibrage pour la mesure de la puissance à l'Institut Fraunhofer de systèmes à énergie solaire (ISE)

Dimensions

Série SF 130/2	Sans cadre	Cadre alu
l x L (mm)	1485 x 663	1491 x 669
Épaisseur (mm)	5	35
Poids (kg)	10,5	12,5

Homologations/Certifications

EN IEC 61215 ed. 2
Classe de protection II
Directive 89/336/CEE (CE)
Directive 73/23/CEE (CE)



Caractéristiques module Solar-Fabrik Série SF 130/2

Type de module	SF 130/2-125	SF 130/2-130	SF 130/2-135
Nombre de cellules (polycristallin)	36	36	36
Tension max. système	840 V	840 V	840 V

Caractéristiques électriques en STC (Standard Test Conditions: 1000 W/m², 25 °C, AM 1,5)

Puissance nominale*	P _{max}	125 W	130 W	135 W
Limites de tri puissance		+/- 2,5 W	+/- 2,5 W	+/- 2,5 W
Tension appr.	U _{MPP}	17,50 V	17,72 V	17,94 V
Tension circuit ouvert appr.	U _{OC}	21,53 V	21,69 V	21,86 V
Courant appr.	I _{MPP}	7,14 A	7,34 A	7,52 A
Courant de court-circuit appr.	I _{SC}	7,84 A	7,96 A	8,08 A

Caractéristiques électriques sous 800 W/m², NOCT, AM 1,5

Puissance en MPP appr.	P _{max}	96 W	100 W	104 W
Tension appr.	U _{MPP}	17,67 V	17,90 V	18,12 V
Tension circuit ouvert appr.	U _{OC}	21,26 V	21,42 V	21,59 V
Courant appr.	I _{MPP}	5,43 A	5,58 A	5,72 A
Courant de court-circuit appr.	I _{SC}	5,88 A	5,97 A	6,07 A

Sous un ensoleillement de 200 W/m² et une température de 25 °C, le rendement diminue de 7 % environ par rapport au rendement en conditions standard STC.

Températures

Coefficient de température tension	T _K (U _{OC})	-72 mV/K
Coefficient de température courant	T _K (I _{SC})	5,45 mA/K
NOCT		45 °C +/- 4K

Autres caractéristiques

Test haute tension	Tension d'essai 3200 V _{DC} /max. 60µA
Tenue à la grêle **	Jusqu'à 25 mm de diamètre à 23 m/s
Résistance à la tempête **	Vitesse du vent jusqu'à 130 km/h = 800 Pa et facteur de sécurité 3
Charge de neige supportée **	Sans cadre: 2400 Pa Δ 245 kg/m ²
Contrainte testée selon IEC 61215	Avec cadre: 5400 Pa Δ 550 kg/m ²

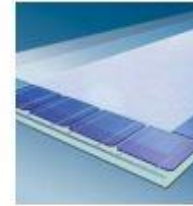
* (tolérance +/- 5 %)

** en combinaison avec notre système de fixation breveté Profilink installé selon les recommandations (BP) Sous réserve de modifications techniques.

Garantie de puissance: 25 ans conformément à nos conditions de garantie supplémentaires, envoyées sur demande.

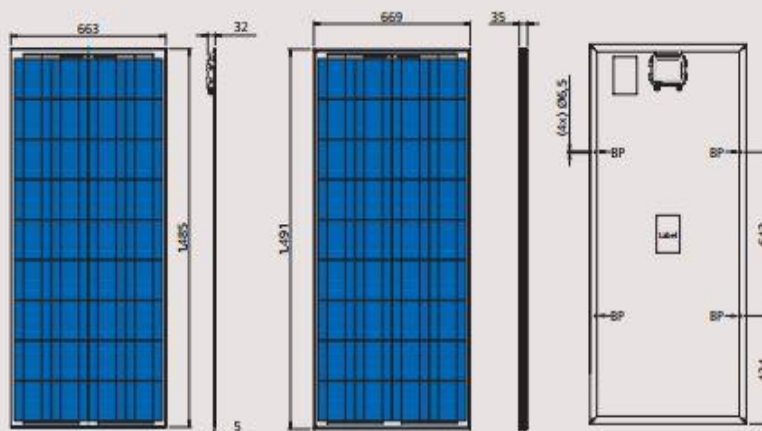


Un système de fixation efficace: Profilink



Structure du module:
verre spécialement trempé à faible teneur en fer/film vinyl transparent en acétate d'éthyle (EVA)/cellules photovoltaïques/EVA/ feuille arrière en Tedlar

Certifié par le VDE (Association des électrotechniciens allemands) selon les normes DIN EN ISO 9001, Reg.Nr. 5002983/QM11.2003 / DIN EN ISO 14001, Reg.Nr. 5002983/UM11.2003



SF 130/2 sans cadre

SF 130/2 avec cadre



Solar-Fabrik AG
Munzinger Straße 10
79111 Freiburg / Allemagne
tél. +49-(0)761-4000-0
fax +49-(0)761-4000-199
www.solar-fabrik.de

Etat: 15.12.2006, Solar-Fabrik AG
Document n° 0612MD8153